THE UNIVERSITY OF CHICAGO

ROLE OF REGULATORY T CELL ANTIGEN SPECIFICITY IN T CELL TOLERANCE, AUTOIMMUNITY, AND SELF-NONSELF DISCRIMINATION

A DISSERTATION SUBMITED TO

THE FACULTY OF THE DIVISION OF THE BIOLOGICAL SCIENCES

AND THE PRITZKER SCHOOL OF MEDICINE

IN CANDIDACY FOR THE DEGREE OF

DOCTOR OF PHILOSOPHY

COMMITTEE ON IMMUNOLOGY

BY

DAVID EDWARD KLAWON JR.

CHICAGO, ILLINOIS

AUGUST 2023

In memoriam of research animals,

to whom we owe an incomprehensible debt.

TABLE OF CONTENTS

LIST OF FIGURES

LIST OF TABLES

ACKNOWLEDGEMENTS

Eight years ago, during a class on Religion in Japan, I learned of the metaphor titled "Indra's Net". I imagined it as a fishing net consisting of square patterns made by intersecting rope, with multicolored diamonds fastened to the crossing points. Each jewel has no intrinsic veneer – it appears as nothing on its own – but instead reflects the vibrancy of those neighboring gems only when contextualized within the net. I think of this image often to remind myself that I am nothing but the culmination of lessons and experiences afforded to me by others. Thank you to all who have been a part of my net.

Thank you to the many people who directly contributed to the work presented in this thesis, as well as those who passed down their unique skills and techniques. When we decided to pursue a project using an infection model, very little institutional memory of pathogen experimentation existed within the University of Chicago community, as few laboratories or members had active pathogen experience. Our infection-centric studies would have been impossible in our hands if not for the time and patience of many pathogen teachers: Thank you to Pablo Penaloza-MacMaster and lab members at Northwestern University for hosting me and providing me with all of the basic skills and materials required for pathogen work; thank you to Nancy Freitag and Bridgett Ryan-Payseur at the University of Illinois at Chicago for welcoming me to the lab, graciously providing all *L.monocytogenes* strains, reagents, and techniques, and working with me for many weeks as I fumbled through the cloning and conjugation processes; thank you to Marisa Alegre for providing IACUC and IRB protocol templates for *L.monocytogenes* work; thank you to Wiola Lisicka and Bana Jabri for helping to translate the pathogen techniques I picked up at other Universities to practical work at the University of Chicago facilities. Thank you to those who provided expertise that was used to create novel tools in our lab: to Shan Kasal – and foundational CRISPR work in

carried out in the Albert Bendelac laboratory – for designing the *Tcaf3(exon5)*-floxed allele and passing on a unique genome editing skillset; to Erin Adams, John Leonard, and Ryan Duncombe for teaching myself and others protein production techniques, creating tetramer constructs, housing cell lines, and providing tetramers on a consistent basis; to Justin Spanier and Brian Fife at the University of Minnesota for providing protocols and technical advice regarding anti-pMHC-II antibody production; to Dana Gilmore for serving as my rotation mentor and teaching me all of the basic skills required for work in the Savage Laboratory. Thank you to those who provided their skills and expertise for novel experimental analyses to our laboratory: to Mark Maienschein-Cline at the University of Illinois at Chicago for executing many iterations of the single-cell RNA and TCR sequencing analyses; and a special thank you to Nicole Pagane and Harikesh Wong at the Ragon Institute/MIT for hosting me on multiple occasions, teaching me all of the basics for image analysis, and working diligently on the bioinformatic portion of the data analysis.

Thank you to the members of my thesis committee: Marisa Alegre, Bana Jabri, and Nicholas Chevrier. While the preparation was cumbersome at times, I truly enjoyed presenting our latest findings at committee meetings, as the members were always engaged, and the discussion left me with no shortage of concepts to consider over the following months. The perspectives and scientific advice afforded to me both within and outside of these meetings served to nudge many scientific directions taken in this thesis, including the creation of $C4^{\Delta TEC}$ mice, anti-C4/I-A^b antibodies, and *Lm* strains expressing linked peptides. Thank you also to the greater Committee on Immunology community at UChicago. Faculty engagement at Work in Progress, Journal Club, and Seminars serves as a critical and irreplaceable facet of student education, and I hope that incoming members continue to hold these events in such regard for years to come. The classes afforded in the curriculum, especially those integral to the first-year coursework, beautifully and

simultaneously fill multiple empty niches to provide the foundational tools required to become a scientist – the work and dedication of the faculty who construct and instruct these courses is very much appreciated.

I'd like to thank the following Core Facilities and individuals for indispensable contributions to the work presented in this thesis: NIH Tetramer Core Facility (contract number 75N93020D00005) for providing tetramers, especially Dale Long and Richard Willis for technical advice; University of Chicago Genomics Facility (RRID:SCR_019196) for RNA sequencing, especially Sandy Arun and Pieter Faber for technical assistance and advice; University of Chicago Cytometry and Antibody Technology Facility (RRID:SCR_017760), especially David Leclerc and Laura Johnson for technical advice, Bert Ladd, Mike Olsen, and Mandel Davis for performing cell sorts, and Mandel Davis for hybridoma expansion and antibody isolation; the University of Chicago Transgenic Mouse and Embryonic Stem Cell Facility (RRID:SCR_019171) for creating *Tcaf3(exon5)*-floxed mice, especially Linda Degenstein for performing microinjections and providing technical advice; the University of Chicago Animal Resource Center for mouse husbandry and sample collection.

Thank you to the many members of the Savage Laboratory who cycled through my tenure: Victoria Lee, Jaime Chao, Christine Miller, Donald Rodriguez, Sharon Zeng, Matthew Walker, Riley Curran, Nicole Ganci, Nikita Maheshwari, and Joseph Guter. Having spent the better part of seven years in the laboratory, I've had a front row seat to a complete generational cycle of the laboratory personnel. There's something special about the process of scientific transformation within a trainee – from novice to intellectual to mentor – and the various roles adopted by each individual over time. It's been a gift to have lived this experience concurrent with so many others, and I hope to carry the lessons of support, humility, and mentorship with me throughout my career.

A special thank you to my desk neighbors Christine and Riley, who were always excited to exchange novel data and get lost in spontaneous scientific discussions and ideas. Thank you to Justin and members of the Kline Laboratory, especially Sravya Tumuluru, Brendan MacNabb, Xiufen Chen, who were always willing to shirk responsibility with me for some company and a beer or five. I look forward to the day when we all meet at a conference, share our awesome research programs, and teach our trainees the importance of hazy early morning connections around a bonfire.

Words cannot express my gratitude for the support and love of my friends; each of whom have been instrumental in shaping both who I am and the life that I'm beyond lucky to live. For friends met throughout graduate school and the many experiences and discussions we've shared – Matt Funsten, Katya Frazier, Brooke Weigel, Peter Flynn, Nick Venturelli, Lari de Wet, Ryan Fuller, Nicole Fuller, Ryan Brown, Curtis Eisen, Maile Hollinger. For my roommates, and filling the time with grilling, brewing, television, and parties – Avi DeLeon, Julian Lutze, Clara Nizard, Eric Bueter. For the triathlon crew, and the excellent company you've been through all four seasons and the countless miles – Jen Allocco, Ryan Duncombe, Matt Walker. For my community mentee Patrick Brown, and all that you have taught me. For my friends met in college, and your consistent, unconditional, and easy friendship through the ups and downs – Sanam Bhalla, Donte Stevens, Nadeera Siddique, Caitlin Tice. For those who met me at a strange time, and the lasting impact your openness and adventure have had on my life – George Nelson, Fréd Blais, Nikita Bruce, Pauline Bö, Nai Rodriguez, Xabier Iñarritu, Roy Ma. For my friends from Buffalo, thank you for always keeping a place for me back home – Ryan O'hara, Adam Roaldi, Scotty Rentz, Mikey McDonnell, Christian Farah, Peter Scaglione, Pat Ryan, John Maher, Tyler Marciniak.

My path to science, this thesis, and what lies beyond is inextricably linked to the

inspirational mentors who willingly invested their time and energy in a curious but intrinsically unfocused and often confused young man without much direction. Thank you to Mr. Hellerer and Mr. Roland, who opened my eyes to the wonder of science and it's ability to answer questions with veracity. To Deacon Hynes, who taught me that it is okay to ask difficult questions and seek answers even when they are difficult or contradictory to my worldview. Thank you to Dr. Candy DeBerry, who inspired my love for research, facilitated my early research experiences, and supported my academic pursuits through times when I had lost faith in myself. To Dr. Anu Shanmuganathan, who showed me the magic of Immunology, demonstrated how to find answers to questions through experimentation, and illuminated how hypothesis-based research unlocks the ability to answer yet unanswered questions. Thank you to those who adopted me into their laboratories and provided vital insight into research techniques and life as a scientist: Dr. Jaime Clements at Kinex Pharmaceuticals, Dr. Qiming Jane Wang at the University of Pittsburgh, and Dr. Manuj Tandon and Dr. Evan Carder.

I would not be here without the mentorship and guidance of Dr. Peter Savage. Pete exhibits admirable qualities that serve as a model for what it means to be a brilliant and well-rounded scientist, including knowing how to intellectually fight for an idea, knowing when to re-evaluate a hypothesis, knowing how to efficiently communicate thoughts and experiments, and understanding when a break is required. In watching many students carry out their training under Pete's guidance, I gather that Pete possesses this rare ability to meet individuals where they are, tailor his mentorship to exploit their strengths, and ultimately manifest their potential into reality. I greatly struggled during my first summer at UChicago; having been denied all research positions the previous summer, was fresh out of undergrad and had been out of the laboratory for two years. Feeling defeated, I had packed my belongings into the car decided to head back to Buffalo and

figure out what to do instead of graduate school. A kind e-mail from Pete inquiring about the summer and my interest in a rotation came the day before I was set to leave, and gave me a reason to stay and try again. There are few moments in life that fork so clearly, and I am forever grateful for the confidence and compassion Pete afforded me in this interaction and many others. I hope to exemplify these qualities and pass them on to others in the future.

Most importantly, I need to thank my family. This is as much yours as it is mine – there's not a chance in hell this would have happened without you. To mom and dad – your countless and incomprehensible sacrifices, your absolute support and encouragement – every experience I've had, lesson I've learned, person I've met, has only been possible by your reassurance and space to grow, even when you didn't understand. To Kyle and Jacquie – growing up with you taught me how to be a friend, how to solve problems, how to be a teach and how to learn. I continue to be amazed by each of you, and am so lucky to have you in my life. To Manisha – there are no words. You're more than I ever imagined a partner could be; thank you for possessing all of the qualities that I aspire to. Your love through all of this has made it worthwhile. To the next adventure!

Funding

This work and stipend support were funded by the National Institute of Allergy and Infectious Diseases (U01-AI154560 to Peter Savage, Ronald Germain, Nancy Freitag; T32-AI007090 to Peter Savage gifted to David Klawon), the National Cancer Institute (P30-CA014599 to the Comprehensive Cancer Center Core), a Chicago Biomedical Consortium Catalyst Award to Peter Savage and Nancy Freitag, an Institute for Translational Medicine Core Subsidy Award to Peter Savage, the Robert E. Priest Fellowship to David Klawon, and a Fitch Scholarship to David Klawon.

EXPERIMENTAL CONTRIBUTIONS

Figure 4
Dana Gilmore performed C4 peptide immunization experiments and collected the data. **Brendan MacNabb** provided BMDC generation protocols and helped to maintain the cultures.

Figure 5
Dana Gilmore performed some T cell transfer experiments that involved C4/I-A^b tetramers and collected the data.

Figure 7
Christine Miller was a co-executer of Treg and Tconv isolation and mixing experiments and analyses.

Figure 8
Dana Gilmore generated some mixed chimeras, and performed some experiments and collected the data.

Figure 9
Dana Gilmore executed fetal thymic organ cultures and performed post-surgical treatments. **Dengping Yin** performed surgical procedures.

Figure 10
Victoria Lee and **Christine Miller** helped with vector design of the EAR and GLR clones. **Victoria Lee** assisted with some *in vitro* stimulation experiments.

Figure 11
Christine Miller was a co-executer of Treg depletion experiments and analyses. **Dengping Yin** performed surgical procedures.

Figure 20
Christine Miller was a co-executer of Treg and Tconv isolation and mixing experiments and analyses.

Figure 21
Christine Miller was a co-executer of Treg and Tconv isolation and tetramer depletion experiments and analyses.

Figure 22
Christine Miller was a co-executer of MJ23 Treg isolation and *Tcrb*$^{-/-}$ reconstitution experiments and analyses.

Figure 23
Donald Rodriguez and **Matthew Walker** were co-executers of the C4/I-A^b-specific T cell isolation experiment. **Mark Maienschein-Cline** performed bioinformatic analysis of sequencing data and created some figure panels. Nicole Pagane created some figure panels.

Figure 27
Harikesh Wong and **Nicole Pagane** were co-executers of imaging experiments. Harikesh Wong processed fixed samples, performed image acquisition, segmented some images, and advised he imaging work. Nicole Pagane designed and performed bioinformatic analyses of segmented images and created figure panels.

Figure 28
Nicole Ganci and **Matthew Walker** executed aspects of the experimental setup for the day 14 infection analysis.

Figure 30
Matthew Walker assisted with aspects of the SP33 transfer and infection experiment.

Figure 31
Matthew Walker assisted with aspects of the infection experiment and sample processing.

Figure 32
Montserrat Kwon assisted with the LLO/I-A^b tetramer analysis of fixed TCRβ mice.

Figure 33
Mandel Davis maintained and expanded select hybridoma cultures and purified antibody.
Justin Spanier and **Brian Fife** provided protocols and technical advice for hybridoma production

General
Matthew Walker performed or assisted with the design, construction, expression, and validation of some *L. monocytogenes* strains. **Bridgett Ryan-Payseur** assisted with the construction and expression of some *L. monocytogenes* strains. **Nicole Ganci** generated MJ23 chimeras for some experiments and assisted with various infections and experiments in Chapter 3. **Ryan Duncombe** and **John Leonard** engineered, produced, and isolated the monomers used to assemble C4/I-A^b, F1/I-A^b, and 2W1S/I-A^b tetramers in some experiments. **Mary Schoenbach** engineered and assembled the SP33 vector used for retrogenic expression. **Darshan Kasal** designed the *Tcaf3(exon5)^{flox}* allele, advised on the experimental strategy, and provided protocols. **Linda Degenstein** performed microinjections to create *Tcaf3(exon5)^{flox}* founder mice. **David Leclerc** and the **University of Chicago Cytometry Core Team** performed FACS sorting. **Dale Long**, **Richard Willis**, and the **NIH Tetramer Core Team** provided most monomer reagents used for tetramer production.

ABBREVIATIONS

TCR	T cell receptor
pMHC-II	peptide/MHC class-II
WT	Wild-type
TEC	Thymic epithelial cell
BMC	bone-marrow chimera
LF	low-frequency
CD4 SP	$CD4^+CD8^{neg}$ thymocytes
DP	$CD4^+CD8^+$ thymocytes
SLO	Secondary lymphoid organ
Spl	spleen
LN	Lymph node
pLN	periaortic lymph node
dLN	draining lymph node
Lm	*Listeria monocytogenes*
Tconv	$CD4^+$ $Foxp3^{neg}$ conventional T cell
Treg	$CD4^+$ $Foxp3^+$ regulatory T cell
pTreg	peripherally-induced regulatory T cell
DC	dendritic cell
BMDC	Bone marrow-derived dendritic cell
CFA	Complete Freund's Adjuvant
MPLA	Monophosphoryl lipid A
CTV	CellTrace Violet
PLP	proteolipid protein
IRBP	Interphotoreceptor retinoid-binding protein
C4/I-A^b	C4 peptide complexed with the I-A^b MHC-II molecule
F1/I-A^b	F1 peptide complexed with the I-A^b MHC-II molecule
LLO/I-A^b	LLO-derived peptide complexed with the I-A^b MHC-II molecule
2W/I-A^b	2W peptide complexed with the I-A^b MHC-II molecule
P7/I-A^b	IRBP-derived P7 peptide complexed with the I-A^b MHC-II molecule
MJ23	C4/I-A^b-specific monoclonal T cell
SP33	F1/I-A^b-specific monoclonal T cell
MFI	mean fluorescent intensity
SFI	summed fluorescence intensity
PGE	promiscuous gene expression
TRA	tissue-restricted antigen
scRNAseq	single-cell RNA sequencing
scTCRseq	single-cell paired αβ TCR sequencing
LSL	LoxP-STOP-LoxP DNA cassette
GFP	Green fluorescent protein
YFP	Yellow fluorescent protein
NOD	Non-obese diabetic
Ig	Immunoglobulin

ABSTRACT

Foxp3$^+$ regulatory T (Treg) cells maintain immune tolerance throughout life by preventing the activation of self-reactive CD4$^+$ conventional T (Tconv) cells. T cells recognize protein-derived peptides presented on host MHC-II molecules (pMHC-II antigen complexes) using a unique T cell receptor (TCR). T cell activation is initiated upon TCR recognition of specific pMHC-II ligands. For the large array of self-pMHC-II displayed throughout the body at steady-state, it is unclear whether CD4$^+$ T cell tolerance must be imparted for individual pMHC-II complexes, or if broad mechanisms of suppression maintain immune homeostasis across multiple T cell specificities. During infections, Treg cells must control Tconv cells reactive to self-derived peptide ligands while permitting Tconv cells that recognize pathogen-derived foreign antigens, yet the basis of this selectivity is unknown. Using mice in which T cell selection on a single prostate-specific self-pMHC-II ligand is altered, we demonstrate that tolerance is maintained under homeostatic conditions. In distinct settings of inflammation, including pathogen-associated epitope mimicry or T cell transfer to a lymphopenic environment, mice developed fulminant prostate-specific autoimmunity. Mechanistically, this self-pMHC-II complex directs antigen-specific cells into the Foxp3$^+$ regulatory T cell lineage during development but does not induce clonal deletion to a measurable extent. This single specificity of Treg cells selectively constrains Tconv cell reactive to the same pMHC-II antigen to prevent T cell infiltration of the prostate, but does not impact the concurrent Tconv cell response against multiple foreign pathogen-derived peptides. Our study reveals a two-tiered system of Treg cell-mediated control in which bystander mechanisms of suppression maintain tolerance at steady-state, while self-pMHC-specific Treg cells enforce self-nonself discrimination in settings of inflammation.

INTRODUCTION TO THESIS

The concept of autoimmunity – host pathology mediated by self-directed immune responses – briefly emerged at the dawn of the 20th century alongside the discovery of adaptive immunity, and was subsequently lost for nearly four decades by a preoccupation with foreign-directed immune responses to invading microorganisms termed "pathogens". Following Bordet's discovery of foreign-reactive antibodies in the blood [1], Ehrlich attempted but was unable to elicit such antibodies reactive to self-tissues in the host, leading him to the conclusion of "horror autotoxicus", or the notion that autoimmunity cannot happen [2]. The events to follow ought exist as a cautionary tale against such hubris-laden statements of dogma in the realm of scientific discovery. In their aftermath, Donath and Landsteiner described the existence of human subjects bearing antibodies that could lyse their own red blood cells [3], and Papazolu demonstrated that thyrotoxicotic patients bore sera that could fix complement to thyroid tissue [1]. However, barring a few limited observations following tissue damage vaccination [1], these seminal studies were largely overlooked or forgotten in the pursuit of foreign-directed immunity.

Autoimmunity re-emerged from obscurity in the 1940s as a kind of byproduct of the study and development of immune-inducing adjuvants, when Freund and others demonstrated the emergence of a paralytic disease was the direct result of immunization with brain tissue emulsified in adjuvant [4]. Even in the face of this evidence, the scientists were hesitant to refer to such a disease as "autoimmune", evidencing the pervasiveness of Ehrlich's assertion of impossibility within the immunology community forty years later. The term "autoimmune" was finally used to describe such a disease following the identification of anti-Rh autoantibodies in driving hemolytic anemia in 1951. Once the veil of impossibility had been lifted, a decade of studies linked previously observed pathologies across human tissues to autoreactivity [1]. The arrival of autoimmunity as a

mainstay culminated in 1957 with Burnet's formulation of the clonal selection theory of adaptive immunity, which carved out a provision for clones of self-reactivity [5].

Burnet introduced the first formal communion on Immunology in 1967 at Cold Spring Harbor, where the cellular basis for his theory on clonal selection had been confirmed with the description of adaptive T and B lymphocytes [6,7]. αβ T cells are a specialized subset of immune lymphocytes that play a critical role in vertebrate host defense against pathogens. A pathogen is an invasive uni- or multi-cellular organism defined as "nonself" by the host which infects the host to elicit disease or pathology, and include a biologically diverse group of bacteria, viruses, fungi, parasitic worms, and yeast. The basic biological role of a T cell is to recognize when a pathogen infection occurs and to orchestrate an immune response by both T and B lymphocytes which specifically targets and eliminates the pathogen without promoting destruction of host tissues – a concept commonly referred to as self-nonself discrimination.

The first formal mention of self-nonself discrimination arrived in 1959 on the coattails of Barnet's clonal selection theory and widespread acceptance of the existence of autoimmune lymphocytes. Lederberg first postulated a "rescue" model of self-nonself discrimination in which the default program for all antibody-producing cells was unresponsiveness (which he termed "paralysis"), and such cells could only be induced to respond if foreign antigen was available in this temporal window [8]. Bretscher and Cohn revised this theory in 1970 [9] to incorporate a "plastic" model, where antibody-producing cells could simultaneously maintain unresponsive or responsive potential depending on external factors. Importantly, this is the first postulation of the existence of a "Signal 2" which complements the "Signal 1" of antigen recognition and is required for immune responsiveness. They postulated that "Signal 2" was a carrier antibody bound to the antigen that caused a conformational change for subsequent binding. Interest in this theory was overshadowed

for more than a decade by excitement over discoveries of basic lymphocyte biology, including major histocompatibility complex (MHC) restriction of T cells and the molecular basis of lymphocyte receptor diversity and specificity by VDJ recombination [10]. In 1989, following the identification of dedicated antigen presenting cells (APCs) expressing MHC molecules that required accessory costimulatory molecules to elicit a productive T cell response [11-13], Janeway re-imagined "Signal 2" as the recognition of molecular patterns only found in "nonself" molecules (termed "PAMPs"), which enable the provision of costimulatory signals to T cells [14]. The definition of "nonself" was expanded in 1994 by Matzinger to include "dangerous self", which she proposed to include self-derived molecules associated with tissue inflammation or damage [15]. The discovery of the first PAMP receptor (TLR) in 1997 established a direct link between nonself-derived molecules and the provision of "Signal 2" in an immune response [16]. The discovery of subsequent TLRs and other pattern recognition receptors capable of recognizing self-derived molecules like DNA [17] provided support for Matzinger's postulate.

To enable host protection from nonself pathogens, the host periphery is populated with a diverse array of T cells expressing T cell antigen receptors (TCRs) that recognize protein-derived peptide antigens displayed by host MHC molecules. Each T cell generates a unique TCR during development in the thymus using a quasi-random gene rearrangement process of VDJ recombination and is subsequently selected for the peripheral T cell repertoire based on reactivity to self-derived peptides displayed on MHC (self-pMHCs). The result is an anticipatory repertoire of $CD4^+$ and $CD8^+$ T cells with the potential to recognize unknown pathogen-derived nonself peptides displayed by MHC class II (MHC-II) and MHC-I molecules, respectively. This approach to host defense, based on the formation of a repertoire capable of recognizing self-MHC, followed by the clonal selection of rare T cells during infection that recognize pathogen-derived antigens,

creates a challenging logistical problem: the immune system must establish self-nonself discrimination to maintain tolerance to a multitude of self-pMHCs displayed throughout the body.

The thymus is a key site at which two major forms of T cell tolerance are established. Here, developing T cell precursors undergo VDJ recombination to create a unique TCR and are subsequently selected by reactivity to self-pMHCs. In the process of negative selection, some thymocytes exhibiting overt reactivity to self-pMHC ligands are eliminated by clonal deletion, or diversion into innate-like T cell lineages. Other thymocytes that display reactivity to self-pMHC-II ligands differentiate into Foxp3-expressing regulatory T (Treg) cells, which are a subset of $CD4^+$ T cells with suppressive and host-protective functions in the periphery. The processes of negative selection and Treg differentiation are robust but incomplete, as evidenced by the appearance of mature self-reactive conventional T (Tconv) cells in the periphery that can elicit self-pMHC-directed responses to promote autoimmune disease and tissue pathology in various contexts.

One setting that is particularly ripe for the productive activation of self-reactive Tconv cells is during pathogen infection. Here, inflammatory stimuli such as PAMPs, DAMPs, and innate immune molecules are particularly abundant and enable the provision of "Signal 2" to T cells by triggering the upregulation of costimulatory molecules on APCs. In addition, tissue damage caused by the pathogen may promote the release-self antigens and increase the density of self-pMHC ligands, which will effectively increase TCR-dependent "Signal 1" in self-reactive T cells. Given the nature of T cell repertoire formation and self-selection, some Tconv clones that respond to pathogen-derived antigens may also cross-react with self-pMHCs – a phenomenon termed "molecular mimicry" – which has been proposed as an initiation event for autoimmune disease [18].

Paradoxically, the host T cell repertoire regularly enables pathogen clearance without developing autoimmunity following infection, indicating the existence of robust peripheral

tolerance mechanisms capable of selectively preventing self-directed T cell responses. Self-reactive Tconv cells are actively restricted in the periphery at steady-state via dominant immune suppression by Treg cells, as the depletion of Treg cells in mice results in rapid systemic autoimmunity [19]. In humans, mutations or polymorphisms in genes encoding IL-2, CD25, and CTLA-4 – three molecules critical for Treg development – are associated with various autoimmune diseases, suggesting that deficiencies of Treg cell differentiation or function may underlie disease susceptibility [20-26]. Additionally, polymorphisms in the MHC-II loci often associate with autoimmune diseases [27]. Most described mechanisms of Treg-mediated suppression function in a "bystander" fashion to indiscriminately dampen T cell activation signals, inversely analogous to the broad upregulation of costimulatory molecules during infection. Therefore, it remains unclear how Treg cells coordinate self-nonself discrimination during infection and how the breakdown of factors along this axis leads to autoimmune disease.

In this thesis, we review current knowledge of the processes coordinating Treg cell development, mechanisms of Treg-mediated suppression at homeostasis and during infection, and attempt to understand the mechanisms by which Treg cells enforce self-nonself discrimination by studying endogenous Treg and Tconv specificities. We also highlight key outstanding questions stemming from our work, which we expect to extend beyond autoimmunity to broaden our understanding of basic immune biology in settings of allergy, organ transplantation, and antitumor immunity.

Regulatory T cell development[†]

A major advance in the understanding of immune regulation came with the identification and characterization of a population of $CD4^+$ T cells, termed Treg cells, that function in a dominant fashion to prevent autoimmune reactions, including organ-specific autoimmunity, systemic autoimmunity, and colitis. Initial evidence of the existence of Treg cells came from early experiments demonstrating that the removal of the thymus in three-day-old mice induced organ-specific autoimmunity, but thymectomy of seven-day-old mice did not [28,29]. This established the existence of a thymus-dependent mechanism that is required for the prevention of autoimmunity and implied that this mechanism was first implemented within an early developmental window. Extensive research using T cell fractionation and reconstitution experiments in rodents demonstrated that regulatory activity could be conferred by phenotypic subsets of $CD4^+$ T cells expressing markers of prior antigen experience. A key advance in this area was the demonstration in mice that regulatory activity could be attributed to $CD4^+$ T cells expressing CD25, the IL-2 receptor α chain[30]. Consistent with this, it was shown that day three thymectomy leads to the transient loss of $CD25^+$ $CD4^+$ T cells in the periphery [31], providing a link between the autoimmunity induced by neonatal thymectomy and immune suppression conferred by $CD25^+$ $CD4^+$ T cells. Despite evidence of the existence of Treg cells, it remained unclear whether these cells represented a population of activated $CD4^+$ conventional T cells or a distinct, stable lineage of cells with specialized regulatory function. In 2003, collective evidence from three reports provided the formal demonstration that the transcription factor Foxp3 uniquely defines Treg cells

[†] Portions of this section are reproduced or adapted from Savage, P.A., Klawon, D.E.J., and Miller, C.H. (2020). Regulatory T cell development. Annual Reviews of Immunology. *38*, 421-453.

and is required for Treg cell differentiation [32-34]. Prior to these studies, interest in Foxp3 stemmed from genetic studies showing that human subjects with the X-linked autoimmune syndrome immunodysregulation polyendocrinopathy enteropathy X-linked (IPEX) harbored loss-of-function mutations in FOXP3 [35-37], coupled with genetic studies showing that scurfy mutant mice [38], which develop an X-linked autoimmune wasting syndrome that is similar to IPEX [39], harbor a loss-of-function frameshift mutation in Foxp3 [40]. The importance of Treg cells in the prevention of autoimmunity, the regulation of inflammation, and the suppression of antitumor immunity triggered a firestorm of interest in elucidating the fundamental biology of Treg cell development and function. Specifically, what are the signals that induce Treg cell differentiation, and what is the nature of ligands recognized by these cells?

Signals required for Regulatory T cell development

A major question lies in understanding the molecular signals that are required for Treg cell development in the thymus. Given the importance of Treg cells in various aspects of health and disease, it is conceivable that dysregulation of these molecular pathways could lead to inefficient or aberrant Treg cell differentiation, thereby predisposing individuals to autoimmune disease or inflammatory disorders. Signals driving Treg lineage specification may also remain operative and critical for function in the periphery. It is clear that Treg cell development requires at least three major signals: TCR-dependent recognition of pMHC-II ligand, CD28-dependent signaling triggered by the costimulatory ligands CD80 or CD86, and cytokine signaling triggered by sensing of IL-2, IL-15, and/or IL-7.

TCR sequencing studies revealed that the TCR repertoire expressed by peripheral Treg cells is largely distinct from that of conventional $CD4^+$ T cells, with some degree of overlap [41-43].

This suggested that Treg cell differentiation is a TCR-directed process in which the recognition of distinct pMHC-II ligands either directs de novo Treg cell differentiation of distinct T cell clones or promotes the survival or retention of select Treg cell specificities after an initial stochastic Treg cell differentiation process. A formal demonstration that the TCR directs cells into the Treg lineage in the thymus came from two seminal studies [44,45] which observed that the expression of Treg cell–derived TCRs promoted Treg cell differentiation in the thymus, while the expression of TCRs derived from $CD4^+$ conventional T cells did not. As with most biological processes, this phenomenon was not black-and-white; the efficiency of skewing to the Treg cell lineage varied from TCR to TCR. These studies also revealed that for Treg-biased clones, the efficient induction of Treg cell selection required the introduction of monoclonal precursors at low clonal frequencies, revealing the existence of a limited saturable resource, or niche, that supports the development of each Treg cell clone. The finding that the niche size – defined as the maximum number of $Foxp3^+$ cells of a given specificity that can populate the thymus at any given time – varied for different Treg cell clones suggested that competition for access to a limited pool of pMHC-II ligands was the likely driver of this effect. Peripheral Treg cell differentiation in lymphoreplete or lymphopenic hosts was negligible, suggesting that the thymus is uniquely permissive for Treg cell differentiation for the clones analyzed.

Direct information regarding the ligand-binding properties of these and other endogenous Treg-derived TCRs, such as affinity and half-life, remains limited. To date, most studies into the role of biochemical TCR properties in Treg selection have relied on the use of surrogate markers of TCR/pMHC-II affinity. For example, Nur77-GFP reporter serves as a useful measure of TCR signal strength in some instances, as the intensity of GFP signal increases following *in vitro* T cell stimulation with peptide ligands of increasing potency [46]. However, in vivo studies demonstrate

that the intensity of Nur77-GFP fluorescence wanes over time following cessation of TCR signaling [47]. Thus, for Treg cells exhibiting intermediate Nur77-GFP fluorescence intensities, it is not possible to distinguish whether these are Treg cells expressing intermediate-affinity TCRs that are actively engaging ligand, or Treg cells expressing high-affinity TCRs that have not been recently triggered by pMHC-II ligand. Thus, data using surrogate markers of TCR signal strength should be interpreted with caution. Studies using biochemical measurements of the pMHC-II binding properties of Treg TCRs reactive to natural endogenous ligands are necessary to support such conclusions. As a case-in-point, one report on biochemical properties of Treg-derived TCRs [48] demonstrated that TCR half-life for pMHC-II rather than affinity was a predictor of tTreg selection.

A second class of signals required for Treg cell development involves signaling through the T cell–expressed CD28 costimulatory receptor, which is triggered by recognition of CD80/86 ligands expressed by APCs. This principle was first revealed in studies using *Cd28*$^{-/-}$ and *Cd80/86*$^{-/-}$ mutant mice [49]. Given the importance of the CD28 pathway in providing costimulation for T cell activation, it was expected that *Cd28*$^{-/-}$ or *Cd80/86*$^{-/-}$ mutant mice on the diabetes-susceptible NOD (nonobese diabetic) background would be resistant to diabetes. In stark contrast, it was found that diabetes was exacerbated in such mice. Analysis of mutant mice revealed a paucity of CD4^{+} CD25^{+} Treg cells in the thymus and periphery. Moreover, treatment of wild-type NOD mice with recombinant CTLA-4-Ig fusion protein, which blocks CD80/86 ligands in vivo, induced a substantial loss of CD4^{+} CD25^{+} cells and accelerated diabetes development. Thus, these early studies demonstrated that the triggering of CD28 signaling by CD80 and/or CD86 ligands is crucial for optimal Treg cell development. Subsequent work has further illuminated the mechanisms by which CD28 signaling impacts Treg cell biology. One study [50] used mixed

chimeric mice to demonstrate that the requirement for CD28 signaling in Treg cell differentiation is cell intrinsic. Another study [51] showed that the Treg TCR repertoire is largely unaltered in CD28-deficient mice, suggesting that CD28 does not impact the range of specificities undergoing Treg cell differentiation. Thus, CD28 signaling likely does not function by altering TCR signaling thresholds but instead functions to ensure optimal proliferation or survival of Treg-destined thymocytes that have received appropriate TCR-dependent signals.

A third class of signals required for optimal Treg cell development and fitness includes the sensing of IL-2 or the related common γ-chain cytokines IL-15 and IL-7. Early evidence for this came from observations that $CD4^+$ $CD25^+$ T cells were largely absent in IL-2-deficient mice as well as mice lacking the IL-2Rα or IL-2Rβ chains [52-54]. These findings were refined in following the discovery of Foxp3 in studies which defined general principles about the role of IL-2. First, IL-2 plays a major role in supporting Treg cell development and maintenance, as injection of neutralizing anti-IL-2 antibodies induced a rapid reduction of Treg cell numbers in the thymus and periphery and the development of organ-specific autoimmunity in various mouse strains [55,56]. Second, IL-2 contributes to optimal Treg cell fitness in the periphery but is not absolutely required for Treg cell differentiation due to compensatory contributions from IL-15 and IL-7 [57-60]. This principle was revealed through studies using compound mutant mice that demonstrated that IL-15 and IL-7 signaling can partially compensate for the lack of IL-2 sensing, and that Treg cell development is fully abolished in mice that cannot perceive any signals triggered by IL-2, IL-7, and IL-15 [57,59,61,62]. Third, models which engineered Treg-specific deletion or constitutive activation of STAT5 – a signal transducer downstream of common γ-chain – revealed a key role for this molecule in driving Treg cell differentiation or expansion, [57,63,64].

Given that CD28 signaling is known to promote IL-2 production in activated conventional

T cells, it is important to consider whether the requirements for CD28 signaling and IL-2 signaling are interrelated. In this regard, multiple lines of evidence suggest that the effects of CD28 signaling in Treg cell development are distinct from those of IL-2 signaling. It was reported that the frequency of $CD25^{+}$ $Foxp3^{neg}$ Treg cell precursors is diminished approximately twofold in *Cd28*$^{-/-}$ mice [51,65], suggesting that CD28 may function in an early phase of Treg cell development that precedes IL-2 signaling. In addition, the fact that overexpression of constitutively active STAT5 leads to major shifts in the Treg cell TCR repertoire [63], whereas CD28 deficiency does not [51], suggests that the two signaling pathways function in different ways. Consistent with this, a study [66] used intrathymic cell transfers of TCR transgenic thymocytes to demonstrate that early $CD25^{neg}$ $Foxp3^{neg}$ $GITR^{+}$ Treg cell precursors required CD80/86 signals to proceed through Treg cell differentiation but later $CD25^{+}$ $Foxp3^{neg}$ precursors did not. Thus, cumulative evidence suggests that CD28 likely functions in the early TCR-instructive phase of Treg cell development – independent of clonal Treg selection [51] – but is dispensable for a subsequent cytokine-dependent phase.

Beyond TCR-, CD28-, and IL-2/IL-15/IL-7 signaling, additional pathways have been shown to promote the survival of developing Treg cell clones by conferring resistance to clonal deletion, including TGF-β receptor signaling [67] and engagement of CD70 ligand by the T cell-expressed CD27 receptor [68]. These findings suggest that the strong agonist TCR signals that direct Treg cell differentiation must be counterbalanced by mechanisms to protect developing Treg cells from apoptosis. Lastly, other work has demonstrated that signaling through TNFRSF members GITR, OX40, or TNFR2 augments cytokine responsiveness and facilitates Treg cell differentiation [69].

Developmental signals in space and time

Whereas the molecular requirements of Treg cell differentiation are now well defined, questions remain about which cell subsets act as signal donors. As discussed below, pMHC-II ligands are derived from and displayed by a diverse network of APC types which appear to collaborate to establish a diverse Treg repertoire. CD80/86 costimulatory signals are required on bone marrow-derived cells but not radioresistant thymic epithelial cells for the optimal Treg cellularity [70], but, little more is known about the cellular context in which CD80/86 signals are conferred. Moreover, it is unclear whether costimulatory ligands must be displayed by the same APC presenting pMHC-II ligand, or whether pMHC-II and CD80/86 signals can be conferred by different cells. Regarding IL-2, an early study observed halos of IL-2 expression around cells with T cell morphology [71], suggesting that IL-2 production is localized to regional clusters of cells. A more recent study [72] used an *Il2*-floxed allele on an *Il15*$^{-/-}$ background to define the cellular sources of IL-2 supporting thymus-derived Treg (tTreg) cell development, and found that IL-2 production by T cells but not B cells or DCs was uniquely required to support Treg cell differentiation. Expanding this notion, a related study [73] demonstrated that the major producers of IL-2 in the thymus represent CD4 SP thymocytes that display hallmarks of self-reactivity, and that at least some of these IL-2-producing cells are Treg cell precursors. It should be noted that DC-derived IL-2 has been shown to promote Treg cell differentiation of OT-II T cells in *in vitro*–cultured thymic slices [74], but the prevailing available evidence suggests that tTreg cell development *in vivo* is dependent on IL-2 produced solely by T cells within the thymus.

Beyond identifying the cell populations providing signals for Treg development, it is also necessary to consider how, when, and where these multiple signals are integrated by a developing Treg cell precursors. A common paradigm from early work suggests that Treg cell differentiation

is a two-step process in which TCR- and CD28-dependent signals trigger differentiation to a $CD25^{+}$ $Foxp3^{neg}$ intermediate, which subsequently proceeds to a mature $CD25^{+}$ $Foxp3^{+}$ Treg cell following sensing of IL-2 or related cytokines [75]. However, two recent studies have suggested the existence of a parallel pathway in which mature Treg cells develop via a $CD25^{neg}$ $Foxp3^{LO}$ intermediate [76,77]. A follow-up scRNAseq study [78] found clonotype sharing between the $CD25^{+}$ $Foxp3^{neg}$ and $CD25^{neg}$ $Foxp3^{LO}$ precursor populations, suggesting that these developmental pathways are likely inter-related rather than distinct. Temporal *in vivo* experiments tracking individual clones over time will shed light on how exactly these pathways converge, and whether distinct signals are provided at distinct stages for progression.

Anatomical location defines the nature of APCs, pMHC ligands, and accessory signals that are encountered by a developing thymocyte, so considering the path of a Treg precursor through the thymus is important to elucidate how these signals are provided. T cell precursors generally follow an orchestrated path through the thymus, first entering the cortex where early T cell development and positive selection occur, then egressing to the medulla where later phases of maturation and T cell commitment to distinct lineages occur. MHC-II expression exclusively in the cortex enables near-normal numbers of Treg cells to develop [79-81], but little is known about the TCR diversity, antigen specificity, and functional capacity of these Treg cells. In contrast, multiple lines of evidence suggest that the thymic medulla is critical for the differentiation of many Treg cells. Almost all Foxp3-expressing thymocytes exist in the medulla or at the cortico-medullary junction [59,80,82-84]. Furthermore, as discussed in a later section, it is known that some Treg cell specificities rely on medullary thymic epithelial cells (mTECs) expressing both Aire and MHC-II for development [85-89]. Relatedly, genetic deficiencies that disrupt the proper formation of the thymic medulla lead to broad alterations in Treg cell development [90].

The disparity in findings regarding the roles of the cortex and medulla may reflect heterogeneity in Treg cell developmental pathways, coupled with differences in the nature of self-ligands triggering Treg cell selection. Thus, it is likely that antigen presentation in both the cortex and medulla contribute to the formation of a replete Treg cell repertoire of appropriate diversity. The exact order and location of Treg differentiation signals remain outstanding due to current limitations in experimental tools. The upregulation of Foxp3 is likely temporally and spatially separated from the initial events that trigger Treg cell differentiation [75-77], but current tools cannot pinpoint the initial TCR-dependent signal that triggers Treg cell selection. Finally, historical studies of developing polyclonal Treg cells likely represent a composite of asynchronous developmental trajectories, making it difficult to decouple temporal signaling events.

Regulatory T cell antigen specificity and presentation

TCR-dependent ligand recognition is one of the key signals required for Treg cell differentiation in the thymus. Initial phenotypic studies of polyclonal Treg cells observed that many Treg cells are proliferative at steady state [41] and express high densities of the Nur77-GFP reporter, a surrogate readout of TCR signal strength [46], which led to the hypothesis that thymus-derived Treg cells exhibit specificity for endogenous self- ligands. This paradigm was further established by a substantial body of indirect evidence [91], such as experiments showing that TCR-transduced cells expressing Treg-biased TCRs undergo proliferation in lymphopenic hosts [41]. Still, it remained possible that some Treg cells recognize commensal or environmental antigens, rather than self-ligands. Therefore, a comprehensive understanding of Treg cell specificity requires identification and characterization of endogenous Treg cell ligands.

Early studies examining the antigenic signals that drive Treg cell development utilized TCR transgenic T cells and engineered systems in which model antigens were ectopically expressed in mice to conclude that the recognition of strong agonist ligands in the thymus promoted Treg cell differentiation [92-100]. In all of these model systems, expression of these engineered antigens concurrently induced clonal deletion of a major fraction of TCR transgenic cells, with only a minor fraction of surviving cells exhibiting a $CD25^+$ $Foxp3^+$ phenotype. This led to the notion that recognition of MHC-II-restricted agonist ligands in the thymus induces both clonal deletion and Treg cell development. However, this "dual fate" effect differs from many TCR transgenic mice expressing endogenous Treg-derived TCRs reactive to natural ligands, for which clonal deletion is negligible [44,45,101-103]. Thus, it is important to consider whether these model antigens accurately mimic the natural biology of endogenous Treg cell ligands with respect to expression patterns, processing and presentation efficiency, APC types, and TCR-pMHC-II binding properties. In this regard, any given Aire-dependent transcript is expressed by only a small percentage of mTECs [104,105], but the expression of model antigens driven by Aire regulatory elements drives antigen expression on a large fraction of mTECs [98,106], which may be supraphysiological. Moving forward, it will be important to validate findings in model antigen systems by studying Treg cell clones reactive to endogenous ligands to gain a comprehensive understanding of the factors driving Treg cell differentiation vs. clonal deletion [107,108].

Regarding the nature of endogenous self-pMHC-II ligands that are displayed to developing thymocytes, analysis of eluted peptides by mass spectrometry revealed that the majority are derived from widely expressed "ubiquitous" antigens [109-111], including nuclear, cytosolic, secretory, and transmembrane proteins. The cellular sources of these peptides are incompletely defined, but they likely reflect a mixture of endogenous antigens expressed by thymic APCs

themselves, coupled with exogenous antigens taken up from the blood or interstitial fluid of the thymus. In this regard, intracellular proteins can be processed and presented on MHC-II in the thymus via the autophagy pathway [112,113], and when this pathway is disrupted, T cell selection and self-tolerance are perturbed [114]. Additionally, injection of antigenic protein in the blood can induce antigen uptake by thymic DCs and subsequent Treg cell selection [115,116], suggesting that the blood could serve as a source of self-ligands presented in the thymus. These studies suggest that the most prevalent self-peptides displayed by APCs in the thymus are derived from abundant proteins that are widely expressed throughout the body. In support of this notion, a recent report provided an expansive view of the antigen specificities of naturally occurring Treg cell clones by identifying 17 self-peptides that were derived from widely expressed self-proteins involved in diverse biological processes [48]. By generating a large panel of immortalized cell lines expressing TCRs expressed by Treg cells from neonatal mice, they showed that 20–35% of these TCRs conferred overt reactivity to splenic DCs. Interestingly, the number of reactive clones was further increased using splenic DCs that had been activated by innate signals, suggesting that some Treg cells are reactive to "cryptic" self-ligands that are differentially displayed by activated DCs.

Low-density ligands also play a significant role in central tolerance, often via a mechanism of promiscuous gene expression (PGE). Early evidence of this phenomenon came from studies of transgenic mice that revealed unexpected transgene expression in the thymus driven by the insulin promoter and other promoters thought to be tissue-restricted [117]. Extensive research has since demonstrated that PGE is not simply an artifact of transgenesis but instead represents a highly orchestrated process that is critical for the establishment of immune tolerance. Aire-mediated PGE is extensively discussed below.

To understand the nature of endogenous ligands that drive Treg selection and clonal deletion, both the relevant APCs and signal context must be considered. The thymus is populated by numerous MHC-II-expressing cell types, including Sirpα$^+$ and CD8α$^+$ conventional DCs (cDCs), plasmacytoid DCs (pDCs), B cells, fibroblasts, macrophages, and both cortical TECs (cTECs) and mTECs [85,118]. Coculture experiments demonstrated that many of these APCs can induce Treg cell differentiation *in vitro* [70,118,119]. This functional redundancy is unlikely to operate *in vivo* given the unique temporal and environmental factors encountered by developing thymocytes during maturation. Of the MHC-II-expressing cell types in the thymus, what is known about their contribution to the selection of a replete Treg cell repertoire? It was shown that the inducible ablation of a large fraction of mTECs resulted in an ~50% reduction in Treg cell numbers [86,88], highlighting the critical role for mTECs in either antigen production or presentation. Analysis of chimeric mice lacking MHC-II expression by bone marrow–derived APCs revealed a significant reduction in polyclonal Treg cell numbers [120], and the loss of numerous Treg-biased specificities [89], indicating a key role for MHC-II expression by bone marrow–derived APCs. Notably, one study demonstrated that the development of several Treg cell clones was abolished in mice lacking CD11c$^+$ DCs [89]. Among the thymic DC subsets, analysis of the roles of distinct subsets has been stymied by the lack of robust approaches to specifically deplete distinct populations or conditionally delete MHC-II. An early report suggested that pDCs can migrate to the thymus from the periphery and impact Treg cell selection [121], but this idea has yet to be substantiated. It was reported that the thymus harbors a subset of Aire expressing B cells that contribute to self-antigen presentation in the thymus. A role for these cells in Treg cell selection has yet to be determined [122], but functional experiments indicate that the prevention of autoimmunity does not require Aire expression by bone marrow–derived cells [123,124]. A recent study found that mice develop hallmarks

of autoimmunity in peripheral organs when a subset of thymic fibroblasts lacks expression of the lymphotoxin β receptor [125]. Such mice exhibited a reduction in Aire-expressing mTEC cells and alterations in the CD8 SP repertoire, but whether these fibroblasts have a direct or indirect effect on Treg development remains unknown. The role of distinct thymic cDC subsets are discussed below in the context of Aire-dependent Treg specificities.

In regard to the APCs that coordinate Treg cell development, it is important to consider the process of antigen transfer between different cell types, as this occurs readily in the thymus and can complicate data interpretation. For example, it has been demonstrated that cytosolic or transmembrane proteins can be transferred from radioresistant cells to bone marrow–derived APCs [89,126-128], but multiple mechanisms of antigen exchange in the thymus have been described and could be operative simultaneously. Thymic APCs may process and cross-present peptides from blood-borne proteins or from proteins acquired from apoptotic bodies of mTECs. Alternatively, intact pMHC-II may be directly acquired from mTEC membranes and presented to developing thymocytes in trans by other APC subsets, such as the observation that mTEC-derived pMHC-II and other cell-surface proteins can be acquired and presented by thymic DCs via the scavenging receptor CD36 [128]. Although nuanced, antigen transfer can have far-reaching implications when determining which APC subsets are providing which signals to developing Treg cells, and where and when these interactions occur.

Regulatory T cell selection on Aire-dependent self-antigens

The search for endogenous Treg cell ligands has been complicated by the immense diversity of the self-proteome, coupled with technical limitations in identifying rare self-peptides displayed by MHC-II molecules at low density. Inspired by observations of transgenic mice, the

finding that transcripts encoding numerous TRAs are expressed by mTECs within the thymus [129] inspired studies that led to the identification and characterization of Aire, which drives PGE of many TRAs. Much of what is known about Treg antigen specificity, clonal development, and antigen presentation has relied on the study of Aire-dependent clones and tissue-restricted antigens (TRAs), given the relatively limited pool of antigens, defined antigen source, and identifiable clones. Here, we recount the discovery of Aire, identify known Aire-dependent specificities, discuss the role for APCs in coordinating Treg development, and high the relevance of such Treg cells for autoimmune protection.

A role for Aire in immune tolerance was implied by genetic studies in humans, which demonstrated that human subjects with loss-of-function mutations in AIRE develop autoimmune polyglandular syndrome 1 (APS-1), an autoimmune disease characterized by mucocutaneous candidiasis, autoimmune destruction of the parathyroid and adrenal glands, and hypogonadism [130,131]. A seminal study demonstrated that Aire-deficient mice developed organ-specific autoimmunity due to defects in radioresistant stromal cells and revealed that Aire functions in part by driving the PGE of hundreds of genes, many of which encode peripheral TRAs [124]. Mechanistically, Aire and its associated factors are thought to act on stalled polymerases at chromatin-accessible regions to promote transcription [132]. Interestingly, a given TRA transcript is only expressed by a small percentage of all mTECs at a given time [104,105], which may be an important consideration for spatial and temporal TCR-dependent signals required for Treg development. Nevertheless, the collective population of mTECs can direct the PGE of thousands of transcripts, encompassing a large fraction of the peripheral transcriptome [133]. The fact that a given gene is only transcribed by a small percentage of mTECs at any given time implies that the

ligand density of Aire-dependent peptides is likely to be very low, a concept that may explain the limited antigenic niches supporting the differentiation of many Treg cell clones.

At the time of Aire discovery, PGE of self-peptides in the thymus was largely thought to promote tolerance by driving clonal deletion of developing thymocytes exhibiting reactivity to these self-peptides. However, a series of later studies demonstrated that Aire is required for thymic differentiation of select Treg cell specificities [87,89,102,134], which are estimated to comprise ~25% of the thymic Treg cell repertoire and ~5% of the peripheral Treg cell repertoire in different studies. TCR profiling of recurrent Tconv cell clones infiltrating the prostates of Aire-deficient male mice revealed that dominant Tconv clones did not represent specificities that evaded clonal deletion in the absence of Aire. Instead, these infiltrating cells represented clones that are normally skewed to the Treg cell lineage in wild-type mice but are misdirected into the Foxp3^{neg} Tconv compartment in settings of Aire deficiency [87]. Related to this finding, functional studies of Aire-deficient disease showed that Aire expression is only required in the first few weeks of life to prevent autoimmune disease [135], and that Aire-dependent Treg cells generated early in life were required for the prevention of organ-specific autoimmunity and that early transfer of Treg cells alone was sufficient to prevent development of autoimmune pathology in Aire-deficient recipients [136]. The Scurfy-like disease observed in Foxp3null mice can be reversed by Treg cells that arise in the first two weeks of life [137], corroborating a unique role for the neonatal-derived Treg cell program or antigen specificities. Collectively, these studies demonstrated a major role for Aire in driving the generation of a substantial fraction of Treg cells, which are uniquely required for prevention of organ-specific autoimmunity. Notably, early studies demonstrated that the frequency and absolute numbers of Treg cells were not significantly diminished in the periphery of Aire-

deficient mice [123], highlighting a role for Treg repertoire diversity and antigen specificity in disease protection.

Focusing on Aire-dependent Treg cell specificities reactive to prostate-associated antigens, foundational work for this thesis [138] identified two endogenous self-peptides recognized by recurrent Treg cell clones. Notably, the two peptides were derived from a single prostatic protein, Tcaf3, which was previously identified as a major autoantigen targeted by antibodies under settings of immune dysregulation [139]. This finding, although limited in scope, suggests that organ-specific Treg cells may be focused on a limited number of antigenic determinants in a given regional site. A subsequent study [103] used pMHC-II tetramers to demonstrate that approximately 30% of endogenous $CD4^+$ T cells reactive to peptides derived from the myelin-associated proteolipid protein are skewed to the $Foxp3^+$ Treg cell lineage. Additional studies reported that peptides derived from the myelin oligodendrocyte glycoprotein and insulin B proteins are recognized by Treg cells in autoimmune models of experimental autoimmune encephalomyelitis and diabetes, respectively [140,141]. However, since these peptides represent key targets of Tconv cells driving autoimmune pathology in these contexts, it is unclear whether these represent specificities that are naturally skewed to the Treg cell lineage in an Aire-dependent fashion.

Given the high expression of Aire in mTECs, these cells were the first obvious orchestrators of Aire-dependent tolerance, as initially demonstrated in thymic grafting and bone marrow chimera experiments [123,124]. Immature mTECs undergo a maturational progression associated with upregulation of Aire, MHC-II, and CD80/CD86 [142]. mTECs also produce key chemokines that coordinate the accumulation and positioning of other APC types within the medulla. For example, the production of mTEC-derived XCL1 and CCL 19/21 is critical for the proper recruitment and positioning of $XCR1^+$ DCs [143] and $CD8\alpha^+$ cDCs [144], respectively. Thus,

mTECs represent a key source of multiple factors that are required for Treg cell development, including antigenic peptide, MHC-II, accessory signals, and chemokines. Considering the communication between mTECs and DCs, it is important to consider which and how each of these APC subsets are providing signals for Treg development.

Since antigen expression is restricted to mTECs but accessory signals are thought to derive from DCs, considerations of antigen transfer are especially poignant. To determine whether whole antigen or pMHC-II molecules are transferred from mTECs to DCs, initial work utilized mice in which components of the MHC-II presentation pathway were selectively silenced in mTECs [85]. Studies using these mice revealed that a minor fraction of Treg cell specificities were lost or significantly reduced in frequency [89], suggesting that direct antigen presentation by mTECs is crucial for the development of some Treg cell specificities. In contrast, studies using model antigens expressed under the dictates of the Aire promoter suggested that clonal deletion, not Treg cell differentiation, is the most common outcome of direct MHC-II-restricted peptide presentation by mTECs [85,145], complicating interpretation. Questions of antigen vs pMHC-II transfer are difficult to elucidate using alterations to the mTEC-intrinsic MHC-II apparatus.

More recent studies have characterized the developmental requirements coordinating the thymic differentiation of individual Aire-dependent Treg cell–biased clones. One study [89] demonstrated that some Aire-dependent Treg cell clones failed to develop in *Batf3*$^{-/-}$ hosts, which exhibit a major reduction in Batf3-lineage CD8α^{+} cDCs [146]. In complete opposition, a separate study [70] showed that the differentiation of two Aire-dependent Treg cell clones was not impacted by Batf3 deficiency and that the polyclonal thymic Treg cell repertoire was largely unaltered in *Batf3*$^{-/-}$ mice. Interestingly, the selection of one Aire-dependent Treg cell clone required MHC-II expression by DCs, implying that the selection process was dependent on both mTEC-derived

antigen and DC-expressed MHC-II. Relatedly, a third study suggested that transfer of intact pMHC-II antigens from mTECs occurs via the scavenger receptor CD36 [128], but this transfer was limited to CD8α$^+$ cDCs. Taken together, it is likely that mTEC-derived antigen is transferred to cDCs to coordinate the development of Aire-dependent specificities, though the exact mechanism remains to be elucidated. Batf3-lineage CD8α$^+$ cDCs may contribute to the selection of some Treg cell clones, but the selection of Aire-dependent Treg cells as a whole does not appear to be a major non-redundant function of CD8α$^+$ cDCs.

In addition to CD8α$^+$ cDCs, Sirpα$^+$ cDCs are the second major class of cDCs found in the thymus. These cells are commonly referred to as migratory DCs, as they have been proposed to originate from the periphery. This is consequential when considering potential Treg-inducing antigens given the novelty of extrathymic ligands for developing thymocytes. However, these conclusions are largely based on parabiotic studies or infusion of supraphysiologic numbers of cells into the bloodstream [147], the former of which can be explained by the arrival of DC precursors from one host to the thymus of the other. Thus, the precise origin of these cells remains an outstanding question due to the lack of experimental approaches to specifically fate-map such cells. For the same reason, the role of Sirpα$^+$ cDCs in promoting Treg cell development *in vivo* also remains largely undefined. A recent study [148] demonstrated that ~50% of Sirpα$^+$ cDCs in the thymus express CD301b and created a model to remove CD103b$^+$ cells, but a role for Treg induction was not tested for this subset of cDC2. Likewise, a novel model that abrogates cDC2 development by deleting enhancer elements in the *Zeb2* enhancer was recently published [149], but the role for Treg development was not tested, nor can this model inducibly remove such cells after the establishment of a replete T cell repertoire. Nonetheless, additional circumstantial evidence is consistent with the possibility that Sirpα$^+$ cDCs may play a prominent role in Treg cell

differentiation. For example, Sirpα^{+} cDCs represent the thymic counterpart of peripheral Batf3-independent CD11b^{+} cDCs, which are thought to be more efficient than Batf3-lineage CD8α^{+} cDCs at presenting MHC-II-restricted antigens [150]. Additionally, two studies report that the loss of CD8α^{+} cDCs in *Batf3*$^{-/-}$ mice is associated with an expansion of both Sirpα^{+} cDCs and absolute Treg cell numbers – but not clonal diversity – within the thymus [70,144], suggesting a potential direct relationship between these populations.

Thus, current evidence suggests that mTECs and DCs collaborate to generate a replete thymus-derived Treg cell repertoire of appropriate diversity, comprising a mixture of Aire-independent and Aire-dependent specificities. Thus far, a major requirement for a distinct bone marrow–derived APC subset has yet to be defined, suggestive of broad functional redundancy. Moving forward, addressing this question with higher resolution will require the development of new approaches to constitutively or conditionally deplete distinct APC subsets in the thymus, paired with new ways to conditionally delete MHC-II or costimulatory ligands on different APC populations. In addition, improved approaches are needed to define the positioning, motility, origin, and half-life of key APC populations within the thymus, as well as the mechanisms by which antigenic proteins and pMHC-II complexes are transferred from one cell to another.

Extrathymic selection of regulatory T cells

Beyond Treg cell specification in the thymus, it is clear that peripherally induced Treg (pTreg) cells can also differentiate from Tconv cells at extrathymic sites. This phenomenon was first evident in studies in which CD4^{+} CD25^{HI} cells could readily be recovered from lymphopenic mice that received purified CD4^{+} CD25^{neg} donor T cells by intravenous transfer [30,151], a phenomenon that was later confirmed by numerous studies following the identification of Foxp3.

A clear understanding of Treg cell biology requires determining whether dedicated mechanisms exist to coordinate pTreg cell differentiation, and whether pTreg cells serve unique functions in immune regulation that are distinct from those conferred by tTreg cells.

Consensus has coalesced around the idea that pTreg cells reactive to environmental antigens, including those derived from commensal microbiota, dietary constituents, and fetal antigens, can play an important role in maintaining immune tolerance and homeostasis at sites of the body that interface with the external environment. An important consideration regarding pTreg development is the anatomical site of selection. The site of origin for pTreg cells is likely to reflect the nature of antigenic peptides recognized by such cells, given that pTreg cell antigens are likely distinct from those available during thymic development, and the accessory signals that are available at that site. Additionally, pTreg cell differentiation may divert $CD4^+$ T cells away from alternate T helper states and alter the local immune environment. For example, mounting evidence suggests that pTreg cell differentiation in the gut is interrelated and antagonistic with the differentiation of pathogenic Th17 cells [152,153].

Building on early work examining the induction of polyclonal pTreg cells in lymphopenic mice, it was shown that $CD4^+$ TCR transgenic T cells reactive to exogenous peptides could be induced to undergo pTreg cell differentiation in wild-type mice using various approaches involving the provision of antigen in the absence of innate signals or inflammation ("signal 2") [154-157]. However, it remained unclear whether pTreg cell differentiation is a common process that makes substantial contributions to the mature Treg cell pool at steady state and in contexts of inflammation, infection, and cancer. To address this question, there has been considerable interest in identifying markers that can be used to reliably distinguish Treg cells of thymic and extrathymic origin. Initial reports suggested that the transcription factor Helios [158] and cell surface receptor

Neuropilin-1 [159,160] are uniquely expressed by tTreg cells, but subsequent reports demonstrated that these are not faithful markers [161-165]. This has restricted progress in understanding the origin of Treg cells in different contexts and necessitated reductionist studies in which the developmental potential of distinct Treg cell specificities can be assessed at the clonal level [44,102]. Given the lack of faithful markers of tTreg and pTreg cells, an insightful report [163] was noteworthy in that it provided the first quantitative assessment of the relative frequencies of pTreg cells and tTreg cells in the peripheral Treg cell pool of healthy mice. To do this, the investigators leveraged the serendipitous finding that two distinct Foxp3 reporter mice exhibited differential patterns of expression on tTreg cells and pTreg cells. Specifically, it was found that a Foxp3 reporter inserted in the endogenous Foxp3 locus was faithfully expressed by both tTreg cells and pTreg cells, whereas a second Foxp3 reporter driven from a BAC transgene was exclusively expressed by tTreg cells. Analysis of mice expressing both reporters revealed that pTreg cells comprised 15–25% of peripheral Treg cells in the spleen and lymph nodes of two-month-old mice, and that this fraction increased to an average of 35% in aged mice. Notably, the pTreg cells defined using the double-reporter system exhibited variable expression of both Helios and Neuropilin-1.

Despite substantial evidence that pTreg cells are prevalent in the peripheral repertoire, it remained unclear whether pTreg cells serve unique functions that cannot be conferred by tTreg cells. The understanding of pTreg cell function was significantly advanced by the identification of a conserved noncoding TGF-β/Smad response element in the *Foxp3* locus, named conserved noncoding sequence 1 (CNS1), that is required for optimal pTreg cell differentiation [166-168]. Using gene-targeted *Foxp3*$^{\Delta CNS1}$ mice lacking this element, a series of studies demonstrated that polyclonal and antigen-specific T cells from CNS1-mutant mice exhibit deficiencies in pTreg cell induction, develop aberrant type 2 immune responses in the lung and gastrointestinal tract, and

have increased absorption of allogeneic embryos during pregnancy [166,168,169]. A parallel study [167] showed that mice harboring a different targeted CNS1-mutant allele exhibited milder phenotypes than *Foxp3*$^{\Delta CNS1}$ mice, including the lack of unprovoked inflammation at mucosal sites and unaltered susceptibility to experimental colitis. The reasons for the observed differences in the two CNS1-mutant mice are unknown, but they could be due to variations in microbiota or the genomic elements that were targeted for deletion. Nonetheless, studies using CNS1-deficient mice provided key evidence that pTreg cells serve critical nonredundant modulatory functions at anatomical sites that interface with the external environment. CNS1-mutant mice do not exhibit widespread organ-specific autoimmunity or immune activation throughout the body, indicating that tTreg cells are sufficient to maintain most aspects of tolerance and immune homeostasis.

Much of what is known about pTreg cell differentiation and function stems from the study of pTreg cells in tissues associated with the gastrointestinal tract. Definitive demonstration that naturally occurring pTreg cells populate the endogenous repertoire and exhibit specificity for microbial peptides came from a landmark study [170] which demonstrated that the TCR repertoire of colonic Treg cells is distinct from that of Treg cells at other lymphoid sites, suggestive of reactivity to a unique set of antigens within the colon. Clonal analysis revealed that multiple colonic Treg cell TCRs conferred reactivity to unidentified peptide antigens derived from commensal bacteria, and that such TCRs facilitated microbiota-dependent pTreg cell differentiation, with no evidence of tTreg cell differentiation, which provided direct evidence that some colonic Treg cells exhibit reactivity to foreign peptides and undergo extrathymic differentiation. Subsequent work has expanded the understanding of commensal microbiota that can promote pTreg cell induction, as well as the mechanisms regulating pTreg cell differentiation [152,153,171-173]. Outside the microbiota, a recent report found that some endogenous Tconv cells reactive to dietary antigens underwent

pTreg differentiation upon feeding in the absence of inflammation [174], but could also adopt other responsive and non-responsive T cell lineages. Building from these findings, a consensus has emerged suggesting that Treg cells in the gastrointestinal tract represent a composite of RORγt-expressing pTreg cells reactive to microbe-derived peptides, together with pTreg cells reactive to dietary antigens and self-specific tTreg cells reactive to self-ligands [175-177].

The APC populations that coordinate pTreg development have remained almost entirely unidentified until recently. It was largely assumed that these APCs were going to be cDCs, at least in part, given their obligatory role in coordinating tTreg development discussed above. One recent study used two pTreg clones reactive to *Helicobacter*-derived antigens to survey the cDC subsets that were promoting pTreg induction [178]. While pTreg induction was lost in *Ccr7*$^{-/-}$ mice that lack migratory DCs, the absence of cDC1s or CD103^{+} cDC2s did prevent the formation of pTreg cells, which suggested functional redundancy amongst cDCs. However, three recent studies [179-181] identified a subset or subsets of APCs in the gut which are not cDCs, but have a dedicated function for inducing microbe-specific RORγt^{+} pTreg cells. While the exact lineage of these cells remains incompletely defined, these cells are derived from an *Rorc*-expressing precursor, are identified as RORγt^{+} MHC-II^{+}, and contain both Aire^{+} and Aire^{neg} subsets. Notably, expression of both MHC-II and subunits of the TGF-β-inducing integrin $\alpha_4\beta_7$ was required on these cells for efficient pTreg induction. Additionally, it was shown that these cells are most prominent during the weaning period, raising questions about whether such cells continue to play a role in establishing tolerance to microbial antigens as the landscape changes throughout life. In this regard, a study using heterozygous reporter alleles to study polyclonal pTregs in the gut of adult mice [182] demonstrated that most emerging pTreg cells were RORγt^{+}, suggesting that the RORγt^{+} APC population remains active following weaning, or other APC subsets fulfill this function in the adult. It also remains

outstanding whether these cells play a role in tolerance to non-microbial antigens such as food and allergens. Given that the intestine has the highest proportion of RORγt^{+} Treg cells of any anatomical site, it is unclear whether analogous populations of dedicated tolerogenic APCs exist throughout the body, and what types of antigens such cells would present. Outside of the gut, a recent report demonstrated that B cells undergoing a germinal center reaction can act as APCs to induce *de novo* pTreg generation of some transgenic Tconv cells reactive to the immunizing antigen [183], which was concurrent with the contraction of the germinal center. Ectopic expression of Foxp3 by such cells was sufficient for germinal-center shutdown, but it remains unclear whether tolerance to the immunizing antigen in this setting is actively imposed by pTreg cells or a product of T_{FH} diversion to the pTreg lineage.

Multiple studies have identified peripheral Foxp3^{neg} CD4^{+} T cell populations that exhibit a propensity to differentiate into pTreg cells, including CD25^{+} Foxp3^{neg} cells [184], recent thymic emigrants exhibiting low-density expression of Qa-2 [185], and FR4^{HI}CD73^{HI} cells [186], suggesting that the peripheral repertoire harbors precursor cells that are poised to differentiate into pTreg cells under distinct conditions. While presently unclear, it is interesting to consider why the immune system would generate a peripheral reservoir of pTreg cell precursors rather than generating mature pTreg cells. In this regard, it is possible that the identified populations simply represent transitional intermediates that have already been triggered to undergo Treg cell differentiation but have yet to adopt the full phenotype of mature Treg cells. Alternatively, these cells could be uniquely plastic and harbor the ability to undergo pTreg differentiation or Tconv effector differentiation depending on the context in which antigen recognition occurs.

The collective evidence discussed above demonstrates that pTreg cells generated extrathymically make unique contributions to immune regulation and can target peptides derived

from environmental antigens. However, critical gaps in knowledge remain regarding pTreg cell differentiation and function. The mechanisms that distinguish pTreg cell induction from alternate $CD4^+$ T cell fates such as ignorance or differentiation to IL-17-producing cells are largely outstanding. While it is now clear that unique APCs in the gut play a non-redundant role in this process, it remains unknown why such APCs promote efficient pTreg generation for microbial peptides [180,181] but not to dietary antigens [174]. Questions regarding the maintenance of pTreg cells also remain unanswered, including the role for continual antigen recognition.

Mechanisms of regulatory T cell suppression

The existence of a common mechanism of peripheral tolerance in vertebrates was first envisioned by the observation that many systemic and organ-specific autoimmune diseases tend to manifest in tandem within the same afflicted individuals [187-192]. A role for lymphocytes in mediating autoimmune disease was demonstrated in a study of diabetes-prone rats, where injection with anti-lymphocyte antiserum both protected non-diabetic animals and reversed disease following onset [193]. Subsequent studies using monoclonal antibodies linked disease to the $CD4^+$ T cell subset in the NOD and NZB/NZW autoimmune mouse models [194,195], and demonstrated autoreactivity of human $CD4^+$ T cell clones that infiltrated the thyroid in Graves' disease [196]. This discovery, together with previous demonstrations that thymectomy could induce multi-organ autoimmune disease in mice and rats [197,198], strongly suggested the existence of a dedicated T cell subset that imposed tolerance on autoreactive $CD4^+$ T cells. The hunt for such a suppressor population hit a critical milestone in 1985 when Sakaguchi et al [199] demonstrated that $CD5^{HI}$ T cells were required to prevent autoimmune disease upon splenocyte transfer to lymphopenic hosts, and that such cells did not exist in the $CD8^+$ T cell compartment, indicating that both suppressor

cells and autoimmune mediators co-existed as $CD4^+$ T cells. A series of studies confirmed this finding and further refined the surface phenotype of the suppressor subset [200-205], but it wasn't until 10 years on that Sakaguchi and a different set of colleagues unified these principles with a series of transfer experiments showing that $CD25^+$ $CD4^+$ T cells are both necessary and sufficient to prevent autoimmunity mediated by $CD25^{neg}$ $CD4^+$ T cells. Thus began the study of $CD25^+$ $CD4^+$ regulatory T cell biology and function.

A second renaissance occurred with a conceptual link between known phenotypes and pathologies in autoimmune scurfy mice, huma IPEX patients, and suppressor cells. Mechanistic studies in scurfy mice had demonstrated that $CD4^+$ T cells are required for disease development and are sufficient to transfer disease to new recipients [206]. Additionally, heterozygous *Foxp3*$^{scurfy/+}$ female mice and $FOXP3^{mutant/+}$ human females in which 50% of T cells express a wild-type allele and 50% express a mutant allele due to X chromosome inactivation, subjects appear phenotypically normal [207,208], suggesting that Foxp3 plays a role in the establishment of dominant tolerance as do $CD25^+$ $CD4^+$ regulatory T cells. Thus, collective evidence suggested that autoimmune pathology observed in Foxp3-mutant mice and humans may be due to a defect in Treg cell fitness or function, and Foxp3 was subsequently confirmed as the lineage-defining transcription factor for Treg cells [32-34]. The identification of Foxp3 provided a molecular handle to identify, characterize, and manipulate Foxp3-expressing Treg cells. The development of mouse strains expressing the human diphtheria toxin receptor under the dictates of the *Foxp3* promoter, definitively demonstrated that Treg cells are required throughout life in otherwise unmanipulated hosts to prevent fatal immune dysregulation and autoimmunity [19,209]. This implied that many self-reactive Tconv cells exist at steady-state within the repertoire which require a second tier of Treg-mediated regulation. In addition to suppression of autoreactive cells, an expanding body of

evidence demonstrates that Treg cells serve other unique functions including the promotion of tissue repair [210,211], metabolic regulation [212], and hair follicle stimulation [213], and are extensively reviewed elsewhere (140–142). In this section, we review known mechanisms by which regulatory T cells maintain conventional T cell suppression at steady-state and their modes of operation in settings of inflammation, with an emphasis on the signals that coordinate their functional states.

Relationship between the regulatory T cell and conventional T cell repertoires[‡]

Following development in the thymus, Treg cells seed the peripheral repertoire alongside Tconv cells. As discussed previously, most of these Treg cells develop in response to self-derived pMHC-II ligands and display hallmarks of self-reactivity in the periphery, while Tconv cells represent a mix of cells with self- and foreign agonist ligand specificities. Experiments that assess Treg cell development and function typically center analysis on quantification of Treg cell frequency and absolute number at various anatomical sites. However, for reasons discussed below, Treg cells can undergo compensatory expansion or contraction in distinct settings or anatomical locations. Furthermore, the Treg cell repertoire represents a diverse array of specificities, including Aire-dependent and Aire-independent clones that are presumably specific for different types of self-antigens. Thus, a comprehensive analysis of Treg cell biology requires approaches that assess the TCR repertoire diversity and antigen specificity of relevant Treg cell populations. As a case in point, early studies noted that the frequency and absolute numbers of Treg cells were not significantly diminished in the periphery of Aire-deficient mice [123]. However, subsequent TCR repertoire profiling of Treg cells in the thymus [89] and periphery [87] revealed that Aire deficiency is

[‡] This section is adapted from Savage, P.A., Klawon, D.E.J., and Miller, C.H. (2020). Regulatory T cell development. Annual Reviews of Immunology. *38*, 421-453.

associated with substantial shifts in the Treg TCR repertoire, with some specificities lost from the Treg cell compartment and others diverted into the Tconv subset. It is therefore important to consider the repertoire composition of both Treg and Tconv subsets as a framework to understand unique signals and functions that may be imparted to Treg cells.

TCR profiling using engineered mice with a quasi-diverse TCR repertoire demonstrated that the repertoire of TCRs expressed by Treg cells is diverse and is largely distinct from that of Tconv cells, with a small fraction of shared TCRs [42,43,214-216]. These data suggest that Treg cells recognize a complex array of antigenic ligands and that Treg cell differentiation is a TCR-instructive process. At least two scenarios can be invoked to explain this bifurcation. First, it is possible that a distinct set of self-pMHC-II ligands drives robust skewing of all antigen-specific cells into the Treg lineage, leading to the observed differences in TCR repertoires. Alternatively, it is possible that for a given self-pMHC-II ligand, unique TCR-pMHC-II binding properties direct some antigen-specific clones into the Treg cell subset, leaving other antigen-specific clones in the Tconv compartment. Studies using pMHC-II tetramers bearing self-peptides have provided key insight into this question, demonstrating that for any given self-pMHC-II complex, the skewing of antigen-specific cells to the Treg cell lineage is incomplete [48,138,140,141,217,218]. Thus, for many endogenous self-pMHC-II ligands, both clonal deletion and diversion to the Treg cell lineage are incomplete, establishing a scenario in which Treg and Tconv cells of matched specificity coexist within the endogenous repertoire. This raises key questions the activation and functional capacity of these cells vis à vis their Treg cell counterparts of matched specificity. Another interesting phenomenon is revealed by studies showing that for pMHC-II tetramers bearing any given foreign peptide, the immune repertoire harbors identifiable populations of both Treg cells and Tconv cells, a finding that holds true for both mice and humans, and for innocuous foreign as well as pathogen-

derived peptides [97,98,106,218-220]. This raises fundamental questions about the extent to which Treg cells reactive to foreign peptides regulate the adaptive immune response, and whether these functions differ from self-specific Treg cells at homeostasis or in settings of inflammation.

Recognition of self-antigen by Treg cells in the periphery at steady-state

Thymically-derived Treg cells are selected in part based on reactivity to self-expressed peptide ligands, so it is conceivable that these cells have access to many such ligands in the periphery at steady-state. Indeed, Treg cells were first hypothesized to harbor self-reactivity based on their activated phenotype and apparent proliferation at steady-state relative to their Tconv counterparts [41,46]. TCR stimulation in the periphery could act extrinsically to position Treg cells at anatomical sites with high densities of cognate self-antigens, and intrinsically to impart Treg cells with unique functional programs required for immune suppression or trafficking. A study comparing the repertoires of Treg cells at various SLOs in mice with a fixed TCRβ chain, and found asymmetric clonal distribution amongst these sites [221]. These results suggested that many Treg cells are either retained in regional SLOs following cognate antigen recognition, or undergo significant clonal expansion in response to TCR-dependent signals. Activated CD44HI Tconv cells and Treg cells displayed regional enrichment, while $CD44^{LO}$ Tconv cells were randomly distributed, further suggesting that recognition of self antigen coordinates regional co-enrichment of Treg cells and self-specific Tconv cells. Many specificities within the polyclonal population of Treg cells, such as those dependent on Aire, are expected to harbor self-reactivity to tissue-restricted antigens. This regional reactivity is likely responsible for the anatomical distribution patterns observed for Treg clones. However, it's likely that many of these cells will not be exposed to agonist self-antigen signals as they circulate through the SLOs. What is known of the phenotypic

changes that occur in Treg cells which depend on TCR signaling? A study in 2004 provided insight to this question with the first description of two phenotypically-distinct Treg subsets in the periphery [222]. Microarray analysis of Treg cells separated by expression of Integrin α_E revealed a host of phenotypic markers that were distinct in these subsets. Specifically, the α_E^{neg} subset had uniformly high expression of CD25 and CD62L, suggesting an IL-2-responsive naïve-like subset, while hallmarks of α_E^+ Treg cells included CD44, ICOS, and various chemokine receptors, implying that this population was uniquely activated and antigen-experienced. Furthermore, the activated Treg population had a heightened ability to home to sites of inflammation, while the naïve-like population could more readily circulate through SLOs, suggesting distinct functions for these populations. Based on these findings, these subsets were given the nomenclature central Treg ("cTreg"; $CD62L^{HI}$ $CD44^{LO}$) and effector Treg ("eTreg"; $CD62L^{LO}$ $CD44^{HI}$) [223]. Additional studies further elucidated the relationship and functional dichotomy between these populations. cTreg cells were shown to uniquely give rise to eTreg cells upon transfer into secondary hosts, indicating that cTreg cells are a precursor population of eTreg cells [224]. This study also found that maintenance of the cTreg population in the periphery required IL-2, while eTreg cells accumulated with increased numbers of DCs and ICOS expression, suggesting that antigen-presentation and TCR signals played a key role in eTreg differentiation.

A definitive demonstration that TCR-dependent signals are necessary for eTreg differentiation and function came from two studies that used complementary models to conditionally ablate TCRα on Treg cells in the periphery [225,226]. Removal of the TCR resulted in a near-complete loss of eTreg cells, indicating that continual TCR signaling is required for continual conversion from the cTreg to eTreg lineage, and may play a role in survival and maintenance of eTreg cells. Notably, the cTreg population and Foxp3-instructed Treg identity were maintained

absent the TCR, and the cells remained IL-2 responsive, indicating that peripheral TCR signals were playing a critical role in cTreg differentiation but not maintenance. Given that TCR ablation serendipitously enabled inducible depletion of eTreg but not cTreg cells, these studies were also able to demonstrate a critical role for eTreg cells in maintaining immune homeostasis, as TCR ablation on all Treg cells enabled the accumulation and inflammatory cytokine production in effector Tconv and $CD8^+$ T cells in the SLOs. cTreg cells are unlikely to be devoid of immune suppressive function, given that they are localized with IL-2 expressing Tconv cells [224] – which are thought to be receiving strong TCR signals [227] –where they likely compete with such cells for IL-2. However, the non-redundant role for eTreg cells in maintaining immune homeostasis argues that an IL-2 deprivation mechanism of immunosuppression is insufficient to prevent the activation of self-reactive T cells. It is notable that cTreg cells have elevated expression of Nur77, suggesting that most of these cells perceive some basal TCR signals at steady-state [224], and it remains unclear whether tonic signals or agonist self-ligand enables eTreg conversion. Since these studies, multiple cellular pathways have been shown to rely on TCR signaling in Treg cells to impart the eTreg program and are reviewed elsewhere [108].

While both cTreg and eTreg cells exist in the SLOs, eTreg cells are the exclusive residents of tissues [228]. A recent study revealed a stepwise process for eTreg infiltration into non-lymphoid tissues marked by the downregulation of Id3 [229], confirming that a second differentiation event following cTreg to eTreg conversion imparts such cells with tissue-entering capabilities. What is known of the signals that enable Treg cells to enter non-lymphoid organs, and do such resident cells play a role in immunosuppression? Most insight into this question came from the recent work [230], which demonstrated that the acquisition of a unique Treg cell signature associated with residency in the visceral adipose tissue (VAT) was first triggered in the spleen but required

additional differentiation upon arrival in the VAT. Interestingly, such a signature was established in part by the transcription factor PPARγ, whose expression is enriched in adipocytes and adipose tissue [231]. TCR transgenic cells derived from a VAT-infiltrating Treg clone specifically homed to and entered the VAT but not other SLOs or non-lymphoid organs, indicating that the TCR plays a critical role not only in the cTreg to eTreg conversion, but also in instructing tissue entry. In addition to the TCR, the IL-33/ST2 signaling axis was also required for VAT entry [232,233], indicating that the TCR is necessary but not sufficient for tissue entry. This is consistent with a host of studies demonstrating a role for various chemokine receptors and integrins, including CCR4 [234], CCR6 [235], and CXCR3 [236], among others, and is reviewed elsewhere [237]. Regarding their function, eTreg cells in non-lymphoid tissues maintain expression of suppressive factors and effector molecules such as IL-10 and CTLA-4 [230], but most functional studies of Treg suppression in tissues come from observations in tumors [228], which may not recapitulate their biology at steady-state. It could be that the primary role of Treg cells in non-lymphoid organs is to regulate the tissue cells themselves, as was demonstrated in the VAT [230], or other non-immunosuppressive functions [238-240], rather than to actively suppress self-reactive T cells.

Regulation by costimulatory ligands and APC activation

The widespread acceptance of a dedicated autoimmune suppressor population catapulted a series of studies seeking to define the mechanisms enabling such control. Many initial studies were performed *in vitro* and came to a series of potential modes of action, including IL-2 inhibition [241] and T cell – T cell contact [242]. The discovery of Foxp3 and advent of Treg cell reporter mice enabled the first investigation of these mechanisms *in vivo*. In 2006, a hallmark study used the contemporaneous technique of two-photon microscopy to visualize the real-time interactions of

Treg and Tconv cells *in vivo* for the first time [243]. Leveraging the NOD mouse model of spontaneous diabetes, this study used co-infusion of TCR transgenic Tconv cells and *in vitro*-induced iTreg cells to demonstrate that Treg cells influence the activity of Tconv cells via interactions with the APC rather than through direct T-T interactions. Specifically, iTreg cells specific for a pancreatic antigen could inhibit the proliferation of Tconv cells of shared antigen specificity, and Tconv cells specific for a different pancreas-associated antigen, suggesting that one primary function of Treg cells *in vivo* is to modulate the activation status and costimulatory ligands of the APC.

The molecule CTLA-4 became immediately obvious as a potential mechanism of Treg-APC crosstalk. While upregulated on activated $CD4^+$ T cells, CTLA-4 expression is constitutive in Treg cells [49,244,245] owing to transcriptional control by Foxp3 [33,246-248]. Critically, CTLA-4 germline knockout mice develop multi-organ autoimmune disease [249,250] and human haploinsufficiency results in systemic autoimmunity [251]. CTLA-4 is a homologue of the T cell-expressed costimulatory receptor CD28 and can bind to the same B7 ligands on the surface of APCs (CD80/86) [252]. Unlike CD28, whose intracellular signaling domains are thought to amplify TCR signal transduction via recruitment of signal transduction elements to the TCR-proximal LAT scaffold [253], CTLA-4 does not have a substantial intracellular region and is generally thought to act as a negative regulator of TCR signals via competition for CD80/86 at the immunologic synapse [254]. Furthermore, CTLA-4 can restrain T cell activation *in trans* [255], suggesting that Treg-expressed CTLA-4 may be able to modulate Tconv activation.

The creation of mice bearing homozygous *Ctla4*^{flox} alleles and a *Foxp3*-dependent Cre recombinase in a 2008 study enabled the first definitive test of the role of CTLA-4 expression in Treg cells [256]. Mice lacking CTLA-4 on Treg cells presented with elevated levels of serum

immunoglobulin, increased production of inflammatory cytokines by Tconv cells, and succumbed to fatal autoimmunity within 3 months of birth, indicating a crucial role in Treg-mediated suppression. Notably, the kinetics of wasting was delayed compared to mice harboring a germline deletion *Ctla4*, suggesting an additional Tconv-intrinsic role in modulating activation. Remarkably, CTLA-4-deficient Treg cells did not appear to be at a developmental disadvantage compared to their sufficient counterparts, implicating an active role for CTLA-4 in the maintenance of tolerance by Treg cells in the periphery. Mechanistically, *in vitro* co-culture experiments revealed increased levels of CD80/86 costimulatory ligands on the surface of DCs cultured with CTLA-4-deficient Treg cells, suggesting that CTLA-4 removes these ligands from APCs to reduce their activating potential, and was confirmed in subsequent independent studies [257-259]. While it is clear that Treg-expressed CTLA-4 is critical to maintain tolerance, the settings that require CTLA-4-dependent suppression are less clear. Conflicting reports using parallel lines of *Foxp3*-CreERT2^{+} x *Ctla4*-floxed mice to remove CTLA-4 in adult lymphoreplete mice highlight the uncertainty surrounding the essence of its function. The initial study of such mice [260] reported that, following CTLA-4 ablation on Treg cells, adult mice were unexpectedly protected from MOG peptide-induced EAE. The number of Tconv cells and their activation status was increased in the periphery of such mice, but Treg cells were also hyperactivated and expressed additional molecules associated with suppression including IL-10 and Lag-3. A conflicting report released by another group [261] found that CTLA-4 ablation in mice on the same genetic background also causes increased numbers and activation phenotypes of Treg and Tconv cells in the periphery, but that this promoted multi-organ autoimmunity, albeit not lethal as was observed in mice lacking Treg-expressed CTLA-4 from birth [256]. Puzzlingly, this report found that CTLA-4 ablation did delay the onset of MOG-induced EAE in line with the previous report, but increased susceptibility

to arthritis following collogen immunization. Collectively, these studies suggest that the target organ, mode of autoimmune induction, and Tconv antigen specificities may all impact the effectiveness of CTLA-4-dependent suppression by Treg cells.

PD-1 is another prominent inhibitory molecule that is upregulated on activated Treg and Tconv cells. Much of what is known of PD-1 mechanism of action comes from studies of Tconv and $CD8^+$ effector T cells, where it has been well-documented to operate in a cell-intrinsic manner to dampen TCR stimulation upon ligation with its ligands PD-L1/2 [262]. Whether Treg-expressed PD-1 played a critical role in immune tolerance remained speculative until 2020 [263] following the generation of mice harboring a *Pdcd1*-floxed allele (encoding PD-1). In mice lacking PD-1 on Treg cells from birth, the proportion of activated eTreg cells was increased in the periphery, suggesting that PD-1 may restrain the transition from cTreg to eTreg by dampening the TCR-dependent signals required for differentiation discussed above. Accordingly, such conditional knockout mice were protected from MOG peptide-induced EAE and mice on the NOD background were protected from diabetes. PD-1-deleted Treg cells had a proliferative and organ-infiltration advantage in the disease settings. Cumulatively, the available evidence suggests that PD-1 acts in a cell-intrinsic manner to limit TCR signal transduction in Treg cells as it does in Tconv cells, which effectively results in enhanced immune suppression rather than Tconv escape and autoimmunity. Notably, this model and study did not discern whether PD-1 alters the development or repertoire of Treg cells, nor how mice harboring the conditional deletion respond to immune challenge.

CTLA-4-dependent removal of costimulatory ligands from APCs by Treg cells [256] agrees with a model of bystander Treg suppression proposed by the intravital imaging study of 2006 [243]. Additional evidence suggests that Treg cells can modulate the activation potential of APCs via

other mechanisms. CTLA-4 has been shown to modulate IFN-γ and IDO expression in DCs [264], which has been proposed to create a tryptophan-sparce environment that is suboptimal for Tconv cell priming. Treg-expressed LAG-3 binding to MHC-II has been proposed as a mechanism that prevents the maturation of the underlying DC [265]. Treg-exclusive Neuropilin-1 has been shown to enable prolonged interactions of Treg on APCs following TCR ligation of antigen, which could act to sequester pMHC-II complexes from Tconv cells of matched specificity that do not have this advantage [266]. In addition to DCs, antigen-presenting B cells have also been implicated as a direct target of CTLA-4-mediated tolerance both within and outside germinal centers [267].

Modulation of soluble factors in the local environment

A second category of bystander suppression mechanisms by which Tregs are known to constrain autoreactive T cells include the modulation of cytokines or soluble factors within the local environment [268,269]. Three of the most well described molecules are the growth factor IL-2, the suppressive cytokine IL-10, and the peripheral Treg conversion factor TGF-β. IL-2 modulation has been hypothesized as a mechanism of Treg-mediated suppression since the discovery of Treg cells, given that Tconv cells are the primary producers of IL-2 [227], that IL-2 promotes robust Tconv effector responses [270], and that Treg cells constitutively express the high-affinity IL-2 receptor CD25 [30]. Indeed, IL-2 itself is required for Treg cell development [271] and to maintain Treg cell function [60,272], indicating an intrinsic role in Treg homeostasis or function. A body of evidence also supports an extrinsic role for the IL-2 sensing by Treg cells in mediating Tconv suppression by acting as an IL-2 "sink" for local cytokine deprivation [273], including an early descriptive study documenting that Treg cells sense IL-2 before antigen-activated Tconv cells [274]. A landmark study investigated IL-2-dependent extrinsic regulation by Treg cells by imaging self-reactive Tconv cells

in situ in the LN at homeostasis [275], and demonstrated that Treg cell microdomains accumulate around IL-2-producing Tconv cells to limit the overt activation of such cells. Notably, microdomain formation was dependent on TCR expression on the Treg cell, while IL-2 sensing by Treg cells was required for optimal control of the Tconv cells, suggesting that both antigen and IL-2 deprivation may function in tandem to direct compartmentalized suppression within the SLOs. In this regard, Treg microdomain formation was a product of local Treg proliferation [276], and the radius of IL-2 diffusion becomes smaller as local IL-2 consumers increase [277]. Given that IL-2 signaling in Tconv cells primarily acts in a paracrine rather than autocrine manner in the periphery [227] – activated Tconv cells can provide IL-2 to other cells but receive it from activated neighbors – IL-2 constraint by Treg cells within a microdomain may effectively create IL-2 "deserts" in locations with a high density of self-derived antigens capable of activating Tconv cells. In addition to its role in the periphery, IL-2 availability has been shown to tune polyclonal Treg production in the thymus [73], where a greater number of IL-2-producing thymocytes that are escaping central tolerance function to promote Treg development by transiently widening the Treg niche.

IL-10 was first described in the context of the classical Th1/Th2 $CD4^+$ T cell paradigm under the moniker "Cytokine Synthesis Inhibitor Factor" as a molecule produced by Th2 cells to antagonize Th1 response elements such as IFN-γ [278]. Despite definitive evidence of the existence of a dedicated autoimmune suppressor population at the time, the observation that IL-10-deficient mice develop spontaneous colitis [279] highlighted a role for this cytokine in immune homeostasis. While initial characterization of IL-10-producing cells *in vivo* revealed expression across multiple subsets [280], the finding that IL-10-producing $CD4^+$ T cells were sufficient to prevent colitis in a T cell transfer model [281] and the emerging knowledge of a dedicated regulatory T cell subset in the

$CD4^+$ compartment [30,32] piqued broad interest in understanding the role of IL-10 for the prevention of autoimmunity. The development of an IL-10 reporter mouse [282] enabled characterization of the relationships between IL-10-producing $CD4^+$ T cell subsets and elucidated their relative contributions to autoimmune protection in the gut and associated lymphoid tissue. This study revealed the existence of $Foxp3^+$ and $Foxp3^{neg}$ subsets of IL-10-expressing $CD4^+$ T cells that produced fewer inflammatory cytokines than their $IL\text{-}10^{neg}$ counterparts. Transfer studies revealed that $Foxp3^{neg}$ cells could give rise to $IL\text{-}10^+$ $Foxp3^{neg}$ and $IL\text{-}10^+$ $Foxp3^+$ cells, suggesting that the IL-10-expressing Tconv subset may be a precursor to bona-fide $IL\text{-}10^+$ $Foxp3^+$ Treg cells. Furthermore, IL-10 itself was not necessary for IL-10 production by $CD4^+$ T cells, but TGF-β promoted both IL-10 production and Foxp3 upregulation by Tconv cells, suggesting that tolerance in the gut is mediated by IL-10 produced by pTreg cells. $Foxp3^+$ Treg-derived IL-10 was indeed confirmed to play a non-redundant role in mediating tolerance within the gut in a study of mice with conditional ablation of IL-10 in Foxp3-expressing cells [283]. These aged mice developed spontaneous colitis and were more susceptible to allergic inflammation in the lung and skin than their IL-10-competent counterparts. Thus, Treg-expressed IL-10 appears to play a critical role in autoimmune suppression at barrier sites, especially in settings of immune challenge. However, it is dispensable for protection from systemic autoimmunity observed following Treg ablation [19], suggesting that it does not play a universal immunosuppressive role throughout the body.

Shortly after the discovery of IL-10, it was observed that MBP-derived peptide administration at steady-state protected mice from immunization-induced EAE by promoting a regulatory $CD4^+$ T cell population that concurrently produced IL-10 and the molecule TGF-β [284,285]. A similar phenomenon was later appreciated in response to microbial antigens in the gut [286], where IL-10 was the direct mediator of colitis suppression while TGF-β did not play a role

following the onset of disease. This finding highlighted the interrelated nature of these regulatory molecules, but suggested distinct regulatory mechanisms by which they orchestrate tolerance; further supported by the fact that TGF-β-null mice develop systemic autoimmune disease [287] while *Il10*$^{-/-}$ mice only develop colitis [279]. The unique mechanism of action for TGF-β was uncovered by the finding that TGF-β-induced signal transduction converts Tconv cells to stable pTreg cells *in vitro* [288] and *in vivo* [156] under conditions of suboptimal antigen priming and low levels of IL-2. At this same time, a substantial body of evidence [289-293] had converged on the existence of a novel lineage of "Th17" Tconv cells that could function as both pro- and anti-inflammatory mediators in various autoimmune settings, including colitis. Within a year, the connection had been made between TGF-β and the Th17 Tconv population when a study demonstrated that pathogenic Th17 cells arose from a shared TGF-β-induced Treg precursor in the presence of the inflammatory molecule IL-6 [294], demonstrating that the suppressive nature of TGF-β was critically dependent on environmental context. This knowledge enabled subsequent investigations into the mechanistic circuit between TGF-β, IL-10, and Treg cells that enables immune suppression. Two simultaneous and complementary studies [295,296] converged on a model whereby Treg cells, presumably induced by TGF-β signaling at steady-state [156], both produce IL-10 and receive IL-10 signals to amplify its production, which act on Tconv cells to inhibit their expression of IL-17 and resultant autoimmune colitis. In addition to TGF-β, retinoic acid has been shown to play a role in pTreg induction from Th17 precursor cells [176,297]. As discussed above, it is now appreciated that a designated APC in the gut is necessary for inducing Treg cells from Th17 precursors [298], but how such a cell co-opts TGF-β, retinoic acid, and inflammatory cytokines such as IL-6 and IL-21 [299] to orchestrate pTreg induction remains to be elucidated.

Suppression of conventional T cells with matched antigen specificity

Over the last decade, researchers have begun to consider whether Treg cells, given their predilection for self-antigen reactivity, regulate self-reactive responses by modulating the pMHC-II complex. In this model, a given Treg clone would preferentially or exclusively suppress Tconv cells reactive to the same antigenic pMHC complex, rather than broadly suppress Tconv cells with no regard for antigen specificity via the bystander mechanisms discussed above. Antigen-specific Treg suppression has largely subsisted in the realm of esoterica for a few key reasons, including continually-emerging evidence supporting the operation of bystander mechanisms of suppression, the lack of dedicated tools required to test this hypothesis *in vivo*, and misinterpretation of existing data. Despite this, a handful of studies have showcased experiments that imply a non-redundant role for Treg specificity in autoimmune suppression, including observations in *Aire*$^{-/-}$ mice that Treg cells that arise during the neonatal period are uniquely capable of suppressing disease [136], and that such disease is manifested when some clones fail to populate the Treg repertoire [87]. At present, it is becoming accepted that antigen-specific Treg suppression *can* happen in various circumstances and contrived models [237], but it is extremely unclear if such a mechanism operates *in vivo* for endogenous populations of Treg cells, and if it does, exactly where, when, and how such a mechanism would function.

The first direct assessment of the role of Treg specificity in peripheral immune tolerance came from a study in 2017 that used an inducible and conditional system to restrict Treg TCR diversity following normal polyclonal repertoire development in the thymus [300]. In such mice, tamoxifen administration caused ~75% of Treg cells in the periphery to switch to the same monoclonal transgenic TCR derived from a Treg cell reactive to a skin antigen. While monoclonal Treg cells maintained Treg identity and gene expression signature, mice containing these Treg

cells harbored activated Tconv cells and ultimately succumbed to autoimmune disease, indicating that a replete and diverse Treg repertoire is a necessary component for autoimmune suppression. The fact that the Treg signature was maintained in monoclonal Treg cells, together with the autoimmune phenotypes observed in mice with full ablation of the TCR on peripheral Treg cells [225,226], suggested that the TCR may play a non-redundant, extrinsic role in suppression of autoreactive Tconv cells. In this regard, a study which used quantitative imaging of the LN at steady-state to investigate endogenous self-reactive Tconv cells and Treg-mediated control [275] found that Treg cells were enriched around such autoreactive cells and limited IL-2 bioavailability, but this enrichment and autoimmune control was dependent on expression of the TCR rather than IL-2 sensing.

The results of the above study demonstrate the requirement for a diverse Treg repertoire for peripheral tolerance, but an alternative explanation to antigen-specific Treg suppression is that the TCR is critical for placing the proper Treg cells in the proper anatomical locations, which is an established function of Treg-expressed TCRs as discussed above [221]. A formal test of antigen-specific Treg suppression requires the select depletion of a single rare specificity of Treg cells without impacting the antigen-matched Tconv cells, or the provision of Treg cells specific to an autoimmune target antigen. In this regard, three recent studies used *in vitro*-induced monoclonal iTreg cells to test antigen-specific suppression following *in vivo* co-infusion with monoclonal Tconv equivalents. In the first study [152], *H. hepaticus*-specific iTreg cells could suppress colitis induced by their transgenic Tconv counterparts when infused at a 50:1 Treg/Tconv ratio. In the second study [301], monoclonal OT-II iTreg cells could suppress the proliferation of OT-II Tconv cells but not SMARTA Tconv cells, and vice versa, following *in vivo* infusion with DCs that were co-pulsed with both OT-II and SMARTA cognate peptides. This study, perhaps the most in-depth

characterization of this mechanism of suppression, concluded that iTreg cells remove MHC-II complexes from APCs using *in vitro* imaging and cytometry experiments. As in the first study, these experiments infused millions of iTreg cells at times with matched Tconv cells at supraphysiologic ratios, raising ambiguity in whether such mechanisms, if operative *in vivo*, would apply for small numbers of Treg and Tconv cells existing amongst an overwhelming polyclonal population. The third study [302] found that pancreatic islet-antigen-specific BDC2.5 iTreg cells suppressed NOD-mediated diabetes following co-transfer to lymphodeplete recipient mice, though it is unclear whether diabetes was prevented by antigen-specific Treg suppression or by bystander mechanisms of suppression, as was observed previously in a similar system [243] discussed above.

The recent development of a technique to deplete antigen-specific T cells *in vivo* enabled the first and only characterization of autoimmune responses in the presence and absence of an endogenous T cell specificity [303]. This study engineered a cytotoxic CAR T cell to express a pMHC-II antigen complex with an intracellular signaling domain, enabling the specific killing of $CD4^+$ T cells specific for the CAR-expressed antigen. Additionally, a modified "high-avidity" CAR was engineered to deplete both high and low-avidity T cell populations, enabling a direct comparison of the contribution of low-avidity and high-avidity clones to autoimmune disease. In the MOG peptide-induced immunization model, it was observed that lower-avidity MOG peptide-specific T cells had to be depleted along with high-avidity cells to improve disease, suggesting both that Tconv cells with low-avidity for self-antigens contribute to autoimmune disease and that the autoimmune reaction can be stymied by the depletion of the single driving specificity of T cells. While the authors made conclusions about the relative contribution of antigen-specific Treg and Tconv cells to disease using arguments of average affinity, the specific depletion of Treg cells at the exclusion of all high- and low-avidity Tconv cells was not confirmed and is unlikely to be

possible using the CAR system as currently engineered. Thus, a system capable of specifically removing a single endogenous specificity of Treg cell while leaving the Tconv compartment intact has not been established, and will be required to determine the extent to which antigen-specific suppression by Treg cells is required *in vivo* to maintain immune tolerance.

Regulatory T cells in settings of inflammation

Regulatory T cells are enriched alongside their Tconv counterparts in multiple settings of inflammation, including autoimmune lesions [304], tumors [305], allergic disease [219,306], and in transplanted organs [307,308]. While many disparate functions have been attributed to Treg cells acting in these unique settings, few studies have characterized the trajectory of Treg cell activation to uncover generalized behavior in settings of inflammation. Two exceptional studies used the *Foxp3*^{DTR} model to transiently induce systemic inflammation, and characterized the polyclonal Treg population during immune activation and following the resolution of inflammation [309,310]. Importantly, these studies leveraged both inflammation-naïve Treg cells and analogous Tconv populations to systematically characterize changes in the global transcriptome and epigenome during and following inflammation. These studies revealed that polyclonal Treg cells numerically accumulate during inflammation, and upregulate Foxp3 and other dependent effector molecules including CD25 and CTLA-4. Somewhat paradoxically, while these activated Treg cells were transcriptionally more similar to effector Tconv cells than their naïve Treg counterparts, many Foxp3-bound loci were epigenetically repressed, suggesting that such cells were poised to return to an unactivated state [309]. Indeed, following the resolution of inflammation, "memory" Treg cells retuned to a transcriptional state more similar to inflammation-naïve Treg cells than those in an active inflammatory environment [310], but could return to an activated state upon secondary

inflammatory exposure. However, Treg cells with a history of inflammatory exposure retained a heightened capacity to infiltrate tissues, suggesting that a key feature of Treg "memory" may be to position such cells at relevant sites for rapid activation upon re-exposure, and perhaps to recruit such cells into non-suppressive roles in tissue repair [210]. Thus, Treg cells appear to be plastic in their ability to switch between activated and homeostatic states during inflammation and following its resolution, respectively.

Tconv cells differentiate into distinct "helper" lineages of cells during inflammatory responses, which include Th1, Th2, Th17, and Tfh, defined by the transcription factors T-bet, GATA-3, RORγt, and Bcl-6, respectively. Lineage choice is instructed by the local cytokine milieu, nature of the inflammatory challenge, and inflamed tissue, and is required in many cases for efficient host protection [311]. Phenotypic characterization of Treg cells following the identification of Foxp3 revealed subsets of Treg cells that were analogous to some Tconv helper lineages adopted following immune challenge [312]. Leveraging the observation that CXCR3$^+$ Treg cells exist at steady state, together with the fact that CXCR3 is induced on Th1 Tconv cells during inflammation, a 2009 study demonstrated that a subset of Treg cells adopt a Th1-like phenotype at homeostasis that depends on the expression of T-bet [313]. Following inflammatory treatment with αCD40 activating antibody, the population of T-bet$^+$ Treg cells increased, although it was unclear whether this was due to *de novo* upregulation, expansion of pre-existing T-bet$^+$ Treg cells, or both. Further characterization revealed that many Th1-like Treg cells expressed CD103, suggesting that such cells may harbor unique tissue-homing capacity over other Treg subsets. Functionally, T-bet-deficient Treg cells could not effectively suppress Th1 Tconv responses or associated inflammation in Foxp3^{null} mice following Treg cell transfer, suggesting a critical role for this Treg subset in controlling Tconv cells during this type of inflammation. A concurrent study

investigating Treg subsets in the gut [314] identified a similar phenomenon for Th17-mediated colitis, whereby STAT3 – a signal transducer downstream of Th17-inducing cytokines – was required in Treg cells to prevent Th17 Tconv differentiation and ensuing tissue pathology. Expession of RORγt and adoption of a Th17-like phenotype by this Treg subset was subsequently determined as the requisite for suppression of Th17 Tconv cells and intestinal inflammation in two parallel studies [176,177]. Notably, one of these studies found that RORγt expression by Treg cells also prevented Th2 Tconv responses [176], highlighting ambiguity in whether such Treg subsets specifically suppress matched Tconv subsets or broadly control Tconv inflammatory responses.

In addition to the uncertainty surrounding lineage specificity of Treg-mediated control, it was also unclear whether such lineage-defining transcription factors were actively required during inflammation, or whether their differentiation programs were responsible for suppression in these settings. A recent study [315] used a fate-mapping reporter system to demonstrate that T-bet$^+$ Treg cells persist for months in the steady-state periphery and continually express T-bet at steady-sate or following infection. Although a properly-controlled experiment to test the requirement of T-bet$^+$ Treg cells for Th1 Tconv was not performed, a sufficiency experiment showed that depletion of all non T-bet-expressing Treg cells results in the activation of autoimmune Tconv cells that secrete the Th2 and Th17 cytokines IL-4, IL-13, and IL-17, but not Tconv cells that secrete the Th1 cytokine IFNγ. This study revealed that Th1-like Treg cells are a stable lineage that preferentially prevents Th1 Tconv differentiation or activation in a setting of autoimmune-mediated inflammation. The mechanism coordinating this selectivity, and the fate of controlled Tconv cells in these settings, remain completely unresolved. Furthermore, given that T-bet expression in Treg cells is primarily induced by Tconv-derived IFNγ [235], it remains unclear where and how T-bet expression is induced in Treg cells in the steady-state mouse, although the recent

identification of IFNγ-expressing cells in the thymus [316] suggests that differentiation could occur during thymocyte development. Finally, the finding that T-bet$^+$ Treg cells appear to be a stable lineage following inflammatory challenge [315] is discordant with the previous study by the same research group (discussed above [310]) demonstrating that most activated Treg cells return to a resting-like state following transient inflammation. Future inquiries will require analysis of tractable populations of Treg cells with known antigen specificity, together with carefully-defined inflammatory environments, to understand the stability and response of such Th-like Treg cells to repeated inflammatory and antigenic challenges.

Regulatory T cell responses during infection

As discussed above, Treg cells employ a host of known mechanisms to prevent the overt activation of self-reactive Tconv cells and overt autoimmunity. The relative contribution of each mechanism to the maintenance of tolerance appears to depend on context, whereby both the tissue and the inflammatory milieu (or lack thereof) dictate the Treg subsets and suppressive molecules required to prevent autoimmune tissue damage. The requirement for such a tolerogenic cell type is intellectually satisfying from an evolutionary perspective when the host population is considered in isolation, as those members unable to prevent self-directed inflammatory responses will both figuratively and literally self-destruct. But the immune system did not emerge to prevent inflammatory responses – it arose from a necessity to manifest inflammation that protects the host during an attack by an infectious nonself threat. The emergence of a regulatory T cell population likely occurred in the context of these dichotomous requirements, necessitating a mechanism to discern between host-protective and host-destructive inflammatory responses.

This paradox has not been lost on the research community – there has been great interest in understanding the mechanisms and consequences of Treg action during infection since their mainstream inception. The first major study into the role of Treg cells during infection was published in 2002, prior to the discovery of Foxp3, in a model of *Leishmania major* infection, which latently persists in the dermis following the acute phase of infection [317]. During the latency phase, $CD25^+$ $CD4^+$ T cells accumulated at the infection site alongside their $CD25^{neg}$ $CD4^+$ counterparts. Isolation and transfer of these populations into infected recipients revealed that the $CD25^{neg}$ $CD4^+$ population promoted pathogen clearance while the $CD25^+$ $CD4^+$ population dominantly inhibited this protection, indicating that $CD25^+$ $CD4^+$ cells were suppressing protective host immune responses during infection. Mechanistically, $CD25^+$ $CD4^+$-derived IL-10 played a critical role in pathogen persistence, as mice that received both $CD25^{neg}$ $CD4^+$ and IL-10-deficient $CD25^+$ $CD4^+$ cells recovered the ability to clear the pathogen. However, rechallenge experiments revealed that deprivation of IL-10 during the primary response to infection prevented protective immunity upon secondary infection, suggesting that $CD25^+$ $CD4^+$ Treg cells enigmatically both prevent optimal effector responses against the pathogen yet enable optimal memory T cell formation. A follow-up study revealed that Treg cells could both promote and prevent immunity to *L. major* within the same host at acute or latently-infected sites, respectively [318], suggesting that the mechanism of Treg action during infection is highly context-dependent. These foundational studies built a conceptual framework for the role of Treg cells during infection that persists 20 years on: Treg cells are positioned on a knife's edge between protective host immunity and detrimental immune suppression, and their function must be carefully coordinated in space and time to ensure pathogen clearance without allowing excessive tissue damage by the pathogen or the host.

The intervening years have been peppered with studies which aim to manipulate endogenous polyclonal Treg populations in various pathogen models and measure the impact on pathogen-directed effector and memory T cell responses at various stages of infection. The first inquiry of this nature occurred in 2008; enabled by the creation of the *Foxp3*^{DTR} mouse and using a model of vaginal HSV-2 infection [319]. This study demonstrated that acute Treg ablation within the first 5 days of infection counterintuitively prevented pathogen and accelerated host death, and suggested that Treg cells coordinate chemokine gradients emanating from the infected tissue in the early stages of infection to ensure proper homing of protective conventional T cells. A separate study that employed lethal *T. gondii* infection [320] of the gut found that polyclonal Treg cells increase during the early stages of infection but are rapidly pruned at the acute phase just before lethality. Efforts to enhance Treg survival in this period prevented lethal pathology yet increased pathogen burden. A parallel observation was made in a separate study of *L.monocytogenes*-infected pregnant female mice [321]. Allogeneic pregnancy increases the baseline abundance of polyclonal Treg cells in the periphery, and such pregnant dams displayed impaired pathogen clearance. Upon Treg ablation, effective pathogen defense was restored, but concomitantly promoted the accumulation of IFNγ^+ alloantigen-specific T cells and fetal rejection. These studies collectively support the notion that Treg cells prevent autoimmunity at the expense of protective anti-pathogen responses.

In the study of *T. gondii* infection [320], collapsing Treg cells at the acute phase of the response adopted a Th1-like phenotype highlighted by T-bet and IFNγ expession prior to lethality, suggesting that this population may dictate the choice to continue the T cell response or resolve the inflammation. Two subsequent studies used models of *L. monocytogenes* [235] and LCMV [322] infection to study these Th1-like Treg and Tconv subsets at this inflection point. These studies

revealed that IFNγ signaling in Treg cells promoted T-bet expression and transiently inhibited the proliferative and suppressive competency of such cells, which was essential for robust anti-pathogen conventional T cell responses and optimal pathogen clearance. Furthermore, Treg and Tconv cells harbored kinetic differences in their capacity to integrate inflammatory IL-12 signals following IFNγ signaling, such that delayed expression of the IL-12R on Treg cells prevented such cells from expressing IFNγ and sustaining an inflammatory environment. Taken together, these studies support a model whereby Treg cells must attenuate their suppressive function during the peak of the T cell response and rapidly rebound following pathogen clearance to effectively promote pathogen-directed effector responses and limit immunopathology.

It has also been suggested that Treg cells play a role in anti-pathogen T cell memory and recall following secondary challenge. A 2012 study [323] tracked *L.monocytogenes*-specific primary and secondary $CD8^+$ T cell responses when Treg cells were depleted early during the primary infection. While pathogen-specific $CD8^+$ T cells stained bright for tetramer in non-depleted mice during the primary response, Treg-depleted mice harbored an analogous population with much dimmer tetramer intensity. Accordingly, Treg-depleted mice failed to expand a robust population of antigen-specific memory T cells following secondary challenge, suggesting that Treg cells act as a filter to restrict low-avidity T cell responses that are less protective during the primary response and do not efficiently consolidate to protective memory. A complementary study using LCMV infection [324] confirmed that pathogen-specific $CD8^+$ T cell memory consolidation and recall was influenced by polyclonal Treg cells during the primary challenge, and demonstrated that the mechanism of memory formation relies on Treg-derived IL-10. A recent study extended these findings of $CD8^+$ memory formation by temporally tracking Treg cells over the course of *L. monocytogenes* infection [325]. Temporal analysis revealed transient "waves" of Treg expansion that

occurred at day 1 and day 7 post-infection. The first wave displayed high expression of IL-10 and molecules associated with the CD73 enzymatic pathway, which was found to be crucial for the formation of pathogen-specific $CD8^+$ T cells. Collectively, these studies suggest that Treg cells act as a "filter" during the early stages of infection to select the most optimal pathogen-specific $CD8^+$ T cells and facilitate the formation of protective memory. Notably, the reliance on bystander mechanisms of action such as IL-10 and CD73 implies indirect regulation through modulation of the local environment or relevant APCs.

The aforementioned studies relied on the characterization or manipulation of polyclonal Treg populations. What is known about antigen-specific populations of Treg cells during infection? A handful of studies have identified or engineered populations of pathogen-specific Treg cells. A 2009 study engineered *L. monocytogenes* to express the model antigen "2W", and identified a minor fraction of 2W-specific Treg cells in the endogenous repertoire during infection [326]. These pathogen-specific Treg cells failed to expand throughout the primary infection, did not display recall upon secondary challenge, and were ultimately dwarfed by a robust 2W-specific Tconv response. A complementary study of *M. tuberculosis* infection identified a similar minor fraction of Treg cells specific for the endogenous pathogen derived antigen "ESAT" [220]. Upon infection, these Treg cells transiently persisted but were ultimately eliminated by the peak of the ESAT-specific Tconv response. Notably, the contraction of such cells required T-bet and IL-12, in line with the previous finding for polyclonal Treg cells elicited during LCMV and *L. monocytogenes* infection, discussed above [235,322]. Contrasting these findings, another study found that Influenza-specific Treg cells could re-expand upon secondary challenge with the same pathogen [327], but accumulation was short-lived and the number of antigen-specific Treg cells rapidly returned to baseline. A final study demonstrated that transgenic HA-specific Treg cells

could form memory cells following infection with HA-expressing influenza or vaccinia virus [328], and that such memory Treg cells prevented the expansion of $CD4^+$ Tconv cells of matched specificity, but whether such a mechanism occurs for endogenous pathogen-specific Treg cells has yet to be demonstrated. At present, it remains unclear whether pathogen-specific Treg cells play a unique role, if any, during infection. As discussed previously, the identity of endogenous self-ligands recognized by Treg cells had remained elusive until only 6 years ago, and studies of such self-reactive Treg populations during infection are yet to be established.

This thesis aims to understand the fundamental immunological paradox of self-nonself discrimination as it applies to $CD4^+$ T cells: how do $Foxp3^+$ Treg cells ensure the suppression of autoreactive Tconv cells while selectively permitting Tconv responses against infectious pathogens? As an investigative platform, I study antigen-specific populations of $CD4^+$ T cells within the C57BL/6 mouse, focusing on a single self-reactive population of Treg and Tconv cells which target a prostate-derived antigen. I engineer genetically modified mice to specifically manipulate expression of this self antigen, and I perform comparative studies in these mice using tetramer reagents and monoclonal T cells to track the phenotype and behavior of this self-reactive T cell specificity. In Chapter 1, I define the role of this single prostatic peptide antigen in shaping the antigen-specific population of Treg and Tconv cells, and describe the consequence for tolerance and autoimmune disease. In Chapter 2, I engineer strains of the pathogen *L. monocytogenes* to define how self-reactive and pathogen-reactive T cell populations respond during infection, and describe a role for antigen-specificity in mediating specific control of autoreactive Tconv cells during infection. In Chapter 3, I investigate the mechanisms by which

antigen-specific Treg suppression is conferred, and define the nature of autoimmunity elicited by a tolerogenic breakdown against the single self-antigen.

MATERIALS AND METHODS[§]

Mice

The following mice were purchased from the Jackson Laboratory, and bred and maintained at the University of Chicago: C57BL/6J (B6) mice, CD45$^{.1/.1}$ B6.SJL-*Ptprc^{a} Pepc^{b}/BoyJ* mice; *Rag1$^{-/-}$* B6.129S7-*Rag1^{tm1Mom}/J* mice; *Aire$^{-/-}$* B6.129S2-*Aire$^{tm1.1Doi}$*/J mice; *Tcra$^{-/-}$* B6.129S2-*Tcra^{tm1Mom}*/J mice; *Bim$^{-/-}$* B6.129S1-*Bcl2l11$^{tm1.1Ast}$*/J; *Foxp3^{GFP}* B6.Cg-*Foxp3^{tm2Tch}*/J; CD4-Cre B6.Cg-Tg(Cd4-cre)1Cwi/BfluJ mice; *Foxp3*$^{\text{DTR-eGFP}}$ B6.129(Cg)-*Foxp3$^{tm3(DTR/GFP)Ayr}$*/J; and *Foxn1*$^{\text{Cre}}$ B6(Cg)-*Foxn1$^{tm3(cre)Nrm}$*/J; *Tcrb$^{-/-}$* B6.129P2-*Tcrb^{tm1Mom}*/J; *Ighm$^{-/-}$* B10.129S2(B6)-*Ighm^{tm1Cgn}*/J; MD4 C57BL/6-Tg(IghelMD4)4Ccg/J; *Ccr2$^{-/-}$* B6.129S4-*Ccr2^{tm1lfc}*/J; BALB/cJ (Balb/c) mice. MJ23tg *Rag1$^{-/-}$* CD45$^{.1/.1}$ and ‘‘TCRβtg’’ mice expressing a fixed TCRβ chain of sequence TRBV26-ASSLGSSYEQY were generated as described previously [102]. *Tcaf3(C4)$^{-/-}$* mice (also called *C4$^{-/-}$*) were generated as described previously, under the alias “*Tcaf3^{tm1}*” [138]. All mice were generated on a pure B6 background or were fully backcrossed to the B6 background. All mice were initially bred and maintained under specific pathogen–free conditions in accordance with the animal care and use regulations of the University of Chicago, Association for Assessment and Accreditation of Laboratory Animal Care Unit #001020, Public Health Service Policy on Humane Care and Use of Laboratory Animals policy assurance #D16-00322 (A3523-01), and United States Department of Agriculture registration #33-R0151. Prior to infection with *L.monocytogenes*, experimental mice were transferred to an isolated ABSL-2 facility. Where applicable, infected mice were housed

---

§ Portions of this section are reproduced or adapted from:
Klawon, D.E.J., Gilmore, D.C., *et al.* (2021). Altered selection on a single self-ligand promotes susceptibility to organ-specific T cell infiltration. Journal of Experimental Medicine *218 (6)*, e20200701.
Klawon, D.E.J., *et al.* Regulatory T cells enforce self-nonself discrimination by constraining conventional T cells of matched self-specificity during infection. *In preparation as of May 2023*.

in separate cages from uninfected littermates. Mice were housed in sterile and ventilated microisolation cages, up to five mice per cage, and fed irradiated standard pellet chow and reverse osmosis water ad libitum in a 12-h light/dark cycle, with room temperature at 22 ± 1°C. All cages contained sterile quarter-inch corncob bedding and a nestlet for environmental enrichment. Mice for experiments were age-matched, littermates when possible and where indicated, and assigned to experimental groups based on genotype.

Generation of C4$^{\Delta TEC}$ mice

Tcaf3(exon5)^{floxed} mice were generated via CRISPR/Cas9-mediated insertion following the *Easi*-CRISPR method described in [329]. Guide sites targeting the introns immediately upstream and downstream of exon 5 of the *Tcaf3* locus were designed using the IDT design tool and were templated from the antisense strand. A 595bp single-stranded ODN Megamer (IDT) templated from the sense strand was used to replace the region between the guide cut sites: it was designed to span the entire exon 5 region, and included two unidirectional *loxP* sites at each guide cut site with 68bp and 80bp homology arms upstream and downstream of the respective *loxP* inserts. Alt-R CRISPR-Cas9 crRNA, tracrRNA, and Cas9 nuclease were purchased from IDT. The following sequences were used for crRNA: 5'-GACCACATGAAAAGATAGCT-3' (upstream) and 5'-CTCCATCAAATTATGTCAGG-3' (downstream). For microinjections, gRNA was assembled with crRNA and tracrRNA at a 1:2 molar ratio via annealing rampdown from 95ºC to 25ºC at 5ºC/min. gRNAs were subsequently complexed with Cas9 in separate reactions at 250ng/ul gRNA and Cas9 for 15min at room temperature. Final injection mix was created at 50ng/ul each gRNA/Cas9 complex and 10ng/ul ssODN Megamer, and spun at 21,000g for 5min prior to injection. Mixes were injected into the nuclei of C57BL/6J embryos. Successful integrations were

determined by PCR using three primer sets designed to generate products that span the upstream *loxP* site only, the downstream *loxP* site only, and the entire inserted region out beyond the homology arms, and was verified by Sanger sequencing. *Tcaf3(exon5)*^{floxed} founder mice were crossed with C57BL/6J mice for two generations, and progeny were subsequently intercrossed with mice of the same founder line and *Foxn1*^{Cre} mice to generate *C4*$^{\Delta TEC}$ (*Tcaf3(exon5)*$^{flox/flox}$ *Foxn1*-Cre^{+}) mice and *C4*^{WT} (*Tcaf3(exon5)*$^{flox/flox}$ *Foxn1*-Cre^{neg}) littermate controls. Since *Foxn1* is expressed in the male gametes [330], only *Foxn1*-Cre^{+} females were used for breeding. Proper genotype and Cre-mediated excision was confirmed for each mouse using both a generic Cre primer set and the primer set spanning the entire inserted region of *Tcaf3(exon5)* beyond the homology arms.

Cell lines and bacteria

High Five insect cells (Trichoplusia ni, female, ovarian) were used for production of recombinant Tcaf3; cells were grown in Insect-XPRESS Protein-Free Insect Cell Medium supplemented with additional L-glutamine (2 mM) and gentamicin sulfate (50 μg/mL), in suspension culture shaking at 120 rpm and 27ºC. Drosophila S2 cells were used for recombinant production of I-A^{b}; cells were transfected according to the Drosophila Expression System manual (Thermo Fisher) in Schneider's Drosophila medium supplemented with 10% FBS, 1X Pen/Strep (100 U/mL penicillin, 0.1 mg/mL streptomycin), and 20 μg/mL gentamicin, and maintained in stationary cultures at 27ºC. S2 transfectants were selected with 25 μg/mL Blasticidin, and stable lines were expanded for expression in Express Five SFM supplemented with 25 μg/mL Blasticidin, 1X Pen/Strep, and 20 μg/mL gentamicin, in suspension culture shaking at 120 rpm and 27ºC. Plat-E cells (Cell Biolabs) were used for retroviral packaging of SP33, EAR, or GLR TCRα-containing pMGflThy1.1

plasmid; cells were grown in Dulbecco's Modified Eagle's Medium (Gibco) supplemented with 10% FBS, 1X Pen/Strep, 10 μg/mL Blasticidin, and 1 μg/mL Puromycin and maintained in stationary cultures at 37ºC. Plat-E transfectants were cultured in the absence of Blasticidin and Puromycin. *E. coli* DH5α (New England Biolabs) was used for cloning and propagation of TCRα-containing pMGflThy1.1 plasmid. *L. monocytogenes* strains used for infection were received from Dr. Nancy Freitag's laboratory at the University of Illinois Chicago and were maintained in BHI media or broth (Difco) per the manufacturers protocol, with antibiotic selection where necessary as described below. SP2/0-Ag14 (ATCC) myeloma cells used for hybridoma production were maintained in DMEM media (Gibco) supplemented with 10% FBS and 1% Penicillin/Streptomycin prior to fusion.

Retrovirus production, infection, and generation of retrogenic mice

SP33rg, EARrg, and GLRrg mice were generated as described previously [138,331]. In brief, the TCRα was cloned into a retroviral construct modified from Turner et al. [331,332]. Plat-E cells, also previously described [333], were used to generate retrovirus. *TCRα*$^{-/-}$ CD4-Cre^{+} TCRβtg^{+} mice on a B6 background were injected with 5-fluorouracil (APP Pharmaceuticals) 3 days prior to bone marrow harvest. Bone marrow cells were cultured for 2 days in X-Vivo 10 (Lonza) containing 15% FCS, 1% penicillin/streptomycin, 100 ng/mL mouse SCF, 10 ng/mL mouse IL-3 and 20 ng/mL mouse IL-6 (Biolegend). Cells were infected with retro- virus by spinfection in the presence of 6 μg/mL polybrene (EMD Millipore) and cultured for an additional 24 hr. All spinfected cells were then mixed with 5 x 10^6 freshly harvested bone marrow ''filler'' cells from *Rag1*$^{-/-}$ mice and injected into lethally irradiated (900 rad) CD45$^{.1/.1}$ *B6.SJL* recipient mice to generate ''retrogenic'' mice. T cells were isolated from retrogenic mice 6-8 weeks after bone marrow reconstitution. CD4^{+}

T cells were FACS-purified from retrogenic mice following CD4 MACS enrichment (Miltenyl Biotech) and staining with the following antibodies: anti-CD8b (Ly-3), anti-CD45.1 (A20), anti-CD45.2 (104), and anti-Thy1.1 (OX-7).

TCR gene usage and CDR3 sequences

The MJ23 TCR contains the alpha chain TRAV14-LYYNQGKLI, utilizing TRAJ23, and the beta chain TRBV26-ASSLGSSYEQY, utilizing TRBJ2-7. The SP33 TCR contains the alpha chain TRAV9D-ALSMSVNYQLI, utilizing TRAJ33, and the beta chain TRBV26-ASSLGSSYEQY, utilizing TRBJ2-7. The GLR TCR contains the alpha chain TRAV6-7/DV9-ALGLRESSGSWQLI, utilizing TRAJ22, and the beta chain TRBV26-ASSLGSSYEQY, utilizing TRBJ2-7. The EAR TCR contains the alpha chain TRAV4D-4-AAEARVPGNTGKLI, utilizing TRAJ37, and the beta chain TRBV26-ASSLGSSYEQY, utilizing TRBJ2-7.

In vitro T cell stimulation and CellTrace labeling

$CD4^+$ T cells were isolated from $MJ23tg^+$ *Rag1*$^{-/-}$ $CD45.1/.1$ female donor mice and purified by MACS (Miltenyi Biotech) enrichment. $CD4^+$ SP33rg T cells were purified by FACS as described above. $CD4^+$ T cells were CellTrace-Violet (ThermoFisher) labeled per manufacturer instructions with slight modification. In brief, cells were pelleted, resuspended in CellTrace-Violet (CTV) at 1:1000 dilution and incubated for 20 min at 37ºC. The reaction was quenched by the addition of 13 mL of PBS. To isolate splenic dendritic cells, splenocytes were isolated from B6 mice and enriched for $CD11c^+$ cells by via MACS (Miltenyi Biotech) positive selection. 1 x 10^4 CTV-labeled T cells were co-cultured with 5 x 10^4 $CD11c^+$ splenocytes, 100 U/mL recombinant mouse IL-2 (Miltenyl Biotech), and prostatic extract or peptide as indicated. Cell cultures were set up in

384-well ultra-low attachment, round-bottom plates (Corning). Dilution of CTV was assessed by flow cytometry on day 5.

T cell transfer experiments

Polyclonal CD4$^+$ donor transfer into lymphodeplete mice

Cells from pooled spleen and lymph nodes (axillary, brachial, cervical, inguinal, pancreatic, periaortic) from 8-12 week old *Tcaf3(C4)*$^+$ or *Tcaf3(C4)*$^{-/-}$ male mice were enriched for CD4$^+$ T cells by MACS (Miltenyi Biotech), combined, and 10^7 cells were injected retro-orbitally into 6-10 week old *Tcrb*$^{-/-}$ male hosts.

Reconstitution of lymphodeplete hosts with mixed Treg and Tconv cells

Cells from pooled spleen and lymph nodes (axillary, brachial, cervical, inguinal, pancreatic, periaortic) from 8-12 week old *Foxp3*^{GFP} mice were enriched for CD4$^+$ T cells by MACS (Miltenyi Biotech) and sorted as by FACS as Foxp3$^+$ Treg and Foxp3^{neg} A mixture of 1 x 10^6 Foxp3$^+$ and 7 x 10^6 Foxp3^{neg} cells combined from mice of the indicated genotypes was injected retro-orbitally into 6-10 week old *Tcrb*$^{-/-}$ male hosts, and the fate of donor cells was assessed by flow cytometry at time indicated in figure legend.

Reconstitution of lymphodeplete hosts with tetramer-depleted T cells

Cells from pooled spleen and lymph nodes (axillary, brachial, cervical, inguinal, pancreatic, periaortic) from 8-12 week old *Foxp3*^{GFP} mice were enriched for CD4$^+$ T cells by MACS (Miltenyi Biotech) and sorted as by FACS as Foxp3$^+$ Treg and Foxp3^{neg}. Following sort, the Foxp3$^+$ Treg fraction was split and stained with the indicated dual tetramers per the protocol, incubated with

anti-PE and anti-APC microbeads (Miltenyi Biotech) for 15 min on ice per the manufacturer protocol, washed, and enriched over a single gravity MACS magnetic column. Fllowing depletion, a mixture of 1 x 10^6 Foxp3$^+$ and 7 x 10^6 Foxp3^{neg} cells combined from mice of the indicated genotypes was injected retro-orbitally into 6-10 week old *Tcrb*$^{-/-}$ male hosts, and the fate of donor cells was assessed by flow cytometry at time indicated in figure legend.

MJ23 Tconv cell transfers

Splenocytes derived from MJ23tg$^+$ *Rag1*$^{-/-}$ CD45$^{.1/.1}$ mice were isolated into a single-cell suspension in RPMI 1640 medium supplemented with 10% FBS and 1X pen/ strep (R10) using a 70-µm filter, and enriched for CD4$^+$ T cells via MACS (Miltenyi Biotec) following the manufacturer's protocol. MJ23$^+$ CD4$^+$ T cells do not develop into Foxp3$^+$ Treg cells in MJ23tg$^+$ *Rag1*$^{-/-}$ mice due to niche overload [102] and are therefore Tconv cells. The indicated number of enriched MJ23 Tconv cells were injected retro-orbitally into males hosts and identified at the indicated timepoint as CD45.1$^+$ CD4$^+$ T cells.

Retrogenic SP33 or EAR T cell transfers

Splenocytes derived from retrogenic mice were isolated into a single-cell suspension in RPMI 1640 medium supplemented with 10% FBS and 1X pen/ strep (R10) using a 70-µm filter, and enriched for CD4$^+$ T cells via MACS (Miltenyi Biotec) following the manufacturer's protocol. Retrogenic cells were further isolated via FACS strategy discussed above. The indicated number of enriched retrogenic cells were injected retro-orbitally into hosts and identified at the indicated timepoint and identified using the Thy1.1 congenic marker.

MJ23 Treg cell transfers

For transfers into *Tcrb-/-* hosts: cells from pooled spleen and lymph nodes (axillary, brachial, cervical, inguinal, pancreatic, periaortic) from 8-12 week old naïve MJ23 low-frequency chimeras or *Foxp3*^{GFP} mice were pooled, enriched for CD4^{+} T cells by MACS, MJ23 chimera cells were depleted of CD45.2^{+} cells with biotin-conjugated antibody and EasySep^{TM} streptavidin beads (StemCell Technologies) per the manufacturer protocol with slight modification, and CD45.1^{+} Foxp3^{+} MJ23 Treg cells or Foxp3-GFP^{+} polyclonal cells were isolated via FACS. In parallel, cells from pooled spleen and lymph nodes (axillary, brachial, cervical, inguinal, pancreatic, periaortic) from 8-12 week old *Tcaf3(C4)*$^{-/-}$ male mice were enriched for CD4^{+} T cells by MACS (Miltenyi Biotech). 200 Treg cells and 7x10^{6} polyclonal CD4^{+} cells were combined, injected retro-orbitally into *Tcrb*$^{-/-}$ hosts, and analyzed at the indicated day post-infection. For transfer into *C4*$^{\Delta TEC}$ hosts: cells from the spleens of low-frequency MJ23 chimeras 4 days pot-infection with *Lm[C4]*, enriched for CD4^{+} T cells by MACS, and MJ23 Treg cells were sorted by FACS. 8000 MJ23 Treg cells were injected retro-orbitally into *C4*$^{\Delta TEC}$ hosts which were immediately challenged with *Lm[C4]*, and mice were analyzed at the indicated timepoint post-infection.

LN cell transfers

LNs from the indicated anatomical site were harvested from mice, pooled, and isolated into a single-cell suspension in RPMI 1640 medium supplemented with 10% FBS and 1X pen/ strep (R10) using a 70-μm filter. Following isolation, cells were enumerated, injected retro-orbitally into *Tcrb*$^{-/-}$ hosts and identified at the indicated timepoint.

Cell isolation and flow cytometry

Cells from secondary lymphoid organs were isolated into a single cell suspension in RPMI-1640 media supplemented with 10% FBS, 1X P/S (R-10) using a 70μm filter. Thymocytes were isolated in R-10 using a 100um filter. To harvest prostatic lymphocytes, prostates were isolated from the genitourinary tract via microdissection, injected and digested with Liberase TL (10mg/mL, Roche) and DNase (20mg/mL, Roche) in RPMI-1640 for 30 minutes at 37ºC. Digested tissue was mechanically disrupted with frosted microscope slides and viable lymphocytes were enriched using Histopaque 1119 (Sigma). All antibodies used were from Biolegend, eBioscience, or BD Biosciences. Cells were stained with conjugated antibodies specific for the following proteins (with clone name in parentheses): CD4 (GK1.5), CD8α (53-6.7), CD8β (Ly-3), CD3 (17A2), CD45.1 (A20), CD45.2 (104), CD69 (H1.2F3), Foxp3 (FJK-16s), B220 (RA3-6B2), CD11b (M1/70), CD11c (N418), F4/80 (BM8), anti-Thy1.1 (OX-7), anti-Vβ3 TCR (KJ25), anti-PD-1 (RMP1-30), anti-CD44 (IM7), anti-TCRβ (H57-597), Egr2 (erongr2), Ki67 (SolA15), CXCR6 (SA051D1), CCR2 (475301), TCF-1 (C63D9), CXCR5 (L138D7), FR4 (12A5), CD73 (TY/11.8), CD25 (PC61), rabbit IgG anti-Myc (D84C12), anti-rabbit IgG (polyclonal, Invitrogen). For chemokine receptors CXCR6 and CCR2, cells were stained for 30min at room temperature in PBS with 2% FCS prior to staining for other surface markers. For surface markers, cells were stained for 20 min at 4ºC in staining buffer (phosphate-buffered-saline with 2% FCS, 0.1% NaN_3, 5% normal rat serum, 5% normal mouse serum, 5% normal rabbit serum, with all sera from Jackson Immunoresearch, and 10 μg/mL 2.4G2 antibody). In experiments involving tetramer staining, cells were instead stained for 20 min at 4ºC in minimal staining buffer (described above) and chemokine receptors were stained for 1 hr at room temperature with the tetramers. Intracellular staining for Egr2, Ki67, Foxp3, TCF-1, and Myc was performed using fixation and permeabilization buffers

(eBioscience) with an overnight antibody incubation at 4°C. In experiments involving Myc staining, a secondary stain was performed the following morning using AF647-conjugated anti-rabbit IgG for 1hr at 4°C in permeabilization buffer (eBioscience). For infected samples, cell isolation, staining, and fixation was performed in a designated BSL-2 safety cabinet. Flow cytometry was performed on an LSR Fortessa (BD Biosciences), and data were analyzed using FlowJo software (Tree Star v10.1).

I-A^b tetramer production

Tetramers were obtained from the NIH Tetramer Core Facility (C4 – THYKAPWGELATD; F1 – GAPIAVHSSLASLVNIL; LLO – NEKYAQAYPNVS; 2W1S – EAWGALANWAVDSA) or produced in-house. For in-house production, C4/I-A^b tetramers bearing the Tcaf3$_{646–658}$(648Y) peptide (THYKAPWGELATD) and F1/I-A^b tetramers bearing the Tcaf3$_{88-107}$ peptide (CPGAPIAVHSSLASLVNILG) were produced using methods similar to those described previously [334]. I-A^b was expressed in Drosophila S2 cells, using separate plasmids to encode the alpha and beta chains, as described previously [334]. Constructs were co-transfected into Drosophila S2 cells together with a plasmid encoding the BirA biotin ligase. Protein expression was induced with the addition of 0.8 mM $CuSO_4$, in the presence of 2 μg/mL biotin (Sigma-Aldrich). Biotinylated I-A^b protein was purified from culture supernatant by nickel affinity chromatography with His Bind Ni-IDA resin (EMD Millipore) and by avidin affinity chromatography with Pierce Monomeric Avidin UltraLink Resin (Thermo Fisher). Tetramers were formed by mixing biotinylated I-A^b with streptavidin-APC (Prozyme PJ27S) or streptavidin-PE (Prozyme PJRS34) at a slight molar excess of I-A^b to biotin binding sites. Saturation of the streptavidin conjugate was verified by non-reducing SDS-PAGE without boiling samples.

I-A^b Alpha Chain

The extracellular domain of the I-A^b alpha chain (underlined) was fused at its N terminus to a secretion signal sequence (boundary denoted by ‘‘/’’), and at its C terminus to an acidic leucine zipper, and a recognition sequence for the BirA biotin ligase.

MPCSRALILGVLALTTMLSLCGG/EDDIEADHVGTYGISVYQSPGDIGQYTFEFDGDELF
YVDLDKKETVWMLPEFGQLASFDPQGGLQNIAVVKHNLGVLTKRSNSTPATNEAPQAT
VFPKSPVLLGQPNTLICFVDNIFPPVINITWLRNSKSVADGVYETSFFVNRDYSFHKLSYL
TFIPSDDDIYDCKVEHWGLEEPVLKHWEPEIPAPMSELTETGGGGSTTAPSAQLEKELQA
LEKENAQLEWELQALEKELAQGGSGGSGLNDIFEAQKIEWHE.

I-A^b Beta Chain with Tcaf3$_{646–658}$(648Y) Peptide (C4)

The extracellular domain of the I-A^b beta chain (underlined) was fused at its N terminus to a secretion signal sequence (boundary denoted by ‘‘/’’), the Tcaf3$_{646–658}$(648Y) peptide (in **bold**), and a linker sequence, and at its C terminus to a basic leucine zipper and a 6xHis tag.

MALQIPSLLLSAAVVVLMVLSSPGTEG/**THYKAPWGELATD**GGGGTSGGGSGGSERHF
VYQFMGECYFTNGTQRIRYVTRYIYNREEYVRYDSDVGEHRAVTELGRPDAEYWNSQP
EILERTRAELDTVCRHNYEGPETHTSLRRLEQPNVVISLSRTEALNHHNTLVCSVTDFYP
AKIKVRWFRNGQEETVGVSSTQLIRNGDWTFQVLVMLEMTPRRGEVYTCHVEHPSLKS
PITVEWRAQSESAWSKGGGGSTTAPSAQLKKKLQALKKKNAQLKWKLQALKKKLAQH
HHHHH.

I-A^b Beta Chain with Tcaf3$_{88-107}$ Peptide (F1)

The extracellular domain of the I-A^b beta chain (underlined) was fused at its N terminus to a secretion signal sequence (boundary denoted by ''/''), the Tcaf3$_{88-107}$ peptide (in **bold**), and a linker sequence, and at its C terminus to a basic leucine zipper and a 6xHis tag.

MALQIPSLLLSAAVVVLMVLSSPGTEG/**CPGAPIAVHSSLASLVNILG**GGGGTSGGGSG
GSERHFVYQFMGECYFTNGTQRIRYVTRYIYNREEYVRYDSDVGEHRAVTELGRPDAE
YWNSQPEILERTRAELDTVCRHNYEGPETHTSLRRLEQPNVVISLSRTEALNHHNTLVCS
VTDFYPAKIKVRWFRNGQEETVGVSSTQLIRNGDWTFQVLVMLEMTPRRGEVYTCHVE
HPSLKSPITVEWRAQSESAWSKGGGGSTTAPSAQLKKKLQALKKKNAQLKWKLQALK
KKLAQHHHHHH.

I-A^b tetramer staining and enrichment

Tetramer staining was adapted from Tungatt et al. [335]. Cells were treated with dasatinib (AdooQ Bioscience) at a final concentration of 50 nM for 30 min at 37°C in minimal staining buffer (phosphate-buffered-saline with 0.1% NaN_3, 2% normal rat serum, 2% normal mouse serum, all from Jackson Immunoresearch, and 10 μg/mL 2.4G2 antibody). PE- or APC-labeled tetramers were added directly to dasatinib-treated cells in minimal staining buffer (without washing) at a final concentration of 100 nM (C4 and F1 tetramers) or 10nM (LLO and 2W1S tetramers) for 1 hr at room temperature. Cells were washed and incubated with unconjugated mouse anti-PE antibody (clone PE001, Biolegend) and mouse anti-APC antibody (clone APC003, Biolegend) at a concentration of 10 μg/mL for 20 min at 4°C in minimal staining buffer. In some experiments, tetramer-binding cells were not stained with unconjugated anti-PE and anti-APC antibody, but were instead enriched via one of two methods, which were adapted from Legoux and Moon [336].

For analysis of naïve mice and for 10X tetramer isolation, cells were incubated with anti-PE and anti-APC microbeads (Miltenyi Biotech) for 15 min on ice per the manufacturer protocol, washed, and enriched over an AutoMACS magnetic column. For mice immunized with peptide, cells were treated with EasySep™ PE/APC Positive Selection Kits (StemCell Technologies) per the manufacturer protocol with slight modification and enriched using a column-free magnet. The resulting bound fraction was stained and analyzed by flow cytometry as described below. The total number of tetramer-positive events was calculated as described by Legoux and Moon [336].

Genetic engineering of L.monocytogenes

All *L.monocytogenes* strains were engineered using the pPL6-myc shuttle vector as described in [337] with modifications in some strains as follows. The peptide or protein of interest to be expressed in *L.monocytogenes* was codon-optimized for expession in *L.monocytogenes* (Genscript), and the coding sequence was synthesized and inserted into the pUC18 vector immediately flanked by BamHI restriction sites (Genscript). Coding sequence fragments were amplified with a Phusion PCR (NEB) using M13 universal forward and reverse primers (IDT) and gel-purified (Qiagen) via the manufacturer's protocol. Amplified fragments and pPL6-myc vector (Freitag Lab) were digested with 1ul BamHI in Cutsmart Buffer (NEB) for 1hr @ 37C, gel-purified, and ligated with 1ul T4 Ligase in Ligation Buffer (NEB) overnight @ 16C using a 1:6 vector:fragment molar ratio. DH5-alpha *E. coli* were heat-transformed using the ligation reaction mix via the manufacturer's protocol (NEB), and transformed colonies were selected on LB agar plates (Sigma) containing 25ug/ml chloramphenicol (CAM) (Sigma) overnight @ 37C. DNA from selected colonies was purified via Miniprep (Qiagen) using the manufacturer's protocol and sequence integration and directionality was confirmed via Sanger sequencing using the pPL6-Myc_Seq primer

(TATTCCTATCTTAAAGTTACTTTTATGTGGAGGC). Correctly-integrated plasmids were subsequently transformed into electrocompetent SM10 *E.coli* (Freitag Lab) via electroporation using a Gene-pulser and 0.1cm Gene-pulser cuvettes (Biorad) and the following settings: capacitance 25uF, resistance 200Ω, voltage 1.8kV. Electroporated SM10 were selected overnight in LB broth (Gibco) + 25ug/ml CAM @ 37C shaking, subsequently incubated overnight on LB agar plates + 25ug CAM @ 37C, and selected colonies were expanded. Shuttle vector was introduced and stably integrated into *L.monocytogenes* genome via conjugation with SM10. Transformed SM10 and *L.monocytogenes* parent strains (*Lm[parent]*) were grown to lawns overnight @ 37C on agar plates under the following conditions: LB agar + 25ug/ml CAM and BHI agar (BD)+ 200ug/ml streptomycin (Strep), respectively. The following day, SM10 was replated in ~1in square on fresh antibiotic-free BHI agar plates, *Lm[parent]* was replated directly on top of SM10, and conjugation proceeded for 4hr @ 37C. Following incubation, conjugation mix was selected overnight @ 37C shaking in BHI broth (BD) containing 7.5ug/ml CAM + 200ug Strep. Cultures were further selected overnight @ 37C on BHI agar plates (BD) containing 7.5ug/ml CAM + 200ug Strep. Colonies were isolated, expanded, and stored as 15% glycerol stocks @ -80C. Stable integration was subsequently confirmed by sequencing and using cellular assays. The final engineered *Lm* strains expressed peptides with the following amino acid sequences: *Lm[C4]* THSKAPWGELATD; *Lm[F1]* GAPIAVHSSLASLVNIL; *Lm[C4+F1]* THSKAPWGELATDGSGRMKLPKGSGMSMDMNGSGCPGAPIAVHSSLASLVNILG.

Infection with L.monocyogenes

L.monocytogenes strains used in this study are described in [337]. Attenuated strains were derived from the 10403S *prfA(G155S)* Δ*actA* parent strain (NF-L974 in reference). Non-attenuated strains

were derived from the 10403S *actA gus plcB prfA(G155S)* parent strain (NF-L943 in reference). The day before infection, glycerol stock of the infecting strain was scraped, dropped in starter culture, and grown overnight @ 37C shaking (225rpm) in BHI broth (Difco) under Chloramphenicol (CAM) (Sigma) selection (7.5ug/ml). On the day of infection, starter culture was diluted 1:20 in BHI+CAM and grown under analogous conditions and expanded to experimentally-determined logarithmic growth phase (~3hrs). Culture was removed and placed on ice for a minimum of 30min to stall growth. Optical density (OD_{600}) of culture was measured and concentration was calculated using the following experimentally-determined equation: For attenuated strains, $Log_{10}[CFU/ml] = 0.6245(OD_{600}) + 8.707$; for non-attenuated strains, $Log_{10}[CFU/ml] = 0.3134(OD_{600}) + 8.585$. Culture was diluted in PBS inoculum to desired concentration, and mice were infected intravenously with 10^7 CFU (attenuated strains) or $5x10^3$ CFU (non-attenuated strains) in 400ul. To confirm infecting dose, following the infection, limiting dilutions of inoculum were plated on antibiotic-free BHI agar plates (Difco), grown overnight at 37C, and CFUs were quantified the following day.

Immunizations

For CFA immunizations, mice were given a single subcutaneous injection on the flank of 100 μg of peptide in 100 μL of CFA emulsion (Sigma-Aldrich). CFA emulsion consisted of a 1:1 ratio peptide:CFA. Mice were analyzed 14 days later. For LPS, mice were given a single intravenous injection of 100 μg peptide and 5 μg LPS (Sigma-Aldrich) and analyzed 7 days later. For MPLA, mice were given a subcutaneous injection of 100 μg peptide and 25 μg MPLA (Sigma-Aldrich). MPLA/peptide mixture consisted of 1:10 DMSO/PBS solvent. and analyzed 14 days later. For splenic DC immunization, splenocytes were isolated from B6 mice, treated with Liberase TL

(10mg/mL, Roche) and DNase (20mg/mL, Roche) in RPMI-1640 for 20 minutes at 37ºC and enriched for $CD11c^+$ cells by via MACS (Miltenyi Biotech) positive selection. 10^6 DCs/ml were incubated with 100 ng/ml LPS and 25 µg/ml peptide in R-10 for 6 hours at 37ºC, subsequently enumerated and $1.75x10^6$ DCs per mouse were injected intraveneously, and mice were analyzed 7 days later. For BMDC immunization, bone marrow was harvested and incubated in R-10 containing 25 ng/ml GM-CSF (Biolegend) at 10^6 cells/ml for 7 days at 37ºC to create BMDCs. At day 7, 100 ng/ml LPS and 25 µg/ml peptide was added to BMDCs and incubated for 6 hours at 37ºC. BMDCs were subsequently enumerated and 10^6 BMDCs per mouse were injected intraveneously, and mice were analyzed 7 days later.

Treatment with anti-CD40, LPS, Poly I:C

Mice were treated with a single injection of either *InVivo*Plus anti-mouse CD40 (clone FGK4.5, BioXCell), *InVivo*Plus rat IgG2a Isotype mAb (clone 2A3, BioXCell), *E. coli*-deriver LPS (Sigma), or Poly I:C (Sigma). Each agent was administered in 200µL of corresponding solvent as follows: 100µg anti-mouse CD40 or isotype antibody intraperitoneally, 5µg LPS intravenously, 20µg Poly I:C intravenously.

Generation of low-frequency MJ23tg chimeric mice

Bone marrow cells from $MJ23tg^+$ *Rag1*$^{-/-}$ $CD45^{.1/.1}$ and B6 females were T-cell-depleted in parallel via CD90.2 MACS beads (Miltenyi Biotech). A mixture consisting of 5% $MJ23tg^+$ *Rag1*$^{-/-}$ bone marrow and 95% B6 "filler" bone marrow was prepared and 5 x 10^6 cells were retro-orbitally injected into sublethally (500 rads) irradiated host mice. When MJ23 donor mice contained the

Foxp3^{DTR} allele, a 20/80 mix of MJ23/B6 marrow was used. Mice were analyzed at 6-12 weeks after engraftment.

Generation of Bim$^{+/+}$ / Bim$^{-/-}$ mixed bone marrow-chimeric mice

Bone marrow cells from *Bim*$^{-/-}$ CD45$^{.2/.2}$ and B6.SJL CD45$^{.1/.1}$ males were isolated and enumerated. A mixture consisting of 50% *Bim*$^{-/-}$ CD45$^{.2/.2}$ and 50% B6.SJL CD45$^{.1/.1}$ was prepared and 5 x 10^6 cells were retro-orbitally injected into lethally (900 rads) irradiated male B6.SJL CD45$^{.1/.1}$ host mice. 5-8 weeks post-engraftment, mice were immunized with 100µg C4 peptide emulsified 1:1 in CFA

Generation of low-frequency MJ23tg Ccr2$^{+/+}$ / Ccr2$^{-/-}$ chimeric mice

Bone marrow cells from MJ23tg$^+$ *Ccr2*$^{+/+}$ CD45$^{.1/.2}$ and MJ23tg$^+$ *Ccr2*$^{-/-}$ CD45$^{.2/.2}$ mice were isolated and enumerated. A mixture consisting of 10% MJ23tg$^+$ *Ccr2*$^{+/+}$ CD45$^{.1/.2}$ + 10% MJ23tg$^+$ *Ccr2*$^{-/-}$ CD45$^{.2/.2}$ + 80% B6.SJL CD45$^{.1/.1}$ was prepared and 5 x 10^6 cells were retro-orbitally injected into sublethally (500 rads) irradiated male B6.SJL CD45$^{.1/.1}$ host mice. Mice were analyzed 6 weeks pos-engraftment.

Diphtheria-toxin mediated depletion of Treg cells

Diphtheria toxin (Sigma) was reconstituted at 5 µg/ml in sterile molecular grade water following manufacturer's protocol and stored at -80°C prior to use. Diphtheria toxin aliquots were frozen and thawed once. Each injection of 1 µg of diphtheria toxin was administered intraperitoneally to Treg cells at the frequency indicated in the figure.

Serial bleeds of low-frequency MJ23 chimeras

Blood was collected via submandibular puncture into clean 1.5 ml tubes and 50 µl immediately transferred to new 1.5 ml tubes containing 50 µl 10 mM EDTA in PBS to prevent coagulation. Samples were subsequently incubated with RBC lysis buffer (Sigma) for 5 min at room temperature, and stained as described for flow cytometric analysis.

Thymectomy of Foxp3^{DTR} mice

8-10 week-old mice were surgically thymectomized or sham operated and allowed to recover for three weeks. Mice received 5 mg/kg Meloxicam via intraperitoneal injection each day for 3 days post-surgery, then every other day for the following week. Following recovery, mice were depleted of Foxp3+ Treg cells via two 1 µg intraperitoneal injections on subsequent days, followed by similar injections every other day for the duration of the experiment. Individual mice were analyzed if moribund was reached prior to endpoint.

Thymic grafting of nude mice

Donor thymi were isolated from 2 day old neonatal mice, lobes separated, and cultured on a saturated Gelfoam sponge (Patterson Veterinary Supply) in the presence of 2-deoxyguanosine (Sigma) in DMEM + 10% FBS + 1% Penicillin/Streptomycin for 8 days at 37ºC and 8% CO_2 to deplete endogenous thymocytes. Following culture, a single thymic lobe was surgically implanted beneath the kidney capsule of each mouse. Mice received 5 mg/kg Meloxicam via intraperitoneal injection each day for 3 days post-surgery, then every other day for the following week. Mice were rested for 3 months prior to analysis.

Immunohistochemistry image acquisition

H&E and anti-CD3 IHC slides were prepared as described above and examined with an Olympus BH2 light microscope with a 10x or 20x objective and with a 10x eyepiece, and were photographed with the Lumenera Infinity 1-5 camera; Image Sensor Micron MT9P031 connected to an Apple computer. No post-image processing of color or contrast was performed.

Prostate tissue histology and immunohistology

Prostates were isolated as described below and fixed in 10% buffered formalin solution (Sigma) for 24-36 hours. Paraffin embedded, 5-micron-thick prostate sections were stained with hematoxylin and eosin (H&E) for blinded histopathology interpretation. Inflammation was graded from 0 to 4 (0 = none, 1 = very focal, 4 = extremely severe with loss of glandular section; scores 2 and 3 were increments between 1 and 4). For immunoperoxidase staining of mouse T cells, adjacent 5-micron-thick prostate sections were de-paraffinized and hydrated. Endogenous peroxidase was blocked by Peroxidase Alkaline Phosphatase Blocking Reagent (Dako), and incubated overnight at 4ºC with hamster anti-mouse CD3 monoclonal antibody (145-2C11, eBioscience) followed by goat anti-hamster IgG (1:100, Vector Laboratories) at room temperature. Samples were subsequently incubated with Avidin-Biotin Complex (Vector Laboratories), and peroxidase was detected by 3,3'diaminobenzidine tetrahydrochloride (Vector Laboratories) until optimal color intensity was achieved. Counterstain was methylene blue.

Immunofluorescence confocal microscopy of lymph node sections:

Sample preparation

Mice were sacrificed and lymph nodes were immediately and carefully isolated and placed in RPMI 1640 medium supplemented with 10% FBS and 1X pen/ strep (R10) on ice. Lymph nodes were trimmed of fat using a stereo dissection microscope and fine forceps, and fixed for 16-20hrs at 4C with agitation in BD Cytoperm/Cytofix (BD Bioscience) diluted to 1% paraformaldehyde in PBS. LNs were subsequently washed 3x in PBS for 10 minutes per wash with agitation at 4C, and stored overnight on ice. The following day, LNs were further trimmed of remaining fat and dehydrated for 24hr in a 30% sucrose solution made in 0.1 M phosphate buffer. LNs were then embedded in optimal cutting temperature (O.C.T.) compound (Sakura Finetek), frozen on dry ice, and stored at -80C. 18-50um sagittal LN sections were prepared using a cryostat (Leica) equipped with a Surgipath DB80LX blade (Leica). Cryochamber and specimen cooling was set to -17C.

Immunofluorescence staining and image acquisition

Tissue sections were adhered to Superfrost Plus microscopy slides (VWR), permeabilized using 0.1% Triton X-100 for 10min at 22C, blocked in 5% mouse serum for 1hr at 22C, and washed in PBS. Tissue sections were next incubated with directly conjugated primary antibodies diluted in PBS for 15hr at 4C. After washing 3x in PBS for 10min per wash at 22C, samples were mounted in Fluoromount-G (SouthernBiotech), which was allowed to cure for a minimum of 14hr at 22C. All imaging was performed using No. 1.5 coverglass (VWR). For pStat5 immunostaining, fixed tissue sections were permeablized in pre-chilled 100% methanol for 18min at -20C, washed extensively in PBS, blocked in 5% donkey serum for 1hr at 22C, and washed further in PBS. Tissue sections were next incubated with unconjugated anti-pSTAT5 (C11C5) diluted in PBS for

15hr at 4C. Following washing in PBS at 22C, tissue sections were incubated with F(ab')2 fragments (Jackson ImmunoResearch Laboratories) for 2hr at 22C. Sections were then washed 4x in PBS for 10min per wash at 22C prior to mounting in Fluoromount-G as described above. Digital images were acquired using an upright or inverted Leica TCS SP8 X spectral detection system (Leica) equipped with a pulsed white light laser, 4 Gallium-Arsenide Phosphide Hybrid Detectos, 1 photomultiplier tube, 40x (NA = 1.3) and 20x (NA = 0.75) oil immersion objective lenses, and a motorized stage. For tissue sections, images were acquired using the 40x objective with a pixel size of 0.271-0.286um, and detector bit-depth of 12. Image acquisition was controlled using LAS X software.

Image processing and segmentation

Image files generated in LAS X software were converted into ".ims" files in Imaris software (Bitplane) and subjected to a 1 pixel Gaussian filter on all channels to reduce noise. Due to high background following infection, the PD-1 channel was subjected to an additional baseline subtraction and 2x2x2 median filter. Image segmentation was performed in Imaris using the "Surface Object Creation" module, which employs a seeded region growing, k-means, and watershed algorithm to define individual cells of interest. To create surfaces on nuclear molecules, the following parameters were used: surface detail = 0.3, background subtraction = 7µm, seed points = 3.2µm, voxel filter > 100. To create surfaces on membrane molecules, the following parameters were used: surface detail = 0.3, background subtraction = 14µm, seed points = 6.8µm, voxel filter > 100. Polyclonal Treg cells were segmented using Foxp3. MJ23 Treg cells were initially segmented using Foxp3, and refined using Foxp3 and CD4 filters. MJ23 Tconv cells were initially segmented using CD45.1, and refined using Foxp3 and CD4 filters. PD-1^{+} polyclonal

Tconv cells were identified by creating artificial nuclei using the CD4 channel and Fiji [276], creating surfaces on the artificial nuclei, and using PD-1 and Foxp3 filters. In all cases, segmentation artifacts were excluded using volume and non-specific staining thresholds. Each MJ23 Treg, MJ23 Tconv, and PD-1^{+} polyclonal Tconv cell was manually reviewed and corrected when necessary. For images depicting MJ23 Treg and Tconv cells, the CD45.1 fluorescence was masked in Imaris to improve visual clarity.

Quantitative image and spatial analysis

Each segmented MJ23 Tconv, MJ23 Treg, and polyclonal Treg in Imaris was saved with their spatial coordinates in addition to the MFI and SFI of each fluorescent marker. The MFI/SFI of a marker on each single cell per imaging day/experiment was normalized to the average MFI/SFI marker from the all the cells of the same cell type in the matched imaging day/experiment in the $C4^{WT}$ mice. Cells with artificially high fluorescence values, here designated as 100 times the average SFI and/or MFI of a given marker, were removed. Additionally, duplicated MJ23 Tregs were removed from the segmented polyclonal Treg objects. The average Treg (both MJ23 and polyclonal) density of the paracortex of a given lymph node tissue section was determined by 1) counting the number of Tregs within the entire tissue section, 2) finding the semi minor and semi major axis in the XY plane and the height of the tissue section in the Z plane, (3) computing the volume of the elliptic cylinder, (4) performing a 2D KDE on the entire tissue section to remove artificially low Treg regions from the total volume to find the effective volume, and finally (5) dividing the total number of Tregs by the effective volume to yield the average Treg density across the tissue section. The value was chosen by finding the fraction of elements in the 2D KDE (with elements) that had a probability of Tregs. The local polyclonal Treg densities around MJ23 Tconv

cells were found by 1) counting the number of Tregs within 30 μm of the Tconv, 2) computing the volume of the cylinder, and 3) dividing the number of Tregs in the local niche by the volume of that local niche. If the local polyclonal Treg density around that MJ23 Tconv cell was greater than that tissue's average Treg density then it was indicative of micro-domain formation; no micro-domain formed if there were average of less than average Tregs in that given niche than you would expect throughout that given lymph node's paracortex. Random permutation null models were performed to shuffle cell type labels to look for specific enrichment of either polyclonal Treg densities or MJ23 Treg densities around MJ23 Tconv cells. The densities for each MJ23 Tconv label were averaged over 499 Monte Carlo (MC) sampling iterations and plotted for visual aid; but the hypothesis that there were greater Treg densities around the true MJ23 Tconv labels over the shuffled labels was evaluated by computing the empirical p-value by 1) averaging over all MJ23 Tconv labels in a given MC permutation and comparing against the true MJ23 Tconv labels, 2) counting how many MC iterations had average densities from the random permutation null model greater than or equal to the actual MJ23 Tconv labels' densities, and 3) determining the empirical p-value with MC sampling iterations. Hierarchical clustering of the local Tregs was implemented in Python with seaborn's clustermap and in R with pheatmap using the UPGMA clustering method with the correlation metric rather than the Euclidian distance. The normalized SFI of each marker on each cell was log2 transformed prior to hierarchical clustering, and the log2-transformed data's z-scores were then visualized with a heatmap. Any -Inf values arising from the log2 transformation were set to the minimum log2 transformed value for that given marker and cell type. Additionally, the "local MJ23 Treg number" was set to -0.5 for all Tregs from the $C4^{\Delta TEC}$ genotype to account for the global deletion of MJ23 Tregs throughout the host in addition to any local depletion within a 30um radius. If the global bias is not set, the hiearchical clustering results remain the same (i.e.

the same major cluster identities and compositions) but a subset of the activated MJ23 Tregs instead cluster with C2 instead of C1. The number of clusters was defined through setting the argument "cutree_cols=7" in R's pheatmap function and "color_threshold=0.77" in Python's scipy.cluster.hierarchy.dendrogram function. The majority vote of the local Treg cluster identities was used to report a specific given MJ23 Tconv cluster identity.

Single-cell RNA/TCR sequencing of C4/I-A^b tetramer$^+$ cells

Cell isolation and library preparation

To maximize cell viability, cell isolation, staining, enrichment, and FACS sorting was performed over a 12hr period directly before sequencing, and cells were kept cold or on ice whenever possible. Cells were isolated from the spleens of infected mice as described above in two "batches": the first consisting of 4 *C4^{WT}* and 5 *C4$^{\Delta TEC}$* mice, and the second consisting of 5 *C4^{WT}* and 5 *C4$^{\Delta TEC}$* mice. For each batch, individual spleens were first enriched for CD4$^+$ T cells using CD4$^+$ T cell negative selection kit (Miltenyi Biotec) following the manufacturers protocol. Individual samples were subsequently stained with C4/I-A^b tetramers as described above. Following tetramer staining, individual samples were incubated with anti-PE and anti-APC microbeads (Miltenyi Biotec) for 15 min on ice (100ul each antibody cocktail / ml), washed, and enriched over an autoMACS magnetic column. Following enrichment, the individual bound fractions were stained with separate surface marker antibody master mixes as described above in minimal staining buffer. Each surface stain master mix contained uniform surface markers common to all mixes, but contained 1 of 10 Totalseq^{TM}-C030X hashing antibodies used to identify cells derived from each mouse. Following surface staining, all samples within a batch were pooled and C4/I-A^b tetramer$^+$ cells were sorted by FACS using a BD FACSAria Fusion 5-18 cytometer.

Ultimately, two sorted samples (one per batch) containing C4/I-A^b tetramer$^+$ cells from pooled and hashtagged mice resulted after isolation. These samples were resuspended in 45ul of sequencing buffer (0.04% BSA in PBS), and 40ul of each sample was loaded into one of two lanes of a sequencing chip and then subjected to Drop-seq (10X Genomics) to coencapsulate individual cells in reverse emulsion droplets in oil together with one uniquely barcoded mRNA-capture bead. Libraries were derived from single cells, then subjected to next-generation sequencing.

10X single-cell RNA-seq quantification

Gene expression matrices for single cells were obtained from raw reads of RNA-seq and feature barcode libraries quantified using CellRanger count v4.0.2 (10X Genomics). TCR sequences for single cells were obtained using CellRanger vdj v.4.0.2 (10X Genomics). Individual samples were further demultiplexed based on feature barcodes, which were used to mark original samples out of the 9 or 10 samples combined in each capture. The maximum feature expression was determined for each cell, and the original sample identity was assigned accordingly as long as the maximum feature expression constituted at least 80% of the total feature expression for that cell. Otherwise the cell was discarded. TCR sequences were matched to gene expression tables based on shared cell barcodes.

Clustering

All samples from both captures were analyzed together for clustering analysis in the Seurat package in R [338]. Percent mitochondrial expression was quantified, and cells with >15% mitochondrial expression, <750 genes expressed, or <2000 total UMI counts were removed. Gene expression was normalized using NormalizeData() in Seurat, and the top 5000 variable features

were identified using FindVariableFeatures(), both with default parameters. Variable features were z-scored, and principal component analysis (PCA) was run. JackStraw p-values and PCA heatmaps were computed to determine the informativeness of each principal component, and the top 45 were selected as features for clustering. Clustering was performed using the Louvain algorithm at resolutions of 0.25, 0.5, 0.75, and 1. Cell types per cluster were determined by comparing the expression level of specific marker genes in those clusters, as well as looking at the percent of cells expressing a functional TCR. Based on these comparisons, a final resolution of 1 was retained for further analysis. Two non-T cell clusters were further removed from the analysis. Dimensionality reduction was performed by UMAP to visualize cells and clusters.

Genotype contribution to each cluster

Composition analysis of cell subpopulations with respect to genotype was performed by first counting the number of cells in each cluster from each individual sample. Differential statistics between genotypes was computed using edgeR [339,340] on these counts, without computing TMM factors.

Differential gene expression

Cluster-specific genes were identified using differential expression statistics (AUC test) between cell clusters using FindAllMarkers() in Seurat with default settings. Differential expression between genotypes was computed using Wilcox test with the FindMarkers() function within each cluster in turn, in each case setting logfc.threshold = 0 to test all genes and using the FDR correction to adjust p-values for multiple testing.

Identification of top clones

Only cells with complete TRA and TRB sequences were retained. Complete TCR sequences were obtained by concatenating the V, D, J, C and CDR nucleotide sequence for both TRA and TRB for each cell. The total number of times each TCR sequence appeared was counted across all cells, as well as the fraction of cells within each cluster and original sample that expressed the TCR. TCRs with at least 5 counts were retained as the top clones. The fraction expressed per cluster and sample was plotted in a heatmap for the top clones.

Production of anti-C4/I-Ab antibodies

Immunization regiment

Antibodies were produced following the methods of [341] with immunization modification as increasing dose regiment based on [342]. In brief, three Balb/c female mice were immunized subcutaneously with 100 µl total of increasing doses of biotinylated C4(S1Y)/I-A^b monomer (NIH tetramer core) in MPLA (Sigma) on the following days with the following doses: d0, 0.02 µg monomer + 0.05 µg MPLA; d2, 0.052 µg monomer + 0.13 µg MPLA; d6, 0.136 µg monomer + 0.34 µg MPLA; d8, 0.5275 µg monomer + 1.32 µg MPLA; d10, 0.9125 µg monomer + 2.29 µg MPLA; d13, 2.3775 µg monomer + 5.94 µg MPLA; d15, 6.1775 µg monomer + 15.45 µg MPLA. On d28, each mouse was boosted with 25 µg monomer intravenously.

B cell enrichment and hybridoma production

4 days post-boost, cells from pooled spleen and lymph nodes (axillary, brachial, cervical, inguinal, pancreatic, periaortic) were isolated, incubated with tetrablock for 10 min at 4ºC followed directly by C4/I-Ab tetramer-PE at 20nM for 30min at 4ºC, washed, and incubated with 50 µl anti-PE

antibody-conjugated beads (Miltenyi) for 30 min at 4ºC. Tetramer-binding B cells were magnetically enriched using a gravity MACS column and subsequently subjected to hybridoma production using the ClonaCell-HY Hybridoma Generation Kit (StemCell) per the manufacturers protocol with slight modification. Enriched B cells were combined in Media B and placed on ice. Sp2/0 myeloma cells (ATCC) were harvested and $2x10^7$ cells were added to the isolated B cell fraction. Cells were spun, pellet was mechanically disrupted by tapping, and 1ml PEG was added dropwise for 1 min without disrupting the cells followed by a minute of stirring. 4 ml Media B was added to the pellet over the next 4 minutes with continual stirring, spun, and gently washed twice with Media A. Cells were subsequently resuspended in Media C and incubated for 16-24hrs. Following incubation, cells were resuspended in semisolid Media D, plated in 14cm dishes, and incubated for 12 days at 37ºC to allow clonal selection. Colonies were subsequently picked and placed in MEDIA E in 96 well-plates with 1 colony per well and incubated for 3 days at 37ºC.

ELISA screen for C4/I-A^b reactivity

On the evening before, High-bind flat bottom plates (Corning) were coated with 50 ng C4/I-A^b monomer or negative control CLIP/I-A^b monomer (NIH tetramer core) at 4ºC. Plates were blocked with 5% BSA for 30 min at room temperature and washed with TBST (Pierce). Supernatant from hybridoma plates was diluted 1:2.4 in TBST, added to coated plates, and incubated for 1 hr at room temperature. Following TBST wash, plated were incubated with 1:2000 horse radish peroxidase-conjugated anti-mouse IgG (Jackson Laboratories) in TBST. ABTS solution (Invitrogen) was added for detection and absorbance was immediately determined at 405 nm. C4/I-A^b-specific hybridoma clones were determined by subtracting the A_{405} for CLIP/I-A^b from that of C4/I-A^b with a difference > 70% required for specificity.

In vitro T cell blocking assays

$CD4^+$ T cells were isolated from $MJ23tg^+$ *Rag1*$^{-/-}$ $CD45.1/.1$ $OT\text{-}IItg^+$ $CD45.1/.1$ female donor mice and purified by MACS (Miltenyi Biotech) enrichment. $CD4^+$ T cells were CellTrace-Violet (ThermoFisher) labeled per manufacturer instructions with slight modification. In brief, cells were pelleted, resuspended in CellTrace-Violet (CTV) at 1:1000 dilution and incubated for 20 min at 37ºC. The reaction was quenched by the addition of 13 mL of PBS. To isolate splenic dendritic cells, splenocytes were isolated from B6 mice and enriched for $CD11c^+$ cells by via MACS (Miltenyi Biotech) positive selection. 1 x 10^4 CTV-labeled T cells were co-cultured with 5 x 10^4 $CD11c^+$ splenocytes, 100 U/mL recombinant mouse IL-2 (Miltenyl Biotech), 1.6 nM C4 peptide or $OVA_{323\text{-}339}$ peptide (Genscript), and 10 μg/ml purified antibody from hybridoma supernatants. Recombinant Balb/c anti-I-A^b blocking antibody (Biolegend) was used as a positive control. Cell cultures were set up in 384-well ultra-low attachment, round-bottom plates (Corning). Dilution of CTV was assessed by flow cytometry on day 3.

Flow cytometry of peptide-pulsed DCs

Splenic dendritic cells were isolated from B6 mice and enriched for $CD11c^+$ cells by via MACS (Miltenyi Biotech) positive selection. Cells were subsequently pulsed with C4 peptide, V5 peptide (GKPIPNPLLGLDST) or a V5-C4 fusion peptide (GKPIPNPLLGLDSTGSGTHSKAPWGELATD) by incubating 10^6 DCs/ml incubated with 100 ng/ml LPS and 25 μg/ml peptide in R-10 for 4 hours at 37ºC. Cells were subsequently stained with anti-C4/I-Ab antibodies at 1:50 or anti-V5 antibody (TCM5, eBioscience) at 1:20 in superblock with antibody-containing cocktail for 20 min at 4ºC and analyzed by flow cytometry.

Statistical analysis

All data except single-cell RNA sequence analysis and confocal immunofluorescence image analysis were analyzed using Prism software (GraphPad v8.1.2). Aforementioned analyses were performed using R. Significance testing was performed as specified in the figure legends. No statistical methods were used to predetermine sample size.

CHAPTER 1:

ROLE OF SELF-ANTIGEN AND CD4^{+} T CELL ANTIGEN-SPECIFICITY IN AUTOIMMUNE DISEASE

INTRODUCTION[§]

$CD4^+$ T cells recognize short peptides complexed with MHC class II molecules (pMHC-II) displayed on the surface of antigen presenting cells (APCs). At steady state, antigen processing leads to the presentation of thousands of self-pMHC-II complexes derived from both ubiquitous and tissue-restricted self-proteins. A critical question lies in understanding how the immune system confers T cell tolerance to this vast array of self-pMHC-II ligands while enabling productive T cell responses to pathogen-derived peptides complexed with MHC-II. One model suggests that $CD4^+$ T cell tolerance is pMHC-II-specific, and must be imparted for each self-pMHC-II complex separately. pMHC-II-specific tolerance may be conferred via multiple mechanisms, including deletion or functional inactivation of self-pMHC-II-specific $CD4^+$ T conventional (Tconv) cells, diversion of such cells into the $Foxp3^+$ regulatory T (Treg) cell lineage, and extrinsic pMHC-II-specific suppression of Tconv cells by antigen-matched Treg cells [301,343]. In a competing model, T cell tolerance is conferred in part via pMHC-II-non-specific mechanisms in which Treg cells engage self-pMHC-II complexes displayed by APCs and suppress the activation of Tconv cells reactive to both cognate and unrelated self-pMHC-II ligands. This idea is based on proposed mechanisms of Treg cell-mediated "bystander" suppression, which include the production of suppressive paracrine factors, depletion of stimulatory factors, or broad dampening of APC stimulatory potential [268,344]. The extent to which pMHC-II specific tolerance and “bystander” suppression operate *in vivo* for a single T cell specificity, the specific contexts under which these occur *in vivo*, and the mechanisms underlying these processes *in vivo* remain largely undefined.

[§] Portions of this section are reproduced or adapted from Klawon, D.E.J., Gilmore, D.C., *et al.* (2021). Altered selection on a single self-ligand promotes susceptibility to organ-specific T cell infiltration. Journal of Experimental Medicine *218 (6)*, e20200701.

Seminal studies demonstrated that thymic expression of select tissue-restricted proteins, including the proteins encoded by *Ins2* [345] and *Rbp3* [346], are required for the prevention of spontaneous organ-specific autoimmunity. Given that these proteins each yield multiple antigenic MHC-II-restricted peptides [347,348], it is not clear whether autoimmunity in these settings is due to a break in T cell tolerance to a single pMHC-II ligand or to multiple pMHC-II specificities acting in concert to promote organ-specific autoimmunity. Here, we examine the role of T cell specificity to pMHC-II in immune tolerance by perturbing the pool of $CD4^+$ T cells reactive to a single self-pMHC-II complex, and use $CD4^+$ T cell transfer to βδ T cell-deficient mice to define the impact on organ-specific T cell infiltration within a diverse polyclonal T cell repertoire. To do this, we focused on T cell responses to peptides derived from the prostate-specific protein Tcaf3, which is recurrently targeted by autoantibodies and Tconv cells in settings of immune dysregulation [87,139,349]. Tcaf3 yields two known I-A^b-restricted self-peptides (termed "C4" and "F1" peptides) that are recognized by naturally occurring Treg cell populations and direct thymic Treg cell differentiation via Aire-dependent processes [87,138]. Using mice engineered to express Tcaf3 protein specifically lacking the C4 peptide, we demonstrate that impaired T cell selection on the C4/I-A^b pMHC-II complex reduces the ratio of C4/I-A^b-specific Treg to Tconv cells elicited by immunization and renders T cell-reconstituted mice susceptible to prostate-specific T cell infiltration. Our findings demonstrate that selection on a single self-pMHC-II ligand can be critical for the prevention of organ-specific T cell infiltration, revealing potential vulnerabilities in pMHC-II non-specific bystander mechanisms of tolerance and suggesting that altered T cell selection on a single pMHC-II ligand can predispose to autoimmunity.

RESULTS**

In this study, we defined how selection on the C4/I-A^b complex impacts the repertoire of antigen-specific T cells in the thymus and periphery, and determined the extent to which alterations in this single T cell specificity influence the development of prostatic T cell infiltration in a T cell reconstitution setting. In previous work, we used T cell receptor profiling and T cell stimulation assays to demonstrate that Tconv cells reactive to the Tcaf3-derived C4 and F1 peptides recurrently infiltrate the prostates of Aire-deficient mice [87]. Consistent with this, here we utilized peptide/MHC tetramer staining to demonstrate that both C4- and F1-specific Tconv cells can be readily and recurrently detected in the prostates of *Aire*$^{-/-}$ male mice (Figure 1, A-B). Thus, both C4/I-A^b and F1/I-A^b pMHC-II complexes are antigenic and susceptible to spontaneous T cell attack when thymic T cell selection is perturbed via Aire deficiency, which prevents the expression of Tcaf3 in the thymus, among other TRAs.

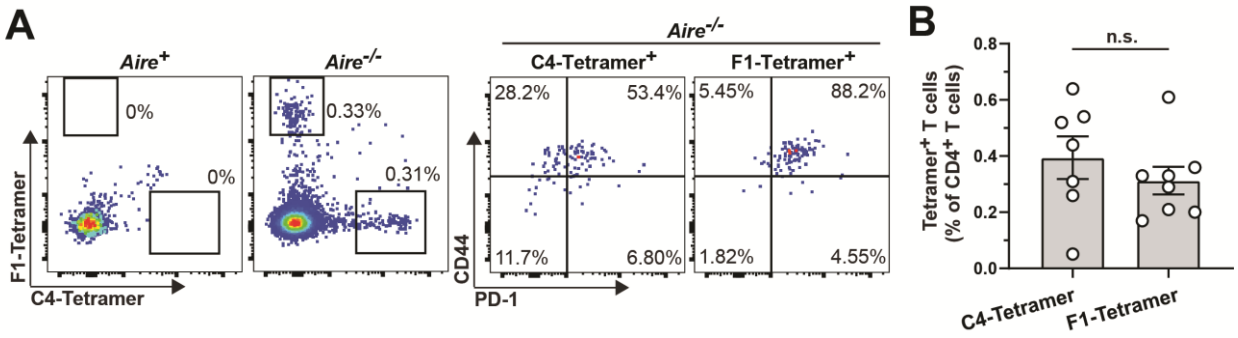

FIGURE 1. Endogenous C4/I-A^b- and F1/I-A^b-specific T cells are found in prostatic autoimmune lesions of *Aire*$^{-/-}$ mice

Both C4/I-A^b and F1/I-A^b are antigenic and recurrently targeted by CD4$^+$ T cells in settings of Aire deficiency. Lymphocytes were enriched from the prostates of >15 week old *Aire*$^+$ or *Aire*$^{-/-}$ male littermate mice and analyzed by flow cytometry for C4/I-A^b tetramer- and F1/I-A^b tetramer-binding cells. (A) Representative flow cytometric analysis of CD4$^+$ T cells isolated from the prostates of mice of the indicated genotype. The left plots depict C4/I-A^b tetramer-APC vs. F1/I-A^b tetramer-PE staining of polyclonal CD4$^+$ T cells, whereas the right plots depict PD-1 vs. CD44

** Portions of this section are reproduced or adapted from Klawon, D.E.J., Gilmore, D.C., *et al.* (2021). Altered selection on a single self-ligand promotes susceptibility to organ-specific T cell infiltration. Journal of Experimental Medicine *218 (6)*, e20200701.

FIGURE 1, continued
expression by tetramer$^+$ T cells. The frequency of cells within the indicated gates is denoted. Data are representative of two independent experiments. (B) Summary plot of the pooled data from (A, Left) showing the frequency of C4/I-A^b tetramer$^+$ and F1/I-A^b tetramer$^+$ cells amongst polyclonal CD4$^+$ T cells isolated from the prostates of *Aire*$^{-/-}$ mice. Each symbol represents one mouse. n = 7, C4; n = 8, F1. Mean ± SEM is indicated. (n.s., not significant $p > 0.05$; two-tailed Mann-Whitney test). Data are pooled from two independent experiments.

Presentation and recognition of the Tcaf3-derived F1 peptide is unaltered in Tcaf3(C4)$^{-/-}$ mice

To create a scenario in which T cell selection on a single pMHC-II complex is altered, we utilized gene-targeted mice in which the germline sequence encoding the 13-amino acid region of the Tcaf3 protein spanning the C4 peptide is deleted (*Tcaf3(C4)*$^{-/-}$ or *C4*$^{-/-}$ mice, referred to previously as *Tcaf3*$^{tm1/tm1}$ mice [138]). Given that deletion of this 13-amino acid segment could impact the presentation of the F1 peptide via alterations in Tcaf3 protein expression, stability, or processing, we first set out to determine whether the presentation of the F1 peptide is altered in *Tcaf3(C4)*$^{-/-}$ mice. As expected, primary Tconv cells expressing the C4-specific "MJ23" TCR [102] proliferated robustly when cultured with splenic dendritic cells and prostatic lysates from C4-sufficient *Tcaf3(C4)*$^{+/+}$ and *Tcaf3(C4)*$^{+/-}$ mice (collectively denoted *Tcaf3(C4)*$^+$ or *C4*$^+$ mice henceforth), but failed to proliferate when extracts from *Tcaf3(C4)*$^{-/-}$ mice were used (Figure 2, A-B). In contrast, Tconv cells expressing the F1-specific "SP33" TCR [138] underwent robust proliferation when cultured with prostatic extracts from mice of both genotypes, indicating that C4 peptide deficiency does not impact the presentation of the F1 peptide in this setting (Figure 2, A-B). To assess whether presentation of the F1 peptide was unaltered by C4 peptide deletion in vivo, we used naive SP33 Tconv cells as a "probe" for antigen recognition. In one setting, we transferred SP33 Tconv cells into *Tcaf3(C4)*$^+$ or *Tcaf3(C4)*$^{-/-}$ males, and found comparable enrichment and activation of SP33 T cells in the prostate-draining paraaortic lymph nodes (pLNs) (Figure 2, C-E),

suggesting that endogenous F1 peptide is available for T cell recognition in *C4*$^{-/-}$ male mice. In a second setting, we analyzed multiple SLOs of primary retrogenic SP33 mice created in *Tcaf3(C4)*$^{+}$ and *Tcaf3(C4)*$^{-/-}$ hosts, which harbor endogenous tractable populations of SP33 Tconv cells. Given that CD4^{+} T cell clones, including the MJ23 clone, are known to be enriched in regional LNs in a TCR-dependent manner [70,221], we expected SP33 to exist at a higher frequency in the pLNs of male mice if F1 peptide expression is intact. Indeed, we observed an enrichment of SP33 T cells in the pLNs of retrogenic hosts of both genotypes, and this elevated frequency did not differ between genotypes (Figure 2, F-G). Collectively, these results indicating that F1 peptide presentation is unaltered *in vivo* in *Tcaf3(C4)*$^{-/-}$ mice, and suggest that only the C4 peptide is altered in *Tcaf3(C4)*$^{-/-}$ mice.

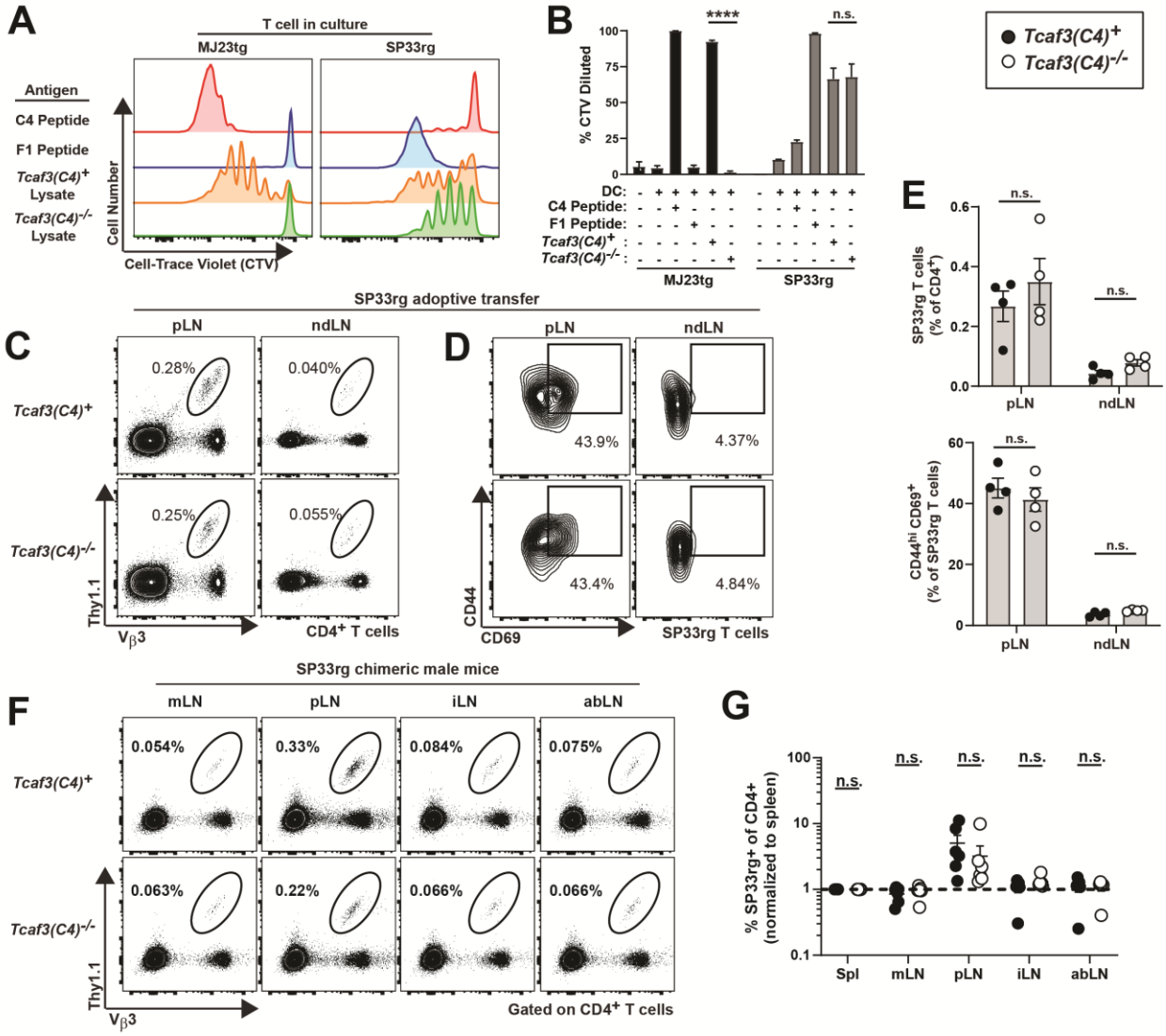

FIGURE 2. Presentation and recognition of the Tcaf3-derived F1 peptide are unaltered in *Tcaf3(C4)*$^{-/-}$ mice.

(A-B) In vitro stimulation of MJ23tg or SP33rg Tconv cells by prostatic lysates. 1 x 10^4 MJ23tg or SP33rg T cells were co-cultured with 5 x 10^4 CD11c$^+$ cells isolated from B6 spleens +mIL-2, with the indicated peptide or prostatic lysates prepared from *Tcaf3(C4)*$^+$ or *Tcaf3(C4)*$^{-/-}$ male mice. Dilution of CTV was assessed by flow cytometry on day 5. Data are representative of two independent experiments. (A) Representative flow cytometric analysis of CTV dilution by CD4$^+$ MJ23tg or SP33rg T cells. (B) Summary plot of pooled data showing the frequency of MJ23tg or SP33rg cells that have diluted CTV from the indicated co-cultures as in (A). Each sample represents an individual co-culture. Mean ± SEM is indicated. n = 2, T cell only; n = 2 DC; n = 3, C4; n = 3, F1; n = 3, *Tcaf3(C4)*$^+$; n = 3, *Tcaf3(C4)*$^{-/-}$. SP33rg + lysate Proliferation Index: *Tcaf3(C4)*$^+$ 1.600 ± 0.118, *Tcaf3(C4)*$^{-/-}$ 1.520 ± 0.159. (**** $p < 0.0001$; n.s., not significant $p > 0.05$; two-tailed Student's t-test). Data are pooled from two independent experiments.

(C-E) 1 x 10^5 purified SP33rg T cells were transferred intravenously into congenically disparate *Tcaf3(C4)*$^+$ or *Tcaf3(C4)*$^{-/-}$ male littermate hosts. 7 days after transfer, cells were isolated from

FIGURE 2, continued
the prostate-draining lymph node (pLN) and non-draining inguinal lymph node (ndLN) and analyzed by flow cytometry. Data are representative of two independent experiments. (C) Representative flow cytometric analysis of Thy1.1$^+$ and Vβ3$^+$ SP33rg T cells amongst polyclonal CD4$^+$ T cells isolated from the indicated lymph node sites in the indicated host mice. The frequency of cells within the indicated gates is denoted. (D) Representative flow cytometric analysis of CD44 vs. CD69 expression by CD4$^+$ Vβ3$^+$ SP33rg T cells isolated from the indicated lymph node sites in the indicated host mice. The frequency of cells within the indicated gates is denoted. (E) (Top) Summary plot of pooled data from (C,D) showing the frequency of CD4$^+$ Vβ3$^+$ SP33rg T cells amongst polyclonal CD4$^+$ T cells (Top), or the frequency of CD44^{HI} CD69$^+$ SP33rg T cells amongst all CD4$^+$ Vβ3$^+$ SP33rg T cells (Bottom) isolated from the indicated lymph node sites in the indicated host mice. Each symbol represents one mouse. n = 4, *Tcaf3(C4)*$^+$; n = 4, *Tcaf3(C4)*$^{-/-}$. Mean ± SEM is indicated. (n.s, not significant $p > 0.05$; two-tailed nonparametric Mann-Whitney test).
(F-G) SP33rg Thy1.1$^+$ retrogenic mice were created in *Tcaf3(C4)*$^+$ or *Tcaf3(C4)*$^{-/-}$ hosts. >6 weeks post-engraftment, cells were isolated from the indicated LN and analyzed by flow cytometry. Data are representative of three independent experiments. (F) Representative flow cytometric analysis of Thy1.1$^+$ and Vβ3$^+$ SP33rg T cells amongst polyclonal CD4$^+$ T cells isolated from the indicated lymph node sites in the indicated host mice. The frequency of cells within the indicated gates is denoted. (G) Summary plot of pooled data from (F) showing the frequency of CD4$^+$ Vβ3$^+$ SP33rg T cells amongst polyclonal CD4$^+$ T cells isolated from the indicated lymph node sites in the indicated host mice, normalized to the chimerism in spleen. Each symbol represents one mouse. n = 6, *Tcaf3(C4)*$^+$; n = 6, *Tcaf3(C4)*$^{-/-}$. Mean ± SEM is indicated (n.s, not significant $p > 0.05$; two-way ANOVA)

Isolation and phenotypic analysis of endogenous C4/I-A^b tetramer$^+$ T cells in the periphery of naïve mice

Having confirmed that *Tcaf3(C4)*$^{-/-}$ mice lack a single self-peptide, we sought to characterize the endogenous circulating population of C4/I-A^b-specific T cells in the presence and absence of the C4 peptide. The repertoire of these antigen-specific T cells could be shaped by numerous factors, including clonal deletion in the thymus or periphery, differential expansion or survival of Treg cells and Tconv cells in the periphery, induction of anergy in C4-specific Tconv cells, and differentiation of peripherally induced Treg (pTreg) cells. To identify such cells and begin to test these possibilities, we created C4/I-A^b tetramers using two fluorophores, and stained the pooled SLOs from mice of either genotype. In a naïve T cell repertoire, CD4$^+$ T cells specific

for any single foreign antigen are extremely rare, constituting only 30-300 cells per mouse [350], so we employed iterative rounds of enrichment in an effort to faithfully identify C4 tetramer-binding T cells [334]. We identified 24 C4/I-A^b-specific T cells per mouse, on average, which is at the lowest end of the naïve T cell range to other defined I-Ab-restricted peptides. Interestingly, the absolute number of C4/I-A^b tetramer$^+$ T cells did not differ between *Tcaf3(C4)*$^+$ and *Tcaf3(C4)*$^{-/-}$ mice (Figure 3, A-B), suggesting that thymic selection on C4/I-A^b and peripheral antigen recognition by C4/I-A^b-specific T cells does not promote the deletion of these self-reactive cells. Consistent with this notion, C4/I-A^b tetramer MFI did not differ between mice of either genotype (Figure 3, C), which might otherwise be expected if the C4 peptide was purging strongly self-reactive cells from *Tcaf3(C4)*$^+$ mice [106,351]. C4/I-A^b tetramer$^+$ T cells did not adopt a $CD73^{HI}$ $FR4^{HI}$ "anergic phenotype" in *Tcaf3(C4)*$^+$ mice (Figure 3, A, D), further suggesting that peptide recognition in the periphery does not measurably inactivate this self-reactive population of cells [186]. Collectively, these data suggest that selection on C4/I-A^b does not promote the deletion or functional inactivation of self-reactive C4/I-A^b specific T cells, necessitating the existence of other mechanisms to control the autoimmune potential of these self-reactive cells.

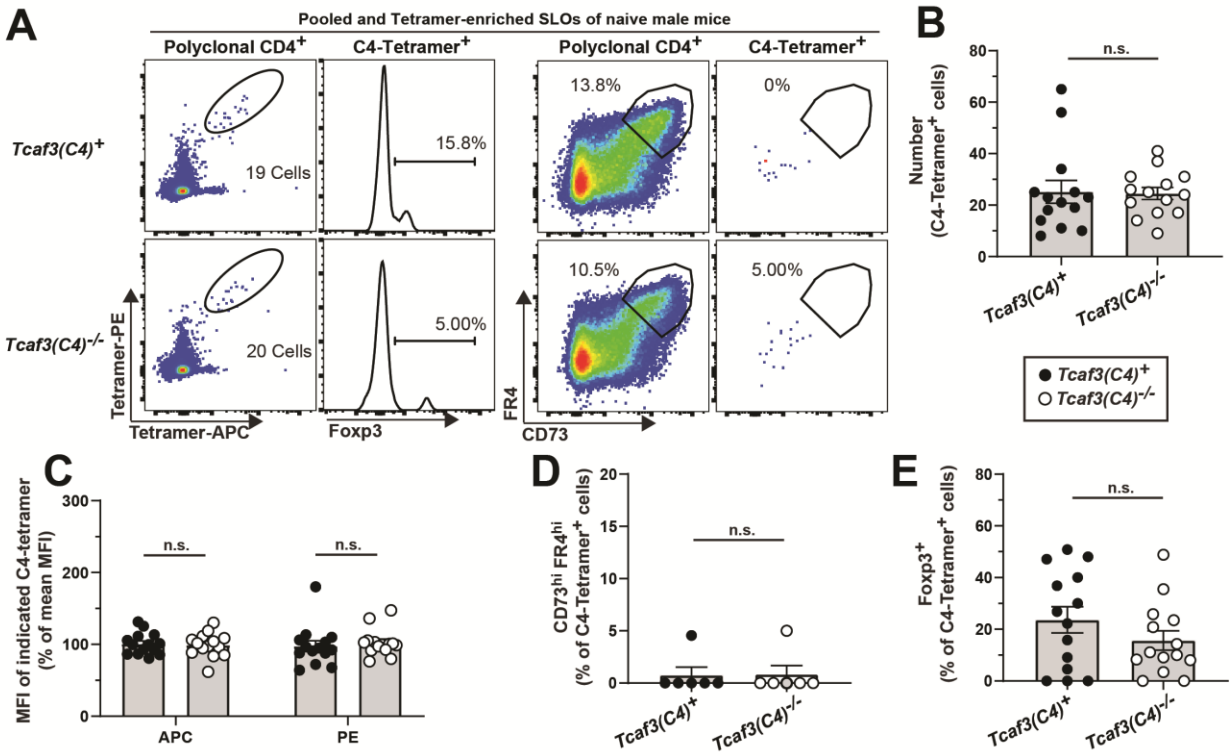

FIGURE 3. Isolation and phenotypic analysis of endogenous C4/I-A^b tetramer$^+$ T cells in the periphery of naive male mice

(A) Representative flow cytometric analysis of CD4$^+$ T cells, enriched from the pooled secondary lymphoid organs (SLOs) from 4-8 week old mice of the indicated genotype. The left plots depict dual C4/I-A^b tetramer expression by polyclonal CD4$^+$ T cells and Foxp3 expression by double C4/I-A^b tetramer$^+$ CD4$^+$ T cells, whereas the right plots depict CD73 vs. FR4 expression by polyclonal CD4$^+$ T cells and double C4/I-A^b tetramer$^+$ CD4$^+$ T cells. The absolute number of cells or frequency of cells within the indicated gates is denoted. (B) Summary plot of pooled data from (A) showing the absolute number of double C4/I-A^b tetramer$^+$ CD4$^+$ cells enriched from the pooled SLOs from mice of the indicated genotype. Each symbol represents one mouse. Mean ± SEM is indicated. (C) Summary plots of pooled data from (A) showing the mean fluorescent intensity (MFI) of C4/I-A^b tetramer-APC and C4/I-A^b tetramer-PE by double C4/I-Ab tetramer$^+$ CD4$^+$ cells enriched from mice of the indicated genotype, normalized to the mean MFI of all double C4/I-A^b tetramer$^+$ CD4$^+$ cells in each independent experiment. Each symbol represents one mouse. Mean ± SEM is indicated. (D) Summary plot of pooled data from (A) showing the frequency of double C4/I-A^b tetramer$^+$ CD4$^+$ cells expressing CD73 and FR4, enriched from the pooled SLOs from mice of the indicated genotype. Each symbol represents one mouse. Mean ± SEM is indicated. (E) Summary plot of data pooled from (A) showing the frequency of double C4/I-A^b tetramer$^+$ CD4$^+$ cells expressing Foxp3, enriched from the pooled SLOs from mice of the indicated genotype. Each symbol represents one mouse. Mean ± SEM is indicated. (n.s., not significant $p > 0.05$; two-tailed nonparametric Mann-Whitney test). n = 13, *Tcaf3(C4)*$^+$, n = 14 *Tcaf3(C4)*$^{-/-}$. Data are representative of 2-4 independent experiments.

T cell selection on C4/I-A^b promotes a Treg-dominated antigen-specific response to C4 peptide immunization

In naïve male mice, the frequency of Foxp3 expression amongst C4/I-A^b tetramer$^+$ T cells did not differ between *Tcaf3(C4)*$^+$ and *Tcaf3(C4)*$^{-/-}$ mice, with the majority of cells existing as Foxp3^{neg} Tconv cells (Figure 3, E), which was unexpected given that the C4 peptide promotes the development of MJ23 Treg cells [138] and that many Aire-dependent CD4$^+$ T cell clones heavily populate the Treg lineage in mice with a fixed TCRβ chain under steady-state conditions [87]. This result could intriguingly suggest that the endogenous polyclonal population of C4/I-A^b-specific T cells in wild-type male mice exists primarily as Tconv cells, and that qualitative differences enable the minor fraction of Treg cells to outcompete such Tconv cells upon antigen recognition. Less excitingly, it's possible that C4/I-A^b-specific T cells could not be faithfully identified in the periphery of naïve mice using current available tools or the enrichment method, and it remains unclear which of these scenarios is closest to reality (see Conclusions and Discussion).

Given the uncertainty surrounding C4/I-A^b-specific CD4$^+$ T cell detection in naive mice, we instead used an established immunization approach in which antigen-specific CD4$^+$ T cells are expanded via immunization with peptide antigen in CFA, which elicits antigen-specific T cells that are reflective of the relative size of the pre-immunization T cell pool [334,350]. *Tcaf3(C4)*$^+$ and *Tcaf3(C4)*$^{-/-}$ mice were immunized, and enriched C4/I-A^b tetramer$^+$ T cells from the pooled SLOs were enumerated and phenotyped two weeks post-immunization [352]. This approach revealed three notable findings. First, analysis of *Tcaf3(C4)*$^+$ males demonstrated that C4-specific T cells elicited by immunization are skewed to the Treg cell compartment, and that skewing is incomplete, averaging 62±14% Foxp3$^+$ cells in 6-8 week old males (Figure 4, A-B). Second, only 21±13% of C4/I-A^b tetramer$^+$ cells elicited by immunization in *Tcaf3(C4)*$^{-/-}$ mice expressed Foxp3,

demonstrating loss of skewing to the Treg cell lineage in C4-deficient mice. Third, the absolute number and tetramer MFI of C4/I-A^b tetramer$^+$ cells recovered after immunization was comparable between *Tcaf3(C4)*$^+$ and *Tcaf3(C4)*$^{-/-}$ males (Figure 4, C-D) Our cumulative findings indicate that C4/I-A^b-specific Tconv cells and Treg cells co-exist in the peripheral repertoire of wild-type mice, and that a primary function of the C4 peptide is to direct antigen-specific T cells to the Treg cell lineage rather than delete or inactivate such cells in the thymus or periphery. Importantly, C4/I-A^b-specific Tconv cells expanded in this immunization setting in *Tcaf3(C4)*$^+$ mice, providing direct evidence that these cells harbor autoimmune potential and require other layers of tolerance for their control.

In the course of our studies, we were unable to characterize the endogenous population of F1/I-A^b-specific T cells, as multiple immunization approaches with the F1 peptide failed to elicit robust expansion of F1/I-A^b tetramer$^+$ T cells (Figure 4, E). This could suggest that these cells exist at lower frequency in the repertoire than C4/I-A^b-specific cells, that F1-specific cells are entrenched in tissues, or could reflect the fact that the F1 peptide is difficult to solubilize in the immunization solution. Regardless, the fact that the F1 peptide appears unaltered in *Tcaf3(C4)*$^{-/-}$ mice (Figure 2) implies that F1/I-A^b-specific Treg cells exist in the repertoires of both mice, as has been observed at the clonal level in fixed TCRβ mice [87].

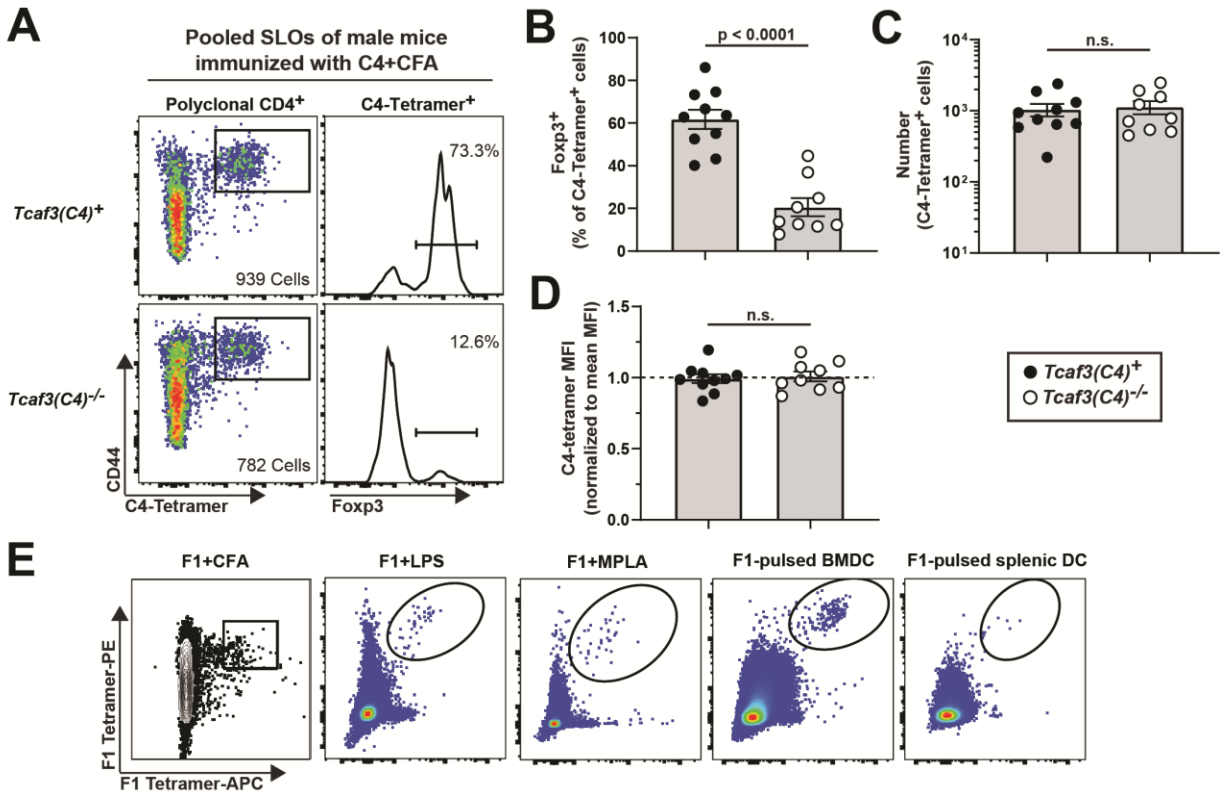

FIGURE 4. T cell selection on C4/I-A^b promotes a Treg-dominated antigen-specific response to C4 peptide immunization.

(A-D) 4-8 week old naïve *Tcaf3(C4)*$^+$ or *Tcaf3(C4)*$^{-/-}$ male littermate mice were immunized subcutaneously with 100mg of C4 peptide emulsified in CFA. 14 days after immunization, CD4$^+$ T cells were isolated and C4/I-A^b tetramer-binding cells were enriched from the pooled SLOs and analyzed by flow cytometry. Data are pooled from three independent experiments and representative of 7 independent experiments where C4/I-A^b tetramer$^+$ T cells were FACS-sorted for single-cell paired ab TCR chain sequencing. (A) Representative flow cytometric analysis of CD4$^+$ T cells enriched from the pooled SLOs of mice of the indicated genotype. The left plots depict CD44 vs. C4/I-A^b tetramer-PE expression by polyclonal CD4$^+$ T cells, whereas the right plots depict Foxp3 expression by CD44^{HI} C4/I-A^b tetramer$^+$ CD4$^+$ T cells. The absolute number of cells (left) and frequency of cells (right) within the indicated gates is denoted. (B) Summary plot of data pooled from (A) showing the frequency of CD44^{HI} C4/I-A^b tetramer$^+$ CD4$^+$ cells expressing Foxp3, enriched from the pooled SLOs from mice of the indicated genotype. Each symbol represents one mouse. n = 10, *Tcaf3(C4)*$^+$; n = 9 *Tcaf3(C4)*$^{-/-}$. (C) Summary plot of pooled data from (A) showing the absolute number of CD44^{HI} C4/I-A^b tetramer$^+$ CD4$^+$ cells enriched from the pooled SLOs from mice of the indicated genotype. Each symbol represents one mouse. n = 10, *Tcaf3(C4)*$^+$; n = 9 *Tcaf3(C4)*$^{-/-}$. (D) Summary plots of pooled data from (A) showing the mean fluorescent intensity (MFI) of C4/I-Ab tetramer-PE for CD44^{HI} C4/I-A^b tetramer$^+$ CD4$^+$ cells enriched from mice of the indicated genotype, normalized to the mean MFI of all CD44^{HI} C4/I-A^b tetramer$^+$ CD4$^+$ cells in each independent experiment. Each symbol represents one mouse. n = 10, *Tcaf3(C4)*$^+$; n = 9 *Tcaf3(C4)*$^{-/-}$. Mean ± SEM is indicated. (n.s., not significant $p > 0.05$; two-tailed nonparametric Mann-Whitney test). (E) Wild-type B6 male mice were immunized with the F1 peptide using the following strategies: subcutaneous in CFA,

FIGURE 4, continued
intravenously using peptide-pulsed and LPS-stimulated BMDCs or splenic DCs, co-administered intravenously with LPS or MPLA. Following immunization, F1/I-A^b tetramer-binding cells were isolated from the pooled SLOs and analyzed by flow cytometry. Representative flow cytometric analysis of $CD4^+$ T cells isolated from the pooled SLOs of mice. Data are representative of 1-2 independent experiments per condition.

In a T cell reconstitution setting, selection on C4/I-A^b is required to prevent T cell infiltration of the prostate

Given that *Tcaf3(C4)*$^{-/-}$ mice mount a C4/I-A^b-specific response dominated by Tconv cells upon immunization, we sought to determine whether T cell selection on the C4/I-A^b complex alone has functional implications for prostate-specific autoimmunity in the absence of additional repertoire changes to other Treg or Tconv specificities. *Tcaf3(C4)*$^{-/-}$ mice lack expression of the C4 peptide in the prostate and therefore do not develop prostatic T cell infiltration or hallmarks of prostatitis (data not shown). To create an experimental system in which T cell-dependent prostatitis could be assessed, we performed cell transfer experiments in which 10^7 bulk $CD4^+$ T cells isolated from *Tcaf3(C4)*$^+$ or *Tcaf3(C4)*$^{-/-}$ males were transferred into αβ T cell-deficient *Tcrb*$^{-/-}$*Tcaf3(C4)*$^+$ male recipients, and assessed the impact on T cell infiltration of the prostate 9 weeks post-transfer (Figure 5, A). In this way, $CD4^+$ T cells that developed in the presence or absence of the C4 peptide (from *Tcaf3(C4)*$^+$ or *Tcaf3(C4)*$^{-/-}$ donor males, respectively) were engrafted into male mice that express the C4 peptide in the prostate. Strikingly, our data revealed that in most recipient mice, the transfer of donor $CD4^+$ T cells from *Tcaf3(C4)*$^{-/-}$ males resulted in prostatic infiltration by C4/I-A^b-specific T cells and polyclonal $CD4^+$ T cells (Figure 5, B-E). In stark contrast, transfer of $CD4^+$ T cells from *Tcaf3(C4)*$^+$ males induced negligible T cell infiltration of the prostate (Figure 5, B-E). Importantly, C4/I-A^b tetramer$^+$ cells were readily isolated from control cohorts of *Tcrb*$^{-/-}$ recipients that received $CD4^+$ T cells from *Tcaf3(C4)*$^+$ donors and were subsequently immunized

with the C4 peptide plus complete Freud's adjuvant (CFA), demonstrating that C4/I-A^b-specific T cells exist in the peripheral repertoire of *Tcaf3(C4)*$^+$ donor mice and repopulate the peripheral repertoire of recipient mice following T cell transfer (Figure 6, A-B). For recipient mice that received T cells from *Tcaf3(C4)*$^{-/-}$ donors, C4/I-A^b tetramer$^+$ T cells in the prostate were largely Foxp3^{neg} (Figure 5, F), whereas Foxp3$^+$ Treg cells accounted for ~23% of polyclonal C4/I-A^b tetramer-negative CD4$^+$ T cells at this site (Figure 5, G). Consistent with these observations, histological analysis demonstrated that some mice receiving T cells from *Tcaf3(C4)*$^{-/-}$ donors developed mild or severe experimental autoimmune prostatitis [353], characterized by overt hallmarks of disrupted tissue architecture and massive infiltration of CD3$^+$ T cells within prostatic glandular structures (Figure 6, C). Notably, F1/I-A^b tetramer$^+$ T cells were rare or not detected in the prostates of recipients reconstituted with T cells from *Tcaf3(C4)*$^{-/-}$ donors (Figure 5, H-I), demonstrating that the breach in tolerance to C4 peptide did not extend to the Tcaf3-derived F1 peptide. These collective findings demonstrate that in this cell transfer setting, T cell selection on a single self-pMHC-II complex, C4/I-A^b, during formation of the T cell repertoire is required to prevent prostatic T cell infiltration by C4-specific Tconv cells and additional polyclonal CD4$^+$ T cells of undefined specificity. Importantly, other Treg cell specificities in the donor cell repertoire, including those reactive to the F1 peptide, were unable to functionally compensate for alterations in the pool of C4-specific T cells, suggesting that pMHC-II-nonspecific "bystander" mechanisms of Treg cell suppression were unable to prevent autoimmune attack by C4-specific Tconv cells in this setting.

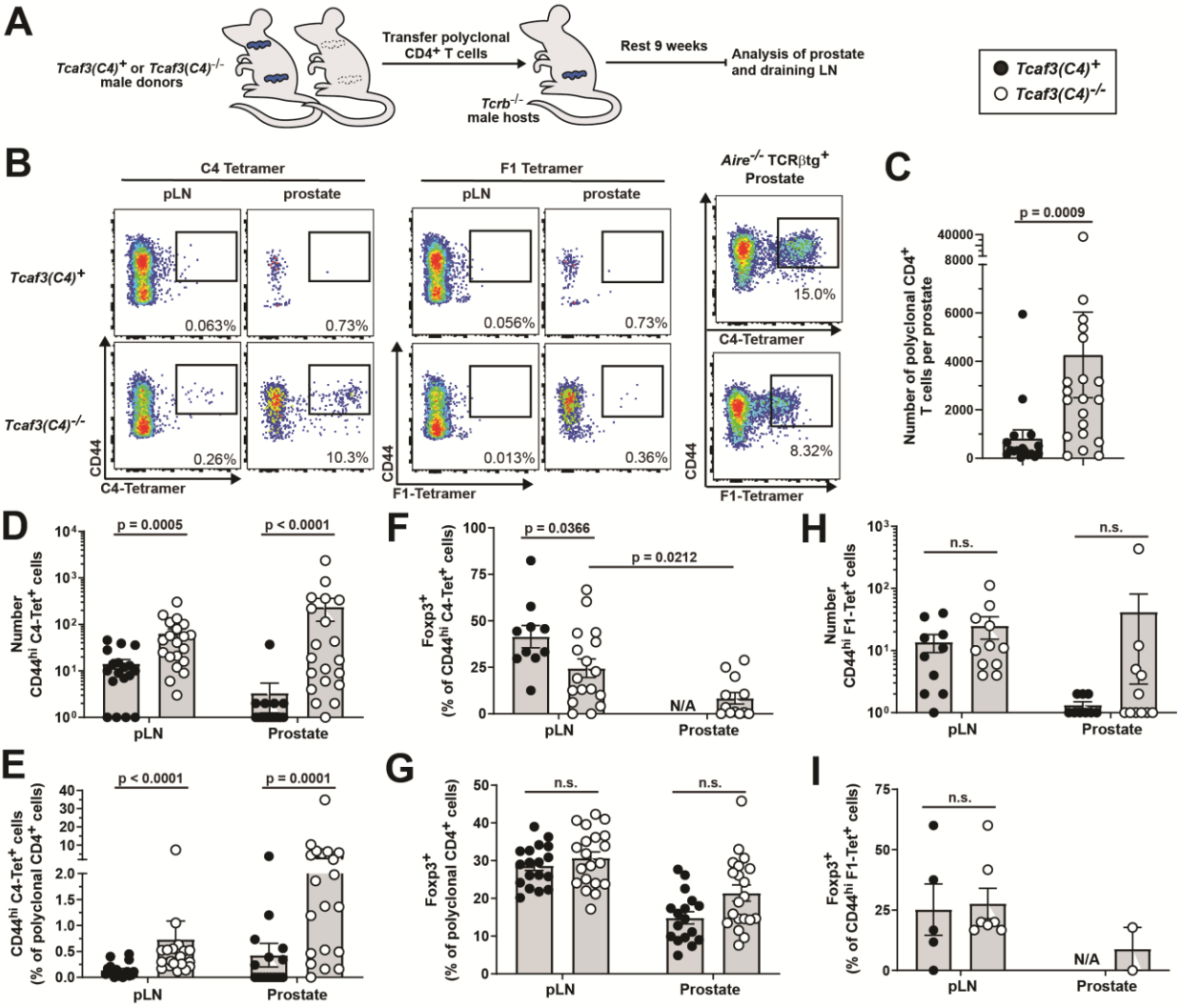

FIGURE 5. In a T cell reconstitution setting, T cell selection on C4/I-A^b is required to prevent T cell infiltration of the prostate.

(A) 10^7 polyclonal CD4$^+$ T cells were isolated from the pooled secondary lymphoid organs (SLOs) of 8-12 week old *Tcaf3(C4)*$^+$ or *Tcaf3(C4)*$^{-/-}$ male donors and transferred intravenously into *Tcrb*$^{-/-}$ *Tcaf3(C4)*$^+$ male littermate recipients. 9 weeks after transfer, the fate of transferred T cells was assessed in the prostate-draining lymph nodes (pLN) or prostate. Data are pooled from 3-6 independent experiments. (B) Representative flow cytometric analysis of CD4$^+$ T cells isolated from the indicated *Tcrb*$^{-/-}$ host males of the indicated genotype. The left plots depict CD44 vs. C4/I-A^b tetramer-PE expression by polyclonal CD4$^+$ cells, whereas the right plots depict CD44 vs. F1/I-A^b tetramer-APC expression by polyclonal CD4$^+$ cells. The frequency of cells within the indicated gates is denoted. (Right) Representative flow cytometric analysis of CD4$^+$ T cells isolated from the prostate of an *Aire*$^{-/-}$ male expressing a fixed TCRβ transgene as C4/I-A^b and F1/I-A^b tetramer staining positive controls. (C) Summary plot of pooled data showing the absolute number of polyclonal CD4$^+$ cells isolated from the prostates of host mice. Each symbol represents one mouse. n = 18, *Tcaf3(C4)*$^+$ pLN; n = 17, *Tcaf3(C4)*$^+$ prostate, n = 20 *Tcaf3(C4)*$^{-/-}$. Mean ± SEM is indicated. (two-tailed nonparametric Mann-Whitney test). (D) Summary plot of the pooled data showing the absolute number of CD44^{HI} C4/I-A^b tetramer$^+$

FIGURE 5, continued
$CD4^+$ cells isolated from the indicated organs of host mice. Each symbol represents one mouse. n = 18, *Tcaf3(C4)*$^+$ pLN; n = 17, *Tcaf3(C4)*$^+$ prostate, n = 20 *Tcaf3(C4)*$^{-/-}$. Mean ± SEM is indicated. (two-tailed nonparametric Mann-Whitney test). (E) Summary plot of the pooled data showing the frequency of $CD44^{HI}$ C4/I-A^b tetramer$^+$ $CD4^+$ cells amongst polyclonal $CD4^+$ T cells isolated from the indicated organs of host mice. Each symbol represents one mouse. n = 18, *Tcaf3(C4)*$^+$ pLN; n = 17, *Tcaf3(C4)*$^+$ prostate, n = 20 *Tcaf3(C4)*$^{-/-}$. Mean ± SEM is indicated. (two-tailed nonparametric Mann-Whitney test). (F) Summary plot of the pooled data showing the frequency of $CD44^{HI}$ C4/I-A^b tetramer$^+$ $CD4^+$ cells expressing Foxp3, isolated from the indicated organs of host mice. Each symbol represents one mouse. n = 10, *Tcaf3(C4)*$^+$ pLN; n = 17 *Tcaf3(C4)*$^{-/-}$ pLN; n = 12 *Tcaf3(C4)*$^{-/-}$ prostate. Mean ± SEM is indicated. (N/A, not applicable; two-tailed nonparametric Mann-Whitney test). (G) Summary plot of the pooled data showing the frequency of polyclonal $CD4^+$ T cells expressing Foxp3, isolated from the indicated organs of host mice. Each symbol represents one mouse. n = 18, *Tcaf3(C4)*$^+$ pLN; n = 17, *Tcaf3(C4)*$^+$ prostate, n = 20 *Tcaf3(C4)*$^{-/-}$. Mean ± SEM is indicated. (n.s., not significant $p > 0.05$; two-tailed nonparametric Mann-Whitney test). (H) Summary plot of the pooled data showing the absolute number of $CD44^{HI}$ F1/I-A^b tetramer$^+$ $CD4^+$ cells isolated from the indicated organs of host mice. Each symbol represents one mouse. n = 10, *Tcaf3(C4)*$^+$ pLN; n = 9, *Tcaf3(C4)*$^+$ prostate, n = 11 *Tcaf3(C4)*$^{-/-}$. Mean ± SEM is indicated. (n.s., not significant $p > 0.05$; two-tailed nonparametric Mann-Whitney test). (I) Summary plot of the pooled data showing the frequency of $CD44^{HI}$ F1/I-A^b tetramer$^+$ $CD4^+$ cells expressing Foxp3, isolated from the indicated organs of host mice. Each symbol represents one mouse. n = 5, *Tcaf3(C4)*$^+$ pLN; n = 7 *Tcaf3(C4)*$^{-/-}$ pLN; n = 2 *Tcaf3(C4)*$^{-/-}$ prostate. Mean ± SEM is indicated. (n.s., not significant $p > 0.05$; N/A, not applicable; two-tailed nonparametric Mann-Whitney test).

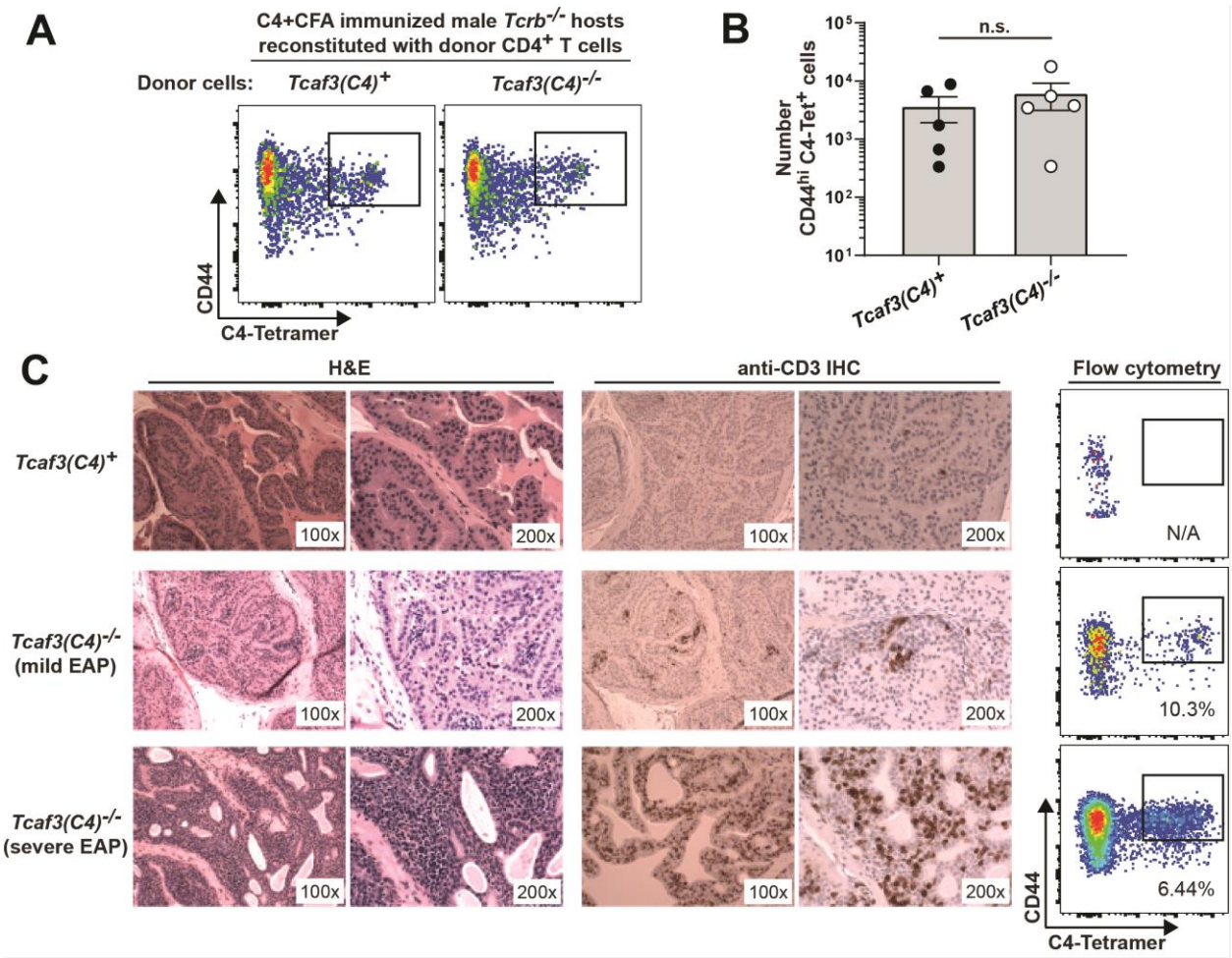

FIGURE 6. In a T cell reconstitution setting, C4/I-A^b-specific T cells drive prostatitis only when derived from *Tcaf3(C4)*$^{-/-}$ donors. Related to Figure 5

(A-B) Following T cell transfer, C4/I-A^b-specific T cells are detectable in recipient mice following peptide immunization. 10^7 polyclonal CD4$^+$ T cells were isolated from the pooled secondary lymphoid organs (SLOs) of 8-12 week old *Tcaf3(C4)*$^+$ or *Tcaf3(C4)*$^{-/-}$ male donors and transferred intravenously into *Tcrb*$^{-/-}$ *Tcaf3(C4)*$^+$ male littermate recipients. 3 weeks post-transfer, host mice were immunized subcutaneously with 100 µg of C4 peptide emulsified in CFA. 14 days after immunization, CD4$^+$ T cells were isolated from the pooled SLOs and analyzed by flow cytometry. (A) Representative flow cytometric analysis depicting CD44 vs. C4/I-A^b tetramer expression by polyclonal CD4$^+$ T cells, isolated from the pooled SLOs of recipient *Tcrb*$^{-/-}$ males of the indicated genotype. (B) Summary plot of pooled data showing the absolute number of CD44^{HI} C4/I-A^b tetramer$^+$ CD4$^+$ T cells isolated from the pooled SLOs of recipient *Tcrb*$^{-/-}$ males of the indicated genotype. Each symbol represents one mouse. n = 5, *Tcaf3(C4)*$^+$; n = 5 *Tcaf3(C4)*$^{-/-}$. Mean ± SEM is indicated. (n.s., not significant $p > 0.05$; two-tailed Mann-Whitney test). Data are representative of three independent experiments. (C) T cell-deficient mice reconstituted with CD4$^+$ T cells from *Tcaf3(C4)*$^{-/-}$ donors can develop mild or severe prostatitis. *Tcrb*$^{-/-}$ mice were reconstituted as in (A). 9 weeks after transfer, lobes from one side of the prostate were taken for tissue pathology, while lobes from the contralateral side were analyzed by flow cytometry. Representative hematoxylin and eosin (H&E) images (left),

FIGURE 6, continued
anti-CD3 immunohistochemistry (IHC) images (middle), and flow cytometric analysis depicting CD44 vs. C4/I-A^b tetramer expression by polyclonal $CD4^+$ T cells (right) of the prostates from host mice. The image magnification (left and middle) and frequency of cells within the indicated gates (right) is denoted (N/A, not applicable); scale bars 100μm at 10x, 50μm at 20x. Of 6 recipient mice that received $CD4^+$ donor cells from *Tcaf3(C4)*$^{-/-}$ males and were subjected to histological analysis, 2 presented with experimental autoimmune prostatitis (EAP) and 3 contained $CD3^+$ cell clusters in the prostate. 0 of 5 mice that received $CD4^+$ cells from *Tcaf3(C4)*$^+$ donors developed EAP or contained $CD3^+$ cell clusters in the prostate.

C4 peptide immunization does not induce the peripheral differentiation of C4/I-A^b-specific Treg cells from Tconv cells

Collective evidence from previous studies [87,102,138] demonstrates that C4/I-A^b directs Treg cell differentiation in the thymus. Consistent with this, we found that C4/I-A^b tetramer$^+$ cells elicited by peptide immunization uniformly express high densities of Helios (Figure 7, A-B), which has been implicated as a potential marker of thymus-derived Treg cells [158]. Nonetheless, it remained possible that pTreg cells contribute to the pool of C4/I-A^b tetramer$^+$ cells following T cell transfer to lymphodeplete hosts, and that this could artificially contribute to the observed autoimmune disease or lack thereof. To assess this possibility, *Tcrb*$^{-/-}$ male recipients were reconstituted with 1 x 10^6 $Foxp3^+$ cells purified from *Foxp3*^{GFP} reporter mice, together with 7 x 10^6 $Foxp3^{neg}$ cells purified from congenically distinct *Foxp3*^{GFP} mice. Three weeks later, recipient mice were immunized with C4 peptide plus CFA and analyzed at two weeks post-challenge (Figure 7, C). Of the C4/I-A^b tetramer$^+$ $Foxp3^+$ Treg cells elicited by immunization, nearly all $Foxp3^+$ cells were derived from the pre-existing $Foxp3^+$ donor cell population, whereas C4/I-A^b $Foxp3^{neg}$ cells were largely derived from the $Foxp3^{neg}$ donor cell population, indicating that immunization-induced pTreg cells make minimal contributions to the pool of C4-specific Treg cells following *Tcrb*$^{-/-}$ reconstitution or peptide immunization (Figure 7, D-E).

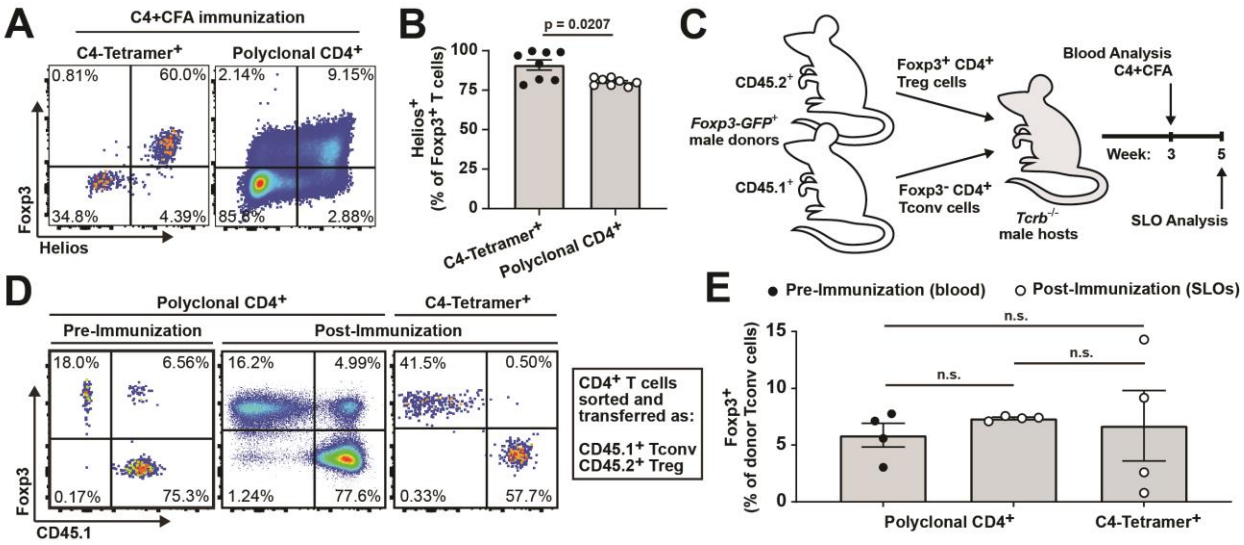

FIGURE 7. C4 peptide immunization does not induce the peripheral differentiation of C4/I-A^b-specific Treg cells from Tconv cells

(A-B) 4-6 week old naïve *Tcaf3(C4)*$^+$ or *Tcaf3(C4)*$^{-/-}$ male and female littermate mice were immunized subcutaneously with 100µg of C4 peptide emulsified in CFA. 14 days after immunization, CD4$^+$ T cells were isolated and C4/I-A^b tetramer-binding cells were enriched from the pooled SLOs, and analyzed by flow cytometry. Data are representative of two independent experiments. (A) Representative flow cytometric analysis of CD4$^+$ T cells enriched from the pooled SLOs of mice of the indicated genotype depicting Foxp3 vs. Helios expression by double C4/I-A^b tetramer$^+$ CD4$^+$ T cells (left) and polyclonal CD4$^+$ T cells (right). The frequency of cells within the indicated gates is denoted. (B) Summary plot of data pooled from (A) showing the frequency of double C4/I-A^b tetramer$^+$ CD4$^+$ Foxp3$^+$ Treg cells or polyclonal CD4$^+$ Foxp3$^+$ Treg cells expressing Helios, enriched from the pooled SLOs from mice of the indicated genotype. Each symbol represents one mouse (n = 8). Mean ± SEM is indicated. (two-tailed nonparametric Mann-Whitney test). (C) Experimental schematic for panels (D-E). 1 x 10^6 Foxp3$^+$ CD45.2$^+$ and 7 x 10^6 Foxp3^{neg} CD4$^+$ CD45.1$^+$ T cells were sorted from congenically disparate Foxp3-GFP male donors and co-transferred into *Tcrb*$^{-/-}$male littermate recipients. 3 weeks after transfer, blood was collected and analyzed by flow cytometry, and mice were immunized subcutaneously with 100µg C4 peptide emulsified in CFA. 14 days after immunization, CD4$^+$ T cells were isolated from the pooled SLOs of recipient mice, stained with C4/I-A^b tetramer, and analyzed by flow cytometry. Data are representative of two independent experiments. (D) Representative flow cytometric analysis depicting CD45.1 vs. Foxp3 expression by CD4$^+$ T cells isolated from host mice. The left plot depicts polyclonal CD4$^+$ T cells isolated from the blood pre-immunization, the middle plot depicts polyclonal CD4$^+$ T cells isolated from the pooled SLOs post-immunization, and the right plot depicts double C4/I-A^b tetramer$^+$ CD4$^+$ T cells isolated from the pooled SLOs post-immunization. The frequency of cells within the indicated gates is denoted. (E) Summary plot of pooled data from (D) showing the frequency of Foxp3$^+$ cells amongst congenically-marked CD4$^+$ T cells that were initially transferred as Foxp3^{neg} Tconv cells. Each symbol represents one mouse (n = 4). Mean ± SEM is indicated. (n.s., not significant $p > 0.05$; two-tailed nonparametric Mann-Whitney test).

Bim deficiency does not impact the C4/I-A^b tetramer staining intensity of polyclonal C4-specific CD4$^+$ T cells

Given the critical nature of T cell selection on the C4/I-A^b complex, whose action seems to be most evident in the thymus, we set out to define how selection on C4/I-A^b impacts the thymic development of C4-specific T cells. In previous work, we demonstrated that the thymic development of monoclonal MJ23tg Treg cells requires Aire [102], and is dependent on expression of the C4 peptide [138]. Because Aire has been proposed to promote both clonal deletion and Treg cell generation [107], we sought to determine whether thymic presentation of the C4 peptide drives one or both of these alternate cell fates. Extensive characterization of monoclonal MJ23 T cells in the thymus of *Tcaf3(C4)*$^+$ and *Tcaf3(C4)*$^{-/-}$ mice revealed no evidence of clonal deletion, but confirmed a critical requirement for the development of MJ23 Treg cells [101]. However, Experimental limitations precluding the faithful identification of endogenous C4-specific T cells in naïve mice (discussed with Figure 3) hindered our ability to perform a similar characterization of endogenous C4/I-A^b-specific thymocytes. To circumvent this, we instead performed studies to determine the extent to which clonal deletion impacts the polyclonal peripheral pool of C4-specific CD4$^+$ T cells. To do this, we utilized mice lacking the pro-apoptotic protein Bim, which exhibit defects in T cell clonal deletion [354], with the rationale that *Bim*$^{-/-}$T cells would constitute a greater relative proportion of the peripheral C4/I-A^b-specific T cell pool than *Bim*$^{+/+}$ cells if they were able to circumvent clonal deletion.

We generated mixed BMCs in which lethally irradiated wild-type host mice were reconstituted with a 50%-50% mixture of T cell-depleted bone marrow from congenically disparate *Bim*$^{+/+}$ and *Bim*$^{-/-}$ donors. 5-8 weeks later, we immunized chimeric mice with C4 peptide plus CFA, and quantified the relative contributions of the *Bim*$^{+/+}$ and *Bim*$^{-/-}$ compartments to the

pool of C4/I-A^b tetramer$^+$ T cells. In immunized BMC mice, we found that C4/I-A^b tetramer$^+$ C4-specific T cells derived from *Bim*$^{-/-}$ bone marrow accounted for a major fraction (71.4±13%) of C4/I-A^b tetramer$^+$ cells (Figure 8, A-B). However, this percentage was comparable to that of tetramer-negative polyclonal CD4$^+$ T cells derived from *Bim*$^{-/-}$ precursors in the same mice (74.4±7%). Likewise, the fraction of CD8□$^+$ T cells and B220$^+$ B cells derived from the *Bim*$^{-/-}$ compartment was also elevated (accounting for 78.3±9% and 88.8±2% of cells, respectively) in chimeric mice (Figure 8, A-B). These findings raised the possibility that the increased proportions of lymphocytes derived from *Bim*$^{-/-}$ bone marrow could be due in part to preferential engraftment and survival of *Bim*$^{-/-}$ hematopoietic precursors, rather than a lack of Bim-dependent deletion of T cells or B cells, making it challenging to draw conclusions by examining relative ratios of T cells derived from the *Bim*$^{-/-}$ and *Bim*$^{+/+}$ compartments. For this reason, we focused our analysis on a paired comparison of C4/I-A^b tetramer$^+$ T cells derived from *Bim*$^{-/-}$ and *Bim*$^{+/+}$ precursors of immunized mice. If high-avidity C4-specific clones undergo clonal deletion, we reasoned that the mean fluorescent intensity (MFI) of C4/I-A^b tetramer staining, a surrogate marker of TCR-pMHC-II avidity [355,356], would be greater for C4/I-A^b tetramer$^+$ cells derived from *Bim*$^{-/-}$ precursors. However, this comparison revealed no detectable differences in the MFI of tetramer staining between *Bim*$^{-/-}$ and *Bim*$^{+/+}$ C4/I-A^b tetramer$^+$ T cells (Figure 8, C), suggesting that Bim deficiency does not impact the average avidity of polyclonal C4-specific T cells elicited by peptide immunization. Taken together, our studies of monoclonal and polyclonal populations suggest that C4-dependent clonal deletion has a negligible impact on the peripheral pool of antigen-specific T cells.

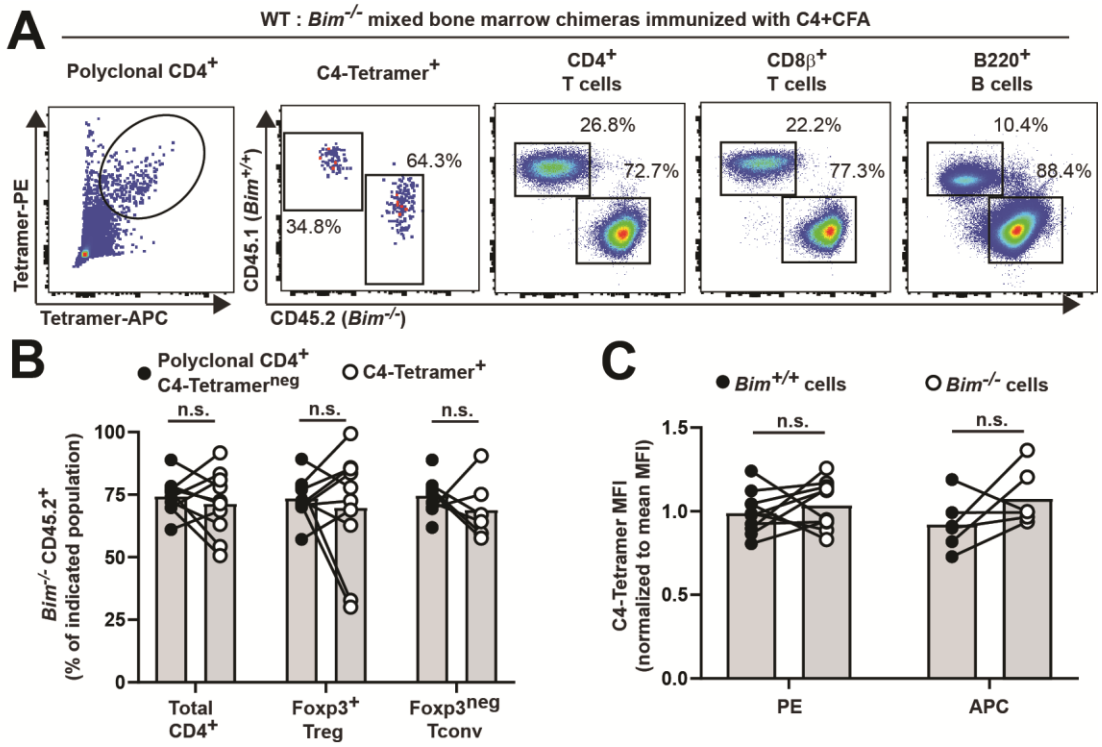

FIGURE 8. C4/I-A^b-dependent clonal deletion does not impact the endogenous pool of C4/I-A^b- specific polyclonal CD4$^+$ T cells

6-8 week-old B6.SJL (CD45$^{.1/.1}$) male littermate mice were lethally irradiated and reconstituted with a 1:1 mixture of *Bim*$^{+/+}$ (CD45.1) and *Bim*$^{-/-}$ (CD45.2) bone marrow. 5-8 weeks post-engraftment, mice were immunized subcutaneously with 100 µg of C4 peptide emulsified in CFA. 14 days after immunization, CD4$^+$ T cells were isolated and C4/I-A^b tetramer-binding cells were enriched from the pooled SLOs and analyzed by flow cytometry. Data are representative of two independent experiments. (A) Representative flow cytometric analysis of polyclonal C4/I-A^b tetramer$^+$, CD4$^+$, CD8β$^+$, and B220$^+$ cells enriched from the pooled SLOs of immunized mixed bone marrow-chimeric mice. The left plot depicts dual C4/I-A^b tetramer expression by polyclonal CD4$^+$ T cells, whereas the right plots depicts CD45.2 vs. CD45.1 expression by C4/I-A^b tetramer$^+$, CD4$^+$, CD8β$^+$, and B220$^+$ cells. The frequency of cells within the indicated gates is denoted. (B) Summary plot of data pooled from (D) showing the frequency of C4/I-A^b tetramer^{neg} and C4/I-A^b tetramer$^+$ CD4$^+$ T cells expressing CD45.2, enriched from the SLOs of immunized mixed bone marrow-chimeric mice. Each symbol represents one mouse (n = 10). Mean ± SEM is indicated. (n.s., not significant $p > 0.05$; Wilcoxon matched-pairs signed rank test). (C) Summary plots of pooled data from (A) showing the mean fluorescent intensity (MFI) of C4/I-A^b tetramer-PE and C4/I-A^b tetramer-APC by C4/I-A^b tetramer$^+$ CD4$^+$ CD45.2$^+$ and C4/I-A^b tetramer$^+$ CD4$^+$ CD45.1$^+$ cells enriched from the SLOs of immunized mixed bone marrow-chimeric mice, normalized to the mean MFI of all C4/I-A^b tetramer$^+$ CD4$^+$ cells in each independent experiment. Each symbol represents one mouse. n = 10, PE; n = 6, APC. Mean ± SEM is indicated. (n.s., not significant $p > 0.05$; Wilcoxon matched-pairs signed rank test).

Thymic-grafted Nude mice do not develop spontaneous prostatitis in the absence of thymic C4 peptide expression

The experimental results laid out in this study indicate that 1) T cell selection on C4/I-A^b promotes the development of antigen-specific Treg cells in the thymus that seed the periphery, 2) C4/I-A^b-specific Treg and Tconv cells expand upon immunization of *Tcaf3(C4)*$^+$ male mice with minimal conversion to pTreg cells, and 3) a T cell repertoire that developed in the absence of the C4 peptide, and is therefore largely devoid of C4/I-A^b-specific Treg cells, can elicit prostatic autoimmunity upon transfer into secondary lymphodeplete recipients that harbor the C4 peptide. However, since the repertoire that develops in a *Tcaf3(C4)*$^{-/-}$ male host lacks C4 peptide expression in both the thymus and periphery, it remained unclear whether C4 peptide is exclusively required in the thymus to prevent autoimmune disease, or if C4/I-A^b recognition in the periphery also played a role in maintaining tolerance. To test this, we performed grafting experiments in which fetal thymi from *Tcaf3(C4)*$^+$ or *Tcaf3(C4)*$^{-/-}$ donor mice were depleted of endogenous thymocytes and grafted under the kidney capsule of nude (*Foxn1*$^{-/-}$) male recipients which lack endogenous thymi but retain C4 peptide expression in the prostate. In this way, thymocytes in the grafted mice would develop in the presence or absence of thymic C4 peptide, but would have access to C4 peptide in the periphery upon thymic egress and without the need for T cell transfer. Unexpectedly, we were unable to identify many C4/I-A^b tetramer$^+$ cells in the pooled SLOs of mice with grafts of either genotype (Figure 9, A-B), nor did *Tcaf3(C4)*$^{-/-}$-grafted hosts develop overt signs of prostatic T cell infiltration (Figure 9, C-E). These results potentially indicate that C4 peptide expression in the thymus alone is not required to protect mice from autoimmunity and that peripheral C4 peptide may add an additional layer of tolerance to the host. A noteworthy caveat to this conclusion is that a vast majority of the CD4$^+$ T cell compartment in the grafted mice exhibited an activated CD44^{HI}

phenotype, which starkly differs from the same compartment in wild-type mice (Figure 9, F) likely due to artificial homeostatic proliferation in the lymphodeplete grafted hosts, and may have prevented proper seeding of C4/I-A^b-specific T cells into the periphery of these mice. Nevertheless, potential mechanisms of tolerance mediated by peripheral C4 peptide could include functional inactivation (permanent or temporary) of C4/I-A^b-specific Tconv cells following C4/I-A^b recognition in the periphery [357], or a hypothetical "training" mechanism whereby rare C4/I-A^b Treg cells in *Tcaf3(C4)*$^{-/-}$ grafted mice outcompete their Tconv counterparts in the prostate-draining LNs. These and other possibilities will be addressed and discussed using various model systems in subsequent chapters.

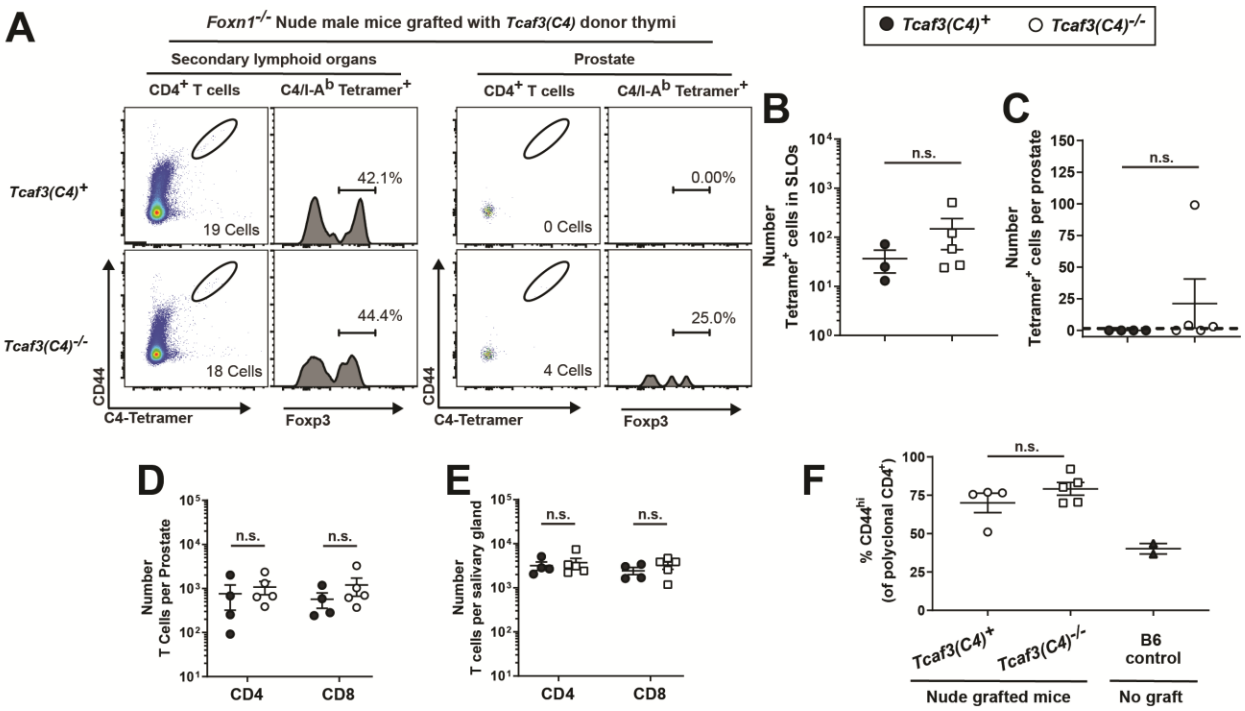

FIGURE 9. *Tcaf3(C4)*$^{-/-}$ thymic-grafted nude mice do not develop spontaneous prostatitis

Foxn1$^{-/-}$ nude male mice lacking an endogenous thymus were surgically grafted in the kidney capsule with *Tcaf3(C4)*$^{+}$ or *Tcaf3(C4)*$^{-/-}$ thymi, which had been depleted of endogenous thymocytes for 7 days in vitro with 2-deoxyguanosine. 10 weeks post-surgery, CD4^{+} T cells were enriched from the pooled secondary lymphoid organs (SLOs) or isolated from the prostates of mice of the indicated genotype. n = 4, *Tcaf3(C4)*$^{+}$, n = 5 *Tcaf3(C4)*$^{-/-}$. Data are representative of two independent experiments. (A) Representative flow cytometric analysis of CD4^{+} T cells isolated from the indicated hosts of the indicated genotype. Plots depict dual C4/I-A^{b} tetramer expression by polyclonal CD4^{+} T cells and Foxp3 expression by double C4/I-A^{b} tetramer^{+} CD4+ T cells, isolated from the SLOs or prostate. (B) Summary plot of pooled data from (A) showing the absolute number of double C4/I-A^{b} tetramer^{+} CD4^{+} cells enriched from the pooled SLOs of mice of the indicated genotype. Each symbol represents one mouse. Mean ± SEM is indicated. (C) Summary plot of pooled data from (A) showing the absolute number of double C4/I-A^{b} tetramer^{+} CD4^{+} cells isolated from the prostate of mice of the indicated genotype. Each symbol represents one mouse. Mean ± SEM is indicated. (D) Summary plot of pooled data from (A) showing the absolute number of polyclonal CD4^{+} or CD8β^{+} cells isolated from the prostates of mice of the indicated genotype. Each symbol represents one mouse. Mean ± SEM is indicated. (E) Summary plot of pooled data from (A) showing the absolute number of polyclonal CD4^{+} or CD8β^{+} cells isolated from the salivary glands of mice of the indicated genotype. Each symbol represents one mouse. Mean ± SEM is indicated. (F) Summary plot of pooled data from (A) showing the frequency of polyclonal CD4^{+} T cells expressing CD44 enriched from the pooled SLOs of mice of the indicated genotype. The frequency of polyclonal CD4^{+} T cells expressing CD44 in the spleen of naive B6 mice are included as a homeostatic control. Each symbol represents one mouse. Mean ± SEM is indicated. (n.s., not significant $p > 0.05$; two-tailed nonparametric Mann-Whitney test).

Phenotype and antigen specificity of Tconv clones identified in the ocular autoimmune lesions of Aire$^{-/-}$ mice

This study addressed whether the absence of a single prostate-derived peptide during T cell repertoire selection rendered mice susceptible to autoimmune disease. While we anticipate that the principles explored for the C4 peptide would extend to other immunodominant autoantigens, and studies in later chapters will continue to use this model system to tackle fundamental questions of autoimmune susceptibility and mechanisms of protection. While the in-depth investigation of the C4 peptide enabled novel insight, demonstrating these principles for a single peptide also remains a limitation of the study. To begin to address this concern, we aimed to 1) identify novel T cell clones that recurrently infiltrate autoimmune lesions, 2) identify the antigen-specificity or class of antigen recognized by these clones, 3) characterize the development and phenotype of these clones at steady-state and upon transfer to secondary immunodeficient or immunodeplete hosts.

We sorted CD4+ T cell clones from the ocular lesions of 5 *Aire*$^{-/-}$ mice, which develop spontaneous autoimmune disease to multiple organs including the eyes [124]. We also crossed these mice to mice expressing the TCRβ chain of the MJ23 T cell clone [102]. In this way, each T cell would express the same TCRβ chain, which restricts repertoire diversity to increase the chance of identifying recurrent clones with deep TCRα sequencing, and enables identification of paired αβTCR clones. This approach identified many clones that were enriched in the eyes compared to the spleen, and were found infiltrating the lesions of multiple mice. We focused on two of these clones for our downstream analyses, given that they constituted 2 of the 5 most abundant clones in the eyes and that their TCRs harbored non-overlapping TRAV/TRAJ/CDR3 regions. We termed these clones "EAR" and "GLR" (see *Materials and Methods; TCR gene usage and CDR3*

sequences) and expressed these clones in vivo using an established retrogenic pipeline [331,358] for downstream analyses.

The EAR clone was readily detected in the thymus where it expressed TCR and populated both the CD4SP and CD8SP lineages (Figure 10, A). Surprisingly, expression of CD4 but not CD8 by EAR thymocytes was low when compared to polyclonal thymocytes, reminiscent of co-receptor reversal and conversion to the $CD8^+$ lineage [359], despite the fact that these cells were identified in the $CD4^+$ T cell compartment of *Aire*$^{-/-}$ mice. In the periphery, EAR also populated the $CD4^+$ and $CD8^+$ lineages, but preferentially skewed $CD8^+$, with a minor fraction of cells expressing neither coreceptor. Phenotyping of $CD4^+$ EAR T cells revealed that most cells did not adopt an anergic $CD73^{HI}$ $FR4^{HI}$ or T_{FH} $CXCR5^+$ $PD\text{-}1^+$ phenotype, but that a fraction were $CD69^+$ and $Foxp3^+$ in multiple regional LNs (Figure 10, B), even upon transfer to secondary hosts (Figure 10, C). Given the supraphysiological frequency of EAR cells in the retrogenic hosts, the latter observations imply that the cognate self-antigen for EAR is highly expressed in multiple tissue sites, as Treg clones have a saturable antigenic niche that usually requires low clonal frequencies to efficiently upregulate Foxp3 [44]. Indeed, $CD4^+$ EAR cells cultured with ex vivo splenic DCs + IL-2 but no exogenous peptide displayed low-level proliferation in vitro in an MHC-II-dependent manner. (Figure 10, D), confirming that this clone either recognizes a ubiquitously-expressed self-antigen or can be tonically stimulated by the $I\text{-}A^b$ molecule. Curiously, despite its apparent self-reactive nature, EAR T cells did not readily infiltrate the organs of primary retrogenic or secondary host mice (data not shown).

The GLR clone displayed a surprising pattern of development distinct from that of EAR. Unlike EAR, which readily expressed TCR and was found in the CD4SP and CD8SP compartments of primary retrogenic hosts, GLR thymocytes expressing TCRβ were extremely rare

(Figure 10, A). This could not be explained by poor retroviral transduction, as a large fraction of transduced donor thymocytes expressed the Thy1.1 reporter. Of the few TCRβ^{+} GLR cells, most remained at the DP stage of development, and there were essentially no CD4SP cells. These patterns pervaded into the periphery, where the few TCRβ^{+} GLR cells that existed expressed neither CD4 nor CD8β (Figure 10, A). We next sought to determine the antigen specificity of the GLR clone. Development of uveitis in *Aire*$^{-/-}$ mice on the B6 background requires the Aire-driven dominant autoantigen IRBP [346], so we screened GLR reactivity to a panel of IRBP-derived peptides that we predicted would have high binding affinity to the I-A^{b} molecule [138,360]. We cultured CTV-labeled DN GLR T cells with splenic DCs + IL-2 and single IRBP-derived peptides, and identified 2 adjacent peptides (O and P peptides) that caused robust division of GLR T cells in an MHC-II-dependent manner (Figure 10, D). Interestingly, the overlapping amino acid residues in the O and P peptides had been identified as the CD4^{+} T cell targeted "P7 Peptide" previously [347], where tetramer analysis revealed that P7/I-A^{b}-specific T cells exist in the repertoire of both *Aire*$^{-/-}$ and wild-type mice. This discrepancy withstanding, cumulative GLR data including low TCR expression, apparent arrest at the DP thymocyte stage, seeding of the periphery by non-natural DN T cells, and robust MHC-II-restricted stimulation despite the lack of CD4 coreceptor, collectively suggests that this clone is under strong pressure to undergo negative selection in the thymus.

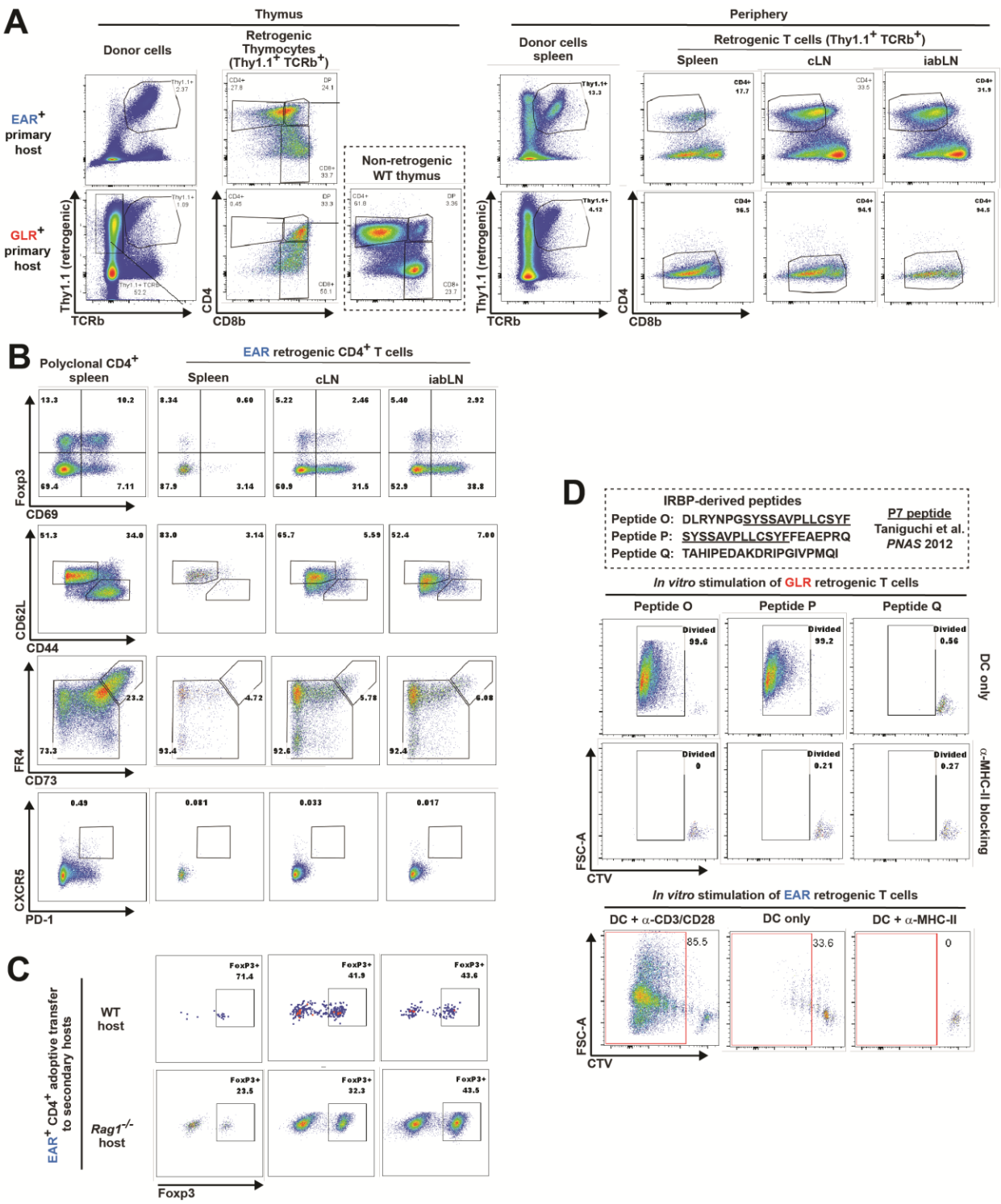

FIGURE 10. Phenotype and antigen specificity of Tconv clones identified in ocular autoimmune lesions of *Aire*$^{-/-}$ mice

CD4^{+} Foxp3^{neg} T cells were FACS sorted from the eyes of *Aire*$^{-/-}$ fixed-β RT3tg^{+} Foxp3-GFP^{+} mice and isolated RNA was subjected to deep TCRα sequencing via the iRepertoire platform. Two of the most abundant TCR clones identified from the sequencing results (termed EAR and

FIGURE 10, continued

GLR) were engineered and expressed in primary retrogenic mice (see Materials and Methods). Data are representative of multiple independent experiments: (A) n = 4; (B) n = 3-4; (C) n = 4; (D) n = 3.

(A) Representative flow cytometric analysis of Retrogenic$^+$ cells isolated from the primary retrogenic host expressing the indicated TCR clone. The plots depict TCRβ vs. Thy1.1 expression by retrogenic donor cells or CD8b vs. CD4 expression by TCRβ$^+$ Thy1.1$^+$ retrognic T cells in the thymus (left) and periphery (right). (B) Phenotype of EAR$^+$ CD4$^+$ T cells in the periphery of mice in (A). The plots depict CD69 vs. Foxp3, CD44 vs. CD62L, CD73 vs. FR4, and PD-1 vs. CXCR5 expression by EAR$^+$ T cells isolated from the indicated organ. (C) 5 x 10^5 EAR$^+$ CD4$^+$ retrogenic cells were FACS sorted and transferred into secondary wild-type or Rag1-deficient recipients. 7 days post-transfer, the Foxp3 status was assessed in the periphery of secondary host mice, The plots depict Foxp3 expression by EAR$^+$ CD4$^+$ donor T cells. (D) In vitro stimulation of GLR$^+$ or EAR$^+$ retrogenic T cells. 1 x 10^4 retrogenic CD4$^+$ T cells were co-cultured with 5 x 10^4 CD11c$^+$ cells isolated from B6 spleens + mIL-2, with the indicated peptide and activating or blocking antibody. Dilution of CTV was assessed by flow cytometry on day 3. Representative flow cytometric analysis of CTV dilution by CD4$^+$ GLR or EAR T cells.

CONCLUSIONS AND DISCUSSION

In this chapter, we use a T cell reconstitution system to demonstrate that altered T cell selection on a single self-pMHC-II complex, C4/I-A^b, renders B6 male mice susceptible to prostate-specific T cell infiltration. This finding indicates that T cell tolerance to the C4/I-A^b self-ligand is pMHC-II-specific, and implies that polyclonal Treg cells reactive to other pMHC-II ligands, including I-A^b complexed with the Tcaf3-derived F1 peptide, are unable to compensate for alterations in the C4/I-A^b-specific T cell pool. Broadly, our findings reveal that pMHC-II non-specific bystander mechanisms of Treg-mediated suppression are insufficient to prevent targeted T cell-mediated autoimmunity in this setting, and imply a crucial requirement for pMHC-II-specific Treg suppression in particular immunological contexts. Ultimately, these concepts demonstrate that vulnerabilities in tolerance to single pMHC-II specificities may predispose individuals to the development of organ-specific autoimmunity, and support a model in which the generation of a diverse Treg cell repertoire spanning a broad array of pMHC-II specificities is essential for maintaining T cell tolerance by providing full "coverage" of antigenic pMHC-II complexes throughout the body.

Pre- and post-immune repertoires of C4/I-A^b-specific T cells

We made an extensive effort to identify and characterize naïve C4/I-A^b T cells in the pre-immune repertoires of *Tcaf3(C4)*$^+$ and *Tcaf3(C4)*$^{-/-}$ mice. We were able to identify ~24 cells per mouse with the tools available at the time (Figure 3). The unexpectedly low number of cells, together with the fact that these cells did not preferentially express Foxp3 in *Tcaf3(C4)*$^+$ mice, bring the quality of the collected data into question. It is noteworthy that a similar study investigating T cell tolerance to proteolipid protein (PLP), a thymus-expressed autoantigen that

drives Treg development of PLP-reactive cells in mice with a fixed TCRβ chain, had naïve precursor frequencies similar to C4/I-A^b-specific T cells and did not overwhelmingly express Foxp3 [103]. TCR recognition of antigen is promiscuous by nature [361] and a relatively low-affinity interaction [362], especially for MHC-II interactions in which long peptides can hang out of the presentation groove and shift register [363], so the conventional C4/I-A^b tetramers used in this study were likely to have missed many low-affinity C4/I-A^b-specific T cells that are elicited during an immune response. Indeed, Jenkins and colleagues recently engineered I-A^b tetramer molecules with an artificially high binding affinity for the CD4 coreceptor and demonstrated a 1.5-4 fold increase in the detectable number of antigen-specific CD4+ T cells elicited by immunization when compared to conventional tetramer reagents [364]. Therefore, while it is clear that C4/I-A^b -specific Treg cells dominate the response following immunization in *Tcaf3(C4)*$^+$ mice (Figure 4) and it can be inferred that the naïve pool of C4/I-A^b -specific T cells is numerically similar between *Tcaf3(C4)*$^+$ and *Tcaf3(C4)*$^{-/-}$ mice [350], the proportion of Foxp3+ cells amongst C4/I-A^b -specific cells in the pre-immune repertoire remains unknown for either genotype. Given that C4/I-A^b is required for the thymic development of monoclonal MJ23 T cells [138], and that many prostate-infiltrating $CD4^+$ T cell clones in Aire-deficient mice are largely directed to the Treg lineage in Aire-sufficient counterparts [87], it is likely that the pre-immune repertoire of C4/I-A^b-specific cells has a higher proportion of Treg cells in *Tcaf3(C4)*$^+$ than in *Tcaf3(C4)*$^{-/-}$ mice. However, not all C4/I-A^b-specific Treg cells develop in a C4 peptide-dependent manner, evidenced by the fact that ~20% of C4/I-A^b-specific T cells elicited by immunization are Treg cells in *Tcaf3(C4)*$^{-/-}$ hosts (Figure 4), which complicates estimations of the relative proportion of Treg cells in the naïve pool that are exclusively directed by C4/I-A^b. It's also known that some tetramer-binding T cells do not contribute to the antigen-specific immune response and responsiveness cannot be predicted by

tetramer staining alone [365], so some C4/I-A^b tetramer-binding cells in the naïve repertoire may not expand at all upon immunization.

Ultimately, the observed Treg phenotypes in the post-immune repertoire of C4/I-A^b-specific cells could be obtained through any of the following pre-immune conditions and scenarios: 1) total reflection - a naïve repertoire that is Treg-dominated in *Tcaf3(C4)*$^+$ but not *Tcaf3(C4)*$^{-/-}$ mice (~60% and 20% Treg, respectively), and all cells expand proportional to one another following immunization, 2) antigen programing - a naïve repertoire that is Tconv-dominated and comparable in mice of both genotypes, but the Tregs have a competitive proliferative advantage upon immunization in *Tcaf3(C4)*$^+$ mice owing to thymic programing of activation thresholds, peripheral ligand training of Treg cells, or antigen-induced anergy of Tconv cells (discussed in Chapter 3), 3) critical clones - a naïve repertoire that is Tconv-dominated in both genotypes, but has a few critical clones populating the Treg compartment in *Tcaf3(C4)*$^+$ mice only, and these clones dominate the response following immunization, 4) absolute number as a fragile parameter - a naïve repertoire that is Tconv-dominated in both genotypes, but *Tcaf3(C4)*$^+$ mice harbor a few more Treg cells with irrelevant clonotypes, and this slight numeric increase provides the Treg population with a competitive advantage over the Tconv population following immunization.

CD4*$^+$ *T cell autoimmune targeting of multiple peptides derived from single immunodominant proteins

Antigen dominance – the tendency for T cell responses against a given agent to be saturated by specificities reactive to a limited set of proteins and epitope derivatives – is a fascinating concept that has been known for decades, observed over a multitude of immune responses and autoimmune diseases, and has been re-exhumed by our current and previous studies [366]. While an

in-depth overview and discussion of antigen dominance hierarchies will be delivered in Chapter 3, the aim here is to direct focus to observations of dominant autoantigens targeted in autoimmune disease. In work foundational to our study, [87,138] the C4 and F1 peptides were identified as recurrent T cell targets derived from a single protein Tcaf3, and it was determined that T cell populations specific for these epitopes are normally enriched for Treg cells at steady-state in wild-type mice, but are dominated by autoimmune-competent Tconv cells absent Aire. Our current study demonstrates the non-redundancy in these two populations: the loss of tolerance to the C4 peptide cannot be compensated by F1/I-A^b-specific T cells that remain tolerant in the system, nor does the breach of tolerance to the C4 peptide break tolerance for T cells reactive to F1 (Figure 5). This independent regulation is corroborated by the observation that C4/I-A^b-specific Treg cells are readily detected in the prostate tumors of TRAMP mice, while F1/I-A^b-specific cells are always absent (data not shown). Notably, C4/I-A^b tetramer$^+$ T cells are relatively easy to identify in wild-type or diseased mice with the proper immune challenge, but F1/I-A^b tetramer$^+$ T cells have been notoriously difficult to elicit with conventional immunization approaches (Figure 4), though not impossible in given proper context (Chapter 3, Figure 31).

The described dominance pattern to Tcaf3 is reminiscent of that observed for other T cell-targeted autoantigens relevant to human and mouse autoimmune disease, including Myelin basic protein [367], Peptidyl arginine deaminase 4 [368,369], proteolipid protein 2 [103,370], insulin 2 [345,348,371,372], and retinol binding protein 3 (or IRBP in mice) [346,347,373]. Specifically, these well-studied autoantigens have a very limited set (two or three per protein) of epitope determinants against which most autoantigen-reactive T cell populations are elicited. Furthermore, the disparate specificities tend to present with distinct patterns of tolerance within the repertoire. Some of these proteins have been demonstrated to be both necessary and sufficient to initiate autoimmune

disease, implying that this entire class of immunodominant autoantigens may sit at the nexus between tolerance and fulminant autoimmune disease. Given their shared pattern with C4 and F1 peptide-responsive T cell populations, we hypothesize that Tcaf3 is also a necessary autoantigen for prostatitis in the mouse, at least to the anterior lobes where Tcaf3 is expressed. Contravening this assertion, it should be noted that multiple prostatic proteins are known targets of Aire in the mouse [133], including Tgm4, which is recurrently targeted by autoantibody targets in humans [374,375]. While this could suggest the existence of T cell populations reactive to multiple immunodominant antigens, it could also be indicative of epitope spreading following a tolerogenic breakdown against a keystone autoantigen (addressed in Chapters 2 and 3). Notably, a Tcaf3 homologue is absent from the human genome, which could provide an opening for a different gatekeeping autoantigen such as Tgm4 in this species.

Insight into the nature of immunodominant antigens might be gleaned from a detailed comparison between Tcaf3, IRBP, and their associated autoreactive T cell populations. An Aire-dependent protein, IRBP has two primary target epitopes in the B6 mouse, termed the "P2" and "P7" peptides [347]. T cells reactive to the "P2" peptide display high susceptibility to deletional tolerance, as evidenced by their presence in *Irbp*$^{-/-}$ but not *Irbp*$^{+/+}$ mice following immunization. Conversely, "P7" reactive T cells are present at similar frequencies in the steady-state repertoires of both genotypes, implying a dependance on peripheral tolerance mechanisms for controlling this population, though Foxp3 expression was never assessed. While F1-specific T cells are certainly not completely absent from the peripheral repertoire (Chapter 3, Figure 31), the difficulty detecting these cells in the steady-state repertoire suggests that their mode of tolerance may be more similar to P2-specific than C4-specific T cells. Accordingly, the apparent tolerance pattern for C4-specific and P7-specific T cells could also be analogous. The assertion is not that the T cell populations

specific for P2/F1 or P7/C4 precisely phenocopy one another, as neither one of these modes of tolerance (central vs peripheral) is absolute for an entire polyclonal population of antigen-specific cells and likely differs on a clonal basis. This is evidenced by our identification of the P7/I-A^b-restricted GLR clone with hallmarks of potent antigen stimulation and an inferred tendency toward clonal deletion (Figure 10), although a formal test of P7-dependent deletion requires a comparison of these metrics between GLR retrogenic mice created in *Aire*$^{+/+}$ and *Aire*$^{-/-}$ hosts and was not performed. The claim instead that immunodominant epitopes may be subjected to differing degrees of central and peripheral tolerance. The basis for this may lie in the concept of "dominant vs cryptic" self epitopes – that some epitopes are readily liberated from proteins and presented ubiquitously while others are only presented in limited contexts [376]. While C4 and F1 antigen are readily presented and accessible in the thymus and periphery of mice, the relative degree of accessibility and context in which these peptides are presented remains unknown. Fundamental differences in presentation between the two sites could include antigen processing via the immunoproteasome [377] and preferential pMHC-II presentation by mTECs or other APC populations. Indeed, thymic APCs differentially present the P2 and P7 peptides following in vitro peptide pulse, though it is unclear whether this can be directly attributed to the different modes of tolerance observed for either specificity. If presentation of C4 and F1 is distinct in the thymus or periphery, this could account for the apparent discrepancy between the peripheral repertoire sizes and how each specificity is subject to tolerance. Moreover, the relative number of C4- vs F1-specific Treg and Tconv cells that seed the repertoire could create inter-specificity competition in the periphery, further contributing to immunodominance at the tissue site and the degree of peripheral tolerance each specificity is subjected to. Ultimately, it remains elusive whether F1 and

C4 can be classified as dominant or cryptic self epitopes, and if this has consequence for why the breach in tolerance to C4 does not extend to F1.

Contexts in which C4/I-A^b-instructed tolerance operates and the relevant cellular performers

It is important to note that the breach in tolerance observed in our experiments occurred following CD4$^+$ T cell transfer to βδ T cell-deficient recipients, a setting that may potentiate T cell activation and differentiation due to homeostatic proliferation of donor cells in the lymphopenic host. This environment mirrors the natural setting of lymphopenia and homeostatic proliferation that is well documented in the neonatal period – a timespan that is crucial for the establishment of T cell tolerance, especially to Aire-dependent tissue-restricted antigens [136]. Relatedly, it is possible that the differentiation of C4/I-A^b-specific Treg cells is especially robust in the neonatal period [136], as has been observed for other Treg cell specificities [48], which may confer these cells with a superior capacity to prevent organ-specific autoimmunity during this window of lymphopenia. A recent report demonstrated that Treg cells arising in the first 2 weeks of life were sufficient to stop ongoing autoimmune disease and prevent inflammation later in life [137], further suggesting that C4/I-A^b-specific Treg cells arise in this early developmental window and may also be relevant for tolerance outside of a lymphopenic setting. We did not directly address questions of temporal ontogeny for C4/I-A^b-specific Treg and Tconv cells, though we did develop several tools over the course of our studies, including *C4$^{fl/fl}$* mice (Chapter 2, Figure 14) and αC4/I-A^b blocking antibodies (Chapter 3, Figure 33), which now enable precise identification of the window for C4/I-A^b Treg and Tconv cell development.

Two critical outstanding questions that remain to be determined are 1) whether altered T cell selection on C4/I-A^b is sufficient to induce prostatic T cell infiltration in a lymphoreplete adult

host in the absence of activation signals, and 2) whether loss of tolerance to C4/I-A^b is due to qualitative or quantitative alterations in C4/I-A^b-specific Treg cells, C4/I-A^b-specific Tconv cells, or both. Knowledge of the answer to the first question will be absolutely essential to determine the mechanisms and cellular compartments responsible for the breakdown of tolerance in the second question. If steady-state mice which lacked C4 peptide expression in the thymus alone were to develop spontaneous autoimmunity, it would reveal a critical axis of tolerance dependent on C4/I-A^b that is instantaneously operative in the thymus or constantly operative in the periphery. In this case, the "rogue" specificities which now arise in the Tconv compartment could be the primary mediators of autoimmunity directed at C4, implicating central tolerance and Treg "shunting" in the thymus as the major way that C4/I-A^b-specific T cells are rendered harmless to the host. Alternatively, C4/I-A^b-specific Treg cells could mediate peripheral tolerance by restricting the activation of Tconv cells in the periphery via direct regulation of these cells or indirect regulation of C4/I-A^b antigen. These possibilities could then be taken to their conclusion by determining whether "rogue" C4/I-A^b Tconv cells can transfer autoimmunity to wild-type males that have endogenous C4/I-A^b-specific Tregs. If instead thymic C4 peptide-deficient mice did not develop prostatitis, it would indicate that polyclonal Treg cells are sufficient to maintain tolerance to C4/I-A^b at steady-state via bystander mechanisms (such as cytokine deprivation, costimulatory masking, or expression of suppressive factors), and that the breach in tolerance to C4/I-A^b requires a triggering event in the periphery akin to homeostatic proliferation. Critically, this result would implicate peripheral tolerance as the primary mode of tolerance to C4/I-A^b, and would hint that mechanisms of C4/I-A^b-specific tolerance are solely operative in inflammatory contexts. Ultimately, this result would provide a conceptual framework in which C4/I-A^b-specific Treg and Tconv cells compete in the same arena following a single triggering event, during which a decision

is made to either mount a pathogenic response against C4/I-A^b or to stop such a response before the veil of tolerance can be ruptured.

CHAPTER 2:

ROLE OF FOXP3^{+} REGULATORY T CELL ANTIGEN SPECIFICITY IN SELF-NONSELF DISCRIMINATION

INTRODUCTION[††]

αβ T cells recognize short peptide antigens bound to host MHC molecules (pMHCs) displayed on the surface of antigen presenting cells (APCs). Such recognition is mediated by a heterodimeric αβ T cell receptor (TCR), which is generated by a quasi-random gene recombination process [378]. As a result, the mature T cell pool is furnished with a diverse collection of T cell clones, each expressing a unique TCR, thereby ensuring that protective T cell responses can be mounted against numerous pathogen-derived (nonself) peptides complexed with host MHC molecules. However, this clonal variation also introduces significant risk because generated TCRs may also recognize self-pMHCs that have the potential to attack the host [343]. This tradeoff necessitates a range of tolerance mechanisms that limit T cell responses against self while enabling those against nonself threats.

The earliest form of control operates in the thymus during T cell development. Here, central tolerance mechanisms filter developing T cells based on TCR reactivity toward an array of self-pMHCs, and many T cells that react too strongly to self-pMHCs are purged from the body through a process known as clonal deletion [379]. However, substantial evidence demonstrates that clonal deletion is incomplete, allowing highly self-reactive conventional T (Tconv) cell clones with autoimmune potential to escape and seed the periphery of the host [186,347,358,380-382]. These Tconv escapees require additional layers of tolerance in the periphery. Foxp3$^+$ regulatory T (Treg) cells are an essential component of peripheral tolerance. This specialized CD4$^+$ T cell subset harbors TCRs that are largely reactive to self-pMHC [271], and Treg cells are required throughout life to

[††] Portions of this section are reproduced or adapted from Klawon, D.E.J., *et al.* Regulatory T cells enforce self-nonself discrimination by constraining conventional T cells of matched self-specificity during infection. *In preparation as of May 2023*.

prevent autoimmunity elicited by self-reactive Tconv cells [19]. Treg cells invoke multiple mechanisms to achieve this outcome, including masking of costimulatory ligands on the surface of antigen-presenting cells (APCs), absorption of T cell growth factors such as IL-2, and production of suppressive cytokines that restrict the differentiation of Tconv cells [256,268,283,344,383,384]. These mechanisms function to raise Tconv cell activation thresholds and limit the progression of ongoing Tconv cell responses through negative feedback. In this regard, previous work documented a local paracrine feedback circuit in which Tregs selectively accumulated around Tconv cells activated by self-pMHCs to limit their activation in the secondary lymphoid organs (SLOs) of healthy hosts [276,385].

The ongoing activation of self-reactive Tconv cells raises a conceptual conundrum related to Treg cell function during pathogen infection, when successful host defense requires Tconv cells reactive to pathogen-derived peptides to be primed, proliferate, differentiate, and effectively traffic. How do Treg cells selectively permit activation of Tconv cell responses against pathogen-derived peptides while maintaining control of autoreactive Tconv cell responses against host-derived self-peptides?

This question has been challenging to answer intuitively considering that inflammatory signals triggered by pathogen infection, including pathogen-associated molecular patterns (PAMPs) [386,387] or damage-associated molecular patterns (DAMPs) [388-390], indiscriminately increase the stimulatory capacity of APCs displaying both self or nonself-pMHCs to enhance Tconv cell responses to both antigens in parallel. Moreover, pathogen-derived peptides can exhibit topological similarities to self-peptides – a phenomenon referred to as epitope mimicry [18,391] – increasing TCR signaling in some self-reactive Tconv clones during infection that could elicit autoimmunity. In this regard, a recent report identified T cell clones expanded in human

autoimmune lesions that cross-react with both self-peptides and microbial peptides [392]. Infection-associated tissue damage may further increase TCR and co-stimulatory signaling in self-reactive Tconv cells due to the release of self-peptides and DAMPs from injured and dying cells. Pathogen infection is therefore a setting poised to overwhelm Treg cell constraints and unleash self-specific Tconv cell responses capable of triggering autoimmunity. Yet autoimmune diseases rarely manifest following a successful pathogen-targeted T cell response, suggesting that Treg cells possess a means to selectively dampen Tconv cells responses against self-peptides while enabling those against nonself-peptides.

One principle that could account for this type of discrimination, at least in part, relates to shared self-pMHC specificities of some Treg cells and Tconv cells. Indeed, several studies have documented the co-existence of mature Treg and Tconv cells that recognize the same self-pMHCs within the endogenous repertoires of healthy mice [87,98,103,140,141,368]. It is noteworthy that some of the peptides identified in these studies were also targeted in murine models of spontaneous and induced autoimmune disease, implying a critical role for this axis in the maintenance of tolerance. In contrast, pMHC-specific T cell pools reactive to foreign, nonself peptides are highly skewed to Tconv cells [97,106,218,220,326]. These observations raise the possibility that self-pMHC-specific Treg cells may preferentially regulate Tconv cells of matched specificity, and that alterations in the Treg/Tconv cell composition of single self-pMHC-reactive pools may contribute to breaches in tolerance, as observed in a previous study [101].

RESULTS‡‡

In this study, we tested the hypothesis that Treg cell specificity for self-pMHC ligands serves as a key determinant of self-nonself discrimination, allowing Treg cells to focus their immunosuppressive functions on self-reactive Tconv cells of shared pMHC specificity. To do this, we analyzed $CD4^+$ T cell responses to a natural self-peptide, termed C4, which is derived from the prostate-specific protein Tcaf3 and selectively displayed on I-A^b, the MHC class II-encoded protein in C57BL/6 mice. C4/I-A^b complexes are normally presented in the thymus, directing a fraction of developing C4-specific T cells into the Treg cell lineage [102,138] without inducing measurable clonal deletion [101]. The net result is a mixture of C4/I-A^b-specific Treg and Tconv cells in the mature peripheral T cell repertoire. Notably, Tcaf3 protein and its derivative peptides are recurrently targeted by autoantibodies and Tconv cells, respectively, in settings of immune dysregulation [87,139,349]. The C4/I-A^b-specific T cell response can be studied using fluorescent C4/I-A^b tetramers [138] and monoclonal T cells from TCR transgenic mice expressing the C4/I-A^b-specific MJ23 TCR (MJ23tg mice) [102]. By combining these tools within gene manipulations and single-cell RNA sequencing, we defined the role of C4/I-A^b-specific Treg cells in regulating Tconv cells of matched specificity and preventing organ-specific autoimmunity, both during homeostatic as well as inflammatory conditions.

‡‡ Portions of this section are reproduced or adapted from Klawon, D.E.J., *et al.* Regulatory T cells enforce self-nonself discrimination by constraining conventional T cells of matched self-specificity during infection. *In preparation as of May 2023*.

Treg-mediated control of Tconv cells is an ongoing process that does not prevent Tconv cells from accessing self-antigen at steady-state or during infection

Systemic depletion of Treg cells, even transiently, unleashes rapid and robust autoimmune infiltration of many tissues by Tconv cells and $CD8^+$ T cells in mice [19], indicating that these cells are required throughout life to control autoreactive T cells. However, both the ontogeny of the infiltrating T cells and the mechanisms normally keeping such cell in check remain unclear. In one possible scenario, Treg cells may constantly suppress Tconv cells in the secondary lymphoid organs throughout the life of such autoreactive cells, and their control is therefore conditional. A second possibility is that Treg cells function by permanently inactivating self-reactive Tconv cells shortly after their egress from the thymus to the periphery, and that the autoimmune disease which manifests upon acute Treg ablation is mediated by recent autoreactive emigrants from the thymus that had yet to be inactivated by Treg cells. To test these possibilities, we subjected *Foxp3*-DTR^+ mice to thymectomy or sham operation and subjected both groups to sustained Treg depletion following surgical recovery. In this way, all Tconv cells in the periphery of thymectomized animals were subjected to Treg-mediated suppression prior to depletion, and would thus fail to elicit autoimmunity if they had been permanently inactivated. Following Treg depletion, thymectomized mice succumbed to autoimmunity at the same rate as sham-operated controls (Figure 11, A), both of which were characterized by elevated frequencies of activated Tconv cells in the SLOs and tissues (Figure 11, B-C). Thus, Treg-mediated control of self-reactive T cells is an ongoing process and inactivation of such cells is readily reversible.

Having established that Tconv control is not permanent, we sought to determine whether Treg-mediated control occurs in a "prophylactic" or "anaphylactic" manner relative to Tconv cell activation. We reasoned that prophylactic mechanisms would prevent Tconv cell activation by

preventing self-antigen recognition by such cells, while anaphylactic mechanisms would include those that occur following the activation of self-reactive Tconv cells. Furthermore, the mechanism of action could be different at steady-state and in inflammatory environments. To address these questions, we tracked the activation of MJ23 Tconv cells that are specific for the C4/I-A^b self-antigen. MJ23 T cells were isolated from female MJ23tg$^+$ *Rag1*$^{-/-}$ CD45.1/.1 mice, which exclusively harbor naïve Foxp3^{neg} Tconv cells [102] due to antigenic niche overload in the thymus [44], and were injected into wild-type B6 male mice, which harbor endogenous C4/I-A^b antigen exclusively in the prostate and prostate-draining paraaortic LNs (pLNs). Following transfer into naïve mice, MJ23 Tconv cells readily upregulated Egr2, a marker of TCR signaling [393], indicating that endogenous Treg cells do prophylactically function to prevent self-reactive Tconv cells from sensing cognate ligand at steady-state (Figure 11, D-E). To determine whether this remained true during inflammation, we performed the same experiments but also infected mice with the pathogen *L. monocytogenes* (*Lm[parent]*) following transfer. *Lm* is a common bacterial pathogen that primarily infects the spleen and liver and triggers multiple innate signaling pathways initiated by both phagosomal and cytosolic innate sensors [394,395]. Infection exposed T cells in the spleen and pLN to innate inflammatory triggers, as measured by upregulation of the activation marker CD69 (Figure 11, F), and MJ23 Tconv cells continued to recognize C4/I-A^b and upregulate Egr2 in the pLN (Figure 11, D-E). Collectively, these data indicate that Treg-mediated control of self-reactive Tconv cells is a constant process that occurs in an anaphylactic manner following the priming of Tconv cells by self-antigen at steady-state and during infection.

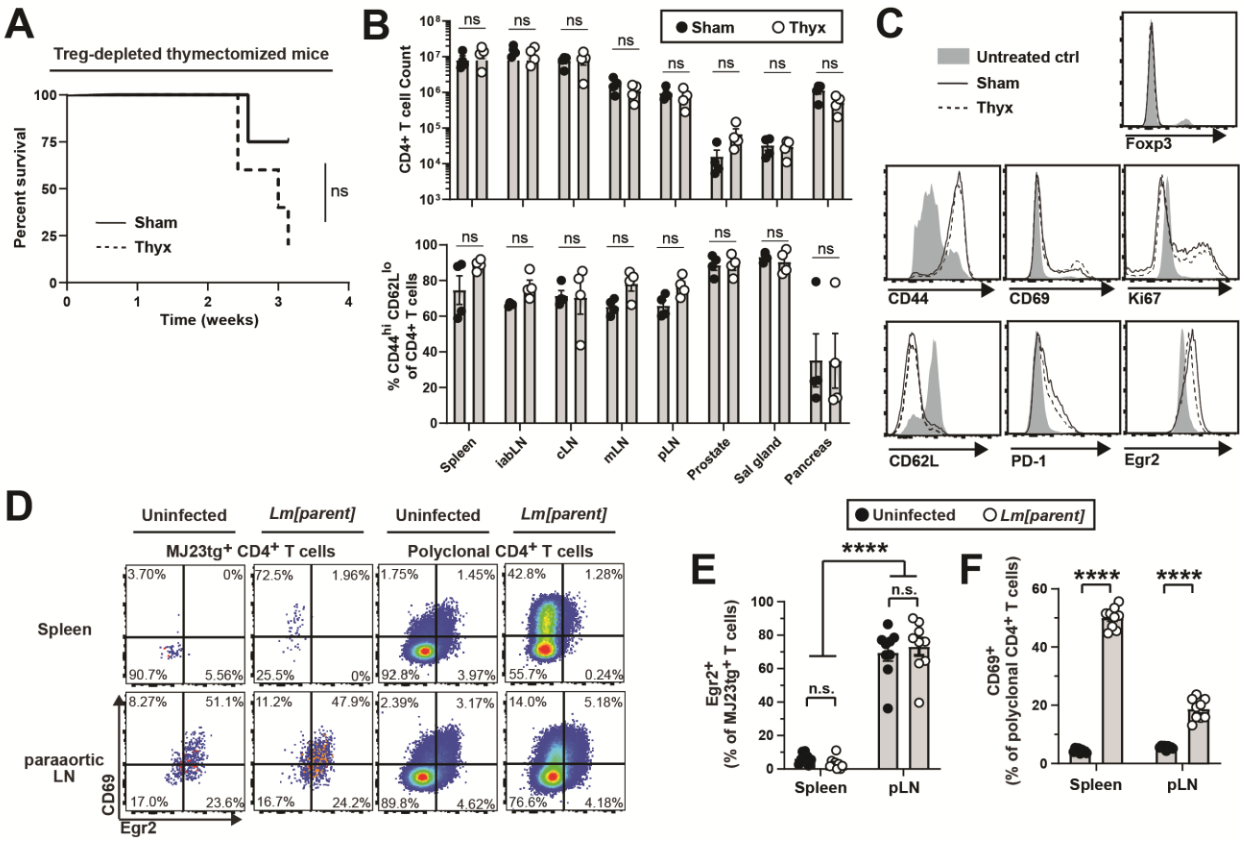

FIGURE 11. Treg-mediated control of Tconv cells is an ongoing process that does not prevent Tconv cells from accessing self-antigen at steady-state or during infection

(A-C) Systemic and sustained depletion of Treg cells in thymectomized mice. Naive Foxp3-GFP^{+} male mice were thymectomized or sham operated. Two weeks post-surgery, Treg cells were systemically depleted via intraperitoneal injection of DT every other day for 21 days or until moribund, at which time mice CD4^{+} T cells were isolated from the SLOs and analyzed by flow cytometry. Data are pooled from 2 independent exepriments, 4 mice per condition. (A) Kaplan-Meier curve depicting survival at day 21 post-depletion. All remaining mice were moribund at day 21. (B) Summary plot of pooled data depicting the frequency of polyclonal CD4^{+} T cells expressing CD44 enriched from the pooled SLOs of mice of the indicated genotype. The absolute number of polyclonal CD4^{+} Tconv cells isolated from the indicated SLOs or mice of the indicated condition (top), and the frequency of polyclonal CD4^{+} Tconv cells expressing an activated CD44^{HI} CD62L^{LO} phenotype (bottom). Each symbol represents one mouse. Mean ± SEM is indicated. (n.s., not significant $p > 0.05$; student's t test). (C) Representative flow cytomeric analysis of CD4^{+} Tconv cells isolated from mice of the indicated condition. Histograms depict Foxp3, CD44, CD62L, CD69, PD-1, Ki67, and Egr2 expression. An untreated wild-type mouse is included as a control.

(D-F) 10^{5} MJ23 Tconv cells were transferred into wild-type male hosts. Mice were infected with *Lm[parent]* 1 day post-transfer or left uninfected, and were assessed in the spleen or paraaortic LN 3 days post-transfer by flow cytometry. Data are pooled from two independent experiments. n = 9, uninfected; n = 9, *Lm[parent]*. (D) Representative flow cytometric analysis of T cells isolated from the indicated organ of untreated and infected mice. Plots depict Egr2

FIGURE 11, continued
vs. CD69 expression by MJ23 $CD4^+$ (left) and polyclonal $CD4^+$ (right) T cells. The frequency of cells within the indicated gates is denoted. (E) Summary plot of pooled data from (D) showing the frequency of $Egr2^+$ cells amongst MJ23 $CD4^+$ Treg and Tconv cells isolated from the indicated organs of host mice. Each symbol represents one mouse. Mean ± SEM is indicated. (**** = $P < 0.0001$; n.s. = $P > 0.05$; ordinary 2-way ANOVA). (F) Summary plot of pooled data from (D) showing the frequency of $CD69^+$ cells amongst polyclonal $CD4^+$ T cells isolated from the indicated organs of host mice. Each symbol represents one mouse. Mean ± SEM is indicated. (**** = $P < 0.0001$; n.s. = $P > 0.05$; Welch's t-test).

Temporal control of single C4/I-A^b- and F1/I-A^b-specific T cell activation enabled by engineered models of pathogen-associated epitope mimicry

Having identified a temporal window in which Treg-mediated control of self-reactive Tconv cells occurs, we sought to understand the importance of Treg specificity for self-antigen in coordinating this process. This required a strategy that could both trigger the timed activation of single endogenous specificities of self-reactive Treg and Tconv cells and enable reliable tracking of these rare cell populations (Figure 3). To this end, we engineered multiple attenuated and non-attenuated *Lm[parent]* strains [337,396-398] to express the recombinant self-peptides C4 and F1 (Figure 12, A). Infecting mice with the resulting strains proved advantageous as it 1) produced inflammatory environments with increased antigen presentation, particularly the spleen, liver, and portal LNs and 2) caused rapid recruitment of C4/I-A^b- or F1/I-A^b-specific T cells to these sites, allowing us to study temporally synchronized responses. Additionally, we engineered strain variants to express linked C4/F1 peptides for simultaneous activation of both specificities, and C4 peptides tagged with the V5 epitope tag to identify APCs that present C4/I-A^b (experiments with these strains will be performed or discussed in Chapter 3). Successful *in vivo* presentation of the C4 and F1 peptides to antigen-specific MJ23 and SP33 T cells was confirmed for all strains except the original *Lm[F1]* strain by measuring proliferation of transferred donor cells labeled with CTV

following infection (Figure 12, B). Unless otherwise stated for the studies contained in this thesis, infections involving *Lm[C4]* refer to the attenuated *Lm ΔActA prfA* G155S* strain engineered to express C4, infections involving *Lm[F1]* refer to the attenuated *Lm ΔActA prfA* G155S* strain engineered to express a truncated form of the F1 peptide (*Lm[trF1]*, see methods), and infections involving *Lm[C4+F1]* refer to the attenuated *Lm ΔActA prfA* G155S* strain engineered to express the C4 and trF1 peptides separated by a spacer containing the N'-terminal and C'-terminal cathepsin cleavage sites flanking the CLIP peptide of the invariant chain CD74 [399]. A comprehensive summary of all engineered *Lm* strains – those employed in this thesis and those used in other studies – can be found in Table 1, which is current as of June 2023.

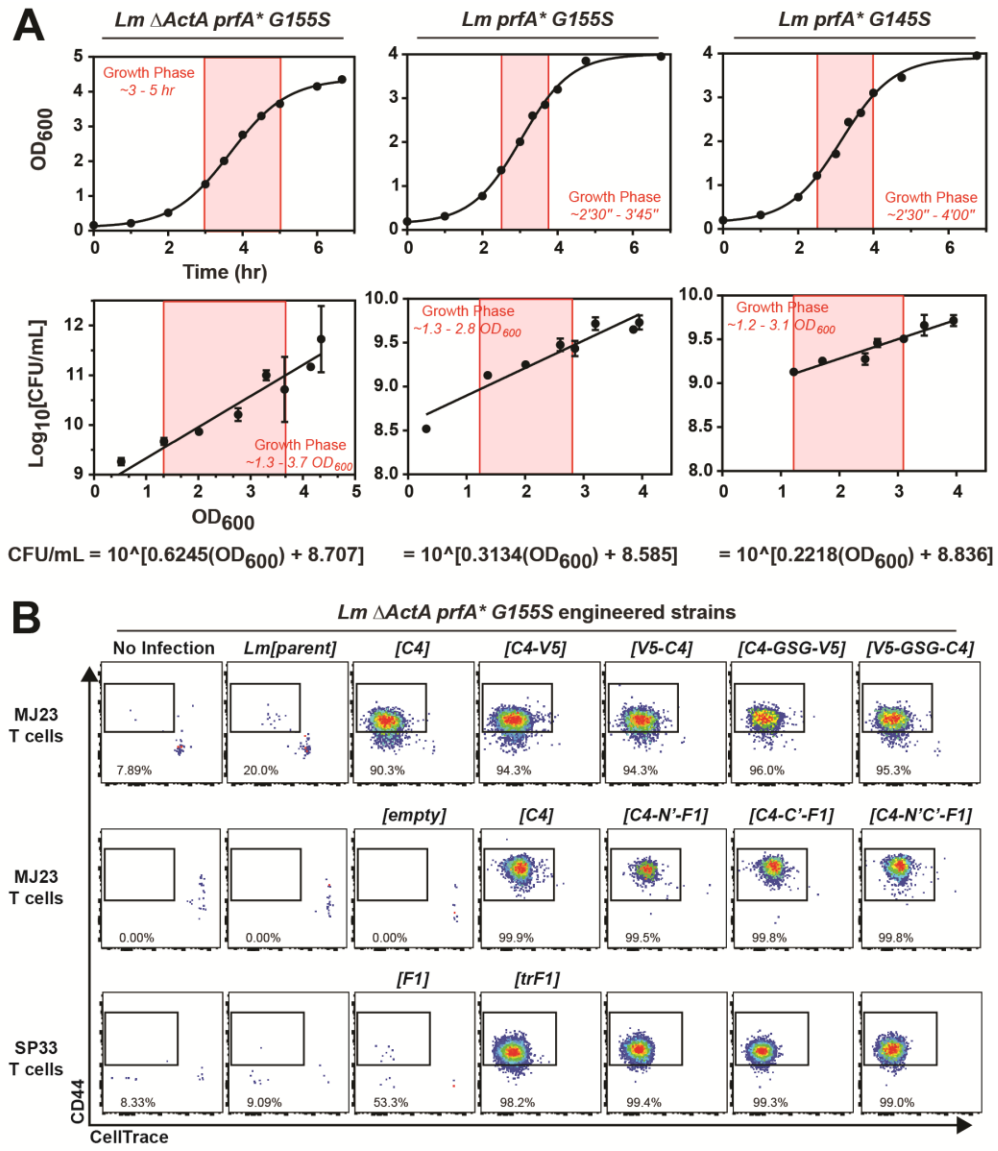

FIGURE 12. Temporal control of single C4/I-A^b- and F1/I-A^b-specific T cell activation enabled by engineered models of pathogen-associated epitope mimicry

(A) Growth curves for three parental strains of *Lm* described in [337]. Starter cultures of *Lm* strains taken from glycerol stock scrapes were grown overnight in 5ml BHI + 200µg/ml Streptomycin at 37ºC with shaking. The next day, starter cultures were diluted 1:20 in 50 mL BHI + antibiotics and grown in the same conditions. At the indicated timepoint, aliquots were taken from the culture, the OD_{600} was measured, and samples were serially diluted and grown in duplicate or triplicate on BHI agar plates overnight at 37ºC. The following morning, colonies at each dilution and timepoint were enumerated. Plots depict the time vs OD_{600} and OD_{600} vs Log_{10}[CFU/mL]. Empirically generated equations were used in corresponding infection experiments to calculate the CFU/mL of the culture and estimate infectious inoculum dose.

(B) In vivo validation of *Lm*-derived antigen presentation to cognate T cells. Wild-type female mice received 105 CTViolet or CTYellow-labelled MJ23 or SP33 Tconv cells isolated from transgenic or retrogenic donor mice, respectively. The following day, recipient mice were

FIGURE 12, continued
infected intravenously with 10^7 CFU of the indicated *Lm* strain engineered to express the indicated peptide, and $CD4^+$ T cells were isolated from the spleens of recipient mice 7 days post-infection and analyzed by flow cytometry. Representative flow cytometric analysis depicts CellTrace dilution vs CD44 expression by MJ23 or SP33 Tconv cells. Data are representative of at least two independent experiments. C4 = C4 peptide, V5 = GKPIPNPLLGDST peptide tag, GSG = linker sequence, F1 = F1 peptide, trF1 = truncated F1 peptide, N' = N-terminal cleavage site of CLIP peptide, C' = C-terminal cleavage site of CLIP peptide.

TABLE 1. Strains of *L. monocytogenes* engineered between April 2019 and February 2023

Strain Name	***Insert sequence***
Lm[C4]	THSKAPWGELATD
Lm[C4-GSG-V5]	THSKAPWGELATD-GSG-GKPIPNPLLGLDST
Lm[C4-V5]	THSKAPWGELATD-GKPIPNPLLGLDST
Lm[V5-C4]	GKPIPNPLLGLDST-THSKAPWGELATD
Lm[V5-GSG-C4]	GKPIPNPLLGLDST-GSG-THSKAPWGELATD
Lm[F1]	CPGAPIAVHSSLASLVNILG
Lm[trF1]	GAPIAVHSSLASLVNIL
Lm[C4-Cclip-F1]	THSKAPWGELATD-GSG-MSMDMN-GSG-CPGAPIAVHSSLASLVNILG
Lm[C4-Nclip-F1]	THSKAPWGELATD-GSG-RMKLPK-GSG-CPGAPIAVHSSLASLVNILG
Lm[C4-N/Cclip-F1]	THSKAPWGELATD-GSG-RMKLPK-GSG-MSMDMN-GSG-CPGAPIAVHSSLASLVNILG
Lm[pPL6-myc]	none
Lm[C4-trF1]	THSKAPWGELATD-GSG-RMKLPK-GSG-MSMDMN-GSG-GAPIAVHSSLASLVNIL
Lm155[C4]	THSKAPWGELATD
Lm155[trF1]	GAPIAVHSSLASLVNIL
Lm155[C4-trF1]	THSKAPWGELATD-GSG-RMKLPK-GSG-MSMDMN-GSG-GAPIAVHSSLASLVNIL
Lm145[C4]	THSKAPWGELATD
Lm145[trF1]	GAPIAVHSSLASLVNIL
Lm145[C4-trF1]	THSKAPWGELATD-GSG-RMKLPK-GSG-MSMDMN-GSG-GAPIAVHSSLASLVNIL
Lm[C4-2W]	THSKAPWGELATD-GSG-RMKLPK-GSG-MSMDMN-GSG-EAWGALANWAVDSA
Lm[mCherry]	*mCherry
Lm[mCherry-C4]	*mCherry-GSG-MSMDMN-GSG-THSKAPWGELATD
Lm[mCherry-OVAp]	*mCherry-GSG-RMKLPK-GSG-MSMDMN-GSG-ISQAVHAAHAEINEAGR
Lm[mCherry-C4-OVAp]	*mCherry-GSG-MSMDMN-GSG-THSKAPWGELATD-GSG-MSMDMN-GSG-ISQAVHAAHAEINEAGR
Lm[sHELd52s]	*sHELd52s
Lm[sHELd52s-C4]	*sHELd52s-GSG-RMKLPK-GSG-MSMDMN-GSG-THSKAPWGELATD
Lm[C4-OVAp]	THSKAPWGELATD-GSG-MSMDMN-GSG-ISQAVHAAHAEINEAGR
Lm[C4-mCherry]	THSKAPWGELATD-GSG-RMKLPK-GSG-MSMDMN-GGGGSGGGSGGGGS-*mCherry
Lm[C4-OVAp-mCherry]	THSKAPWGELATD-GSG-RMKLPK-GSG-MSMDMN-ISQAVHAAHAEINEAGR-GSG-RMKLPK-GSG-MSMDMN-GGGGSGGGGSGGGGS-*mCherry
Lm[fullHELd52s]	*fullHELd52S
Lm[fullHELd52s-C4]	*fullHELd52S-GGGGSGGGGSGGGGS-RMKLPK-GSG-MSMDMN-GSG-THSKAPWGELATD
Lm[C4-fullHELd52s]	THSKAPWGELATD-GSG-RMKLPK-GSG-MSMDMN-GGGGSGGGSGGGGS-*fullHELd52S

TABLE 1, continued.

Strain Name	*Vector*	*Parent Strain*	*Date*	*Does it work?*	*Validation*
Lm[C4]	pPL6-myc	Δ*actA prfA* G155S*	Apr 2019	Yes	MJ23 expansion *in vivo*
Lm[C4-GSG-V5]	pPL6-myc	Δ*actA prfA* G155S*	Apr 2019	pep stimulates	V5 probably won't stain
Lm[C4-V5]	pPL6-myc	Δ*actA prfA* G155S*	Apr 2019	pep stimulates	"
Lm[V5-C4]	pPL6-myc	Δ*actA prfA* G155S*	Apr 2019	pep stimulates	"
Lm[V5-GSG-C4]	pPL6-myc	Δ*actA prfA* G155S*	Apr 2019	pep stimulates	"
Lm[F1]	pPL6-myc	Δ*actA prfA* G155S*	June 2019	No	Does not stim SP33
Lm[trF1]	pPL6-myc	Δ*actA prfA* G155S*	June 2019	Yes	SP33 expansion *in vivo*
Lm[C4-Cclip-F1]	pPL6-myc	Δ*actA prfA* G155S*	June 2019	Yes	MJ23 expansion *in vivo* SP33 expansion *in vivo*
Lm[C4-Nclip-F1]	pPL6-myc	Δ*actA prfA* G155S*	June 2019	Yes	"
Lm[C4-N/Cclip-F1]	pPL6-myc	Δ*actA prfA* G155S*	June 2019	Yes	"
Lm[pPL6-myc]	pPL6-myc	Δ*actA prfA* G155S*	June 2019	n/a	n/a
Lm[C4-trF1]	pPL6-myc	Δ*actA prfA* G155S*	Jan 2021	Yes	MJ23 expansion *in vivo* SP33 expansion *in vivo*
Lm155[C4]	pPL6-myc	*prfA* G155S*	Oct 2021	Yes	ΔTEC autoimmunity
Lm155[trF1]	pPL6-myc	*prfA* G155S*	Oct 2021	Unknown	not validated
Lm155[C4-trF1]	pPL6-myc	*prfA* G155S*	Oct 2021	Unknown	not validated
Lm145[C4]	pPL6-myc	*prfA* G145S*	Oct 2021	Unknown	not validated
Lm145[trF1]	pPL6-myc	*prfA* G145S*	Oct 2021	Unknown	not validated
Lm145[C4-trF1]	pPL6-myc	*prfA* G145S*	Oct 2021	Unknown	not validated
Lm[C4-2W]	pPL6 (no myc)	Δ*actA prfA* G155S*	July 2022	Yes	ΔTEC autoimmunity 2W1S Tetramer expansion
Lm[mCherry]	pPL6 (no myc)	Δ*actA prfA* G155S*	July 2022	Maybe	High OD_{600} Lm culture
Lm[mCherry-C4]	pPL6 (no myc)	Δ*actA prfA* G155S*	July 2022	C4-yes mCherry-no	No MJ23 proliferation Normal OD_{600} Lm culture
Lm[mCherry-OVAp]	pPL6 (no myc)	Δ*actA prfA* G155S*	July 2022	OVAp-no mCherry maybe	No OT-II proliferation High OD_{600} Lm culture
Lm[mCherry-C4-OVAp]	pPL6 (no myc)	Δ*actA prfA* G155S*	July 2022	C4-no, OVAp-no mCherry-no	No MJ23 proliferation No OT-II proliferation Normal OD_{600} Lm culture
Lm[sHEL∆52s]	pPL6 (no myc)	Δ*actA prfA* G155S*	July 2022	No	No MD4 stimulation
Lm[sHEL∆52s-C4]	pPL6 (no myc)	Δ*actA prfA* G155S*	July 2022	C4-yes, HEL-no	MJ23 proliferation No MD4 stimulation
Lm[C4-OVAp]	pPL6 (no myc)	Δ*actA prfA* G155S*	Feb 2023	Yes	MJ23 proliferation OT-II proliferation
Lm[C4-mCherry]	pPL6 (no myc)	Δ*actA prfA* G155S*	Feb 2023	Unknown pep stimulates	not validated MJ23 proliferation
Lm[C4-OVAp-mCherry]	pPL6 (no myc)	Δ*actA prfA* G155S*	Feb 2023	mCherry unclear	OT-II proliferation
Lm[fullHEL∆52s]	pPL6 (no myc)	Δ*actA prfA* G155S*	Feb 2023	No	No MD4 stimulation
Lm[fullHEL∆52s-C4]	pPL6 (no myc)	Δ*actA prfA* G155S*	Feb 2023	No	No MD4 stimulation MJ23 proliferation
Lm[C4-fullHEL∆52s]	pPL6 (no myc)	Δ*actA prfA* G155S*	Feb 2023	C4-yes, HEL-no	No MD4 stimulation

TABLE 1, continued.

Strain Name	*Description*
Lm[C4]	C4 peptide with c-myc tag, used in most experiments
Lm[C4-GSG-V5]	C4 peptide with V5 and myc tags at C terminus, spaced by GSG linker
Lm[C4-V5]	C4 peptide with V5 and myc tags at C terminus
Lm[V5-C4]	C4 peptide with V5 and myc tags at N terminus
Lm[V5-GSG-C4]	C4 peptide with V5 and myc tags at N terminus, spaced by GSG linker
Lm[F1]	full-length F1 peptide with c-myc tag, not used in any experiments
Lm[trF1]	F1 peptide truncated by 3 amino acids, with c-myc tag, used in all Lm[F1] experiments
Lm[C4-Cclip-F1]	Linked C4 and F1 tandem peptide, linked with C-terminal cathepsin sequence of CLIP
Lm[C4-Nclip-F1]	Linked C4 and F1 tandem peptide, linked with N-terminal cathepsin sequence of CLIP
Lm[C4-N/Cclip-F1]	Linked C4 and F1 tandem peptide, linked with N and C-terminal cathepsin sequences of CLIP
Lm[pPL6-myc]	empty vector parent with CAM resistance, used for most Lm[parent] experiments
Lm[C4-trF1]	Linked C4 and truncated F1 tandem peptide, linked with C-terminal cathepsin sequence of CLIP
Lm155[C4]	Lm[C4] strain used above, without deleted *ActA* attenuation
Lm155[trF1]	Lm[trF1] strain used above, without deleted *ActA* attenuation
Lm155[C4-trF1]	Lm[C4-trF1] strain used above, without deleted *ActA* attenuation
Lm145[C4]	Lm[C4] without deleted *ActA* attenuation and high-activity *prfA* to drive peptide expression
Lm145[trF1]	Lm[trF1] without deleted *ActA* attenuation and high-activity *prfA* to drive peptide expression
Lm145[C4-trF1]	Lm[C4-trF1] without deleted *ActA* attenuation and high-activity *prfA* to drive peptide expression
Lm[C4-2W]	Linked C4 and 2W tandem peptide, linked with N and C-terminal cathepsin sequences of CLIP
Lm[mCherry]	Full-length mCherry
Lm[mCherry-C4]	mCherry with C-terminal C4 peptide, linked with C-terminal cathepsin sequence of CLIP
Lm[mCherry-OVAp]	mCherry with C-terminal OT-II agonist peptide, linked with N- and C-terminal cathepsin sequence of CLIP
Lm[mCherry-C4-OVAp]	mCherry with C-terminal C4 and OT-II peptides, interspersed with C-terminal cathepsin sequences of CLIP
Lm[sHELd52s]	HEL protein without N-terminal signal sequence and containing D52S mutation
Lm[sHELd52s-C4]	sHELd52s with C-terminal C4 peptide, linked with N- and C-terminal cathepsin sequences of CLIP
Lm[C4-OVAp]	C4 and OT-II agonist tandem peptide, linked with C-terminal cathepsin sequence of CLIP
Lm[C4-mCherry]	mCherry with N-terminal C4 peptide, linked with N- and C-terminal cathepsin sequence of CLIP
Lm[C4-OVAp-mCherry]	mCherry with N-terminal C4 and OT-II peptides, interspersed with N- and C-terminal cathepsin sequences of CLIP
Lm[fullHELd52s]	full-length HEL with signal sequence and D52S mutation
Lm[fullHELd52s-C4]	fullHELd52s with C-terminal C4 peptide, linked with N- and C-terminal cathepsin sequences of CLIP
Lm[C4-fullHELd52s]	fullHELd52s with N-terminal C4 peptide, linked with N- and C-terminal cathepsin sequences of CLIP

mCherry sequence:

MVSKGEEDNMAIIKEFMRFKVHMEGSVNGHEFEIEGEGEGRPYEGTQTAKLKVTKGGP
LPFAWDILSPQFMYGSKAYVKHPADIPDYLKLSFPEGFKWERVMNFEDGGVVTVTQDS
SLQDGEFIYKVKLRGTNFPSDGPVMQKKTMGWEASSERMYPEDGALKGEIKQRLKLKD
GGHYDAEVKTTYKAKKPVQLPGAYNVNIKLDITSHNEDYTIVEQYERAEGRHSTGGMD
ELYK

sHELs52s sequence:
KVFGRCELAAAMKRHGLDNYRGYSLGNWVCAAKFESNFNTQATNRNTDGSTSYGILQI
NSRWWCNDGRTPGSRNLCNIPCSALLSSDITASVNCAKKIVSDGNGMNAWVAWRNRC
KGTDVQAWIRGCRL

TABLE 1, continued

fullHELd52s sequence:
MRSLLILVLCFLPLAALGKVFGRCELAAAMKRHGLDNYRGYSLGNWVCAAKFESNFNT
QATNRNTDGSTSYGILQINSRWWCNDGRTPGSRNLCNIPCSALLSSDITASVNCAKKIVS
DGNGMNAWVAWRNRCKGTDVQAWIRGCRL

T cell selection on C4/I-A^b selectively prevents the accumulation of self-specific T cells following Lm[C4] infection and protects host mice from prostatitis

The studies in Chapter 1 established that tolerance to the C4/I-A^b self-antigen requires repertoire formation in the presence of the peptide, can be broken in a transfer context when selection occurs in the absence of C4 peptide, and the tolerance breakdown cannot be controlled by Treg cells of polyclonal specificity (Figures 4-6). We therefore aimed to establish whether an activation event analogous to lymphopenic T cell transfer, namely infection with *Lm[C4]*, can break tolerance to the C4/I-A^b peptide. We reconstituted *Tcrb*$^{-/-}$ male mice with CD4$^+$ T cells from *Tcaf3(C4)*$^+$ or *Tcaf3(C4)*$^{-/-}$ male donors (as in Figure 5), then infected these mice intravenously with *Lm[C4]* and measured prostatic T cell infiltration 2 weeks post-infection (Figure 13, A-B). The T cell transfer approach was useful because it enabled us to not only compare endogenous T cell responses to the C4/I-A^b self-antigen, but also to assess the response of CD4$^+$ T cells reactive to a natural I-A^b-restricted *Lm*-derived peptide LLO$_{190\text{-}201}$ [400] within the same host environment (Figure 13, A). Following infection, host mice that had received *Tcaf3(C4)*$^{-/-}$ donor cells developed fulminant prostatic T cell infiltration of C4/I-A^b-specific and polyclonal T cells and expansion of such cells in the SLOs. Notably, these mice had universal infiltration by C4/I-A^b-specific T cells (Figure 13, C-D) and these cells were enriched 100-fold over similarly uninfected mice (Figure 5, D), indicating robust timed activation of such self-reactive cells. Mice receiving donor cells from *Tcaf3(C4)*$^+$ mice had few C4/I-A^b-specific T cells in the SLOs or prostate following infection with *Lm[C4]* (Figure 13, D) despite the fact that C4/I-A^b-specific cells could readily be elicited via peptide + CFA in host mice that had received the donor inoculum alone without infection (Figure 13, C). Surprisingly, the number of LLO/I-A^b-specific T cells elicited by infection was the same whether hosts received donor cells from *Tcaf3(C4)*$^+$ or *Tcaf3(C4)*$^{-/-}$ mice (Figure 13, E). These

results collectively set the stage for our studies with three foundational observations: 1) *Lm[C4]* triggers the rapid activation and accumulation of C4/I-A^b-specific T cells that did not develop in the presence of self-derived C4 peptide, 2) Self-selected tolerance to C4/I-A^b dominantly suppresses the accumulation of pathogenic T cells following *Lm[C4]* infection, 3) the pathogen-specific LLO/I-A^b-restricted T cell response is independent of the response to C4/I-A^b.

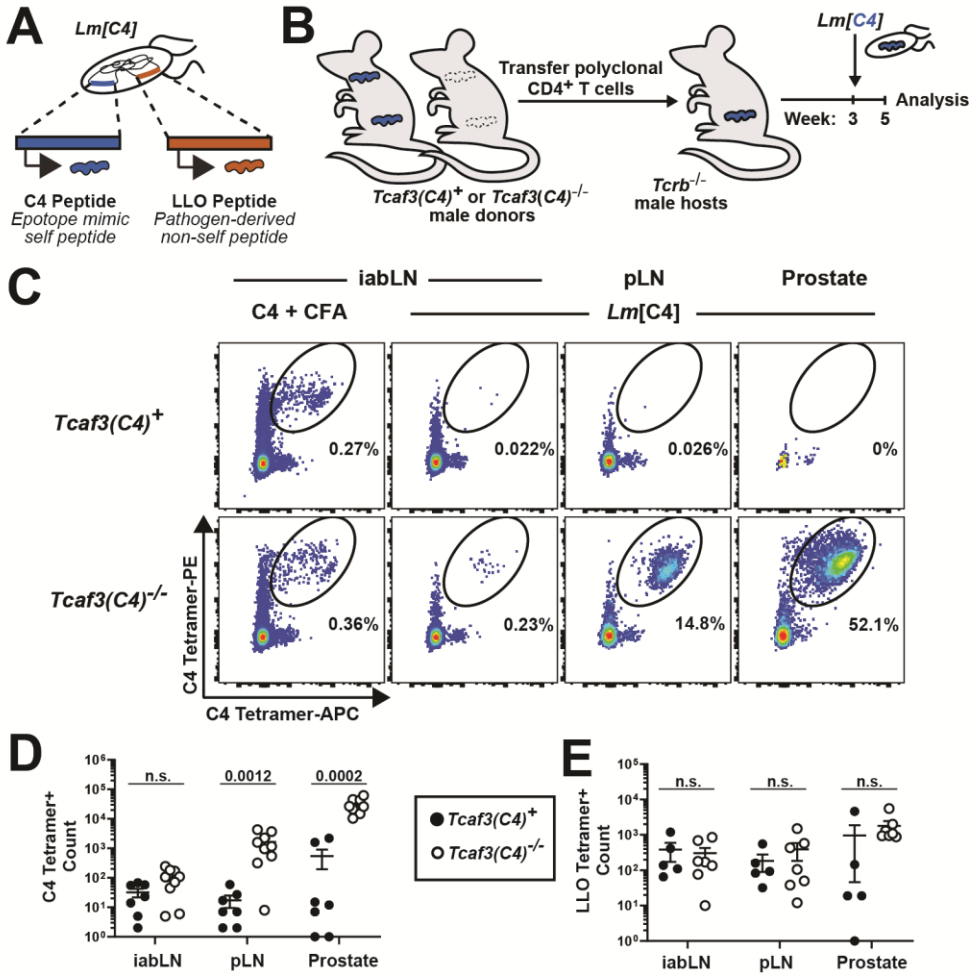

FIGURE 13. T cell selection on C4/I-A^b selectively prevents the accumulation of self-specific C4/I-A^b T cells following *Lm[C4]* infection and protects host mice from prostatitis

(A) Schematic depicting peptide expression in the genetically-engineered *Lm[C4]* pathogen strain. The C4 peptide serves at a pathogen-derived mimetope in during pathogenesis in *C4^{WT}* and *C4$^{\Delta TEC}$* male mice, while the LLO peptide is a pathogen-derived foreign epitope with no known self-expressed analogue in *C4^{WT}* or *C4$^{\Delta TEC}$* mice. (B) 10^7 polyclonal CD4$^+$ T cells were isolated from the pooled secondary lymphoid organs (SLOs) of 8-12 week old *Tcaf3(C4)$^+$* or *Tcaf3(C4)$^{-/-}$* male donors and transferred intravenously into *Tcrb$^{-/-}$ Tcaf3(C4)$^+$* male littermate recipients as in Figure 5. 3 weeks after transfer, recipients were infected intravenously with 10^7 CFU *Lm[C4]* and the fate of transferred T cells was assessed in the prostate-draining lymph nodes (pLN), non-draining LNs (iabLN), or prostate. Host mice that received donor T cells and were immunized subcutaneously with C4 + CFA are included as a control for the presence of C4/I-A^b-specific T cells in the donor inoculum. Data are pooled from 3 independent experiments. n = 5-7, *Tcaf3(C4)$^+$*; n = 8, *Tcaf3(C4)$^+$*. (C) Representative flow cytometric analysis of CD4$^+$ T cells isolated from the indicated *Tcrb$^{-/-}$* host males of the indicated genotype and experimental condition. Plots depict dual C4/I-A^b tetramer staining of polyclonal CD4$^+$ cells. The frequency of cells within the indicated gates is denoted. (D) Summary plot of the pooled data showing the absolute number of C4/I-A^b tetramer$^+$ CD4$^+$ cells isolated from the indicated organs of host mice. Each symbol represents one mouse. Mean ± SEM is indicated.

FIGURE 13, continued
(two-tailed nonparametric Mann-Whitney test). (E) Summary plot of the pooled data showing the absolute number of LLO/I-A^b tetramer$^+$ $CD4^+$ cells isolated from the indicated organs of host mice. Each symbol represents one mouse. Mean ± SEM is indicated. (two-tailed nonparametric Mann-Whitney test).

$C4^{\Delta TEC}$ mice fail to mount a Treg-dominated response against C4/I-A^b but are protected from autoimmunity at steady-state

The development of the *Lm[C4]* strain coupled with T cell reconstitution experiments enabled us to identify a role for self-derived C4 peptide in protecting the host from autoimmunity following infection, and hinted that T cell specific for C4/I-A^b are controlled by mechanisms independent of those regulating other pathogen-derived specificities. However, T cell transfers precluded the ability to define the impact of C4/I-A^b-specific T cells within a complete repertoire at steady-state or precisely track such cells over time following *Lm[C4]*-mediated activation. To this end, we aimed to generate mice deficient in C4/I-A^b-specific Treg but not Tconv cells within natural polyclonal repertoires. We used a gene-targeting strategy to delete the C4 peptide specifically in the thymus, thereby impairing the thymic selection of C4/I-A^b-specific Treg cells without altering the selection of Treg cells reactive to other self-pMHCs (Figure 14, A). We engineered mice in which exon 5 of the *Tcaf3* gene, which encodes the region containing the C4 epitope, is flanked by loxP sites (Figure 14, B). Crossing these mice to *Foxn1*-Cre^+ mice [401] yielded offspring in which *Tcaf3* exon 5 was selectively deleted in thymic epithelial cells (TECs), leaving *Tcaf3* expression in the prostate unaltered (*Foxn1*-Cre^+ *Tcaf3(ex5)$^{flox/flox}$* mice, hereafter referred to as *$C4^{\Delta TEC}$* mice).

Characterization of C4/I-A^b-specific T cells in *$C4^{\Delta TEC}$* and *$C4^{WT}$* (*Foxn1*-Cre^{neg} *Tcaf3(ex5)$^{flox/flox}$*) littermate controls immunized with C4 peptide plus Complete Freund's Adjuvant

(CFA) demonstrated that Treg cells accounted for approximately half of C4/I-A^b-tetramer$^+$ T cells elicited in *C4^{WT}* males, but a significantly smaller fraction of cells (<10%) elicited in *C4$^{\Delta TEC}$* males (Figure 14, C-D), consistent with previous findings in *Tcaf3(C4)$^{-/-}$* mice (Figure 4, B). Despite the difference in C4/I-A^b-specific Treg cell proportion, the average number of C4/I-A^b tetramer$^+$ cells elicited in immunized *C4$^{\Delta TEC}$* males was comparable to that elicited in *C4^{WT}* males (Figure 14, D), indicating that thymic presentation of C4/I-A^b does not measurably restrict the size of the C4/I-A^b-specific T cell pool. These mice finally enabled us to test whether C4/I-A^b-specific Treg cells are required to control C4/I-A^b-specific Tconv cells and maintain tolerance to the prostate at steady state. In the absence of immune challenge, we found that *C4$^{\Delta TEC}$* mice did not develop spontaneous T cell infiltration of the prostate at 4, 6, and 12 months of age (Figure 14, E-F). Thus, while T cell selection on C4/I-A^b renders mice susceptible to prostatitis, C4/I-A^b-specific Tconv cells are controlled by polyclonal Treg cells of unmatched specificity at steady state.

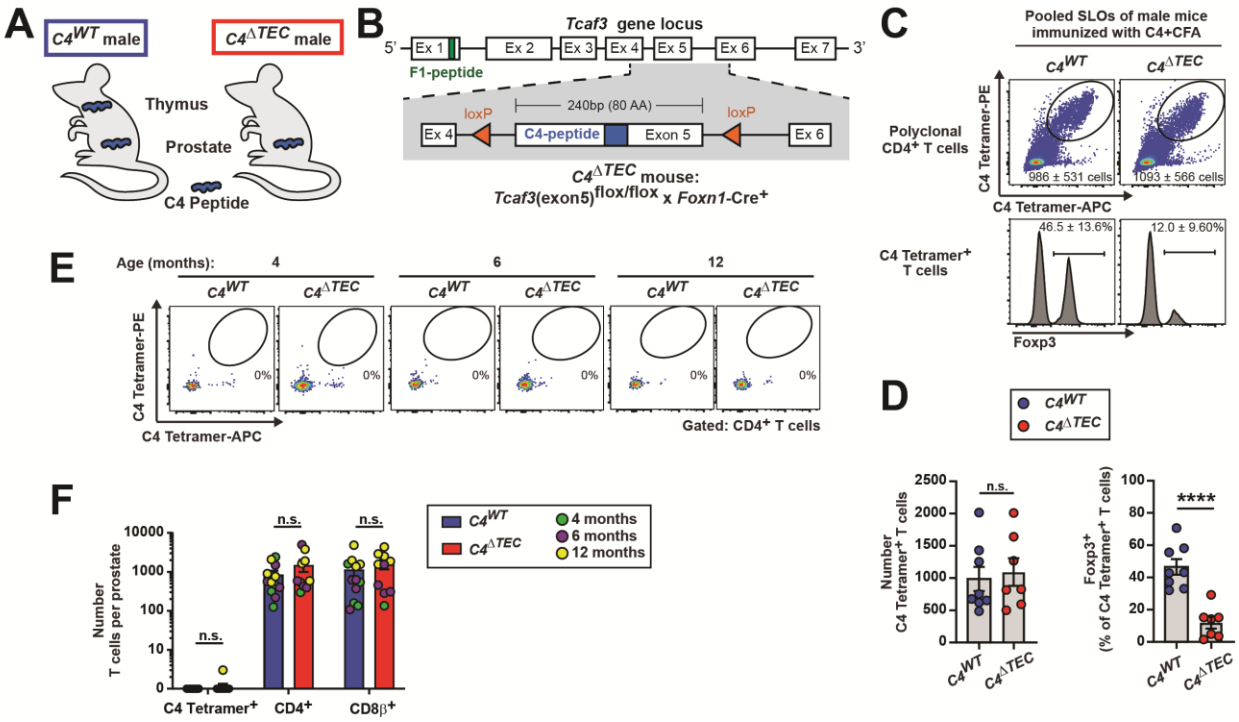

FIGURE 14. *C4$^{\Delta TEC}$* mice fail to mount a Treg-dominated response against C4/I-A^b but are protected from autoimmunity at steady-state

(A) Schematic depicting anatomical location of endogenous C4 peptide expression in *C4$^{\Delta TEC}$* (*Foxn1*-Cre$^+$ x *Tcaf3(exon5)$^{flox/flox}$*) and *C4^{WT}* male mice. In *C4$^{\Delta TEC}$* males, Cre-mediated excision of Tcaf3 exon 5 removes C4 peptide from thymic epithelial cells during T cell development but retains expression in the prostate. (B) Schematic depicting Tcaf3 gene locus. The relative location of the genomic regions encoding the C4 peptide and F1 peptide are depicted in blue and green, respectively. Inset of the Tcaf3(exon5)-floxed allele is shown in grey at the bottom, with inserted loxP sites depicted in orange. See Methods for allele generation.

(C-D) *C4^{WT}* and *C4$^{\Delta TEC}$* littermate mice were immunized subcutaneously with 100µg C4 peptide emulsified in CFA. 14 days after immunization, CD4$^+$ T cells were isolated, and C4/I-A^b tetramer-binding cells were enriched from the pooled SLOs and analyzed by flow cytometry. Data are representative of 2 independent experiments. n = 8, *C4^{WT}*; n = 7, *C4$^{\Delta TEC}$*. (C) Representative flow cytometric analysis of CD4$^+$ T cells enriched from the pooled SLOs of mice of the indicated genotype. The top plots depict C4/I-A^b tetramer-APC vs -PE expression by polyclonal CD4$^+$ T cells, whereas the bottom plots depict Foxp3 expression by dual C4/I-A^b tetramer$^+$ CD4$^+$ T cells. The absolute number of cells (top) and frequency of cells (bottom) ± SD within the indicated gates are denoted. (D) Summary plots of data pooled from (C) showing the absolute number of dual C4/I-A^b tetramer$^+$ CD4$^+$ T cells (left) and frequency of such cells expressing Foxp3 (right) enriched from the pooled SLOs from mice of the indicated genotype. Each symbol represents one mouse. Mean ± SEM is indicated (**** = P < 0.0001; two-tailed Student's t-test).

(E-F) *C4^{WT}* and *C4$^{\Delta TEC}$* littermate naïve male mice were sacrificed at the indicated age, and the prostates were analyzed for CD4$^+$, CD8β$^+$, and C4/I-A^b tetramer-binding T cells by flow cytometry. Data are representative of 3 independent experiments. n = 4, *C4^{WT}* 4mo; n = 1, *C4$^{\Delta TEC}$* 4mo; n = 4, *C4^{WT}* 6mo; n = 4, *C4$^{\Delta TEC}$* 6mo; n = 4, *C4^{WT}* 12mo; n = 5, *C4$^{\Delta TEC}$* 12mo. (E)

FIGURE 14, continued
Representative flow cytometric analysis of $CD4^+$ T cells isolated from the prostates of mice of the indicated genotype and age. The plots depict C4/I-A^b tetramer-APC vs -PE expression by polyclonal $CD4^+$ T cells. The frequency of cells within the indicated gates is denoted. (F) Summary plot of pooled data from (E) showing the number of $CD4^+$, $CD8\beta^+$, and C4/I-A^b tetramer-binding T cells isolated from the prostates of mice of the indicated genotype and age. Each symbol represents one mouse. Mean ± SEM is indicated (n.s. = $P > 0.05$; two-tailed Student's t-test).

Polyclonal Treg cells are sufficient to control C4/I-A^b-specific Tconv cells following inflammatory challenge

The activity of self-specific Tconv cells might be impacted by elevated co-stimulatory and accessory input signals common during inflammation and infection, so we wondered whether the absence of C4/I-A^b-specific Treg cells rendered $C4^{\Delta TEC}$ mice susceptible to autoimmunity following inflammatory triggers. We treated $C4^{\Delta TEC}$ mice with agonists of innate signaling pathways known to activate APCs, and 8-week-old $C4^{\Delta TEC}$ males treated with anti-CD40 agonist antibody, LPS, or poly I:C failed to develop prostatic T cell infiltration by 10 weeks post-treatment (Figure 15, A-D). We also challenged $C4^{\Delta TEC}$ and $C4^{WT}$ males with the virulent parental strain of *Lm* and infection similarly did not induce prostatic T cell infiltration (Figure 15, E-F).

Collectively, these results demonstrate that C4/I-A^b-specific Tconv cells are sufficiently constrained by Treg cells of unmatched specificity, even when APCs and T cells are activated by distinct inflammatory signals. However, C4/I-A^b-specific Tconv cells with autoimmune potential have access to self-derived ligand at steady-state and adopt inflammatory phenotypes following *Lm* infection in the prostate-draining LN (Figure 11, D-E), which suggests that these cells are unable to breach an activation threshold for pathogenicity. Given that that Treg constraint is an ongoing process downstream of TCR-induced priming (Figure 11), it follows that C4/I-A^b-specific Tconv cells are controlled following TCR engagement via bystander suppression mechanisms. In

this scenario, C4/I-A^b-specific Tconv cells would undergo initial priming via TCR signaling, which would enable these cells to transiently increase their activation status to somewhere below the threshold for complete pathogenicity, but their further activation (via TCR-independent factors such as IL-2 and costimulation) would be prevented by polyclonal Treg cells, some of which would be concurrently activated by other self-ligands.

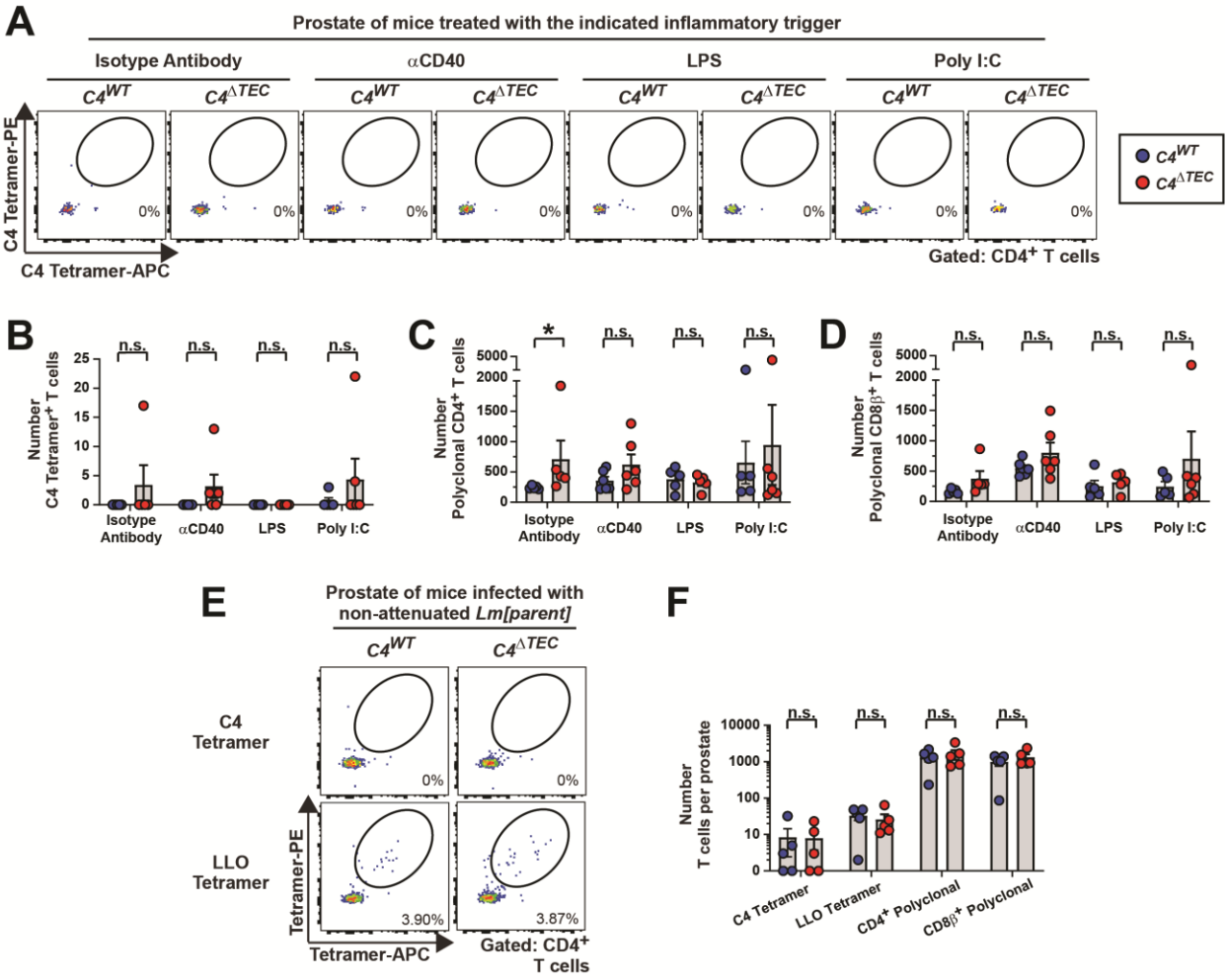

FIGURE 15. Polyclonal Treg cells are sufficient to control C4/I-A^b-specific Tconv cells following inflammatory challenge

(A-D) *C4^{WT}* and *C4$^{\Delta TEC}$* littermate male mice were challenged with a single dose of the indicated innate immune stimuli (see Methods). 10 weeks post-treatment, mice were sacrificed and the prostates were analyzed for CD4$^+$, CD8β$^+$, and tetramer-binding T cells by flow cytometry. n = 5, *C4^{WT}* Iso; n = 5, *C4$^{\Delta TEC}$* Iso; n = 6, *C4^{WT}* αCD40; n = 6, *C4$^{\Delta TEC}$* αCD40; n = 5, *C4^{WT}* LPS; n = 5, *C4$^{\Delta TEC}$* LPS; n = 6 *C4^{WT}* Poly I:C; n = 5, *C4$^{\Delta TEC}$* Poly I:C. Data are representative of two indpenedent experiments. (A) Representative flow cytometric analysis of CD4$^+$ T cells isolated from the prostates of mice of the indicated genotype and treatment. The plots depict C4/I-A^b tetramer-APC vs -PE expression by polyclonal CD4$^+$ T cells. The frequency of cells within the indicated gates is denoted. (B) Summary plot of pooled data in (A) showing the number of C4/I-A^b tetramer-binding T cells isolated from the prostates of mice of the indicated genotype and treatment. Each symbol represents one mouse. Mean ± SEM is indicated (n.s. = P > 0.05; ordinary 2-way ANOVA). (C) Summary plot of pooled data in (A) showing the number of polyclonal CD4$^+$ T cells isolated from the prostates of mice of the indicated genotype and treatment. Each symbol represents one mouse. Mean ± SEM is indicated (n.s. = P > 0.05; ordinary 2-way ANOVA). (D) Summary plot of pooled data in (A) showing the number of polyclonal CD8β$^+$ T cells isolated from the prostates of mice of the indicated genotype and

FIGURE 15, continued
treatment. Each symbol represents one mouse. Mean ± SEM is indicated (n.s. = P > 0.05; ordinary 2-way ANOVA).
(E-F) *C4*^{WT} and *C4*$^{\Delta TEC}$ littermate male mice were infected with 5x10^3 CFU of the non-attenuated parental strain of *L. monocytogenes* (see Methods). 10 weeks post-infection, mice were sacrificed, and the prostates were analyzed for CD4$^+$, CD8β$^+$, and tetramer-binding T cells by flow cytometry. n = 5, *C4*^{WT}; n = 5, *C4*$^{\Delta TEC}$. Data represent two independent experiments. (E) Representative flow cytometric analysis of CD4+ T cells isolated from the prostates of mice of the indicated genotype. The top and bottom plots respectively depict C4/I-A^b tetramer-APC vs -PE and LLO/I-A^b tetramer-APC vs -PE expression by polyclonal CD4$^+$ T cells. The frequency of cells within the indicated gates is denoted. (F) Summary plot of pooled data in (E) showing the number of CD4$^+$, CD8β$^+$, C4/I-A^b, and LLO/I-A^b tetramer-binding T cells isolated from the prostates of mice of the indicated genotype. Each symbol represents one mouse. Mean ± SEM is indicated (n.s. = P > 0.05; ordinary 2-way ANOVA).

Thymic selection on C4/I-A^b is required to prevent prostatitis following Lm[C4] infection and does not impact the T cells response to the Lm-derived LLO peptide

The control of self-pMHC-specific Tconv cells at homeostasis or following innate inflammatory challenge does not require suppression by Treg cells of matched specificity. However, proposed drivers of autoimmunity include scenarios in which self-specific Tconv cells perceive both innate activation and elevated TCR signals, including by pathogen-associated epitope mimicry and in settings where the quantity of self-pMHC ligands is increased by infection-associated cell death. Previous experiments indicate that pathogenic C4/I-A^b-specific Tconv cells can escape polyclonal Treg control following T cell transfer to a lymphopenic environment (Figure 5), further suggesting that a unique role for Treg specificity in controlling such autoreactive cells may arise following a distinct triggering event. We therefore employed our *Lm[C4]* pathogen model to concurrently elevate both innate activation and TCR signals in the same anatomic location, which allowed us to track the activation of antigen-specific Treg and Tconv cells over a precisely defined timeframe.

To define whether Treg cells reactive to C4/I-A^b play a role in controlling Tconv cells of shared specificity and maintaining tolerance in this setting, we infected $C4^{WT}$ and $C4^{\Delta TEC}$ mice with *Lm[C4]* and analyzed C4/I-A^b-specific Tconv responses and prostatic infiltration across time in the spleen and prostate-draining pLN (Figure 16, A). In $C4^{WT}$ mice, infection with *Lm[C4]* failed to induce prostatic T cell infiltration (Figure 16, B-D), demonstrating that the self-selected Treg cell-biased response to C4/I-A^b effectively controlled the C4/I-A^b-specific Tconv cell response triggered by *Lm[C4]* infection in a complete polyclonal repertoire. $C4^{WT}$ mice continued to be protected from autoimmunity more than 180 days after infection (Figure 16, E-F), demonstrating robust suppression of C4/I-A^b-specific Tconv cells long after pathogen clearance and memory T cell formation. In contrast, $C4^{\Delta TEC}$ mice infected with *Lm[C4]* rapidly developed fulminant prostatic T cell infiltration following infection, including infiltration by C4/I-A^b Tconv cells, $CD4^+$ Treg and Tconv cells, and $CD8^+$ T cells (Figure 16, B-D). These findings demonstrate that Tconv cell responses triggered by a pathogen-expressed self-peptide mimetope can be controlled in wild-type mice harboring a Treg cell-biased pool of self-pMHC-specific T cells, whereas control of such Tconv cell responses is lost when thymic selection of antigen-specific T cells is impaired. Critically, all polyclonal Treg cells reactive to other self-pMHC ligands were unable to compensate for altered thymic selection on C4/I-A^b upon *Lm[C4]* challenge.

Given the divergent outcomes in $C4^{WT}$ vs. $C4^{\Delta TEC}$ mice following *Lm[C4]* infection, we sought insight into the forces driving autoimmune protection vs. prostatic T cell infiltration in the two settings. We therefore tracked the fate of endogenous C4-specific Tconvs and Tregs across time in the spleen, which is a primary site of T cell priming during infection where the burden of attenuated *Lm* peaks in the first three days after challenge and rapidly diminishes thereafter [402-404]. In $C4^{WT}$ mice, which were protected from prostatitis, polyclonal C4/I-A^b $tetramer^+$ T cells

identified in the spleens at day 4 were predominantly Treg cells (Figure 16, G-H), as expected. Of note, both C4/I-A^b tetramer$^+$ Treg cells and Tconv cells displayed high expression of Ki67 at this early time point (Figure 16, I), indicating that despite the Treg cell-biased response in *C4^{WT}* mice, C4/I-A^b-specific Tconv cells were readily primed in the early days of *Lm[C4]* infection. The number of splenic C4/I-A^b tetramer$^+$ T cells and the extent of Treg cell skewing of these cells waned progressively at days 7 and 14 (Figure 16, H and J). In *C4$^{\Delta TEC}$* mice, which developed fulminant prostatitis following *Lm[C4]* infection, the number of C4/I-A^b tetramer$^+$ T cells elicited in the spleen at day 4 was comparable to that observed in *C4^{WT}* mice (Figure 16, J). However, the trajectory of C4/I-A^b-specific T cells in *C4$^{\Delta TEC}$* mice was characterized by a Tconv cell-dominated response, continued expansion of C4/I-A^b tetramer$^+$ T cells in the spleen at day 7, and elevated frequencies of antigen-specific T cells in the pLNs and prostate by day 14 (Figure 16, G-J). In the same experiments, we also assessed the response of CD4$^+$ T cells reactive to the *Lm*-derived peptide $LLO_{190\text{-}201}$ and found that the number and phenotype of LLO/I-A^b-specific T cells was indistinguishable in *C4^{WT}* vs. *C4$^{\Delta TEC}$* mice (Figure 16, G-J). Thus, the divergent T cell responses to C4/I-A^b did not impact the T cell response to a second *Lm*-expressed peptide, demonstrating pMHC specificity in the observed responses. Our cumulative data demonstrate that C4/I-A^b-specific Treg cells does not prevent the early activation of C4/I-A^b-specific Tconv cells following infection, firmly establishing that Treg-mediated control occurs in an "anaphylactic" manner after Tconv activation. Thus, C4/I-A^b-specific Treg cells act by selectively stifling the downstream persistence and prostatic infiltration of Tconv cells of matched specificity without altering the response of Tconv cells reactive to a pathogen-specific nonself antigen.

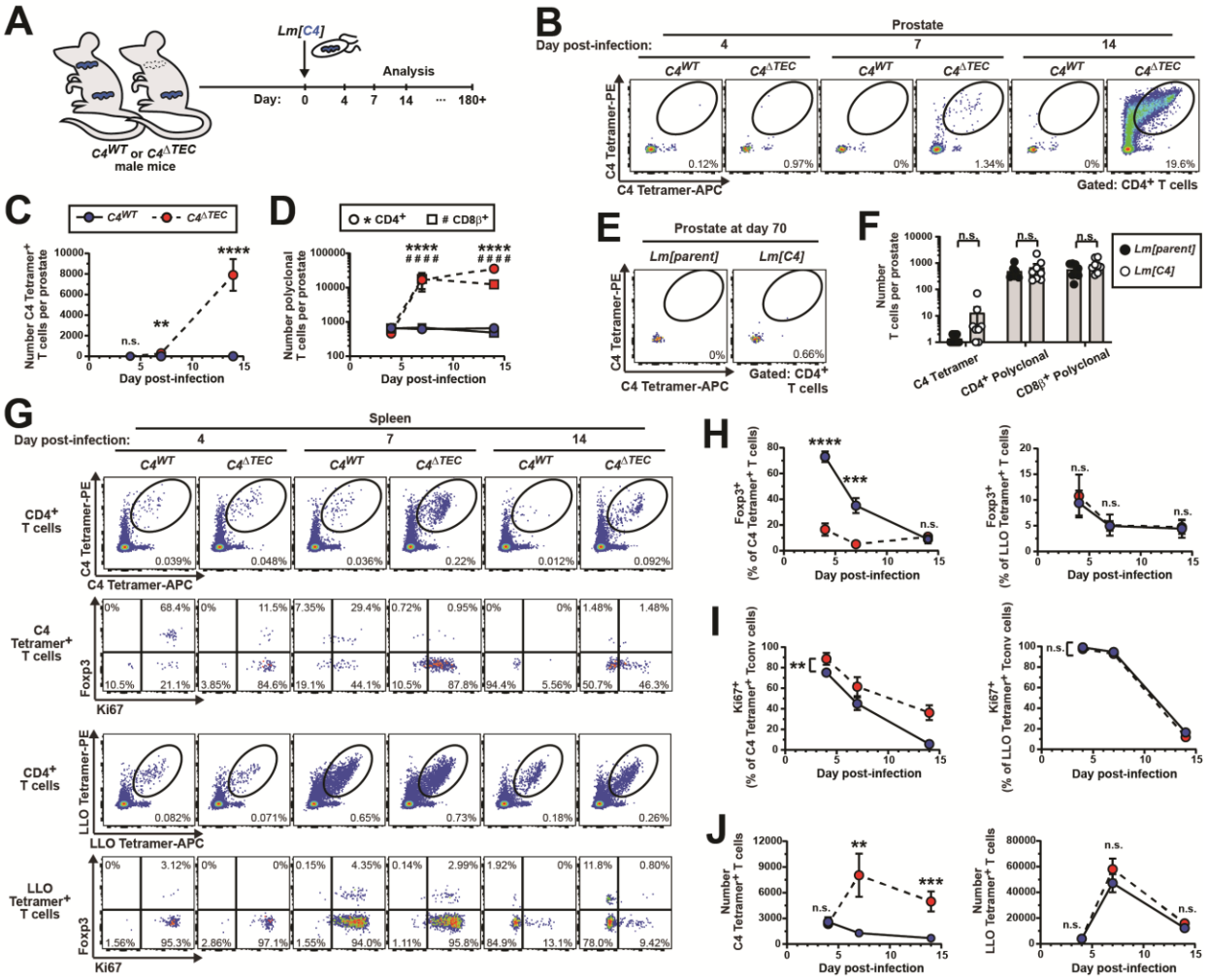

FIGURE 16. Thymic selection on C4/I-A^b is required to prevent prostatitis following *Lm[C4]* infection and does not impact the T cell response to the *Lm*-derived LLO peptide antigen

(A) *C4^{WT}* and *C4$^{\Delta TEC}$* mice were challenged intravenously with 10^7 CFU *Lm[C4]*. On the indicated day post-infection, T cells were isolated from the indicated organ, labelled with C4/I-A^b or LLO/I-A^b tetramers, and analyzed by flow cytometry. Data ae representative of 3-4 experiments. n = 6, *C4^{WT}* d4; n = 7, *C4$^{\Delta TEC}$* d4; n = 6, *C4^{WT}* d7; n = 7, *C4$^{\Delta TEC}$* d7; n = 8, *C4^{WT}* d14; n = 10, *C4$^{\Delta TEC}$* d14. (B) Representative flow cytometric analysis of CD4$^+$ T cells isolated from the prostates of mice of the indicated genotype on the indicated day post-infection. Plots depict C4/I-A^b tetramer-APC vs -PE expression by polyclonal CD4$^+$ T cells. The frequency of cells within the indicated gates are denoted. (C) Summary plot of data pooled from (B) showing the number of dual C4/I-A^b tetramer$^+$ CD4$^+$ T cells recovered from the prostates of mice of the indicated genotype and day post-infection. Each symbol represents the mean ± SEM of pooled mice. (** = P < 0.01; **** = P < 0.0001; n.s. = P > 0.05; two-tailed non-parametric Mann-Whitney test). (D) Summary plot of data pooled from (B) showing the number of CD4$^+$ T cells and CD8β$^+$ T cells recovered from the prostates of mice of the indicated genotype and day post-infection. Each symbol represents the mean ± SEM of pooled mice. (**** = P < 0.0001 CD4+ T cells; #### = P < 0.0001 CD8β$^+$ T cells; two-tailed non-parametric Mann-Whitney test). (E-

FIGURE 16, continued
F) Wild-type male mice were infected with 10^7 CFU *Lm[C4]* or *Lm[parent]*. 6 months post-infection, mice were sacrificed, and the prostates were analyzed for $CD4^+$, $CD8\beta^+$, and C4/I-A^b tetramer-binding T cells by flow cytometry. Data represent two independent experiments. n = 8, *Lm[parent]*; n = 8, *Lm[C4]*. (E) Representative flow cytometric analysis of $CD4^+$ T cells isolated from the prostates of mice infected with the indicated pathogen strain. The plots depict C4/I-A^b tetramer-APC vs -PE expression by polyclonal $CD4^+$ T cells. The frequency of cells within the indicated gates is denoted. (F) Summary plot of pooled data in (E) showing the number of $CD4^+$, $CD8\beta^+$, and C4/I-A^b tetramer-binding T cells isolated from the prostates of mice infected with the indicated pathogen strain. Each symbol represents one mouse. Mean ± SEM is indicated (n.s. = $P > 0.05$; ordinary 2-way ANOVA). (G) Representative flow cytometric analysis of $CD4^+$ T cells isolated from the spleens of mice of the indicated genotype on the indicated day post-infection. The plots depict C4/I-A^b or LLO/I-A^b tetramer-APC vs -PE expression by polyclonal $CD4^+$ T cells, and Ki67 vs Foxp3 expression by C4/I-A^b or LLO/I-A^b $tetramer^+$ T cells. The frequency of cells within the indicated gates are denoted. (H) Summary plot of data pooled from (G) showing the frequency of dual C4/I-A^b $tetramer^+$ (left) or LLO/I-A^b $tetramer^+$ (right) $CD4^+$ T cells expressing Foxp3 in the spleens of mice of the indicated genotype and day post-infection. Each symbol represents the mean ± SEM of pooled mice. (** = $P < 0.01$; n.s. = $P > 0.05$; two-tailed non-parametric Mann-Whitney test). (I) Summary plot of data pooled from (G) showing the frequency of dual C4/I-A^b $tetramer^+$ (left) or LLO/I-A^b $tetramer^+$ (right) $CD4^+$ Tconv cells expressing Ki67 in the spleens of mice of the indicated genotype and day post-infection. Each symbol represents the mean ± SEM of all mice.(** = $P < 0.01$; ordinary 2-way ANOVA). (J) Summary plot of data pooled from (G) showing the number of dual C4/I-A^b $tetramer^+$ (left) or LLO/I-A^b $tetramer^+$ (right) $CD4^+$ T cells recovered from the spleens of mice of the indicated genotype and day post-infection. Each symbol represents the mean ± SEM of pooled mice. (** = $P < 0.01$; **** = $P < 0.0001$; n.s. = $P > 0.05$; two-tailed non-parametric Mann-Whitney test).

The prostate-draining pLN contains a reservoir of proliferating C4/I-A^b-specific T cells in $C4^{\Delta TEC}$ mice following Lm[C4] infection

The presence of activated C4/I-A^b-specific T cells in the spleens of *Lm[C4]* infected mice indicates that the pathogen is capable of triggering self-directed responses at sites distal from the prostate, and imply directed migration of such cells back to the prostate or draining LN following infection, at least in $C4^{\Delta TEC}$ mice that develop autoimmunity. Curiously, stromal cells of the prostate, which produce Tcaf3 and the C4 peptide, do not express MHC-II and thus cannot be directly targeted by $CD4^+$ Tconv cells [405], so we reasoned that activated T cells were likely to first traffic to the draining LN. To capture autoimmune licensing at this site, we measured C4/I-A^b and

LLO/I-A^b-responses in $C4^{WT}$ and $C4^{\Delta TEC}$ mice at the pLN following *Lm[C4]* infection. In $C4^{WT}$ mice, which were protected from autoimmunity, the number of C4/I-A^b-specific T cells remained low and constant throughout infection (Figure 17, A-B), with an approximately equal composition of Treg and Tconv cells (Figure 17, C). In contrast to the spleen, C4/I-A^b Tconv cells never expressed Ki67 (Figure 17, D), suggesting that these cells had either lost their proliferation capacity while trafficking to the pLN or were instructed to turn off the program upon entry. In this regard, a significant fraction of C4/I-A^b-specific Treg cells retained Ki67 in the pLN following infection, which may imply that these cells actively reinforce suppression of C4/I-A^b-specific Tconv cells at this site as an additional layer of autoimmune control.

In $C4^{\Delta TEC}$ mice, C4/I-A^b-specific Tconv cells progressively increased in number following infection in the pLN (Figure 17, B) but not the spleen (Figure 16, J), further supporting the notion that these cells migrate from distal sites following activation. By day 7, more than half of these cells retained Ki67 expression, which was sustained at day 14 long after the pathogen had been cleared (Figure 17, D). Interestingly, the Ki67 expression pattern of C4/I-A^b-specific T cells at day 7 and 14 was distinct, as these cells exhibited high and low fluorescence intensity of Ki67, respectively (Figure 17, A). These data support a model whereby pathogenic C4/I-A^b-specific Tconv cells arrive at the pLN in a hyperactivated state, initiate prostatic T cell infiltration, and take up residence in the pLN to perpetuate the autoimmune reaction following a shift to a basal-proliferative state. A similar phenomenon was recently described for pathogenic $CD8^+$ T cells in diabetic NOD mice immunity [406]. Finally, LLO/I-A^b-specific Tconv cell phenotypes were not different between $C4^{WT}$ and $C4^{\Delta TEC}$ mice in the pLN (Figure 17, C-D), but the number of LLO/I-A^b-specific Tconv cells was higher at this site by day 14 in $C4^{\Delta TEC}$ mice (Figure 17, B), supporting

the notion that pathogen-specific memory cells trafficking from distal sites contribute to the polyclonal prostatic infiltrate in *C4$^{\Delta TEC}$* mice following infection (discussed in Chapter 3).

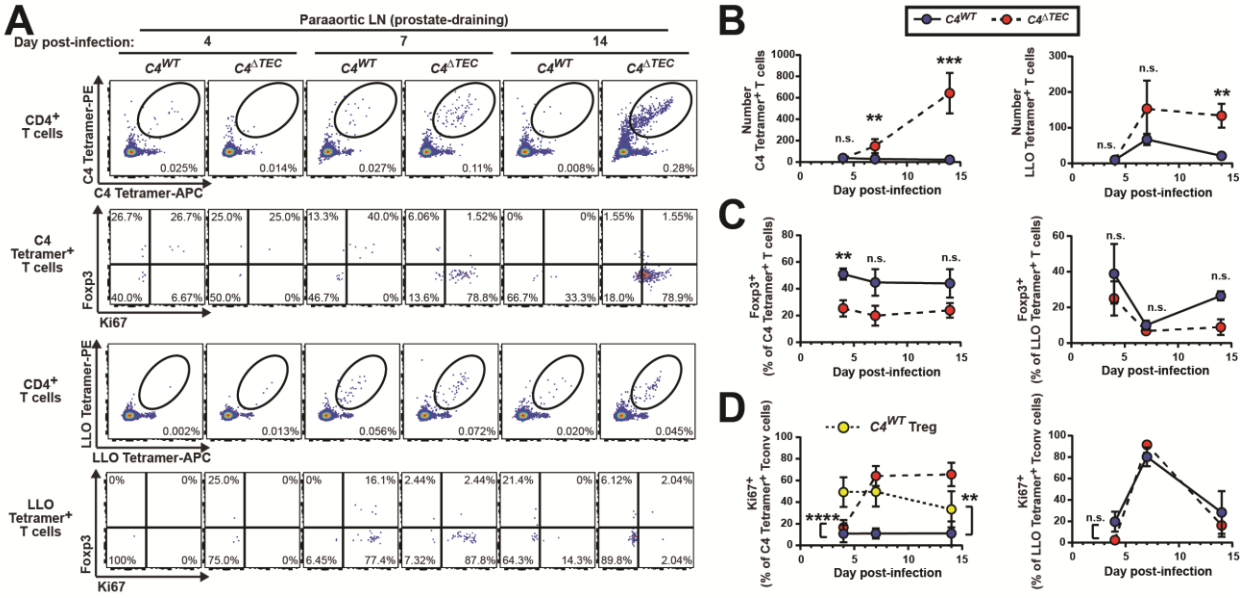

FIGURE 17. The prostate-draining LN contains a reservoir of proliferating C4/I-A^b-specific T cells in *C4$^{\Delta TEC}$* mice following *Lm[C4]* infection

As in Figure 16, *C4^{WT}* and *C4$^{\Delta TEC}$* mice were challenged intravenously with 10^7 CFU *Lm[C4]*. On the indicated day post-infection, T cells were isolated from the indicated organ, labelled with C4/I-A^b or LLO/I-A^b tetramers, and analyzed by flow cytometry. Data ae representative of 3-4 experiments. n = 6, *C4^{WT}* d4; n = 7, *C4$^{\Delta TEC}$* d4; n = 6, *C4^{WT}* d7; n = 7, *C4$^{\Delta TEC}$* d7; n = 8, *C4^{WT}* d14; n = 10, *C4$^{\Delta TEC}$* d14. (A) Representative flow cytometric analysis of CD4$^+$ T cells isolated from the paraaortic LNs of mice of the indicated genotype on the indicated day post-infection. The plots depict C4/I-A^b or LLO/I-A^b tetramer-APC vs -PE expression by polyclonal CD4$^+$ T cells, and Ki67 vs Foxp3 expression by C4/I-A^b or LLO/I-A^b tetramer$^+$ T cells. The frequency of cells within the indicated gates are denoted. (B) Summary plot of data pooled from (A) showing the number of dual C4/I-A^b tetramer$^+$ (left) or LLO/I-A^b tetramer$^+$ (right) CD4$^+$ T cells recovered from the paraaortic LNs of mice of the indicated genotype and day post-infection. Each symbol represents the mean ± SEM of pooled mice. (** = P < 0.01; *** = P < 0.001; n.s. = P > 0.05; two-tailed non-parametric Mann-Whitney test). (C) Summary plot of data pooled from (A) showing the frequency of dual C4/I-A^b tetramer$^+$ (left) or LLO/I-A^b tetramer$^+$ (right) CD4$^+$ T cells expressing Foxp3 in the paraaortic LNs of mice of the indicated genotype and day post-infection. Each symbol represents the mean ± SEM of pooled mice. (** = P < 0.01; n.s. = P > 0.05; two-tailed non-parametric Mann-Whitney test). (D) Summary plot of data pooled from (A) showing the frequency of dual C4/I-A^b tetramer$^+$ (left) or LLO/I-A^b tetramer$^+$ (right) CD4$^+$ Tconv cells expressing Ki67 in the paraaortic LNs of mice of the indicated genotype and day post-infection. Each symbol represents the mean ± SEM of all mice. C4/I-A^b-specific Treg cells are included in yellow. (** = P < 0.01; **** = P < 0.0001; n.s. = P > 0.05; ordinary 2-way ANOVA).

C4/I-A^b-specific Tconv cells are not permanently inactivated by self-antigen recognition and have pathogenic potential in C4^{WT} mice

In addition to being a *de facto* model of pathogen-associated epitope mimicry, we also propose that *Lm[C4]* infection could reflect a more common infection scenario where a tissue-invading pathogen causes the release of self-derived antigen that serve to enhance TCR signals in an inflammatory environment. However, our experiments suggest that C4/I-A^b-Tconv responses triggered by *Lm[C4]* at sites distal to the prostate are the primary drivers of autoimmunity in the absence of C4/I-A^b-Treg cells, and it remained possible that C4/I-A^b-specific Tconv cells that normally exist the pLN in *C4$^{\Delta TEC}$* mice are functionally incapable of mounting a pathogenic T cell response. In this case, the pathogen-expressed mimetope peptide would be crucial to overcome tolerance since self-reactive Tconv cells at relevant tissue sites would be anergic or inert prior to the infectious trigger. To test whether C4/I-A^b-specific Tconv cells at the pLN are capable of mounting an autoimmune response upon infection, we reconstituted T cell-deficient male mice with bulk cells from the pLN or non-draining LN of *C4$^{\Delta TEC}$* donor mice and measured the autoimmune potential of such cells following *Lm[C4]* challenge of host mice (Figure 18, A). Surprisingly, 50% of the recipients of pLN cells displayed severe prostatic infiltration by C4/I-A^b and polyclonal CD4$^+$ T cells, while none of the ndLN cell recipients developed prostatitis (Figure 18, B-C). Incomplete penetrance of autoimmunity amongst hosts was most probably due to the rarity of C4/I-A^b-specific cells amongst the donor inoculum. Thus, C4/I-A^b-specific Tconv cells at the pLN not only retain autoimmune potential but may be even more pathogenic than the same cells at distal sites, possibly owing to higher-affinity TCRs or lower signaling thresholds by recent recognition of self antigen.

The breach of tolerance in *C4*$^{\Delta TEC}$ mice following *Lm[C4]* infection is critically dependent on the escape of C4/I-A^b-specific Tconv cells. The paucity of C4/I-A^b-specific Treg cells elicited in *C4*$^{\Delta TEC}$ mice, coupled with the prevalence of such cells in autoimmune-protected *C4*^{WT} mice, strongly suggests a non-redundant role for antigen-specific Treg control of Tconv cells following infection. Still, given that thymic selection on C4/I-A^b (and other Aire-dependent specificities) is known to alter the repertoires and presumably affinities/avidities of antigen-specific Treg and Tconv cells [87], it remained possible that thymic selection on C4/I-A^b removes any TCR clones with autoimmune potential from the Tconv repertoire of antigen-specific cells in *C4*^{WT} mice. To formally demonstrate that peripheral tolerance to C4 peptide following infection depends on suppression by Treg cells, we transiently depleted polyclonal Treg cells in *Foxp3*-DTR$^+$ male mice just before and after *Lm[C4]* challenge (Figure 18, D), and found populations of C4/I-A^b-specific, LLO/I-A^b-specific, and polyclonal Tconv cells infiltrating the prostate 14 days after infection (Figure 18, E-F). Therefore, C4/I-A^b-specific Tconv cells retain pathogenic potential in a wild-type repertoire, and their control following *Lm[C4]* infection maps to the Treg compartment.

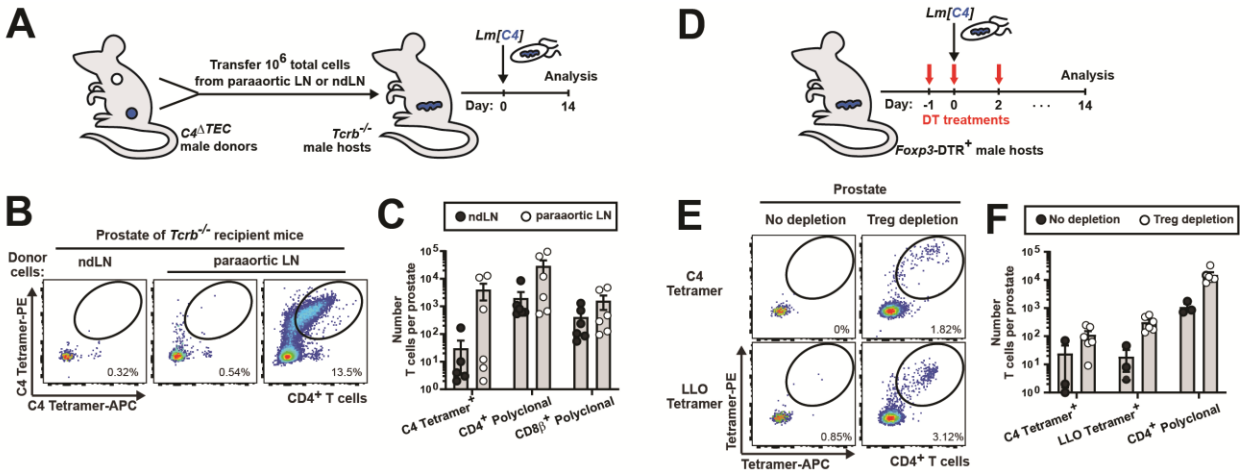

FIGURE 18. C4/I-A^b-specific Tconv cells are not permanently inactivated by self-antigen recognition and have pathogenic potential in *C4^{WT}* mice.

(A-C) Cells isolated from the prostate-draining paraaortic LNs and non-draining inguinal LNs were harvested and pooled from five *C4$^{\Delta TEC}$* donor males and 10^6 total cells were injected into *Tcrb$^{-/-}$* host males, which were subsequently infected intravenously with 10^7 CFU *Lm[C4]*. The prostates of host mice were analyzed by flow cytometry 14 days post-infection. *C4^{WT}*; n = 6, *C4$^{\Delta TEC}$*; n = 6. Data represent one experiment. (B) Representative flow cytometric analysis of CD4+ T cells isolated from the prostates of host mice that received donor cells from the indicated organ. Plots depict C4/I-A^b tetramer-APC vs -PE expression by polyclonal CD4$^+$ T cells. The frequency of cells within the indicated gates are denoted. (C) Summary plot of data pooled from (B) showing the number of T cells recovered from the prostates of host mice that received donor cells from the indicated organ. Each symbol represents one mouse. The mean ± SEM is indicated.

(D-F) Foxp3-DTR$^+$ male mice were infected intravenously with 10^7 CFU *Lm[C4]* and were either transiently depleted of all polyclonal Tregs via DT injection on days -1, 0, and 2 post-infection or left untreated. 14 days post-infection, the cells were isolated from the prostates and analyzed by flow cytometry. No depletion; n = 3, Treg depletion; n = 6. Data represent one experiment. (E) Representative flow cytometric analysis of CD4$^+$ T cells isolated from the prostates of mice that were transiently depleted of Treg cells or left untreated. Plots depict C4/I-A^b tetramer-APC vs -PE expression (top) or LLO/I-A^b tetramer-APC vs -PE expression (bottom) by polyclonal CD4$^+$ T cells. The frequency of cells within the indicated gates are denoted. (F) Summary plot of data pooled from (E) showing the number of T cells recovered from the prostates of mice that were transiently depleted of Treg cells or left untreated. Each symbol represents one mouse. The mean ± SEM is indicated.

Tolerance to the Tcaf3-derived F1 peptide is maintained in C4$^{\Delta TEC}$ mice following Lm[F1] infection

The cumulative evidence supports the notion that *C4$^{\Delta TEC}$* but not *C4^{WT}* mice develop autoimmune disease following *Lm[C4]* infection due to the failure of C4/I-A^b-specific Treg cells

to control of Tconv cells with matched specificity. While presently unknown, the mechanism is presumably one that cannot be mediated by any other specificity of Treg cells (Figure 16). However, as discussed for *Tcaf3(C4)*$^{-/-}$ mice (Figure 2), Cre-mediated deletion of the exon 5 segment in *C4*$^{\Delta TEC}$ mice could impact Tcaf3 expression including presentation of the F1 peptide, and thus *C4*$^{\Delta TEC}$ mice may lack other relevant Treg specificities. We therefore generated attenuated recombinant *Lm* expressing the I-A^b-restricted, Tcaf3-derived "F1" peptide (Figure 12, B), which is encoded by *Tcaf3* exon 1 (Figure 14, B). *Aire*$^{-/-}$ mice, which have exhibit a defect in both C4/I-A^b- and F1/I-A^b-specific Treg cells [87] among others, presented with robust infiltration of the prostate by F1/I-A^b-specific T cells following *Lm[F1]* challenge (Figure 19, A-D). In contrast, neither *C4*$^{\Delta TEC}$ nor *C4*^{WT} mice developed prostatitis following *Lm[F1]* infection. Remarkably, while there were numeric and phenotypic differences between F1/I-A^b-specific T cells elicited in the spleen between *Aire*$^{-/-}$ mice and *C4*$^{\Delta TEC}$ or *C4*^{WT} mice, there was no difference in the response against the LLO peptide despite the presumed loss of many Treg specificities in *Aire*$^{-/-}$ mice (Figure 19, E-H), further supporting the notion that individual specificities can be independently regulated following infection. These data demonstrate that altered T cell selection on C4/I-A^b in *C4*$^{\Delta TEC}$ mice does not impair tolerance to the F1/I-A^b antigen derived from the same source protein.

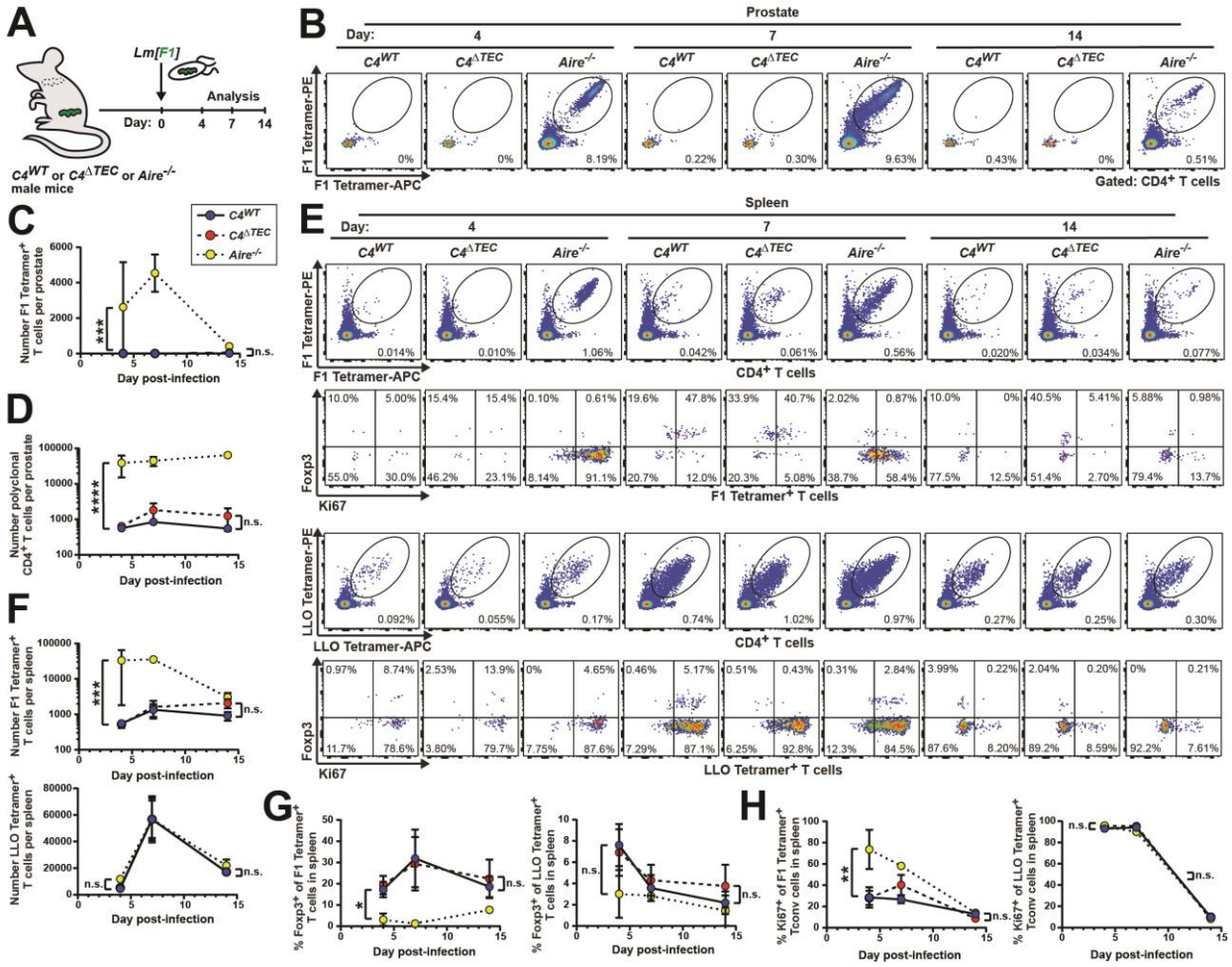

FIGURE 19. Tolerance to the Tcaf3-derived F1 peptide is maintained in *C4$^{\Delta TEC}$* mice following *Lm[F1]* infection

(A) *C4^{WT}*, *C4$^{\Delta TEC}$*, and *Aire$^{-/-}$* mice were challenged intravenously with 10^7 CFU *Lm[F1]*. On the indicated day post-infection, T cells were isolated from the indicated organ, labelled with F1/I-A^b or LLO/I-A^b tetramers, and analyzed by flow cytometry. Data are representative of 2 experiments. n = 4, *C4^{WT}* d4; n = 4, *C4$^{\Delta TEC}$* d4; n = 2, *Aire$^{-/-}$* d4; n = 4, *C4^{WT}* d7; n = 4, *C4$^{\Delta TEC}$* d7; n = 2, *Aire$^{-/-}$* d7; n = 4, *C4^{WT}* d14; n = 4, *C4$^{\Delta TEC}$* d14; n = 2, *Aire$^{-/-}$* d14. (B) Representative flow cytometric analysis of CD4$^+$ T cells isolated from the prostates of mice of the indicated genotype on the indicated day post-infection. Plots depict F1/I-A^b tetramer-APC vs -PE expression by polyclonal CD4$^+$ T cells. The frequency of cells within the indicated gates are denoted. (C) Summary plot of data pooled from (B) showing the number of dual F1/I-A^b tetramer$^+$ CD4$^+$ T cells recovered from the prostates of mice of the indicated genotype and day post-infection. Each symbol represents the mean ± SEM of pooled mice. (*** = P < 0.001; n.s. = P > 0.05; two-tailed non-parametric Mann-Whitney test). (D) Summary plot of data pooled from (B) showing the number of CD4$^+$ T cells recovered from the prostates of mice of the indicated genotype and day post-infection. Each symbol represents the mean ± SEM of pooled mice. (**** = P < 0.0001 CD4+ T cells; two-tailed non-parametric Mann-Whitney test). (E) Representative flow cytometric analysis of CD4$^+$ T cells isolated from the spleens of mice of the indicated genotype on the indicated day post-infection. The plots depict F1/I-A^b or LLO/I-

FIGURE 19, continued
A^b tetramer-APC vs -PE expression by polyclonal $CD4^+$ T cells, and Ki67 vs Foxp3 expression by F1/I-A^b or LLO/I-A^b $tetramer^+$ T cells. The frequency of cells within the indicated gates are denoted. (F) Summary plot of data pooled from (E) showing the number of dual F1/I-A^b $tetramer^+$ (top) or LLO/I-A^b $tetramer^+$ (bottom) $CD4^+$ T cells recovered from the spleens of mice of the indicated genotype and day post-infection. Each symbol represents the mean ± SEM of pooled mice. (*** = $P < 0.001$; n.s. = $P > 0.05$; two-tailed non-parametric Mann-Whitney test). (G) Summary plot of data pooled from (E) showing the frequency of dual F1/I-A^b $tetramer^+$ (left) or LLO/I-A^b $tetramer^+$ (right) $CD4^+$ T cells expressing Foxp3 in the spleens of mice of the indicated genotype and day post-infection. Each symbol represents the mean ± SEM of pooled mice. (* = $P < 0.05$; n.s. = $P > 0.05$; two-tailed non-parametric Mann-Whitney test). (H) Summary plot of data pooled from (E) showing the frequency of dual F1/I-A^b $tetramer^+$ (left) or LLO/I-A^b $tetramer^+$ (right) $CD4^+$ Tconv cells expressing Ki67 in the spleens of mice of the indicated genotype and day post-infection. Each symbol represents the mean ± SEM of all mice.(** = $P < 0.01$; ordinary 2-way ANOVA).

In a reconstitution setting using T cell-deficient hosts, C4/I-A^b-specific Tconv cells cannot be suppressed by increasing the number of endogenous Treg cells of shared specificity

Having demonstrated a requirement for C4/I-A^b-specific Treg cells in preventing autoimmune disease following *Lm[C4]* infection, we next wondered whether these cells were sufficient to prevent the pathogenicity of C4/I-A^b-specific Tconv cells. We performed a series of experiments in an attempt to increase or decrease the numeric ratio of C4/I-A^b-specific Treg over Tconv cells within the host. This was especially alluring since it would enable us to discern whether a numeric Treg advantage is sufficient to prevent disease, or if other factors such as T cell activation states or cellular positioning are important.

In the first experiment, we performed Treg/Tconv "mixing" reconstitutions. Given the loss of $Foxp3^+$ C4/I-A^b-specific Treg cells in C4 peptide-deficient mice following immunization (Figure 4), we reasoned that the frequency of C4/I-A^b-specific Tregs was higher within the polyclonal Treg compartment of *Tcaf3(C4)*$^+$ mice than *Tcaf3(C4)*$^{-/-}$ mice, and that the reverse was true for C4/I-A^b Tconv cells. We sorted polyclonal Treg and Tconv cells from *Tcaf3(C4)*$^+$ and

Tcaf3(C4)$^{-/-}$ donor mice, reconstituted T cell-deficient hosts with one of four inoculum pools containing a unique combination of Treg and Tconv cells, and infected the host mice with *Lm[C4]* following a rest period (Figure 20, A). In this way, host receiving *C4*$^{+}$ Treg cells with *C4*$^{-/-}$ Tconv cells had more C4/I-A^{b}-specific Treg cells than mice reconstituted with Treg and Tconv cells from *C4*$^{-/-}$ mice. Similarly, hosts of *C4*$^{-/-}$ Treg cells with *C4*$^{+-}$ Tconv cells had less C4/I-A^{b}-specific Treg cells than those reconstituted with *C4*$^{+}$ Treg and Tconv cells. Following infection, hosts that had received *C4*$^{-/-}$ Tconv cells developed prostatic T cell infiltration in all cases, while those that had received *C4*$^{+}$ Tconv cells did not (Figure 20, B-E). Notably, the Treg compartment had little effect on the autoimmune outcome. These results suggest that Tconv cells in *C4*$^{-/-}$ mice are more potent potentiators of autoimmunity than those in *C4*$^{+}$ mice. It is important to note that the relative ratio of C4/I-A^{b} Treg and Tconv cells after engraftment is unknown in the host mice, so it is difficult to conclude whether the observed breach in tolerance is due to a failure of sufficient numbers of antigen-specific *C4*$^{+}$ Treg cells to seed the host prior to infection. Similarly, the number of C4/I-A^{b}-specific Tconv cells in the *C4*$^{-/-}$ Tconv inoculum is unknown and may still exceed the Treg/Tconv ratio required to maintain tolerance, if one exists. Finally, given that C4/I-A^{b}-specific Treg cells are not completely absent from *C4*$^{-/-}$ mice (Figure 4, B), these cells may be sufficient to control C4/I-A^{b}-specific Tconv cells from *C4*$^{+}$ hosts, at least in the artificial ratios used in this experiment.

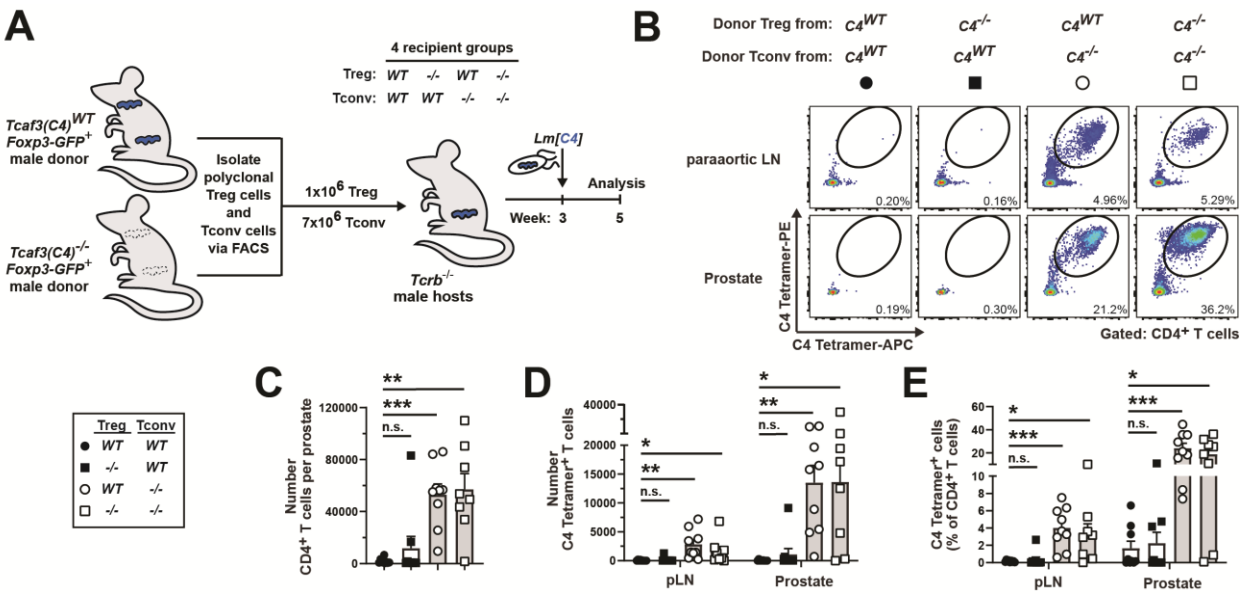

FIGURE 20. In a reconstitution setting using T cell-deficient hosts, C4/I-A^b-specific Tconv cells cannot be suppressed by increasing the number of endogenous Treg cells of shared specificity

(A) Experimental schematic for panels (B-E). Foxp3$^+$ CD4$^+$ Treg cells and Foxp3^{neg} CD4$^+$ Tconv cells were isolated from the pooled SLOs of *Tcaf3(C4)*$^+$ or *Tcaf3(C4)*$^{-/-}$ donor mice that harbored the Foxp3-eGFP reporter allele. The *Tcaf3(C4)*$^+$ Treg pool contains a higher proportion of C4/I-A^b-specific Treg cells than the *Tcaf3(C4)*$^+$ Treg pool, while the *Tcaf3(C4)*$^{-/-}$ Tconv pool contains a higher proportion of C4/I-A^b-specific Tconv cells than the *Tcaf3(C4)*$^+$ Tconv pool (Figure 3). Four groups of *Tcrb*$^{-/-}$ recipient mice received 1 x 10^6 Foxp3$^+$ Treg and 7 x 10^6 Foxp3^{neg} Tconv cells that were mixed by donor genotype as indicated and co-transferred. 3 weeks after transfer, recipient mice were infected intravenously with 10^7 CFU *Lm[C4]*. 2 weeks following infection, CD4$^+$ T cells were isolated from the paraaortic LN and prostate of recipient mice, stained with C4/I-A^b tetramer, and analyzed by flow cytometry. n = 9, *Tcaf3(C4)*$^+$ Treg *Tcaf3(C4)*$^+$ Tconv; n = 9, *Tcaf3(C4)*$^{-/-}$ Treg *Tcaf3(C4)*$^+$ Tconv; n = 9, *Tcaf3(C4)*$^+$ Treg *Tcaf3(C4)*$^{-/-}$ Tconv; n = 8, *Tcaf3(C4)*$^{-/-}$ Treg *Tcaf3(C4)*$^{-/-}$ Tconv. Data are representative of three independent experiments. (B) Representative flow cytometric analysis of CD4$^+$ T cells isolated from the indicated organ of host mice. The plots depict C4/I-A^b tetramer-APC vs -PE expression by polyclonal CD4$^+$ T cells. The frequency of cells within the indicated gates is denoted. (C) Summary plot of pooled data showing the absolute number of polyclonal CD4$^+$ cells isolated from the prostates of host mice. Each symbol represents one mouse. Mean ± SEM is indicated (n.s. = P > 0.05, ** = P < 0.01, *** = P < 0.001; ordinary 1-way ANOVA). (D) Summary plot of pooled data showing the absolute number of dual C4/I-A^b tetramer$^+$ CD4$^+$ cells isolated from the indicated organs of host mice. Each symbol represents one mouse. Mean ± SEM is indicated (n.s. = P > 0.05, * = P < 0.05, ** = P < 0.01; ordinary 2-way ANOVA). (E) Summary plot of pooled data showing the frequency of dual C4/I-A^b tetramer$^+$ CD4$^+$ cells amongst CD4$^+$ cells isolated from the indicated organs of host mice. Each symbol represents one mouse. Mean ± SEM is indicated (n.s. = P > 0.05, * = P < 0.05, *** = P < 0.001; ordinary 2-way ANOVA).

Reconstitution of lymphopenic males with C4/I-A^b tetramer-depleted Tregs does not exacerbate prostatic T cell infiltration following Lm[C4] infection

In the next experiment, we attempted to remove C4/I-A^b-specific Treg cells from the wild-type repertoire and measure the impact on autoimmunity following *Lm[C4]* infection. We sorted polyclonal Treg and Tconv cells from wild-type donor males, then tetramer stained the Treg fraction with C4/I-A^b or irrelevant 2W1S/I-A^b tetramers and magnetically depleted the tetramer-binding cells, and finally reconstituted *Tcrb*$^{-/-}$ mice with tetramer-depleted Treg cells and sorted Tconv cells (Figure 21, A). Following *Lm[C4]* infection, we found that some host mice depleted of C4/I-A^b Treg cells presented with polyclonal and C4/I-A^b-specific T cell infiltration of the prostate, though this penetrance was not complete amongst mice nor did it reach statistical significance over 2W1S/I-A^b tetramer-depleted Treg recipients (Figure 21, B-D). Even so, these results further demonstrate that C4/I-A^b-specific Tconv cells in wild-type mice are capable of eliciting autoimmune prostatitis. Unfortunately, analysis of the pLN and prostate revealed that C4/I-A^b-specific Treg cells were far from absent in host mice that had been tetramer-depleted of such cells (Figure 21, E), indicating a critical caveat in these experiments that again prevents a conclusion on the sufficiency of C4/I-A^b-specific Tregs for protection during infection.

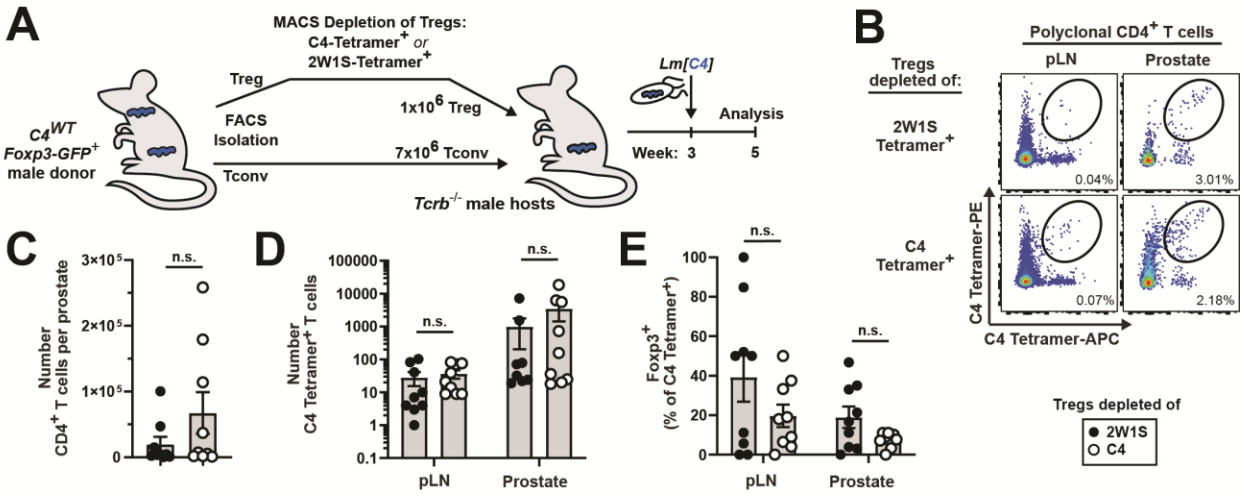

FIGURE 21. Reconstitution of T cell-deficient males with C4/I-A^b tetramer-depleted Tregs does not exacerbate prostatic T cell infiltration following *Lm[C4]* infection

(A) Experimental schematic for panels (B-E). Foxp3$^+$ CD4$^+$ Treg cells and Foxp3^{neg} CD4$^+$ Tconv cells were isolated via FACS from the pooled SLOs of *C4^{WT}* donor mice that harbored the Foxp3-eGFP reporter allele. The Treg pool was split in half, stained with either C4/I-A^b Tetramer-APC and -PE or control 2W1S/I-A^b Tetramer-APC and -PE, and depleted of Tetramer-binding cells over a column using αAPC/PE magnetic beads. The Tconv pool was unmanipulated. *Tcrb$^{-/-}$* recipient mice received 7 x 10^6 Foxp3^{neg} Tconv cells co-transferred with 1 x 10^6 Foxp3$^+$ Treg cells depleted of either tetramer. 3 weeks after transfer, recipient mice were infected intravenously with 10^7 CFU *Lm[C4]*. 2 weeks following infection, CD4$^+$ T cells were isolated from the paraaortic LN and prostate of recipient mice, stained with C4/I-A^b tetramer, and analyzed by flow cytometry. n = 9, C4/I-A^b-depleted Treg; n = 9, 2W1S/I-A^b-depleted Treg. Data are representative of three independent experiments. (B) Representative flow cytometric analysis of CD4$^+$ T cells isolated from the indicated organ of host mice. The plots depict C4/I-A^b tetramer-APC vs -PE expression by polyclonal CD4$^+$ T cells. The frequency of cells within the indicated gates is denoted. (C) Summary plot of pooled data showing the absolute number of polyclonal CD4$^+$ cells isolated from the prostates of host mice. Each symbol represents one mouse. Mean ± SEM is indicated (n.s. = P > 0.05; Welch's t test). (D) Summary plot of pooled data showing the absolute number of dual C4/I-A^b tetramer$^+$ CD4$^+$ cells isolated from the indicated organs of host mice. Each symbol represents one mouse. Mean ± SEM is indicated (n.s. = P > 0.05; ordinary 1-way ANOVA). (E) Summary plot of pooled data showing the frequency of dual C4/I-A^b tetramer$^+$ CD4$^+$ cells expressing Foxp3, isolated from the indicated organs of host mice. Each symbol represents one mouse. Mean ± SEM is indicated (n.s. = P > 0.05; ordinary 1-way ANOVA).

Transfer of low numbers of MJ23 Treg cells does not quench the autoimmune potential of C4/I-A^b-specific Tconv cells

The previous two experiments were unable to successfully toggle a defined number of C4/I-A^b-specific Treg cells in the system. Therefore, we opted to take an approach in which we could both transfer and reliably recover congenically marked C4/I-A^b-specific MJ23 Treg cells. While similar "Treg addback" experiments have been performed by other research groups using foreign-derived antigenic systems [152,301], these contrived experiments introduced hyper-physiological frequencies of millions of Treg cells of a single specificity that had been differentiated *in vitro*. Instead, we sought to introduce natural thymically-derived MJ23 Treg cells that had developed at low clonal frequency in chimeric donor mice (LF MJ23 chimeras) [101,102].

We first attempted to introduce naïve MJ23 Treg cells into a repertoire prone to prostatic autoimmunity. We sorted MJ23 Treg cells from the pooled SLOs of resting LF MJ23 chimeras, and co-transferred 200 cells with $CD4^+$-enriched T cells from *Tcaf3(C4)*$^{-/-}$ donor mice into T cell-deficient recipients (Figure 22, A). We subsequently infected these mice with *Lm[C4]* after a rest period and measured prostatic T cell infiltration. Following infection, host mice variably presented with prostatic disease, including infiltration by polyclonal C4/I-A^b-specific T cells (Figure 22, B-D), which was no less severe than control mice that had received polyclonal Treg cells. Despite the initial transfer into lymphodeplete hosts and subsequent antigenic infection, MJ23 Treg cells were dwarfed in the pLN or prostatic lesions by C4/I-A^b-specific polyclonal cells (Figure 22, E), suggesting that both MJ23 Treg cells and polyclonal C4/I-A^b-specific Treg cells in the previous transfer experiments were unable to optimally function in host mice due to engraftment inefficiencies.

In an attempt to promote MJ23 Treg engraftment, we performed a second iteration of these experiments in which MJ23 Treg cells were activated prior to and at the time of transfer. We first infected LF MJ23 donor mice with *Lm[C4]* to activate and expand the endogenous population of MJ23 Treg cells. We then isolated these cells by FACS and introduced 8000 directly into $C4^{\Delta TEC}$ host males, which we simultaneously infected with *Lm[C4]* to further mobilize these Treg cells and initiate autoimmune reactions in the hosts (Figure 22, F). Despite these efforts, host mice developed fulminant autoimmunity to the same extent as control mice seeded with infection-experienced polyclonal Tregs (Figure 22, G-H), with the few recovered MJ23 Treg cells numerically overwhelmed by polyclonal C4/I-A^b-specific T cells from the host (Figure 22, I-J). Notably, the number of MJ23 Treg cells recovered in this experiment was less than in the previous despite the greater number of transferred cells (Figure 22, E and J), which could imply a temporal ceiling for the proliferation of MJ23 Treg cells akin to that described for "exhausted" $CD8^+$ T cells exposed to chronic antigen [407], given the repeated challenge by *Lm[C4]* in the donor and host mice. Ultimately, this series of sufficiency experiments (Figures 20-22) failed to demonstrate that the autoimmune potential of C4/I-A^b-specific Tconv cells is related to the number of Treg cells of matched specificity in the host. Thus, it remains outstanding whether control of C4/I-A^b-specific Tconv cells by analogous Treg cells following infection is strictly due to quantitative differences between these cells, or if qualitative differences in activation potential or spatial location play a pivotal role in coordinating this process.

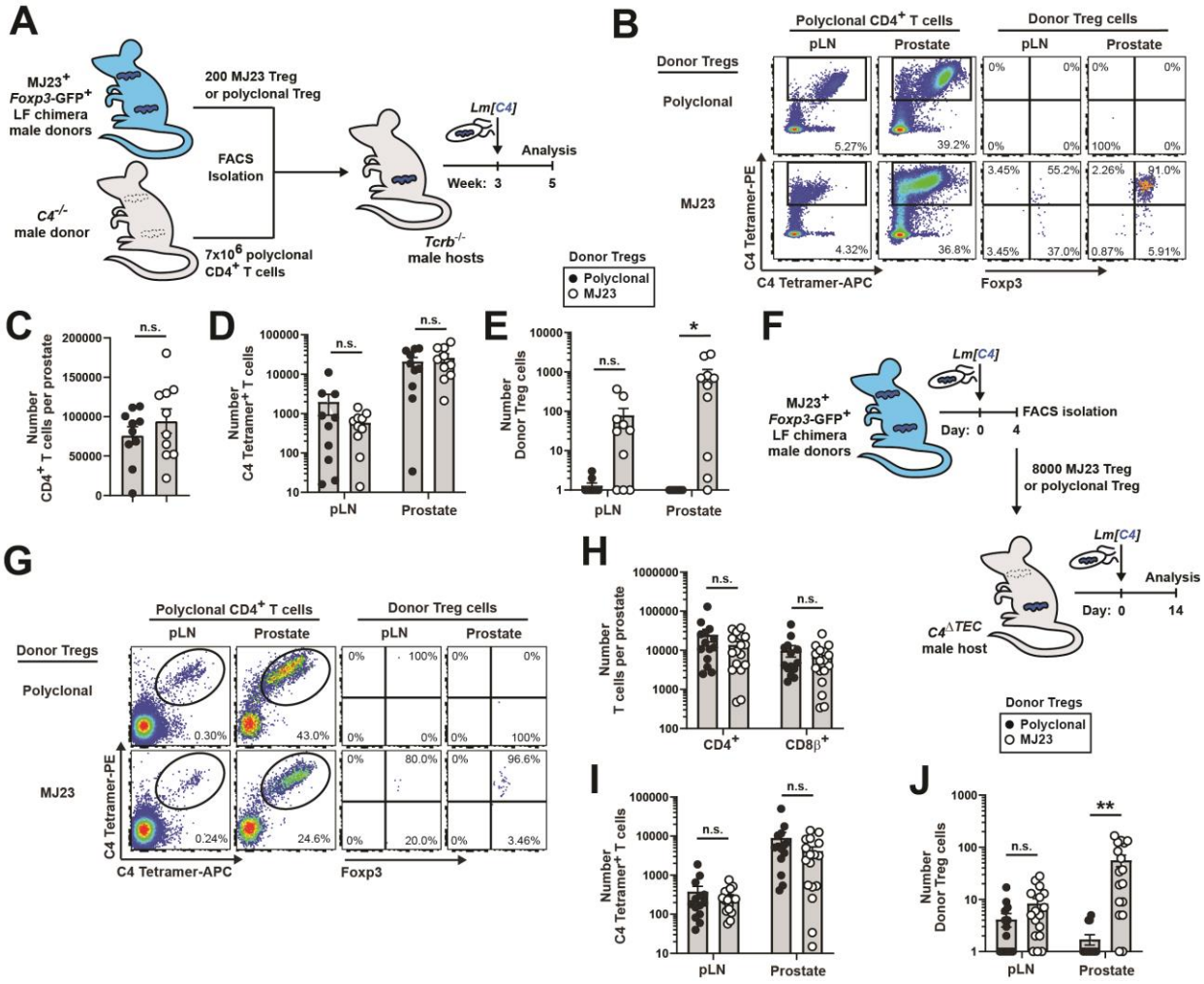

FIGURE 22. Transfer of low numbers of MJ23 Treg cells does not quench the autoimmune potential of C4/I-A^b-specific Tconv cells

(A) Experimental schematic for panels (B-E). Foxp3$^+$ MJ23 Treg cells and polyclonal CD4$^+$ T cells were isolated via FACS or magnetic enrichment from the pooled SLOs of low-frequency (LF) MJ23 bone marrow chimeras or congenically-disparate *C4*$^{-/-}$ donor mice, respectively. *Tcrb*$^{-/-}$ recipient mice received 7 x 10^6 polyclonal Tconv cells co-transferred with 200 MJ23 Treg cells or polyclonal Treg cells sorted from a Foxp3-GFP$^+$ donor. 3 weeks after transfer, recipient mice were infected intravenously with 10^7 CFU *Lm[C4]*. 2 weeks following infection, CD4$^+$ T cells were isolated from the paraaortic LN and prostate of recipient mice, stained with C4/I-A^b tetramer, and analyzed by flow cytometry. n = 9, C4/I-A^b-depleted Treg; n = 9, 2W1S/I-A^b-depleted Treg. Data are representative of three independent experiments. (B) Representative flow cytometric analysis of CD4$^+$ T cells isolated from the indicated organ of host mice. The plots depict C4/I-A^b tetramer-APC vs -PE expression by polyclonal CD4$^+$ T cells (left), or Foxp3 vs C4/I-A^b tetramer-PE expression by donor Treg cells. The frequency of cells within the indicated gates is denoted. (C) Summary plot of pooled data showing the absolute number of polyclonal CD4$^+$ cells isolated from the prostates of host mice. Each symbol represents one mouse. Mean ± SEM is indicated (n.s. = P > 0.05; Welch's t test). (D) Summary plot of pooled data showing the absolute number of dual C4/I-A^b tetramer$^+$ CD4$^+$ cells isolated from the

FIGURE 22, continued
indicated organs of host mice. Each symbol represents one mouse. Mean ± SEM is indicated (n.s. = P > 0.05; ordinary 1-way ANOVA). (E) Summary plot of pooled data showing the absolute number of donor Treg cells recovered from the indicated organs of host mice. Each symbol represents one mouse. Mean ± SEM is indicated (n.s. = P > 0.05; ordinary 1-way ANOVA).
(F) Experimental schematic for panels (G-J). Foxp3$^+$ MJ23 Treg cells were isolated via FACS from the pooled SLOs of LF MJ23 bone marrow chimeras that had been infected 4 days prior with 10^7 CFU *Lm[C4]*. *C4*$^{\Delta TEC}$ recipient mice received 8000 MJ23 Treg cells or polyclonal Treg cells sorted from an infected Foxp3-GFP$^+$ donor, and were immediately infected with 10^7 CFU *Lm[C4]*. 2 weeks following infection, CD4$^+$ T cells were isolated from the paraaortic LN and prostate of recipient mice, stained with C4/I-A^b tetramer, and analyzed by flow cytometry. n = 17, MJ23 Treg recipients; n = 14, polyclonal Treg recipients. Data are representative of four independent experiments. (G) Representative flow cytometric analysis of CD4$^+$ T cells isolated from the indicated organ of host mice. The plots depict C4/I-A^b tetramer-APC vs -PE expression by polyclonal CD4$^+$ T cells (left), or Foxp3 vs C4/I-A^b tetramer-PE expression by donor Treg cells. The frequency of cells within the indicated gates is denoted. (H) Summary plot of pooled data showing the absolute number of polyclonal CD4$^+$ and CD8β$^+$ cells isolated from the prostates of host mice. Each symbol represents one mouse. Mean ± SEM is indicated (n.s. = P > 0.05; ordinay 1-way ANOVA). (I) Summary plot of pooled data showing the absolute number of dual C4/I-A^b tetramer$^+$ CD4$^+$ cells isolated from the indicated organs of host mice. Each symbol represents one mouse. Mean ± SEM is indicated (n.s. = P > 0.05; ordinary 1-way ANOVA). (J) Summary plot of pooled data showing the absolute number of donor Treg cells recovered from the indicated organs of host mice. Each symbol represents one mouse. Mean ± SEM is indicated (n.s. = P > 0.05; ordinary 1-way ANOVA).

C4/I-A^b specific Tconv cells responding to Lm[C4] infection rapidly adopt non-proliferative cell states in C4^{WT} mice

A generalizable picture has emerged from our study. Within the first few days of infection, both self-reactive and pathogen-specific Tconv cells sense antigen, are activated, and begin to proliferate. If Treg cells reactive to the same self-antigen are present, such cells can selectively mute individual self-pMHCII-directed responses in the SLOs without measurably impacting Tconv responses directed at the pathogen. Absent such Treg cells, autoimmunity is unleashed and perpetuated following infection clearance, and can no longer be controlled by Treg cells of other specificities. A critical outstanding question lies in understanding why the activated C4/I-A^b-

specific Tconv cells in *C4^{WT}* mice fail to accumulate while the analogous population in *C4$^{\Delta TEC}$* mice explodes after the four-day branch point (Figure 16, G). Are C4/I-A^b-specific Treg cells selectively killing the Tconv cells? Are they undergoing abortive proliferation, apoptosis, or failing to differentiate?

To gain insight into the nature of these divergent responses, we performed single cell RNA sequencing and paired αβTCR sequencing of C4/I-A^b tetramer$^+$ T cells purified from the spleens of *C4^{WT}* vs. *C4$^{\Delta TEC}$* mice four days after *Lm[C4]* challenge, the time point at which the C4/I-A^b-specific T cell responses are poised to diverge (Figure 16, G). UMAP projection of unsupervised clustering revealed 14 distinct T cell clusters (Figure 23, A), none of which were exclusive to the *C4^{WT}* or *C4$^{\Delta TEC}$* settings, but instead differed in their proportional representation (Figure 23, B-D). Three clusters (Clusters 1 and 9, plus Cluster 10 in *C4^{WT}* only) exhibited expression of *Foxp3* and other Treg cell-defining signature genes (Figure 23, E-F). These Treg cells accounted for 61.7% of C4/I-A^b-tetramer$^+$ T cells from *C4^{WT}* mice, but only 5.92% of cells from *C4$^{\Delta TEC}$* mice. Hierarchical clustering of individual genes identified *Ccr2* as a cluster-defining gene for the most prevalent Treg cell cluster (Cluster 1), implicating the CCR2 chemokine receptor as a marker of Treg cells triggered by agonist ligand during *Lm* infection (Figure 23, G – discussed extensively in Chapter 3, Figure 29).

We next sought to define differences in the transcriptional states adopted by C4/I-A^b-specific Tconv cells elicited in *C4^{WT}* vs. *C4$^{\Delta TEC}$* mice. Our analysis coalesced around select signature genes, including the *Mki67* gene encoding the proliferation marker Ki67, the chemokine receptor-encoding *Ccr2*, *Cxcr6*, and *Ccr7* genes, and the *Tcf7* gene encoding the transcription factor TCF1 (Figure 23, F-G). High CCR2 and CXCR6 expression are hallmarks of inflammatory effector cells capable of migrating into peripheral tissues, whereas high CCR7 expression is

associated with T cell retention in lymphoid tissues [408]. High expression of TCF1 is a hallmark of "stem-like" central-memory T cells [409,410], which reside in lymph nodes and have been implicated as key reservoirs supporting sustained effector T cell responses in contexts of pathogen defense, autoimmunity, and anti-tumor immunity [406,411-413]. In *C4*$^{\Delta TEC}$ mice, which develop prostatitis following *Lm[C4]* infection, Tconv cell clusters 0, 4, and 6 were overrepresented relative to *C4*^{WT} mice (Figure 23, H). Tconv cells in Clusters 0 and 4 were characterized by high expression of *Cxcr6* and *Ccr2*, low expression of *Tcf7* and *Ccr7*, and adoption of a proliferative profile including expression of *Mki67* (Figure 23, F-G), indicative of proliferating Tconv cells that have initiated effector cell programs. Tconv cells in Cluster 6 were also highly proliferative, but exhibited an inverse expression pattern of other signature genes, including low expression of *Cxcr6* and *Ccr2* and high expression of *Tcf7* and *Ccr7* (Figure 23, F-G). Thus, cells in Cluster 6 exhibited numerous hallmarks of cycling "stem-like" central-memory T cells. In contrast, the most abundant Tconv cell cluster enriched in *C4*^{WT} mice, in which Tconv cells were effectively controlled during *Lm[C4]* infection, was Cluster 5 (Figure 23, H). This cluster was characterized by elevated expression of *Ccr2* and *Cxcr6*, low expression of *Tcf7* and *Ccr7*, and low expression of *Mki67* and other cell cycle-related genes (Figure 23, F-G), indicative of short-lived effector cells that have lost proliferative potential. Collectively, these findings demonstrate that the Treg cell-biased C4/I-A^{b}-specific T cell response in *C4*^{WT} mice was associated with stifled Tconv cell differentiation, whereas the disease-potentiating Tconv cell-dominated response in *C4*$^{\Delta TEC}$ mice was characterized by a mixture of stem-like central-memory Tconv cells and proliferative Tconv cells exhibiting hallmarks of effector cell differentiation.

To capture the phenotype of individual activated clones mounting productive or failed responses to C4/I-A^{b}, we analyzed the paired αβTCR sequences and cluster contribution of single

cells. To ensure each cell was derived from the same parent, we defined each clone by identical paired *Tra* and *Trb* genes and exact nucleotide sequences of the CDR3 regions. Furthermore, we restricted our analysis to only clones found >4 times in the dataset, as we reasoned that these cells would have been activated by antigen and were unlikely to be noise. Treg-biased clones dominated the response in $C4^{WT}$ mice as expected, but a minor fraction were also found in $C4^{\Delta TEC}$ mice (Figure 23, I), demonstrating that at least some of the Treg cells that develop independently of C4/I-A^b in the thymus respond to this ligand. Treg-biased clones comprised well over half of the expanded clones in $C4^{WT}$ mice, suggesting that the naive C4/I-A^b-specific repertoire is biased to the Treg lineage, at least for clones capable of responding to C4/I-A^b (Figure 3 and Chapter 1 discussion). Importantly, clones in mice of both genotypes segregated almost exclusively into Treg or Tconv-defined clusters (Figure 23, I), formally demonstrating negligible contribution of pTreg induction to the pool of C4/I-A^b-specific T cells (Figure 7). Individual Tconv-biased clones often populated multiple clusters in mice of both genotypes, though the relative frequency in each cluster varied across clones and between genotypes (Figure 23, I). While this result doesn't preclude a Tconv cell-intrinsic role (such as TCR affinity) in shaping the clonal response, it does importantly demonstrate that factors extrinsic to the Tconv clone influence the cell state adopted by each individual Tconv cell, and imply a degree of spatial heterogeneity within the SLO of different cells derived from the same clone. In this regard, only a few Tconv clones of all responding clones in $C4^{\Delta TEC}$ mice exhibited significant bursting at the timepoint analyzed (Figure 23, I), suggesting heterogeneous signal integration events even at this early timepoint that may be sufficient to instruct extensive cell divisions. This observation also implies that a few escaping Tconv cells could be responsible for fulminant autoimmune disease – implicating the number of activated Tconv cells as a fragile parameter that requires a tightly-regulated mechanism to control.

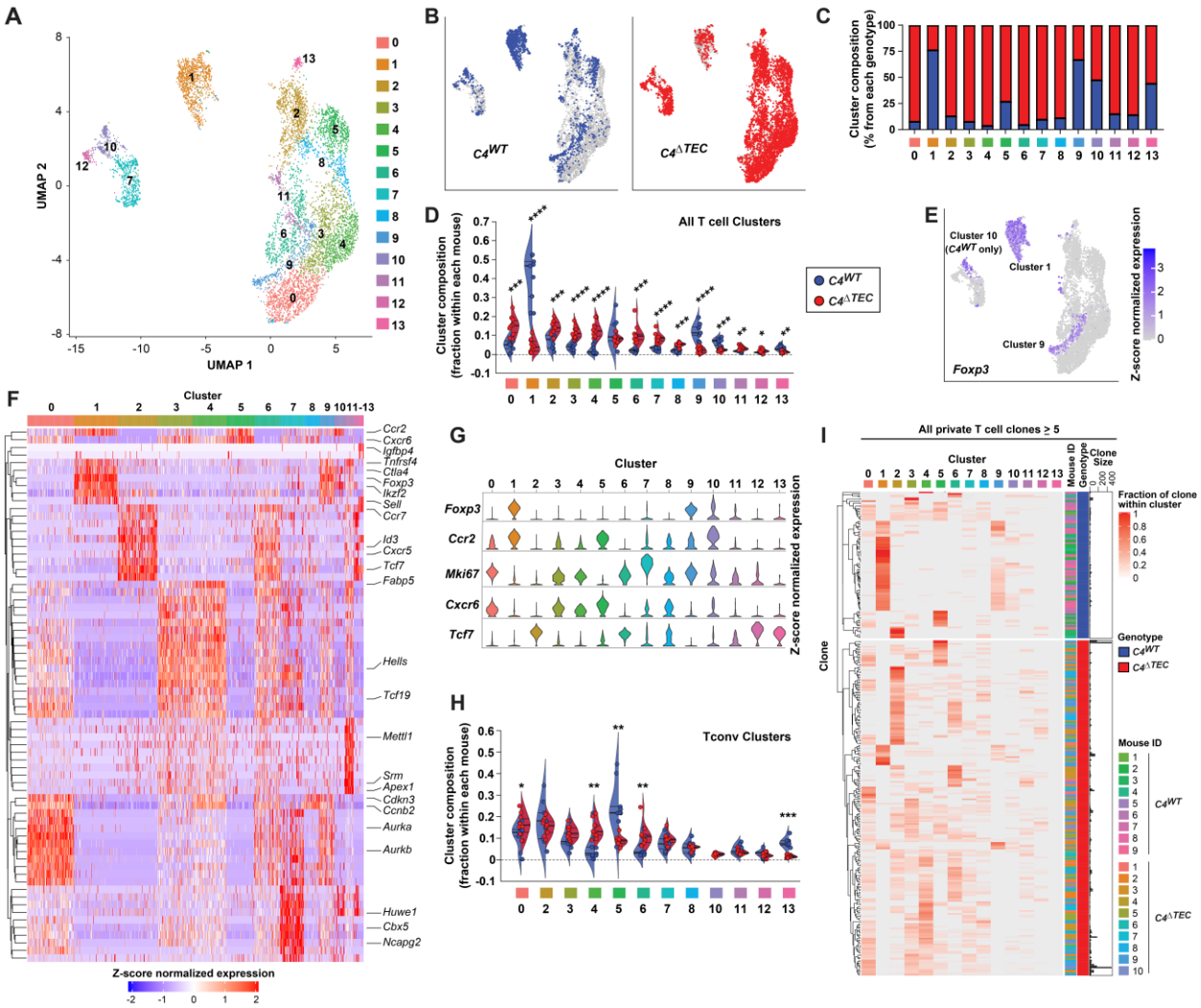

FIGURE 23. C4/I-A^b-specific Tconv cells responding to *Lm[C4]* infection rapidly adopt non-proliferative cell states in *C4^{WT}* mice

C4^{WT} and *C4$^{\Delta TEC}$* male mice were challenged intravenously with 10^7 CFU *Lm[C4]*. At 4 days post-infection, C4/I-A^b tetramer$^+$ CD4$^+$ T cells were FACS sorted from the spleen, pooled, and subjected to paired scRNA-seq and scTCR-seq (10X platform, see Methods). n = 9, *C4^{WT}* mice; n = 10, *C4$^{\Delta TEC}$*. (A) Unsupervised clustering of scRNA-seq 5' gene expression data for C4/I-A^b tetramer$^+$ CD4$^+$ T cells FACS sorted from the spleens of *C4^{WT}* and *C4$^{\Delta TEC}$* male mice 4 days post-infection with *Lm[C4]*. 6839 total cells, 6320 cells with complete TRA and TRB. (B) UMAP embedding of scRNA-seq data in (A) comparing C4/I-A^b tetramer$^+$ CD4$^+$ T cells derived from *C4^{WT}* and *C4$^{\Delta TEC}$* mice (top) and histogram depicting the frequency of cells assigned to either genotype within each cluster (bottom). 1593 *C4^{WT}*- and 5246 *C4$^{\Delta TEC}$* -derived cells. (C) Summary plot of data from (B) depicting the frequency of cells assigned to either genotype comprising each cluster. (D) Summary plots depicting the frequency of all cells in each cluster, expressed as a fraction of all T cells or Tconv cells derived from each individual mouse. Each symbol represents cells derived from one mouse. The mean ± SD is indicated (* = P < 0.05; ** = P < 0.01; *** = P < 0.001 **** = P < 0.0001; Welch's t-test). (E) UMAP embedding of Z-score normalized expression of Foxp3 of scRNA-seq data in (A). All cells in Clusters 1, 9, and

FIGURE 23, continued
all $C4^{WT}$-derived cells in Cluster 10 were designated as Treg, while all other cells were assigned Tconv. (F) Heatmap of the top 10 differentially expressed genes per cluster from scRNA-seq data in (A). Select genes used to define each cluster are highlighted to the right. (G) Summary plots depicting the Z-score normalized expression of select genes across cells in each cluster. (H) Summary plots depicting the frequency of Tconv-assigned cells in each cluster, expressed as in (D). (I) Distribution of TCR clonotypes (≥ 5 cells, 320 total clones) across all clusters. Heatmap depicts the fraction of each clone across all clusters, where 1 means 100% of a clonotype exists in a given cluster. Hierarchical clustering was performed on the clones and clusters, after separating clones by genotype. The mouse identifier, genotype, and size of each clone is indicated to the right.

MJ23 Treg cells are required to suppress the proliferation, differentiation, and accumulation of clonally-matched Tconv cells following Lm[C4] infection

Single-cell sequencing of polyclonal C4/I-A^b T cells responding to *Lm[C4]* in $C4^{\Delta TEC}$ vs. $C4^{WT}$ mice revealed that distinct cell states were being adopted in the presence or absence of C4/I-A^b-specific Treg cells (Figure 23). These disparate states were primarily characterized by proliferation capacity, suggesting that the Tconv cells which go on to elicit autoimmunity in $C4^{\Delta TEC}$ mice adopt effector programs capable of forming memory, while those in $C4^{WT}$ mice can undergo effector differentiation but rapidly lose the ability to self-renew. While the cumulative data suggests that C4/I-A^b-specific Treg cells are responsible for mediating these disparate outcomes, our studies of polyclonal C4/I-A^b-specific Treg and Tconv cells have been unable to definitively demonstrate such a role owing to differences in clonal composition of the Treg and Tconv repertoires between $C4^{WT}$ and $C4^{\Delta TEC}$ mice [87], and that our efforts to selectively modulate C4/I-A^b-specific cells only in one T cell compartment have been unsuccessful (Figures 20-22).

To directly assess the impact of C4/I-A^b-specific Treg cells on the trajectory of C4/I-A^b-specific Tconv cell responses to *Lm[C4]*, we studied the response of monoclonal MJ23 Tconv cells to *Lm[C4]* challenge in the presence or absence of MJ23 Treg cells. Given previous work

showing that clonal deletion does not impact the thymic selection of MJ23 T cells [101], the analysis of Treg and Tconv cells expressing the fixed MJ23 TCR eliminates the variables of clonal deletion and TCR affinity for pMHC [107] between C4/I-A^b-specific Tconv cells in $C4^{WT}$ and $C4^{\Delta TEC}$ mice, facilitating direct assessment of the role of Treg cells in regulating Tconv cells of matched pMHC specificity. For analysis, we developed a panel of antibodies specific for proteins encoded by signature genes defined in the transcriptional analysis (Figure 23, G), allowing quantification of MJ23 Tconv cell phenotypes using flow cytometry.

We infected LF MJ23 chimeras created in $C4^{WT}$ and $C4^{\Delta TEC}$ hosts with *Lm[C4]* and measured MJ23 T cells 6 days post-infection (Figure 24, A). We chose the day 6 timepoint to quantify the cell states by flow cytometry rather than the day 4 timepoint from which the RNA sequencing data originated because changes in protein expression only become apparent after changes in gene expression [414], as evidenced by the fact that C4/I-A^b-specific Tconv cells continued to express Ki67 protein at day 4 post-infection (Figure 16, I) despite having turned off gene expression at this timepoint (Figure 23, G). At day 6, MJ23 Tconv cells elicited in $C4^{\Delta TEC}$ hosts outnumbered MJ23 Tconv cells in $C4^{WT}$ hosts >6-fold in the spleen (Figure 24, B-D), maintained elevated densities of Ki67 (Figure 24, E-F), and exhibited significant shifts in cell states (Figure 24, G), including enrichment of a proliferative $Ki67^+$ $CXCR6^{neg}$ $CCR2^{neg}$ $TCF1^{hi}$ "stem-like" population (akin to cluster 6) and underrepresentation of a non-proliferative $Ki67^{neg}$ $CXCR6^+$ $CCR2^+$ $TCF1^{lo}$ short-lived effector-like population (akin to cluster 5), thereby mirroring some of the phenotypic shifts observed for polyclonal C4/I-A^b-specific Tconv cells in $C4^{\Delta TEC}$ vs. $C4^{WT}$ hosts (Figure 23, G). Oddly, MJ23 T cells capable of responding to *Lm[C4]* also appeared in the $CD8^+$ and DN T cell compartments in the periphery of LF chimeras in both $C4^{WT}$ and $C4^{\Delta TEC}$ hosts (though critically none expressed Foxp3), likely due to an experimental artefact in the

transgenic system. Intriguingly, while MJ23 Tregs suppressed the proliferation of $CD4^+$ MJ23 Tconv cells (Figure 24, C-F), they had no effect on that of $CD4^{neg}$ cells expressing the MJ23 TCR (Figure 24, H-I), suggesting that antigen-specific control by Treg cells may act via a mechanism unique to the $CD4^+$ T cell lineage and not other T cells. In all, these data indicate that MJ23 Treg cells impact the proliferative competency and cell states of Tconv cells of matched specificity.

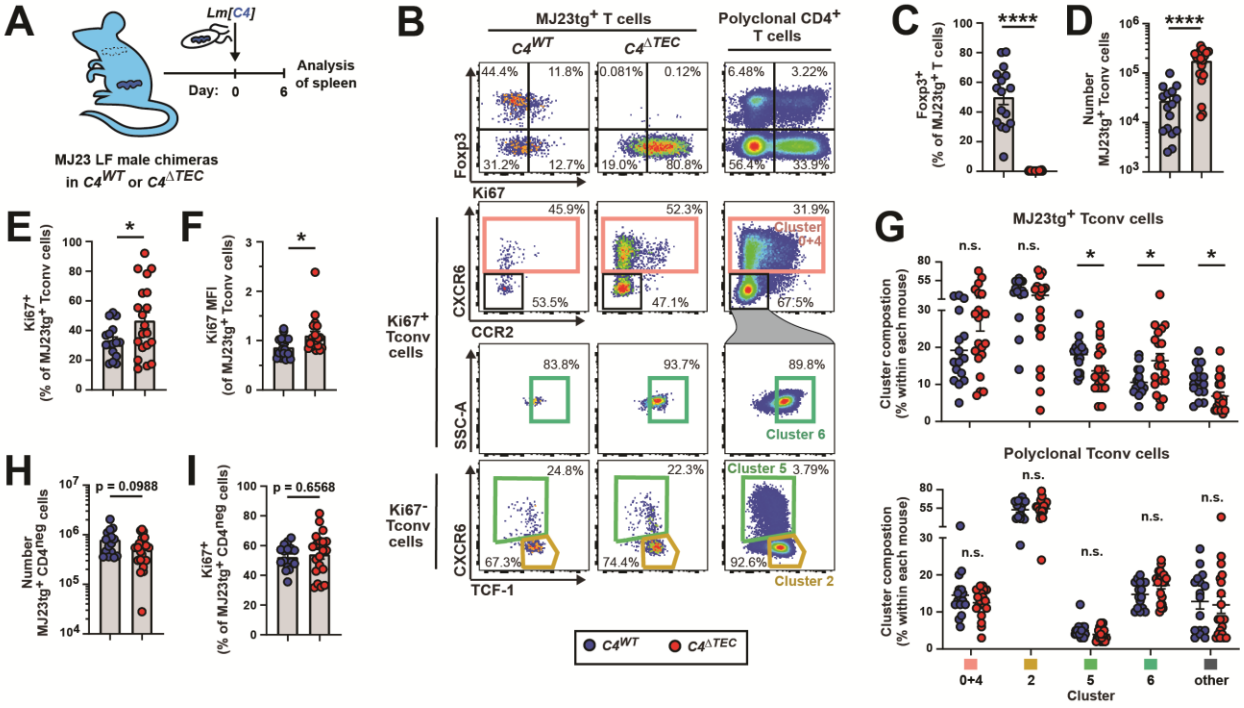

FIGURE 24. MJ23 Treg cells are required to suppress the proliferation, differentiation, and accumulation of clonally-matched Tconv cells following *Lm[C4]* infection

(A) Experimental schematic for panels (B-I). LF MJ23 chimeric mice were generated in $C4^{WT}$ and $C4^{\Delta TEC}$ male hosts. >6 weeks post-engraftment, host mice were infected with 10^7 CFU *Lm[C4]*. 6 days post-infection, the fate of MJ23 T cells were assessed in the spleen by flow cytometry. n = 16, $C4^{WT}$; n = 20, $C4^{\Delta TEC}$. Data represent three independent experiments. (B) Representative flow cytometric analysis of MJ23+ or polyclonal CD4$^+$ T cells isolated from the spleens of LF chimeric mice of the indicated genotype. Plots depict Ki67 vs. Foxp3 expression by MJ23$^+$ or polyclonal CD4$^+$ T cells (top), and the expression of CXCR6, TCF-1, and CCR2 by Ki67$^+$ (middle) and Ki67^{neg} (bottom) MJ23$^+$ or polyclonal CD4$^+$ Foxp3^{neg} Tconv cells. Flow cytometry-identified clusters were defined based on expression of markers observed in the scRNA-seq dataset (Figure 23E). The frequency of cells within the indicated gates is denoted. (C) Summary plot of pooled data showing the frequency of Foxp3$^+$ cells amongst MJ23$^+$ CD4$^+$ T cells isolated from the spleen of host mice of the indicated genotype. Each symbol represents one mouse. Mean ± SEM is indicated. (**** = P < 0.0001; Welch's t test). (D) Summary plot of pooled data showing the number of MJ23+ CD4+ Tconv cells isolated from the spleen of host mice of the indicated genotype. Each symbol represents one mouse. Mean ± SEM is indicated. (**** = P < 0.0001; Welch's t test). (E) Summary plot of pooled data showing the frequency of Ki67$^+$ cells amongst MJ23$^+$ CD4$^+$ Tconv cells isolated from the spleen of host mice of the indicated genotype. Each symbol represents one mouse. Mean ± SEM is indicated. (* = P < 0.05; Welch's t test). (F) Summary plot of pooled data showing the mean fluorescence intensity (MFI) of Ki67 on MJ23$^+$ CD4$^+$ Tconv cells isolated from the spleen of host mice host mice of the indicated genotype. Each symbol represents one mouse. Mean ± SEM is indicated. (* = P < 0.05; Welch's t test). (G) Summary plot of pooled data depicting the frequency of MJ23$^+$ CD4$^+$ Tconv cells (top) or polyclonal CD4$^+$ Tconv cells (bottom) in each cluster, relative to all MJ23$^+$ or polyclonal CD4$^+$ Tconv cells identified in each individual mouse. Each symbol represents one

FIGURE 24, continued
mouse. The mean ± SEM is indicated (* = $P < 0.05$; Welch's t test). (H-I) TCRβ^{+} CD4^{neg} MJ23^{+} cells coexist alongside CD4^{+} MJ23^{+} in LF MJ23 chimeric mice. (H) Summary plot of pooled data showing the number of MJ23^{+} CD4^{neg} cells isolated from the spleen of host mice of the indicated genotype. Each symbol represents one mouse. Mean ± SEM is indicated. (Welch's t test). (I) Summary plot of pooled data showing the frequency of Ki67^{+} cells amongst MJ23^{+} CD4^{neg} cells isolated from the spleen of host mice of the indicated genotype. Each symbol represents one mouse. Mean ± SEM is indicated. (Welch's t test).

MJ23 Treg cells enforce rapid shutdown of cell cycle to limit the proliferation and effector differentiation of clonally-matched Tconv cells following Lm[C4] infection

The striking differences between the MJ23 Tconv responses to infection in LF MJ23 *C4^{WT}* and *C4$^{\Delta TEC}$* hosts strongly suggests that C4/I-A^{b}-specific Treg cells directly orchestrate protective or pathogenic outcomes following *Lm[C4]* challenge by governing the proliferation of Tconv cells with matched antigen specificity. Nevertheless, it remained formally possible that intrinsic differences in signaling capacity linger between MJ23 Tconv cells in either genotype that were imprinted by thymic selection on C4/I-A^{b} [415]. To eliminate this possibility, we generated chimeras in *C4^{WT}* hosts using bone marrow from MJ23 mice expressing the *Foxp3$^{DTR\text{-}EGFP}$* allele, subjected half of these mice to selective MJ23 Treg cell depletion via DT administration, and challenged with *Lm[C4]* (Figure 25, A). The depletion of MJ23 Treg cells did not significantly impact the number of MJ23 Tconv cells elicited by days four and six post-infection (Figure 25, B-E). However, MJ23 Treg cell depletion led to a significant increase in the proliferative potential of MJ23 Tconv cells by day four as measured by elevated expression of the transcription factor Myc (Figure 25, F), which has been shown to serve as a "division destiny" marker predictive of subsequent cell division [416]. Consistent with this, MJ23 Treg cell depletion led to striking increases in the extent and density of Ki67 expression by MJ23 Tconv cells at day 6 post-infection (Figure 25, G-H), along with measurable shifts in phenotypic cell states (Figure 25, I) as defined from the

sequencing data (Figure 23, G). Finally, as observed for MJ23 T cells in $C4^{WT}$ and $C4^{\Delta TEC}$ hosts, MJ23 Treg depletion had no effect on the number or proliferation of $CD4^{neg}$ cells expressing the MJ23 TCR (Figure 25, J-K). Thus, the specific depletion of MJ23 Treg cells led to measurable alterations in the proliferative competency of Tconv cells of matched specificity following *Lm[C4]* challenge, directly and definitively implicating MJ23 Treg cells in altering MJ23 Tconv cell fate.

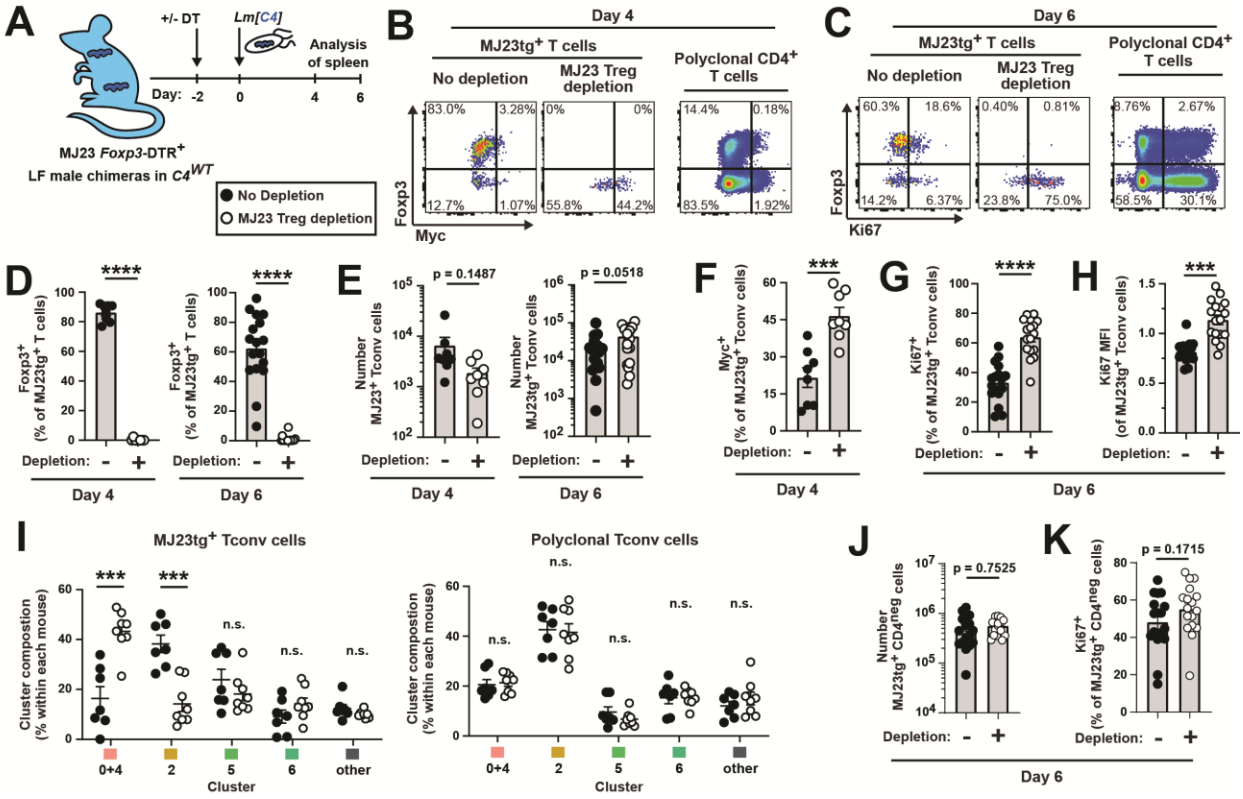

FIGURE 25. MJ23 Treg cells enforce rapid shutdown of cell cycle to limit the proliferation and effector differentiation of clonally-matched Tconv cells following *Lm[C4]* infection

(A) Experimental schematic. LF MJ23 chimeric mice were generated in $C4^{WT}$ male hosts using MJ23$^+$ *Rag1*$^{-/-}$ *Foxp3*-DTR$^+$ marrow. >6 weeks post-engraftment, mice were depleted of MJ23 Treg cells with via a single intraperitoneal injection of DT, or left untreated. 2 days following DT treatment, host mice were infected with 10^7 CFU *Lm[C4]*. 4 or 6 days post-infection, the fate of MJ23 T cells were assessed in the spleen by flow cytometry. n = 8, no depletion d4; n = 8, MJ23 Treg depletion d4; n = 17, no depletion d6; n = 17, MJ23 Treg depletion d6. Data represent two (d4) or four (d6) independent experiments. (B) Representative flow cytometric analysis of MJ23$^+$ or polyclonal CD4$^+$ T cells isolated from the spleens of LF chimeric mice depleted of MJ23 Treg cells or left untreated at 4 days post-infection. Plots depict Myc vs. Foxp3 expression by MJ23$^+$ or polyclonal CD4$^+$ T cells. The frequency of cells within the indicated gates is denoted. (C) Representative flow cytometric analysis of MJ23$^+$ or polyclonal CD4$^+$ T cells isolated from the spleens of LF chimeric mice depleted of MJ23 Treg cells or left untreated at 6 days post-infection. Plots depict Ki67 vs. Foxp3 expression by MJ23$^+$ or polyclonal CD4$^+$ T cells. The frequency of cells within the indicated gates is denoted. (D) Summary plot of pooled data showing the frequency of Foxp3$^+$ cells amongst MJ23$^+$ CD4$^+$ T cells isolated from the spleen of host mice depleted of MJ23 Treg cells or left untreated at the indicated day post-infection. Each symbol represents one mouse. Mean ± SEM is indicated. (**** = P < 0.0001; Welch's t test). (E) Summary plot of pooled data showing the number of MJ23$^+$ CD4$^+$ Tconv cells isolated from the spleen of host mice depleted of MJ23 Treg cells or left untreated at the indicated day post-infection. Each symbol represents one mouse. Mean ± SEM is indicated. (Welch's t test). (F) Summary plot of pooled data from (B) showing the frequency of Myc$^+$ cells amongst MJ23$^+$ CD4$^+$ Tconv cells isolated from the spleen of host mice depleted of MJ23 Treg

FIGURE 25, continued
cells or left untreated at 4 days post-infection. Each symbol represents one mouse. Mean ± SEM is indicated. (*** = $P < 0.001$; Welch's t test). (G) Summary plot of pooled data showing the frequency of $Ki67^+$ cells amongst $MJ23^+$ $CD4^+$ Tconv cells isolated from the spleen of host mice depleted of MJ23 Treg cells or left untreated at 6 days post-infection. Each symbol represents one mouse. Mean ± SEM is indicated. (**** = $P < 0.001$; Welch's t test). (H) Summary plot of pooled data showing the mean fluorescence intensity (MFI) of Ki67 on $MJ23^+$ $CD4^+$ Tconv cells isolated from the spleen of host mice host mice depleted of MJ23 Treg cells or left untreated at 6 days post-infection. Each symbol represents one mouse. Mean ± SEM is indicated. (*** = $P < 0.001$; Welch's t test). (I) Summary plot of pooled data depicting the frequency of $MJ23^+$ $CD4^+$ Tconv cells (left) or polyclonal $CD4^+$ Tconv cells (right) in each cluster (as in Figure 24B), relative to all $MJ23^+$ or polyclonal $CD4^+$ Tconv cells identified in each individual mouse at 6 days post-infection. Each symbol represents one mouse. The mean ± SEM is indicated (*** = $P < 0.001$; Welch's t test). (K-L) $TCR\beta^+$ $CD4^{neg}$ $MJ23^+$ cells coexist alongside $CD4^+$ $MJ23^+$ in LF MJ23 chimeric mice. (J) Summary plot of pooled data showing the number of $MJ23^+$ $CD4^{neg}$ cells isolated from the spleen of host mice depleted of MJ23 Treg cells or left untreated at 6 days post-infection. Each symbol represents one mouse. Mean ± SEM is indicated. (Welch's t test). (K) Summary plot of pooled data showing the frequency of $Ki67^+$ cells amongst $MJ23^+$ $CD4^{neg}$ cells isolated from the spleen of host mice depleted of MJ23 Treg cells or left untreated at 6 days post-infection. Each symbol represents one mouse. Mean ± SEM is indicated. (Welch's t test).

CONCLUSIONS AND DISCUSSION

In this chapter, we investigate how Treg cells impose tolerance to self-antigens during infection without limiting robust effector responses directed at the pathogen. Using mice in which Treg cells reactive to a single self-peptide are removed due to altered thymic selection, and employing a model of pathogen-associated epitope mimicry to initiate robust T cell responses, we demonstrate that self-pMHCII-specific Treg cells selectively control Tconv cells of matched antigen specificity following infection without quantitatively or qualitatively altering the Tconv response to a second pathogen-derived epitope. Functionally, this single specificity of Treg cells did not prevent the activation of self-reactive Tconv cells, but instead rapidly restricted their potential to proliferate, differentiate, and ultimately sustain effector responses. Critically, the loss of a single specificity of self-specific Treg cells enabled fulminant autoimmunity to the prostate following infection, characterized by an antigen-specific and polyclonal T cell infiltrate. Thus, Treg cell specificity for self-pMHC ligands serves as a key determinant of self-nonself discrimination, allowing Treg cells to focus their immunosuppressive functions on self-reactive Tconv cells of shared pMHC-II specificity.

Molecular mimicry and the initiation of autoimmune disease

Molecular homology between bacterial and mammalian species has been apparent for decades [417] and has since sparked a litany of investigations to understand the implications of such blurred self for host tolerance and pathogen protection. The first proof-of-concept experiment demonstrating molecular mimicry as an initiator of autoimmune disease was performed in rabbits immunized with the hepatitis B virus-derived protein HBVP [418], which exhibited amino acid sequence homology to myelin basic protein and triggered EAE disease characterized by

autoantibodies and CNS-infiltrating mononuclear cells. Since this demonstration, many autoimmune diseases have been found to be associated with prior exposure to distinct bacterial or viral agents, but the causal relationships and antigenic mimics, if any, remain largely undefined [18]. Additional host genetic and environmental factors contribute to the development of autoimmune diseases, so the role of a mimetic pathogen in host autoimmune attack must be considered amongst these influences.

The HLA/MHC loci and corresponding allotypes have some of the strongest associations across autoimmune diseases [419], implicating T cells as holding an axial role in disease onset or progression in many cases, and exemplifying one instance of clear genetic predisposition. Since autoimmune risk alleles vary across clinical diseases, it's unlikely that a universal pathogenesis relating to detrimental characteristics in a particular MHC molecule (such as blanket quirks in antigen presentation or a restriction-independent superantigen) are the sole contributors to disease development. In this regard, recent studies have identified T cell clones within autoimmune lesions of HLA risk-allele-bearing human patients that cross-react with self peptides and epitope mimics derived from pathogens [392,420], demonstrating a direct link between autoimmune-relevant T cell specificities and potential for antigen-induced activation by an infectious agent. Furthermore, the fact that the prevalence of nearly all dominant autoimmune diseases has continued to increase through the industrialized era [421,422], indicates that environmental exposures have a clear bearing on disease initiation. Our study defined and studied a self-reactive T cell specificity relevant to autoimmune disease, and controlled host genetic and environmental factors that could play a role in autoimmune disease following infection, including altered T cell selection of a single specificity and the usage of a single molecular mimic epitope. Our results provide four key insights into the pathogenesis of T cell-initiated autoimmune disease: 1) epitope mimicry alone is not sufficient to

initiate autoimmune disease, 2) a host can harbor a potent genetic predisposition to autoimmunity without ever manifesting disease, 3) the onset of autoimmune disease can be initiated by, and may well require, a single inflammatory event, 4) environmental factors that influence T cell selection or repertoire maintenance could predispose genetically tolerant individuals to autoimmune disease.

Wild-type mice infected with *Lm[C4]* did not develop prostatic T cell infiltration months following infection (Figure 16). This was not necessarily the obvious outcome considering the strong antigenic and inflammatory triggers present at multiple anatomical sites, and that successful host defense necessitates robust protective responses from T cells. The existence of this dominant suppressive mechanism – which is capable of tuning self-directed T cell responses without impacting those reactive to foreign epitopes – implies the existence of external evolutionary pressure to select such a system. Unlike the central tolerance mechanism of clonal deletion, which was probably selected independent from external pressures assuming that strongly-self reactive T cell clones are capable of breaching an activation threshold and mounting an autoreactive response at steady-state, the ability for T cells to selectively shut down a self-directed response in an inflammatory environment likely evolved to deal with external pressures imposed by pathogens. What factors contributed to such selection? One intriguing observation is that the line between self and nonself at the level of proteins and peptides is less distinct than is generally appreciated. Indeed, a comprehensive computational analysis found that >90% of 5-mer amino acid sequences observed in the proteomes of dozens of commensal and pathogenic bacteria also exist in the human proteome [423]. Furthermore, 99.7% of human proteins had at least one 7-mer peptide sequence that overlapped with a sequence derived from a microbe included in the dataset. While these percentages drop with each additional residue, the probability of sequence similarity, importance of select residues for TCR activation, and capacity for register shifts in MHC-II alleles implies that

molecular mimicry may be a common event across species that harbor an adaptive immune system [424,425]. If lymphocyte selection and function has evolved alongside foreign-derived epitope mimics, it follows that this selective pressure had a leading role in the emergence of regulatory T cells and their predilection for self-reactivity. In such an evolutionary scenario, immunodominant epitope mimics would have occasionally elicited an autoimmune response in individuals of a population, rendering them sterile or resulting in premature death depending on the target organ. An immunosuppressive lineage of cell would have therefore been required for fitness, and regulatory T cells would have emerged in the population to fill this role. Consequently, this would have increased the susceptibility of the population to pathogen attack owing to broad immunosuppression, and forced a second evolutionary bottleneck for the emergence of a regulatory T cell repertoire selected primarily for strong reactivity to self immunodominant epitopes. Further evidence for this hypothesis of Treg selection is the observation that many regulatory T cells at mucosal sites are reactive to antigens derived from commensal microbes [152,153,170,172,426], and that the Treg repertoire is fluid in its ability to modulate the abundance of regulatory T cells within an antigen-specific population based on the presence or absence of antigen at these sites [427-429]. It is less likely that reciprocal selective pressure was imposed on the pathogen by the antigen-specificity of Treg cells, at least for populations with a diverse pool of MHC allotypes, since "self" would be a sliding definition between individuals in a population and thus impede the pathogen from deliberately evolving immunodominant epitope mimics.

In our system, a single genetic predisposition – the failure to select on the C4/I-A^b antigen and the resulting lapse in antigen-specific Treg selection – predisposed the host to severe autoimmune infiltration but required a specific inflammatory event to manifest disease (Figures 14-16). This observation is potently reminiscent of the apparent chasm between individuals

harboring known genetic risk alleles and the manifestation of diseases. One such example is coeliac disease, where the HLA-DQ2.5, HLA-DQ8, and HLA-DQ2.2 haplotypes are strongly associated with clinical disease, yet the vast majority of individuals with these risk factors lead disease-free lives [430-432]. In this particular disease, it is well described that environmental factors including antigen availability and exposure to inflammation play a critical role in the onset of disease. Might the results from our study broadly integrate with the progression of other diseases with known genetic susceptibilities? It could be that each of these diseases requires a distinct triggering event to initiate the autoimmune cascade. In principle, any inflammatory event capable of sufficiently activating a self-reactive T cell specificity would enable a break in tolerance. This could be analogous to our system, where the event enables a bypass of control via the lack of Treg cells with matched antigen specificity, but could theoretically happen by any mechanism that effectively lowers the activation threshold of a T cell, including high levels of antigen, constitutively active molecules in a signaling cascade, or receptors with abnormally high affinity for their ligands. By this logic, infectious agents should enhance incidence of disease in genetically-susceptible mouse strains by triggering the autoimmune cascade. Indeed, NOD mice prone to autoimmune diabetes exhibit rapid progression of disease following infection with the virus CBV4 [433], and a molecular mimic from a Fusobacteria commensal microbe can activate islet-reactive T cells to potentiate disease [434]. Yet other viral infections can delay disease onset [435,436], suggesting that infection-induced autoimmune disease depends on the context and pathogenesis of infection. Notably, in cases where protection was enhanced, mice manifested an increase in Treg cells and negative regulators of costimulation, implying that these particular scenarios raised rather than lowered T cell activation thresholds. Nevertheless, disease in NOD mice is complex and genetic susceptibility is orchestrated in concert with the microbiota and temporal factors [437]. On

the other hand, *Aire*$^{-/-}$ mice develop a range of disease phenotypes largely due to the loss of Aire-dependent specificities from the Treg repertoire and a concurrent emergence of these clones in the Tconv compartment [87]. Relatedly, owing to spontaneous X inactivation and that the Foxp3 locus resides on the X chromosome, Foxp3$^{+/-}$ heterozygous female mice harbor "Treg wannabes" with a predilection for self-reactivity in the Tconv compartment yet do not develop spontaneous autoimmune disease. Both of these cases are prime candidates to scrutinize the hypothesis of infection-triggered autoimmunity, as pathogen infection could function to create an environment permissible for escape of multiple self-reactive Tconv cells that exist due to genetic abnormalities. To our knowledge, no such experiments have been performed.

Just as most individuals with genetic susceptibility do not go on to develop autoimmune disease, it is also true that not all individuals with disease have an obvious predisposition. Is protection from autoimmunity the genetic default, or can disease occur in any member of a population given the proper context? What might this reveal about environmental influences, hidden variables of susceptibility, and the nature of self? We demonstrate that protection following an instance of pathogen-associated molecular mimicry hinges on a single-specificity of Treg cells. But not every immunodominant epitope that needs to be tolerized as "self" will be available to select for antigen-specific Tregs in the thymus. Antigens associated with post-pubescence and pregnancy, for example, are likely to exist as cryptic epitopes that uniquely arise in the periphery [376], which could implicate these antigens as being uniquely susceptible to autoimmune attack following infection with a mimetic pathogen, even in individuals without an obvious genetic predisposition. Furthermore, given that MHC alleles can have different peptide anchor residues [425], its formally possible that a common immunodominant epitope shared amongst coronaviruses, for example, could exploit a cryptic epitope in a single allotype which wouldn't present as an

obvious autoimmune risk allele in the clinic. Finally, other external factors capable of shaping the Treg and Tconv repertoires of single antigen specificities in the periphery, such as the context or duration of antigen exposure [174,220], may have implications for loss of tolerance not only to self, but also to allergens [219], the tumor [438,439], and organ transplants. Future efforts exploring the events that culminate in loss of tolerance will likely enable the identification of novel therapeutic targets for a host of autoimmune and associated diseases.

Autoimmunity triggered at distal sites

The notion of pathogen-associated molecular mimicry implies that autoimmunity directed toward distinct target tissues can be initiated via T cell activation at distal anatomical locations. Our study supports this model, given the development of prostate-directed autoimmunity in $C4^{\Delta TEC}$ mice following *Lm[C4]* challenge despite the pathogen's strong tropism for the spleen and liver (Figure 16). Similar demonstrations of distally-triggered autoimmunity via mimetic antigens have been described for a host of autoimmune diseases including SLE, RA, MS, T1D, APS, and Uveitis [440-442]. Unlike our study, most investigations of this phenomenon are initiated at the gut, where the triggering event is not infection with a mimetic pathogen but commensal-expressed mimotopes concurrent with an event that causes dysbiosis. What do the pathogenesis features common to each of these models and ours reveal about T cell activation, trafficking, and site-directed inflammation? Recent work using the photoconvertible Kaede mouse model demonstrated a striking degree of immune cell turnover in the colon and rapid trafficking of such cells to distal sites such as the spleen and bone marrow [443]. The rate of trafficking was similar to that observed for antigen-specific T cells following *Lm[C4]* infection, which could be easily detected by day 4 in the spleen but didn't readily appear at the prostate-draining pLN until day 7 (Figures 16-17). These results

indicate that T cells can rapidly distribute to distal sites both at steady-state or following activation, and suggest that regional enrichment of antigen-experienced T cell clones in the SLOs, including Treg cells, is more likely due to transient clonal bursts or delayed egress than static residency at the antigen-draining site [221].

The extensive trafficking of T cells between tissue sites suggests that T cell specificities may originate at distal sites but home to sites of inflammation. In this regard, a critical outstanding question from our work is the trafficking patterns of C4/I-A^b-specific Treg and Tconv cells upon *Lm[C4]* infection. MJ23 Treg cells are enriched, but not exclusively, in the pLN of male LF chimeric mice [70], yet C4/I-A^b-specific Treg cells still dominate the antigen-specific response in the spleen of wild-type mice by day 4 post-infection. Are these Treg cells primarily composed of "wandering" Tregs that are passing through the spleen at the time of infection, or is there a directed migration of such cells from the pLN? Studies of Treg migration from the gut provide additional insight. One such study demonstrated that Treg cells that originated and likely differentiated in the colon were capable of trafficking to an inflamed site of muscle injury within 48 hours [444]. Intriguingly, these Treg cells selectively express CCR2, just as do activated C4/I-A^b-specific Treg cells following *Lm[C4]* infection, and their trafficking is reduced by CCL2 blockade. In a reverse scenario, a separate study observed loss of *S. epidermidis*-specific Treg cell trafficking to the skin following concurrent dysbiosis and *S. epidermidis* colonization of the gut [445], suggesting that responding Treg cells may prolong their stay at sites of inflammation. Assuming these findings are broadly applicable to infection-responsive Treg cells, it's likely that C4/I-A^b-specific Treg cells traffic from the pLN to the spleen following *Lm[C4]* infection to control Tconv cells of matched specificity, and may do so in a CCR2-dependent manner (discussed in Chapter 3). The contribution of migrating C4/I-A^b-specific Treg and Tconv cells to the response at the spleen could be defined

using FTY-720 to block SLO egress during the infection, but such an experiment was not performed.

That autoimmune reactions can be initiated at distal inflammatory sites unintuitively suggests that inflammation itself can be both mobile and self-perpetuating. Classically, a site-specific infection or tissue injury is thought to initiate a T cell response via antigen and inflammatory PAMPs and DAMPs, which ultimately consolidates into memory and resolves upon pathogen clearance or wound healing. Our study significantly challenges this paradigm. Given that C4/I-A^b-specific responses are primarily initiated at the spleen and liver, and that the attenuated *Lm[C4]* pathogen is cleared with days of infection, the prostate is almost certainly devoid of infection-induced inflammation, at least by a week post-infection. Further supporting this claim, infection of mice with *Lm[parent]* or systemic inflammatory triggers did not initiate prostate-directed autoimmunity (Figure 15), even though prostate-derived C4 peptide is readily accessible during infection (Figure 11) and C4/I-A^b-specific cells at the pLN are perfectly capable of eliciting autoimmunity (Figure 18). Therefore, since C4/I-A^b-specific Tconv cells are the sole initiators of prostatitis in $C4^{\Delta TEC}$ mice, these cells intrinsically harbor the capacity to both manifest inflammation at a distal sterile site and sustain an inflammatory response – directly or indirectly. It follows that a single activated Tconv specificity is sufficient to drive an antigen-directed inflammatory response in the absence of any external TCR-amplifying costimulation or cytokine cues. While this revelation has far-reaching implications relevant to both disease and the fundamental nature of the adaptive immune response, our study provides little insight into the questions it has raised. What events occur when C4/I-A^b-specific Tconv cells that have escaped antigen-specific Treg control arrive at the pLN? Our data suggest that these cells may be subject to a second layer of antigen-specific constraint by Treg cells, but ultimately take up residence as a

self-sustaining population of effector cells if left unchecked (Figure 17). Which APCs re-activate these cells upon arrival? Studies in the tumor indicate that migratory DCs arriving from the tissue are the most potent activators of $CD4^+$ T cells in the LN [446,447], yet cDC1s and a novel $Aire^+$ ILC-like cell type present food- and bacterial-derived antigens for pTreg differentiation in the gut [179-181,448], so the identity of the APCs that present prostate-derived C4/I-A^b at steady-state remains speculative. Additional outstanding questions include whether activated C4/I-A^b-specific Tconv cells impose an inflammatory phenotype on the relevant APCs, how C4/I-A^b-specific Tconv cells infiltrate the prostate, and what role polyclonal tetramer-negative bystander T cells play in the autoimmune response. These and other questions will be the subject of discussion and speculation in Chapter 3: *Driver and Passenger T cells and epitope spreading*.

Antigen-specific Treg suppression and modes of T cell activation

The landmark finding that regulatory T cells are required throughout life to prevent T cell-mediated autoimmunity led to a flood of research focused on understanding the mechanisms by which Treg cells impose suppression. The vast majority of these studies have uncovered modes of Treg suppression that function in a bystander fashion to broadly dampen inflammatory cues in the environment, which effectively raise the threshold for T cell activation and accordingly dampen the response to self [237]. This classical mode of Treg function has thus become the default in the field of Treg biology owing to two main factors: 1) studies have almost exclusively manipulated the polyclonal Treg population, 2) studies have investigated Treg cells in naïve steady-state mice, with a few notable exceptions (see Introduction to Thesis). Our study has uncovered a previously unappreciated mode of antigen-specific Treg suppression during infection, which was uniquely enabled through the manipulation of a single specificity of endogenous Treg cells reactive to a

natural self-antigen. While our study is not the first to propose a role for antigen-specificity in Treg suppression, our system precisely identifies the context in which this mode is operative, demonstrates a critical requirement for autoimmune protection and effective self-nonself discrimination, and hones in on the mechanism being a rheostat which responds to Tconv cell activation rather than a prophylactic masking of stimulatory antigen.

The role of antigen specificity in Treg function has yielded historically conflicting results due to the lack of physiologic *in vivo* systems. A study in the NOD model [243] infused mice with islet antigen-specific BDC2.5tg Treg cells induced and activated *in vitro* plus equal numbers of either antigen-matched BDC2.5tg Tconv cells or 4.1tg Tconv cells specific for a different islet antigen. In this contrived system, BDC2.5tg Treg cells could suppress both specificities of Tconv cells, suggesting that Treg suppression occurs in a bystander fashion. Notably, this study found that Treg cells and Tconv cells made stable contacts with antigen-bearing APCs rather than with each other, implying a role for antigen and indirect Treg-mediated suppression at the Treg-APC interface. A more recent study corroborated these results using AAV-mediated Foxp3 delivery to engineer islet antigen-specific Treg cells, finding that such cells could prevent diabetes in NOD mice using both antigen-specific and bystander mechanisms of suppression [302]. A separate study [301] that similarly infused mice with *in vitro* differentiated transgenic Treg and Tconv cells came to the opposite conclusion: Treg cells were able to selectively suppress Tconv activation with matched antigen specificity by removing pMHC-II complexes from the surface of peptide-pulsed DCs. The extensive variables within each experimental system make it difficult to determine the source of this discrepancy. With regard to our study, one possibility could be the differences in APC activation and antigen availability: the former finding that demonstrated bystander suppression relied on endogenous antigen presentation at steady-state, while the latter study

utilized *ex vivo* peptide-pulsed DCs as the antigen source. This explanation suggests that antigen density and environmental factors impact the operative mode of Treg control (bystander vs. antigen-specific), which aligns with the results of our study demonstrating a similar contextual role for antigen-specific Treg suppression (Figures 14-16).

TCR expression on endogenous Treg cells in the periphery is required to maintain tolerance at steady-state [225,226], demonstrating that the TCR/pMHC-II axis is crucial for optimal Treg function. While tantalizing to suppose that this alludes to an antigen-specific mode of Treg tolerance, there are multiple alternative explanations for why the TCR is required, including that TCR positions Treg cells in the proper anatomical sites [221,230] or that it intrinsically confers a phenotype amenable to suppressive function, as has been described for the cTreg to eTreg transition [224]. However, a study addressing the role of a polyclonal repertoire in endogenous Treg function makes a compelling case for the importance of antigen specificity in Treg-mediated control [300]. Here, when most polyclonal Treg cells were made to express a single transgenic Treg-derived TCR, mice developed multi-organ Tconv cell infiltration, albeit at a delayed rate compared to mice in which TCR expression is ablated on Treg cells. The delayed onset of autoimmune disease in this model could be due to compensation from the few remaining polyclonal Treg cells, but may also be due to the lack or delay of an external event that triggers inflammation, which we found to be necessary for autoimmune induction when a single Treg specificity is absent (Figures 5 and 16). Because all Treg specificities except one are absent from these mice, it's possible that an "invisible" autoimmune-initiating event may occur when Tconv cells are triggered by PAMP-bearing microbial flora that are normally tolerized by Treg specificities. Furthermore, monoclonal Treg mice developed histological disease in the skin despite that the Treg-bearing TCR is specific for a single skin-derived antigen, implying that bystander modes of tolerance at the level of the

APC are unlikely to solely account for mechanisms of Treg control as was proposed in [243]. This result supports our findings that tolerance to the F1 peptide is maintained in *C4*$^{\Delta TEC}$ mice following *Lm[F1]* infection (Figure 19) and that all polyclonal Treg cells including F1/I-A^b-specific Treg cells are unable to compensate for the loss of C4/I-A^b-specific Treg cells (Figure 16).

The clear gap in knowledge that arises from these studies and ours concerns the cellular and molecular mechanisms by which Treg cell are selectively controlling Tconv cells with matched specificity. Integrating what is known about the modes of Treg and Tconv cell activation with tolerogenic and autoimmune phenotypes in our studies may provide critical clues. When mounting a response, T cells integrate three classes of activation signals, namely TCR/antigen, costimulation, and cytokines, which geometrically sum to determine the magnitude of the proliferation burst [449]. Since Treg and Tconv cells compete in the same arena for the same signals, these cells will necessarily influence each other's responses. C4/I-A^b-specific Tconv cells do not elicit an autoimmune response in *C4*$^{\Delta TEC}$ mice at steady-state or following inflammatory triggers alone (Figures 14-15), so deprivation of costimulatory and cytokine signals by polyclonal Treg cells must be sufficient to keep these Tconv cells below a critical activation threshold. Tconv cells require continued antigen availability, at least for a few days, to optimally proliferate and take on effector cell functions [450]. Furthermore, sustained TCR/pMHC-II interactions promote memory cell formation [451]. When mice are infected with *Lm[C4]*, which provides an increase in antigen, C4/I-A^b-specific Tregs become critical to keep Tconv cells of matched specificity from breaching tolerance, and do so by limiting their proliferation and effector differentiation. Integration of these studies with our observations strongly argues that C4/I-A^b-specific Treg cells uniquely control Tconv cells of matched specificity following *Lm[C4]* infection primarily by direct competition for C4/I-A^b antigen. Notably, this mechanism would explain why increases in C4/I-A^b Treg cells were

unable to prevent prostatitis in our T cell reconstitution experiments (Figures 20 and 22). pMHC-II-specific control by Treg cells is likely inoperative upon T cell transfer into *Tcrb*$^{-/-}$ mice given the expected increase in cytokine and costimulation availability in the lymphopenic host – a compensatory increase in these activation signals effectively lowers the threshold for T cell activation such that the integration of the TCR signal parameter is rendered irrelevant for breaching tolerance. In our study, MJ23 Treg cells were able to limit the proliferative states of clonally-identical MJ23 Tconv cells (Figures 25-26), which strongly suggests that something intrinsic to the Treg cell program makes these cells superior antigen competitors. Treg-intrinsic signaling machinery could render these cells more sensitive to pMHC-II recognition. Indeed, a recent report demonstrated that Treg cells exhibit greater Nur77 expression following antigen stimulation *in vitro* than Tconv cells expressing the same TCR [452], and aligns with our observations for MJ23 Treg and Tconv cells in the pLN at steady-state (Klawon et al., manuscript in preparation). This implies that Treg cells also have a proliferative advantage following antigen recognition, which may be temporal given that C4/I-A^{b}-specific tolerance is instructed within the first 4 days of infection (Figure 16). In this regard, Tconv cells spend a significantly longer duration of time on antigen-bearing APCs following TCR ligation than do Treg cells [453], and Tconv cells undergo non-linear expansion only after a few days since initial antigen exposure [454,455].

The cumulative evidence hypothesizes a mechanistic model of Tconv activation and antigen-specific Treg suppression as follows: 1) Upon recognition of antigen on an APC, a C4/I-A^{b}-specific Tconv cell arrests and begins to integrate TCR, costimulatory, and cytokine signals, 2) if allowed to maintain prolonged TCR/pMHC-II contact, the Tconv cell is programed to undergo extensive division and differentiation, will eventually disengage, and will give rise to many effector progeny, 3) if a C4/I-A^{b}-specific Treg cell finds the same APC, it will compete with the

Tconv cell for pMHC-II, effectively interrupting the prolonged contacts to prevent the Tconv from adopting pathogenic effector programs, 4) the Treg cell, which doesn't arrest on the APC, undergoes a modest but rapid clonal burst and continues surveying the environment for other antigen-bearing APCs. Critical evaluation of this model will require a combination of temporal data tracking the behavior of C4/I-A^b-specific Treg and Tconv cells in the early hours of infection, spatial data focused on the niches occupied by these cells during signal integration, and data defining the interactions between C4/I-A^b-specific T cells, polyclonal Treg cells, and other relevant T cell specificities.

CHAPTER 3:

MECHANISMS OF FOXP3$^+$ REGULATORY T CELL SUPPRESSION DURING INFECTION AND CONSEQUENCES FOR ANTIGEN-SPECIFIC CD4$^+$ T CELL TOLERANCE

INTRODUCTION

αβ T cells use T cell receptors (TCRs) to specifically identify short peptide antigens bound to host MHC molecules (pMHCs) displayed on the surface of antigen presenting cells (APCs). The mature T cell pool is furnished with a diverse collection of T cell clones expressing unique TCRs that are collectively capable of reacting to a broad array of self-derived and pathogen-derived peptide antigens (pMHCs). While this diversity ensures host protection from foreign threats, it inadvertently generates autoreactive T cells that can attack host tissues if properly activated. Foxp3$^+$ regulatory T (Treg) cells, an immunosuppressive subset of CD4$^+$ T cells that largely recognize self-antigens, enforce immune tolerance of autoreactive CD4$^+$ conventional T (Tconv) cells throughout life using an array of context-dependent mechanisms. We previously demonstrated that bystander mechanisms of Treg-mediated suppression – those that functionally raise the activation barrier for all Tconv cells irrespective of antigen specificity [256,268,283,344,383,384]. – are sufficient to control self-reactive Tconv cells at homeostasis (Figure 14). However, Treg cells reactive to a single self-antigen were indispensable for controlling Tconv cells of matched specificity during infection and preventing fulminant organ-targeted autoimmunity yet had no impact on responses to a pathogen-derived antigen (Chapter 2), demonstrating that bystander mechanisms of Treg-mediated suppression are insufficient in settings of inflammation. This finding raises unanswered questions of how a single Treg specificity can selectively control Tconv cells with matched specificity, and how escape of a single Tconv specificity coordinates a directed assault on the target organ.

Direct competition between Treg and Tconv cells for pMHC antigen via the TCR is an apparent mechanism that could explain antigen-specific Treg suppression. Given the relatively equal numbers of self-pMHC-reactive Treg and Tconv cells that seed the periphery (Figure 14),

this mechanism implies that Treg cells are superior at competing with Tconv cells for antigen. It is unlikely that differences in TCR-intrinsic properties such as affinity or avidity for pMHC confer this advantage, given that a clonal population of Treg cells was able to control Tconv cells expressing the same TCR (Figures 24-25). Indeed, a recent study demonstrated that Treg cells exhibit greater Nur77 expression following antigen stimulation than Tconv cells expressing the same TCR [452], suggesting that the Treg program itself may confer an advantage. Peripheral recognition of antigen prior to infection could support this advantage by instructing the capacity of self-specific Treg and Tconv cells to respond to antigen. Absent inflammatory triggers, prolonged antigen exposure can confer Tconv cells with a hyporesponsive or "anergic" phenotype [456] making it more difficult for these cells to escape Treg constraint. Conversely, TCR-dependent signals at homeostasis confer Treg cells with an "effector" phenotype [225,226], which endows such cells with unique chemokine receptors and trafficking abilities [224,229,310].

TCR-dependent competition may explain antigen-specific suppression of Tconv cells but does not explain how these activated Treg cells fail to impact the response of other specificities through known bystander mechanisms. An APC displaying self- and pathogen-pMHC complexes would bring self-reactive Treg cells in close proximity with pathogen-specific Tconv cells, which would have to compete for TCR-independent activation cues such as IL-2 and costimulatory ligands that could impact their response. It's possible that self-derived and pathogen-derived antigens are exclusively displayed by distinct APC populations, though this possibility is unlikely given a recent report that identified migratory DCs as the primary interacting partners of Treg cells [457]; the same APC population that displays foreign antigens from tissues following immunization [458]. Another scenario could be that Treg cells use their TCRs to remove pMHC complexes from APCs to avoid concurrent display to self- and pathogen-reactive T cells, as proposed in a previous

study [301], but this mechanism is incomplete if operative given that self-reactive Tconv cells are readily primed by antigen following infection (Figure 16). A third possibility is that dominance hierarchies of T cells within antigen-rich microdomains instruct antigen-specific responses such that only one local T cell clone responds to the detriment of all others. In this model, self-specific Treg cells and pathogen-specific Tconv cells would equally compete for activation factors near the APC at the exclusion of self-specific Tconv cells, ultimately driving a large clonal burst for one or the other that would not be captured by enumerating cells contributing to the response. Such microdomain decisions may be critical for the complete breakdown of tolerance following the loss of a single Treg specificity, allowing for organ infiltration by a multitude of T cell specificities that are otherwise tolerant.

RESULTS

In this study, we elucidated the mechanisms that enable antigen-specific Treg control of self-reactive Tconv cells during infection, and defined the cell types and antigen specificities that participate in autoimmune suppression or loss of tolerance. To do this, we analyzed Treg and Tconv cell responses against self-derived peptide antigens following infection with the pathogen *L. monocytogenes*. These two self-reactive specificities respectively recognize the prostate-derived C4 and F1 peptides presented on the MHC-II molecule I-A^b. Presentation of these antigens in the thymus during development directs a fraction of antigen-specific T cells into the Treg lineage [87], enabling both Treg and Tconv cells of each specificity to exist in the normal repertoire of C57BL/6 mice at steady-state. Mice that harbor a conditional deletion of the C4 peptide in the thymus (termed $C4^{\Delta TEC}$ mice) fail to efficiently seed the periphery with C4/I-A^b-specific Treg cells (Figure 14) and develop autoimmune prostatitis elicited by C4/I-A^b-specific Tconv cells following infection with a C4 peptide-expressing pathogen *Lm[C4]* (Figure 16). In contrast, wild-type mice ($C4^{WT}$) infected with *Lm[C4]* are completely protected from autoimmune disease by C4/I-A^b-specific Treg cells that limit the proliferation and differentiation of C4/I-A^b-specific Tconv cells (Figures 23-25) without impacting the response to another pathogen-derived antigen (Figure 16). The C4/I-A^b- and F1/I-A^b-specific T cell responses can be studied using fluorescent tetramers and monoclonal T cells from TCR transgenic or retrogenic mice expressing the C4/I-A^b-specific MJ23 TCR [102] or F1/I-A^b-specific SP33 TCR [138]. By combining these tools within gene manipulations and quantitative multiplexed tissue imaging, we determined the mechanism by which C4/I-A^b-specific Treg cells prevent autoimmunity and defined the cross-talk between these and other specificities following a breach in tolerance.

C4/I-A^b-specific MJ23 Treg cells are intrinsically poised to accumulate earlier than clonally-matched Tconv cells following Lm[C4] infection

Activated C4/I-A^b-specific Tconv cells enable autoimmunity of the prostate in *C4$^{\Delta TEC}$* mice following infection with *Lm[C4]*, but these same cells are controlled in similarly-infected *C4^{WT}* mice by Treg cells of the same specificity (Figure 16). The choice to become pathogenic or abort the response is instructed by day 4 post-infection, as C4/I-A^b-specific Tconv cells in *C4^{WT}* mice have already adopted non-proliferative gene-expression programs at this timepoint (Figure 23). Understanding how C4/I-A^b-specific Treg cells orchestrate this control therefore requires a temporal analysis of C4/I-A^b-specific T cells at timepoints earlier than day 4 post-infection. Since rare C4/I-A^b-specific T cells are difficult to reliably detect using pMHC tetramers in the absence of expansion, we instead tracked congenically-marked MJ23 Treg and Tconv cells at these early timepoints. Additionally, this eliminated any variables inherent to the TCR between the Treg and Tconv compartments, enabling a direct comparison of responses intrinsic to Treg and Tconv cells of matched pMHC specificity.

We performed an early time course of the response to *Lm[C4]* challenge in MJ23 BMCs generated in *C4^{WT}* hosts, which harbor a mixture of MJ23 Treg cells and Tconv cells at baseline (Figure 26, A), and compared this to the response in chimeras generated in *C4$^{\Delta TEC}$* hosts, which exclusively harbor MJ23 Tconv cells due to the lack of C4/I-A^b presentation in the thymus (Figure 24, C). In *C4^{WT}* hosts, MJ23 Treg cell expansion occurred more rapidly than that of MJ23 Tconv cells, preceding MJ23 Tconv expansion by 12 hours or more (Figure 26, A-B). As a result, MJ23 Treg cells outnumbered MJ23 Tconv cells by >15-fold from days 2.5 to 4 (Figure 26, C-D). Strikingly, a similar delay in MJ23 Tconv cell expansion was also observed in *Lm[C4]* challenged *C4$^{\Delta TEC}$* hosts lacking MJ23 Treg cells (Figure 26, B-D), suggesting that this proliferation lag was

an intrinsic feature of the MJ23 Tconv cell response and that Treg cells are able to rapidly proliferate. Despite this delay, MJ23 Tconv cells expanded markedly in $C4^{\Delta TEC}$ hosts beyond day 3 (Figure 26, B-D), indicative of a rapid proliferative burst following the initial lag period and consistent with previous studies of Tconv cells reactive to pathogen-expressed nonself peptides [454,455]. Notably, differences in proliferation between Treg and Tconv cells were not observed at the polyclonal level (Figure 26, E). These results indicate that C4/I-A^b-specific MJ23 Treg cells are intrinsically poised to accumulate more rapidly following *Lm[C4]* challenge relative to Tconv cells expressing the same TCR.

The earlier accumulation of MJ23 Treg cells could occur either because these cells begin proliferating sooner or because these cells divide faster than MJ23 Tconv cells. To determine this, we tracked these cells at day 2 following infection in $C4^{WT}$ mice, which was the earliest timepoint that we could detect a T cell response. At day 2, the absolute number of MJ23 Treg and Tconv cells was comparable to the number of cells in naïve mice (Figure 26, C and F-G), indicating that proliferation had not yet occurred in either population. Despite this, both MJ23 Treg and Tconv cells expressed Ki67 (Figure 26, H-I), suggesting that both populations had sensed antigen and were poised to proliferate. Taken together, these results suggest that MJ23 Treg cells do not initiate the proliferative program sooner than MJ23 Tconv cells but instead undergo a proliferative burst faster than these cells. Notably, the pro-proliferative high affinity IL-2 receptor CD25 was uniformly expressed by MJ23 Treg cells but not Tconv cells at day 2 (Figure 26, J), suggesting that competition for IL-2 may contribute to both the early expansion of MJ23 Treg cells and the paucity of responding MJ23 Tconv cells.

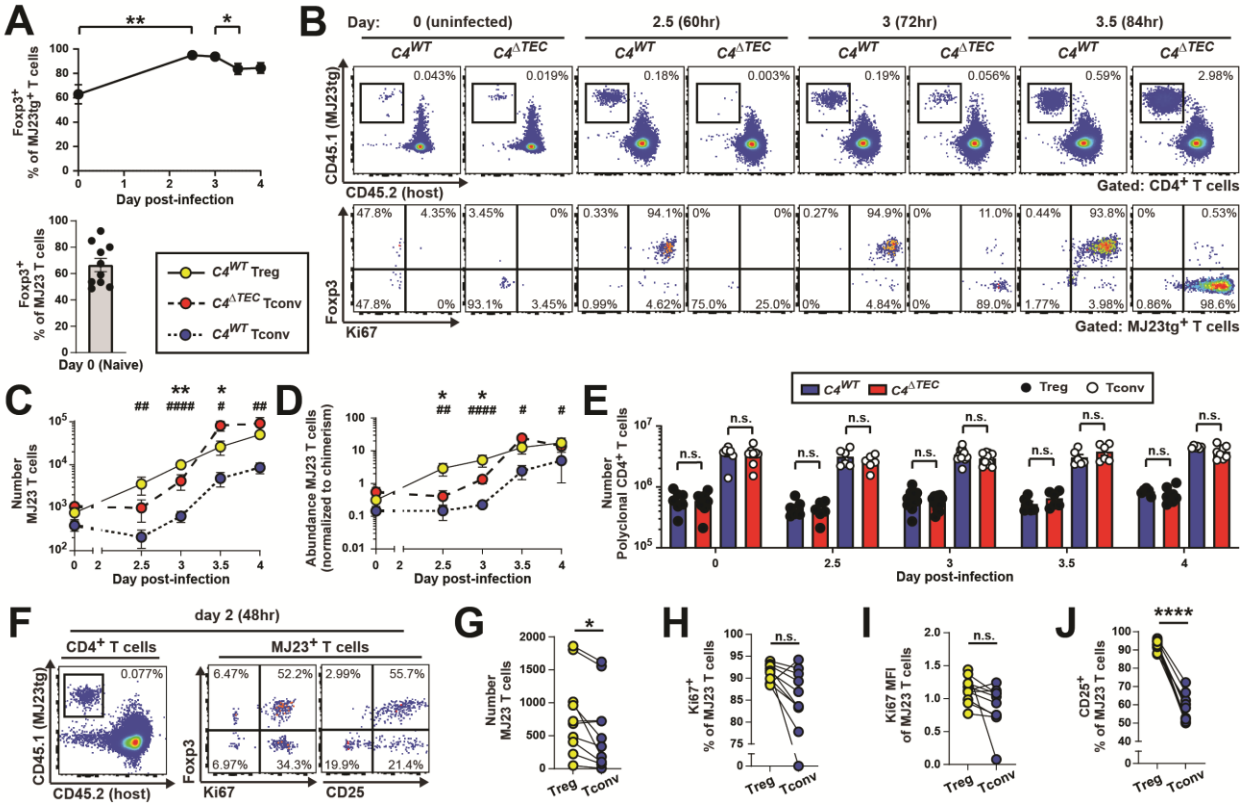

FIGURE 26. C4/I-A^{b}-specific MJ23 Treg cells are intrinsically poised to accumulate earlier than clonally-matched Tconv cells following *Lm[C4]* infection

LF MJ23 chimeric mice were generated in *C4^{WT}* and *C4^{ΔTEC}* male hosts. >6 weeks post-engraftment, host mice were infected with 10^7 CFU *Lm[C4]*. at the indicated day post-infection, the fate of MJ23 T cells were assessed in the spleen by flow cytometry. At 2dpi (F-J), CD4$^+$ T cells were magnetically enriched from the spleen prior to analysis. n = 7, *C4^{WT}* d0; n = 8, *C4^{ΔTEC}* d0; n = 10, *C4^{WT}* d2; *C4^{WT}* d2.5; n = 6, *C4^{ΔTEC}* d2.5; n = 11, *C4^{WT}* d3; n = 12, *C4^{ΔTEC}* d3; n = 6, *C4^{WT}* d3.5; n = 6, *C4^{ΔTEC}* d3.5; n = 6, *C4^{WT}* d4; n = 8, *C4^{ΔTEC}* d4. Data represent 3-5 independent experiments (A-E) and two independent experiments (F-J). (A) Summary plots of pooled data showing the frequency of MJ23$^+$ CD4$^+$ cells expressing Foxp3 in mice at the indicated day post-infection. The bottom plot depicts unchallenged mice for clarity. Each symbol represents the mean ± SEM of pooled mice (top) or one mouse (bottom). (* = P < 0.05; ** = P < 0.01; two-tailed non-parametric Mann-Whitney test). (B) Representative flow cytometric analysis of MJ23$^+$ or polyclonal CD4$^+$ T cells isolated from the spleens of LF chimeric mice of the indicated genotype and timepoint. Plots depict CD45.2 vs. CD45.1 expression by polyclonal CD4$^+$ T cells (top), and Ki67 vs. Foxp3 expression by MJ23$^+$ CD4$^+$ T cells (bottom). The frequency of cells within the indicated gates is denoted. (C) Summary plot of pooled data showing the number of MJ23$^+$ CD4$^+$ Treg and Tconv cells recovered from the spleens of mice of the indicated genotype and day post-infection. Each symbol represents the mean ± SEM of pooled mice. Asterisks (*) indicate statistics comparing *C4^{WT}* Treg to *C4^{ΔTEC}* Tconv, whereas Number signs (#) indicate statistics comparing *C4^{WT}* Treg to *C4^{WT}* Tconv (* = P < 0.05; ** = P < 0.01; **** = P < 0.0001; two-tailed non-parametric Mann-Whitney test). (D) Summary plot of pooled data showing the relative abundance of MJ23$^+$ CD4$^+$ Treg and Tconv cells recovered from the spleens of mice of the indicated genotype and day post-infection. The number of MJ23$^+$ CD4$^+$ T cells was

FIGURE 26, continued
normalized to the number of "antigen-independent" TCRβ^{neg} CD45.1$^+$ cells in each mouse to control for differences in chimerism between mice prior to infection. Each symbol represents the mean ± SEM of pooled mice. Asterisks (*) indicate statistics comparing *C4^{WT}* Treg to *C4$^{\Delta TEC}$* Tconv, whereas Number signs (#) indicate statistics comparing *C4^{WT}* Treg to *C4^{WT}* Tconv (* = P < 0.05; **** = P < 0.0001; two-tailed non-parametric Mann-Whitney test). (E) Summary plot of pooled data showing the number of polyclonal CD4$^+$ cells recovered from mice at the indicated day post-infection. Each symbol represents the mean ± SEM of pooled mice. (n.s. = P > 0.05; two-tailed non-parametric Mann-Whitney test).
(F) Representative flow cytometric analysis of polyclonal or MJ23$^+$ CD4$^+$ T cells enriched from the spleens of LF chimeric mice 2 days post-infection. Plots depict CD45.2 vs. CD45.1 expression by polyclonal CD4$^+$ T cells (left), and Ki67 or CD25 vs. Foxp3 expression by MJ23$^+$ CD4$^+$ T cells (right). The frequency of cells within the indicated gates is denoted. (G) Summary plot of pooled data showing the number of MJ23$^+$ CD4$^+$ Treg and Tconv cells enriched from the spleens of host mice 2 days post-infection. Each symbol represents one mouse. Mean ± SEM is indicated. (* = P < 0.05; two-tailed paired t test). (H) Summary plots of pooled data showing the frequency of Ki67$^+$ cells amongst MJ23$^+$ CD4$^+$ T cells enriched from the spleens of host mice 2 days post-infection. Each symbol represents one mouse. Mean ± SEM is indicated. (n.s. = P > 0.05; two-tailed paired t test). (I) Summary plots of pooled data showing the the normalized MFI of Ki67 amongst MJ23$^+$ CD4$^+$ T cells enriched from the spleens of host mice 2 days post-infection. Each symbol represents one mouse. Mean ± SEM is indicated. (n.s. = P > 0.05; two-tailed paired t test). (J) Summary plots of pooled data showing the frequency of CD25$^+$ cells amongst MJ23$^+$ CD4$^+$ T cells enriched from the spleens of host mice 2 days post-infection. Each symbol represents one mouse. Mean ± SEM is indicated. (**** = P < 0.0001; two-tailed paired t test).

MJ23 Treg cells locally compete with MJ23 Tconv cells for C4/I-A^b antigen and IL-2 signals to orchestrate their suppression

Our collective data demonstrate that C4/I-A^b-specific Treg cells instruct the fate of C4/I-A^b-specific Tconv cells by limiting their proliferation and differentiation potential between days 2 and 4 following *Lm[C4]* infection. Given that C4/I-A^b-specific Treg cells have an intrinsic proliferative advantage over Tconv cells in this same timeframe, we hypothesized that C4/I-A^b-specific Treg cells limit Tconv cell activation by outcompeting such cells for critical antigenic and cytokine input signals necessary for proliferation and differentiation [459,460]. C4/I-A^b-specific Treg cells may especially modulate TCR signaling in C4/I-A^b-specific Tconv cells since such Treg cells

do not constrain the Tconv response to a second *Lm*-derived peptide antigen LLO/I-A^b (Figure 16). To elucidate the mechanism by which self-pMHC-specific Treg cells selectively control Tconv cells of matched specificity following infection, we performed quantitative confocal imaging of *Lm[C4]*-challenged MJ23 BMCs generated in $C4^{WT}$ vs. $C4^{\Delta TEC}$ mice (Figure 27, A). This approach provided phenotypic and spatial information regarding the activation states and relative positioning of MJ23 Treg and Tconv cells of matched specificity, and the relationship of these cells to proximal endogenous Treg cells in settings where C4/I-A^b-specific Tconv cells are effectively controlled ($C4^{WT}$ mice) or where a breach of control results in fulminant organ-specific autoimmunity ($C4^{\Delta TEC}$ mice). Phenotypic features included PD-1 expression to readout TCR signaling intensity, Ki67 to measure proliferative competency, and pSTAT5 staining to readout IL-2 cytokine signaling, whereas spatial features included quantification of local densities of polyclonal or MJ23 Treg cells near each MJ23 Tconv cell. We analyzed the response in the liver-draining portal lymph nodes, which drain a major site of *Lm* propagation, and focused on the day 3 timepoint, reasoning that the mechanisms orchestrating the divergent outcomes in $C4^{WT}$ vs. $C4^{\Delta TEC}$ mice are likely to be captured here (Figure 26).

We observed that MJ23 Treg cells were positioned near some – but not all – MJ23 Tconv cells (Figure 27, B). To investigate whether co-localized MJ23 Treg cells were coordinating MJ23 Tconv constraint, we defined the activation states of MJ23 Treg and MJ23 Tconv cells located proximal to one another (within a 30μm microdomain), and compared these to the activation states of MJ23 Treg and Tconv cells that were not co-localized (distal, not near). MJ23 Treg cells expressed high amounts of Ki67 regardless of whether they were positioned near MJ23 Tconv cells (Figure 27, C), suggesting that most MJ23 Treg cells had already integrated signals required for proliferation by this timepoint, and supporting the notion that Treg cells rapidly enter a

proliferative state following infection (Figure 26). In contrast, proximal MJ23 Treg cells exhibited elevated staining of PD-1 and pSTAT5 relative to distal MJ23 Treg cells, as well as both proximal and distal polyclonal Treg cells (Figure 27, D-E), indicating that MJ23 Treg cells perceived elevated TCR and IL-2-dependent signals when positioned near MJ23 Tconv cells, and suggesting that co-localized MJ23 Treg cells were actively sensing C4/I-A^b antigen. MJ23 Tconv cells in $C4^{WT}$ hosts expressed reduced amounts of PD-1 and Ki67 relative to MJ23 Tconv cells elicited in $C4^{\Delta TEC}$ hosts, regardless of whether they were co-localized with MJ23 Treg cells (Figure 27, F-G), suggesting that MJ23 Treg cells were limiting antigen availability throughout the system. Notably, significant differences in pSTAT5 staining were not observed for MJ23 Tconv cells in $C4^{WT}$ vs. $C4^{\Delta TEC}$ mice irrespective of whether MJ23 Tconv cells were marked by MJ23 Treg cells in close proximity (Figure 27, H), indicating that MJ23 Treg cells did not impact IL-2 sensing by clonally matched Tconv cells at this time point. Collectively, these data demonstrate that the presence of clonally matched Treg cells did not prevent TCR signaling by MJ23 Tconv cells, but instead broadly attenuated the intensity of TCR signals perceived by these cells, and did so despite co-localizing with only a fraction of MJ23 Tconv cells at the time of analysis.

The observation that MJ23 Tconv cells in $C4^{\Delta TEC}$ mice collectively express higher amounts of PD-1 and Ki67 but not pSTAT5 than their counterparts in $C4^{WT}$ mice suggests that MJ23 Treg cells primarily constrain MJ23 Tconv cells by limiting their access to C4/I-A^b. Only a fraction of MJ23 Tconv cells had proximally-located MJ23 Treg cells in $C4^{WT}$ mice, yet the proliferative state and TCR signaling of all MJ23 Tconv cells was attenuated (Figure 27, F-G). Furthermore, only a fraction of MJ23 Tconv cells in $C4^{\Delta TEC}$ mice adopted high expression of Ki67 and PD-1 (Figure 27, F-G) despite the lack of MJ23 Treg cells, implying that polyclonal Treg cells may also play a role in constraint or escape of MJ23 Tconv cells. To understanding the local Treg cell

microenvironments regulating MJ23 Tconv cell responses in the two settings, we defined the full landscape of Treg cells – both MJ23 and polyclonal – positioned within 30μm of each MJ23 Tconv cell in mice of both genotypes. To do this, we linked each Treg cell to its nearest MJ23 Tconv cell and performed unsupervised hierarchical clustering of eight parameters, including the staining intensity of Ki67, PD-1, and pSTAT5 for each Treg cell and its linked MJ23 Tconv cell, plus the local densities of polyclonal and MJ23 Treg cells near this MJ23 Tconv cell (Figure 27, I-K). This analysis defined six major Treg cell clusters that differed in their proportional representations in the $C4^{WT}$ vs. $C4^{\Delta TEC}$ settings (Figure 27, L). We then used these clusters to define the local Treg cell microenvironments associated with the MJ23 Tconv cell activation phenotypes, thereby merging these two perspectives. This was done by plotting PD-1 vs. Ki67 expression for MJ23 Tconv cells elicited in the two settings and color coding each MJ23 Tconv cells based on the most common Treg cell phenotype within close proximity (Figure 27, M-N). To validate this approach, we performed a similar analysis for the MJ23 Tconv cells using the average phenotypes of all proximal Treg cells, which yielded similar results (data not shown).

This holistic analysis revealed that MJ23 Tconv cells that adopted different phenotypes were typically associated with distinct local Treg cell microenvironments. For MJ23 Tconv cells elicited in $C4^{\Delta TEC}$ hosts lacking MJ23 Treg cells, plots of PD-1 vs. Ki67 expression revealed multiple phenotypic patterns (Figure 27, M), including two PD-1^{hi} populations (D1 and D2) exhibiting strong TCR signaling and at least two Ki67^{hi} populations (including D2 and D3) with high proliferative competency. The D1 and D2 MJ23 Tconv cell populations expressed high amounts of PD-1 despite a high local density of polyclonal Treg cells (Treg clusters C4 and C3, respectively) (Figure 27, I), suggesting that such Treg cells were unable to prevent strong TCR signaling by these Tconv cells in the absence of matched MJ23 Treg cells. In addition, the most

prevalent MJ23 Tconv cell phenotype in the *C4*$^{\Delta TEC}$ setting, D3, was characterized by high expression of Ki67 and low expression of PD-1 (Figure 27, M), indicative of cells that have terminated TCR signal integration by this time point but were able to adopt a prolonged proliferative state. For these Tconv cells, the local Treg cell microenvironment featured PD-1^{lo} Treg cells (Treg cluster C5) interspersed with a minor population of highly activated PD-1^{hi} Ki67^{hi} pSTAT5^{hi} Treg cells (Treg cluster C6) (Figure 27, I), suggesting that these MJ23 Tconv cells have entered an activated state that can no longer be controlled by Treg cells.

In contrast, the presence of MJ23 Treg cells in *Lm[C4]*-challenged *C4*^{WT} hosts prevented the emergence of the phenotypic MJ23 Tconv cell subsets highlighted above (D1, D2, and D3) and drove consolidation of MJ23 Tconv cells into a more uniform phenotype characterized by intermediate expression of PD-1 and intermediate to high expression of Ki67 (Figure 27, N). Of note, some MJ23 Tconv cells elicited in *C4*$^{\Delta TEC}$ hosts exhibited this same phenotype (cells falling outside D1, D2, and D3) (Figure 27, M), suggesting that bystander tolerance mechanisms enforced by polyclonal Treg cells controlled a minor fraction of MJ23 Tconv cells elicited in *C4*$^{\Delta TEC}$ mice. MJ23 Tconv cells elicited in *C4*^{WT} hosts were primarily marked by two proximal Treg cell clusters – one containing co-localized MJ23 Treg cells (Treg cluster C2), and one devoid of MJ23 Treg cells (Treg cluster C1) (Figure 27, I and N). Of note, all Treg cells in these clusters expressed high amounts of PD-1 (Figure 27, K), indicative of uniform engagement of self-pMHC by these Treg cells, and suggesting that some polyclonal Treg cells in clusters C1 and C2 represent endogenous C4-specific Treg cells. This contrasted with local Treg cell microenvironments enriched near MJ23 Tconv cells in *C4*$^{\Delta TEC}$ hosts, which contained a substantial fraction of PD-1-negative Treg cells (Figure 27, I and K). Curiously, a fraction of MJ23 Treg cells in *C4*^{WT} hosts that were not co-localized with MJ23 Tconv cells adopted the Ki67^{hi} PD-1^{neg} "D3" phenotype (Figure 27, O)

observed for MJ23 Tconv cells in $C4^{\Delta TEC}$ but not $C4^{WT}$ hosts (Figure 27, M-N), suggesting that MJ23 Treg cells normally occupy this phenotypic niche to restrict entry by MJ23 Tconv cells. Collectively, these data indicate that in a setting of elevated self-antigen presentation during bacterial infection, self-pMHC-specific Treg cells promote the formation of unique Treg cell microenvironments which attenuate TCR signaling by Tconv cells of shared specificity and stifle the emergence of distinct Tconv cell phenotypes.

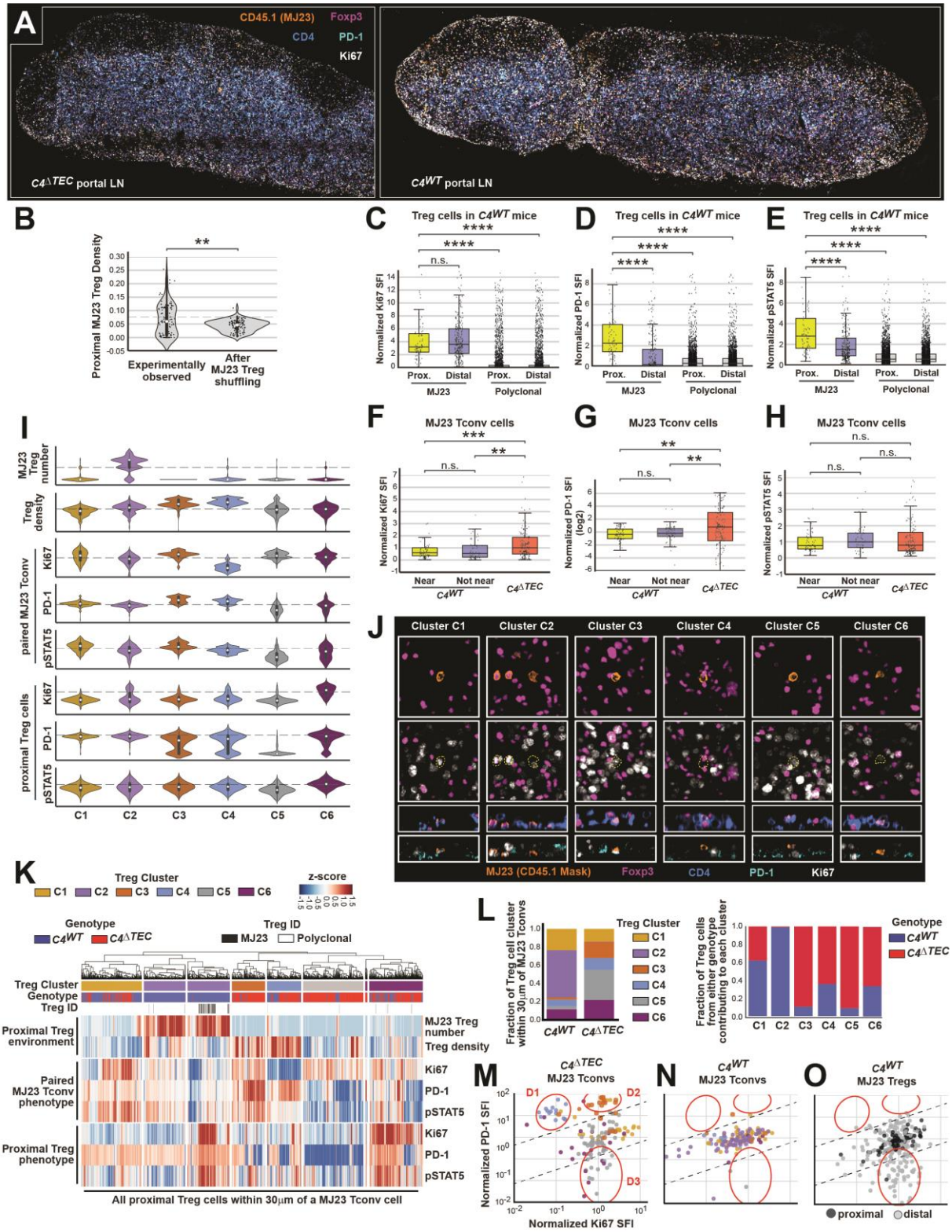

FIGURE 27. MJ23 Treg cells locally compete with MJ23 Tconv cells for C4/I-A^b antigen and IL-2 signals to orchestrate their suppression

FIGURE 27, continued
LF MJ23 chimeric mice were generated in $C4^{WT}$ and $C4^{\Delta TEC}$ male hosts. >6 weeks post-engraftment, host mice were infected with 10^7 CFU *Lm[C4]*. 3 days post-infection, the liver-draining portal LNs were fixed, sectioned, immunostained, and $CD4^+$ T cells were analyzed by high-parameter confocal microscopy. n = 6, $C4^{WT}$; n = 4, $C4^{\Delta TEC}$. Data represent 2-3 independent experiments. (A) Representative images depicting whole LN sections isolated from mice of the indicated genotype. Images depicts CD45.1 (cells from MJ23-derived marrow), Ki67, Foxp3, CD4, and PD-1 expression. (B) Summary plot depicting the observed proximal density of MJ23 Treg cells surrounding MJ23 Tconv cells in LNs from $C4^{WT}$ hosts, compared to the density after the positions of MJ23 Tregs were randomly shuffled with polyclonal Tregs. Each dot represents one MJ23 Tconv cell. (C-E) Summary plots of pooled data depicting Ki67 (C), PD-1 (D), and pSTAT5 (E) standardized fluorescence intensity (SFI) on MJ23 and polyclonal Treg cells in LNs from $C4^{WT}$ hosts. Proximal cells are observed within 30μm of an MJ23 Tconv cell, while distal cells are observed outside of this radius. Each dot depicts one cell. (F-H) Summary plots of pooled data depicting Ki67 (F), PD-1 (G), and pSTAT5 (H) standardized fluorescence intensity (SFI) on MJ23 Tconv cells in LNs from mice of the indicated genotype. "Near" denotes MJ23 Tconv cells identified in $C4^{WT}$ mice where at least one MJ23 Treg cell was observed within 30μm. Each dot depicts one cell. (I-O) All proximal MJ23 and polyclonal Tregs observed within 30μm of each MJ23 Tconv cell in LNs from mice of the indicated genotype were linked to their proximal MJ23 Tconv cell, and subjected to high-dimensional unsupervised clustering analysis. (I) Violin plots showing the normalized z-score of each clustering parameter for the proximal Treg cells. Treg cells were classified into six unique clusters (C1 to C6) based on the clustering parameters. (J) Image gallery depicting cluster-assigned MJ23 Tconv and polyclonal Treg cell microenvironments in LNs isolated from $C4^{\Delta TEC}$ and $C4^{WT}$ mice. (K) Heatmap of unsupervised clustering of proximal Treg cells. Each row depicts a clustering parameter, while each column depicts an individual Treg cell. (L) Histogram showing the proportion of Treg cells in each Treg cluster as a fraction of the total proximal Treg cells identified in mice of either genotype (left), or the fraction of Treg cells from either genotype contributing to each Treg cluster (right). (M-O) Summary plots depicting the expression of Ki67 and PD-1 on MJ23 Tconv cells identified in LNs from $C4^{\Delta TEC}$ (M), MJ23 Tconv in $C4^{WT}$ (N), and MJ23 Treg in $C4^{WT}$ mice (O). Each symbol represents one cell. Colors depict the most abundant Treg cluster observed within 30μm of each MJ23 Tconv cell (M and N), or classify an MJ23 Treg as proximal or distal to an MJ23 Tconv cell (O). Lines depict the prediction interval for the linear regression of MJ23 Tconv cells identified in $C4^{WT}$ mice (N). Three phenotypic regions of interest are depicted in red, classified as D1, D2, and D3.

MJ23 Treg cells restrain MJ23 Tconv cell entry into the blood and prostate following Lm[C4] infection

MJ23 Treg cells have an intrinsic proliferative advantage over Tconv cells of matched specificity (Figure 26), which enables such cells to rapidly accumulate and outcompete MJ23

Tconv cells for C4/I-A^b antigen following *Lm[C4]* infection (Figure 27). While MJ23 Treg cells ultimately limit the potential of MJ23 Tconv cells to sustain effector and consolidate memory responses, they do not prevent activated MJ23 Tconv effector cells from briefly accumulating in the secondary lymphoid organs (Figures 23-25). We therefore wondered whether MJ23 Treg cells also limit the migratory potential of MJ23 Tconv cells to prevent autoimmune infiltration. We first tracked MJ23 T cells in the blood over time in LF MJ23 chimeras generated in $C4^{WT}$ mice post *Lm[C4]*-infection, and compared their prevalence to MJ23 Tconv cells in analogous $C4^{\Delta TEC}$ chimeric mice (Figure 28, A). In $C4^{WT}$ hosts, very few MJ23 T cells were observed in the blood at all timepoints (Figure 28, B-D), and most of those that did enter the blood were MJ23 Treg cells (Figure 28, E). In the absence of MJ23 Treg cells in $C4^{\Delta TEC}$ hosts, MJ23 Tconv cells appeared in the blood 4 days after infection, where they continued to accumulate until the peak of the T cell response at day 6 (Figure 28, B-E). These results suggest that MJ23 Treg cells prevent efficient egress of MJ23 Tconv from SLOs following their initial activation.

We next sought to test whether MJ23 Treg cells impeded the ability of MJ23 Tconv cells to traffic into the prostate. Since endogenous C4/I-A^b-specific cells elicited by Lm[C4] infection in $C4^{\Delta TEC}$ mice enable prostatic infiltration by nonspecific "passenger" T cell clones (Figure 16, B-D), we reasoned that MJ23 Tconv cells would also be subject to a degree of bystander infiltration and it would therefore be improper to compare MJ23 T cells in the prostate between $C4^{WT}$ and $C4^{\Delta TEC}$ host mice. Instead, we generated chimeras in $C4^{WT}$ hosts using bone marrow from MJ23 mice expressing the $Foxp3^{DTR\text{-}EGFP}$ allele, subjected half of these mice to selective MJ23 Treg cell depletion via DT administration, and assessed MJ23 T cells host mice 14 days after *Lm[C4]* infection (Figure 28, F). Even in this system, a high degree of prostatic T cell infiltration was observed in both groups (Figure 28, G-H), likely reflective of irradiation-induced inflammation in

the host mice prior to chimera setup, which precluded a direct comparison of the absolute number of prostate-infiltrating MJ23 Tconv cells. To circumvent this, we compared the number of MJ23 Tconv cells in the prostate to the number of MJ23 Tconv cells observed in the spleen within each group. We reasoned that if MJ23 Treg cells were impairing the egress of MJ23 Tconv cells from SLOs, a higher proportion of MJ23 Tconv cells would exist in the spleen than the prostate of MJ23 Treg-sufficient mice when compared to MJ23 Treg-depleted mice. A greater fraction of MJ23 Tconv cells were observed infiltrating the prostates of MJ23 Treg-depleted mice than non-depleted mice when normalized to the spleen (Figure 28, I), suggesting that MJ23 Tconv cells are preferentially maintained in the peripheral SLOs when MJ23 Treg cells are present. As an additional metric, we plotted the number of MJ23 Tconv cells recovered from the spleen vs. the prostate for each mouse and compared the best-fit lines between the groups. This analysis revealed a significantly steeper slope that favored the prostate for MJ23 Treg-depleted mice, indicating that MJ23 Tconv cells in these mice had an enhanced ability to enter the prostate following *Lm[C4]* infection (Figure 28, J). Taken together, our studies in $C4^{WT}$, $C4^{\Delta TEC}$, and MJ23 Treg-depleted hosts suggest that MJ23 Treg cells impair the ability of MJ23 Tconv cells to exit SLOs and traffic to the prostate following *Lm[C4]* infection.

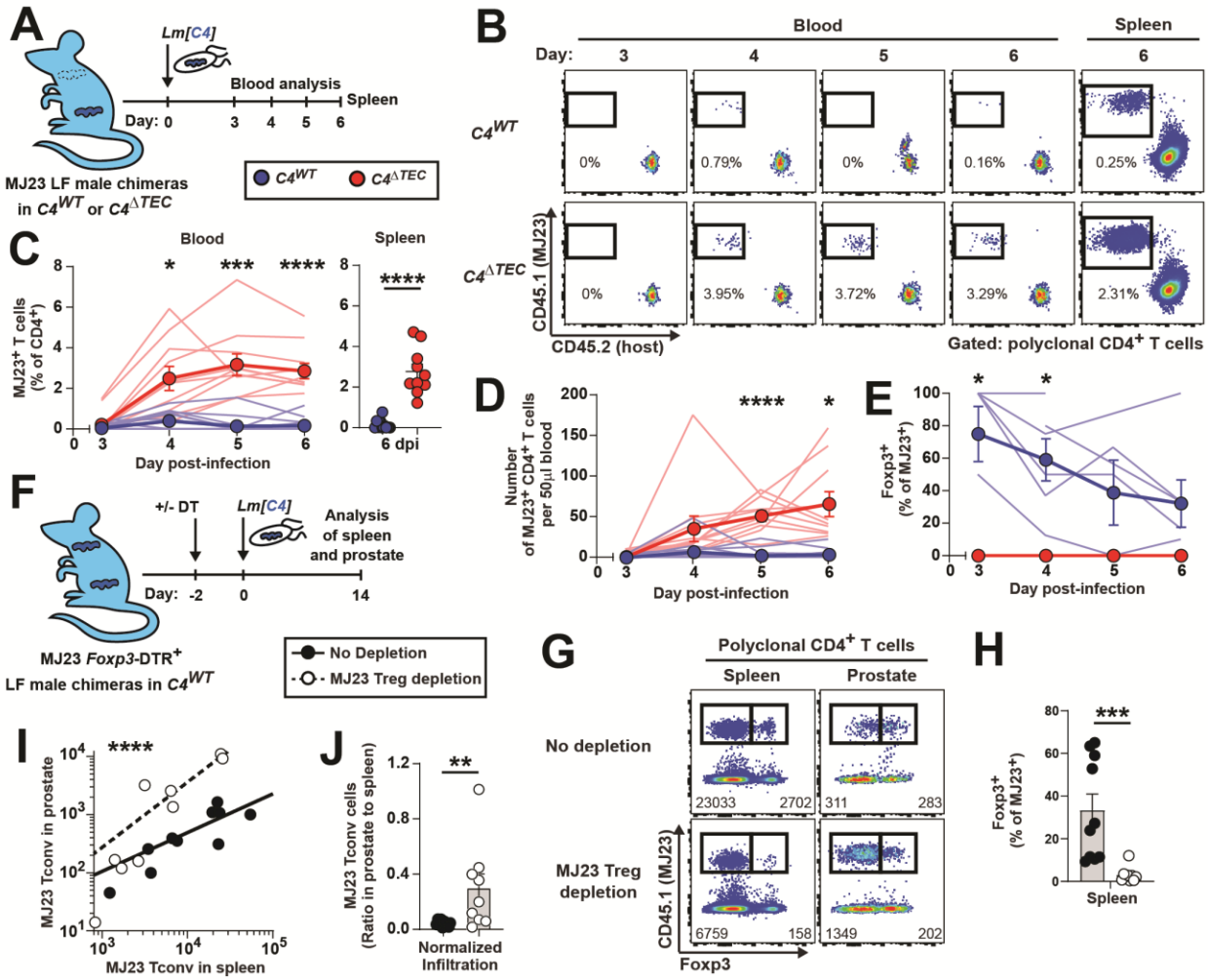

FIGURE 28. MJ23 Treg cells restrain MJ23 Tconv cell entry into the blood and prostate following *Lm[C4]* infection

(A) Experimental schematic for panels (B-E). LF MJ23 chimeric mice were generated in $C4^{WT}$ and $C4^{\Delta TEC}$ male hosts. >6 weeks post-engraftment, host mice were infected with 10^7 CFU *Lm[C4]*. On days 3-6 days post-infection, MJ23 T cells were assessed in the blood by flow cytometry. Mice were sacrificed at day 6 to also assess the fate of MJ23 T cells in the spleen. n = 10, $C4^{WT}$; n = 10, $C4^{\Delta TEC}$. Data represent two independent experiments. (B) Representative flow cytometric analysis of CD4+ T cells isolated from the blood or spleen of LF chimeric mice of the indicated genotype at the indicated timepoint. Plots depict CD45.1 (MJ23) vs. CD45.2 (host) expression by polyclonal $CD4^+$ T cells. The frequency of cells within the indicated gates is denoted. (C) Summary plot of pooled data showing the frequency of $MJ23^+$ T cells amongst $CD4^+$ T cells isolated from the blood or spleen of host mice of the indicated genotype at the indicated timepoint. (Left) Each thin line represents one mouse, while each symbol represents pooled mice. (* = P < 0.05, *** = P < 0.001, **** = P < 0.0001; 2-way ANOVA) (Right) Each symbol represents one mouse. Mean ± SEM is indicated. (**** = P < 0.0001; Welch's t test). (D) Summary plot of pooled data showing the number of $MJ23^+$ $CD4^+$ T cells isolated from the blood of host mice of the indicated genotype at the indicated timepoint. Each thin line represents one mouse, while each symbol represents pooled mice. Mean ± SEM is indicated. * = P < 0.05,

FIGURE 28, continued
**** = P < 0.0001; 2-way ANOVA. (E) Summary plot of pooled data showing the frequency of Foxp3$^+$ cells amongst MJ23$^+$ CD4$^+$ T cells isolated from the blood of host mice of the indicated genotype at the indicated timepoint. Each thin line represents one mouse, while each symbol represents pooled mice. Mean ± SEM is indicated. (* = P < 0.05; 2-way ANOVA).
(F) Experimental schematic for panels (G-J). LF MJ23 chimeric mice were generated in *C4^{WT}* male hosts using MJ23$^+$ *Rag1$^{-/-}$ Foxp3*-DTR$^+$ marrow. >6 weeks post-engraftment, mice were depleted of MJ23 Treg cells with via a single intraperitoneal injection of DT, or left untreated. 2 days following DT treatment, host mice were infected with 10^7 CFU *Lm[C4]*, and the fate of MJ23 T cells was assessed 14 days later in the spleen and prostate by flow cytometry. n = 10, no depletion; n = 9, MJ23 Treg depletion. Data represent two independent experiments. (G) Representative flow cytometric analysis of polyclonal CD4$^+$ T cells isolated from the spleen or prostate of LF chimeric mice depleted of MJ23 Treg cells or left untreated. Plots depict Foxp3 vs. CD45.1 expression by polyclonal CD4$^+$ T cells. The number of cells within the indicated gates is denoted. (H) Summary plot of pooled data showing the frequency of Foxp3$^+$ cells amongst MJ23$^+$ CD4$^+$ T cells isolated from the spleen of host mice depleted of MJ23 Treg cells or left untreated. Each symbol represents one mouse. Mean ± SEM is indicated. (*** = P < 0.001; Mann-Whitney test). (I) Summary plot of pooled data showing depicting the number of MJ23$^+$ Foxp3^{neg} Tconv cells isolated from the spleen vs. prostate of host mice depleted of MJ23 Treg cells or left untreated. Each symbol represents one mouse. The least squares linear regression line for each group is depicted. No depletion, Slope = 0.4990, R2 = 0.5054; MJ23 Treg depletion, Slope = 1.078, R2 = 0.9327. (**** = P < 0.0001; Extra sum-of-squares F test comparing the slopes). (J) Summary plot of pooled data showing the ratio of MJ23$^+$ Foxp3^{neg} Tconv cells isolated from the prostate normalized to the spleen of host mice depleted of MJ23 Treg cells or left untreated. Each symbol represents the ratio for one mouse. Mean ± SEM is indicated. (** = P < 0.01; Mann-Whitney test).

CCR2 is required for MJ23 Treg development but not positive selection in the thymus

The diminished ability for MJ23 Tconv cells to traffic out of the SLOs in the presence of MJ23 Treg cells could reflect a failure of the Tconv cells to differentiate into cell states permissive for egress and organ infiltration. Thus, MJ23 Treg competition may dually function to both prevent MJ23 Tconv cells from adopting long-lived effector states and expressing receptors or integrins required for motility. Alternatively, MJ23 Treg cells may impede MJ23 Tconv trafficing via a direct mechanism that parallels competition, such as the production of chemokines that attract and sequester MJ23 Tconv cells. In this regard, the chemokine receptor CCR2 was highly and ubiquitously expressed by both C4/I-A^b-specific Treg cells in the spleen 4 days after *Lm[C4]*

infection, and C4/I-A^b-specific Tconv cells that had been primed but lost proliferation potential (Cluster 5, enriched in *C4*^{WT} mice; Figure 23, H). We sought to investigate the role of CCR2 in Treg suppression and Tconv constraint following *Lm[C4]* using the MJ23 system. We first bred a *Ccr2*-deficient allele onto the MJ23 transgenic mouse line, then generated chimeras in *C4*^{WT} hosts using bone marrow from MJ23$^+$ *Ccr2*$^{-/-}$ donor mice and infected host mice with *Lm[C4]*. Unexpectedly, MJ23 Treg cells were completely absent in the periphery of these mice following infection but MJ23 Tconv cells were readily recovered (data not shown), suggesting that CCR2 may be uniquely required for the development or maintenance of MJ23 Treg cells at steady-state. While interesting, this result precluded studies testing the requirement for CCR2 on MJ23 Treg cells and Tconv cells during infection. Future studies will require the use of an inducible *Foxp3*$^{Cre\text{-}ERT2}$ x *Ccr2*-floxed system to remove CCR2 on MJ23 or polyclonal Treg cells only during *Lm[C4]* infection.

To identify the requirement for CCR2 in MJ23 Treg cells, we generated new chimeras in *C4*^{WT} hosts using a mixture of congenically-distinct bone marrow from MJ23$^+$ *Ccr2*$^{-/-}$ and MJ23$^+$ *Ccr2*$^{+/+}$ donor mice, and compared MJ23 T cells from these compartments in the thymus and periphery of host mice at steady-state. In the thymus, a fraction of CCR2-sufficient MJ23 thymocytes expressed Foxp3, but Foxp3 was undetectable in CCR2-deficient MJ23 cells (Figure 29, A-B), indicating that CCR2 expression is required for MJ23 Treg development in the thymus. Curiously, CCR2$^+$ MJ23 thymocytes uniformly expressed the CCR7 receptor that promotes transit to the thymic medulla and existed at the MHC-I$^+$ CD69$^+$ "M1" stage of thymocyte development [461], suggesting that CCR2 may function in this window to coordinate Treg development. In stark contrast, most CCR2-deficient MJ23 thymocytes lacked CCR7 expression yet existed at the MHC-I$^+$ CD69^{neg} "M2" late developmental stage (Figure 29, C-D), implying that these cells were ready

to egress from the thymus even though they had not entered the medulla where they would normally receive signals that direct Treg development of Aire-dependent specificities [462]. Accordingly, *Ccr2*$^{-/-}$ MJ23 Treg cells but not *Ccr2*$^{+/+}$ MJ23 Treg cells were absent from the periphery of chimeric mice (Figure 29, E-F). These data reveal that CCR2 is required for MJ23 Treg development in the thymus and acts in a cell-intrinsic manner. Curiously, a previous study investigating the role of CCR2 in Treg cells also described a cell-intrinsic role for CCR2 in polyclonal Treg cells [463]; though CCR2-deficiency did not prevent Treg development and such cells were readily found in the periphery. Instead, the authors demonstrate that CCR2 is required for optimal CD25 expression by Foxp3^{+} cells in the thymus and periphery. Together with our study of MJ23 Treg cells, these collective observations suggest that CCR2 may act to position developing thymocytes in proper Treg niches within the medulla where they receive signals to upregulate CD25. Some Treg specificities may still receive sufficient IL-2 and antigen signals without this niche (ie. the polyclonal *Ccr2*$^{-/-}$ Tregs), while others specificities such as those reactive to C4/I-A^{b} cannot overcome this deficit.

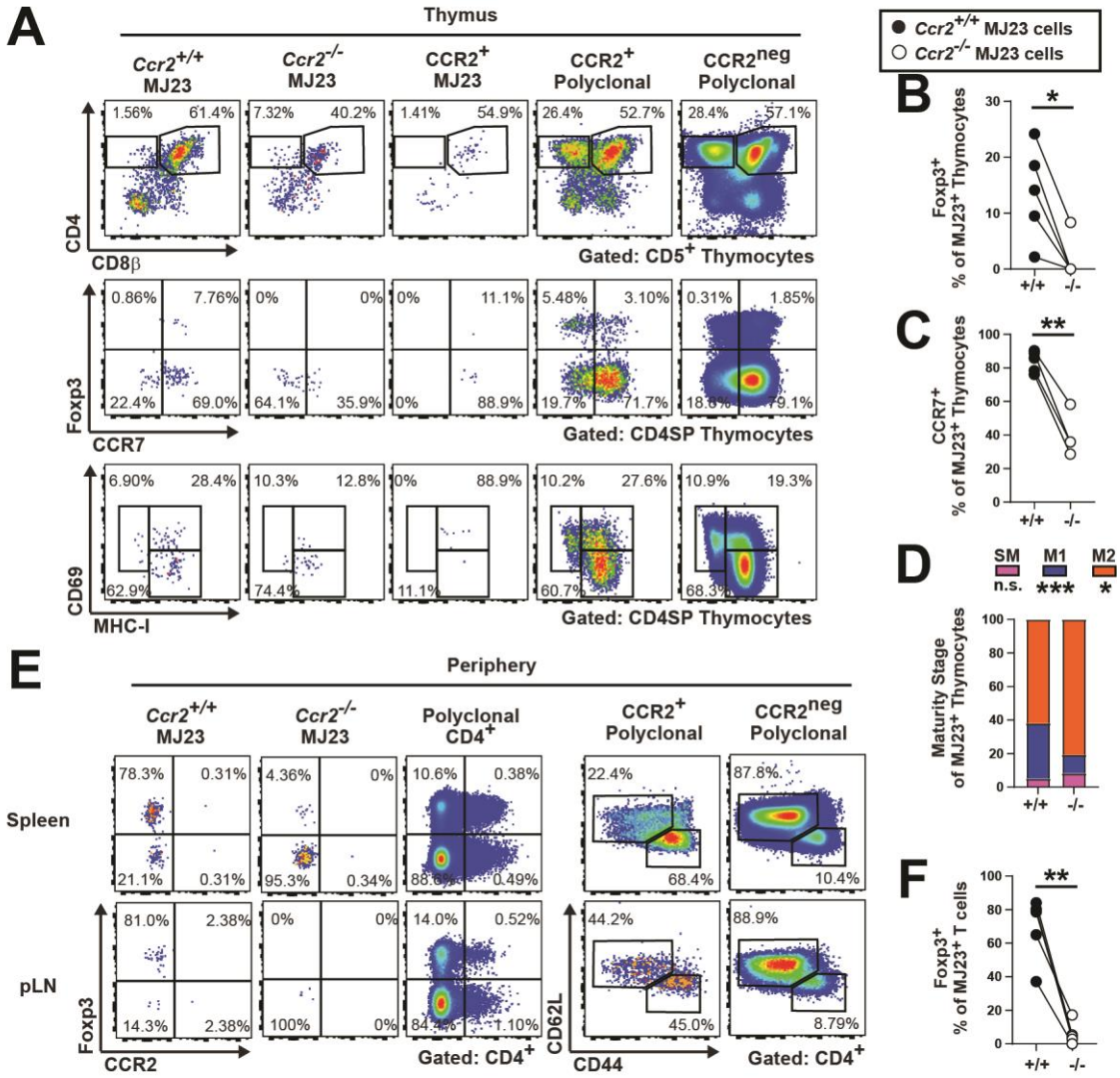

FIGURE 29. CCR2 is required for MJ23 Treg development but not positive selection in the thymus

Mixed LF MJ23 chimeric mice were generated in B6.SJL ($CD45^{.1/.1}$) male hosts using the following donor marrow: $MJ23^+$ *Ccr2*$^{-/-}$ $CD45^{.2/.2}$ and $MJ23^+$ *Ccr2*$^{+/+}$ $CD45^{.1/.2}$. Thus, all Mixed LF MJ23 chimeras contained congenically-disparate $MJ23^+$ T cells that were sufficient or deficient for CCR2. >6 weeks post-engraftment, the fate of MJ23 T cells were assessed in the thymus and spleen by flow cytometry. n = 5 mixed LF chimeras. Data represent one independent experiment. (A) Representative flow cytometric analysis of MJ23 donor$^+$ or polyclonal host$^+$ thymocytes isolated from the thymus of LF chimeric mice. Plots depict CD4 vs. CD8β expression by $CD5^+$ thymocytes (top), CCR7 vs. Foxp3 expression by CD4SP thymocytes (middle), and MHC-I vs. CD69 expression by CD4SP thymocytes (bottom). The frequency of cells within the indicated gates is denoted. (B) Summary plots of pooled data showing the frequency of $Foxp3^+$ cells amongst $MJ23^+$ *Ccr2*$^{+/+}$ or $MJ23^+$ *Ccr2*$^{-/-}$ CD4SP thymocytes enriched from the thymus of chimeric mice. Each symbol pair represents one mouse. (* = $P < 0.05$; two-tailed paired t test). (C) Summary plots of pooled data showing the frequency of $CCR7^+$ cells amongst $MJ23^+$ *Ccr2*$^{+/+}$ or $MJ23^+$ *Ccr2*$^{-/-}$ CD4SP thymocytes enriched from the

FIGURE 29, continued
thymus of chimeric mice. Each symbol pair represents one mouse. (** = $P < 0.01$; two-tailed paired t test). (D) Summary plots of pooled data showing the frequency of $MJ23^+$ *Ccr2*$^{+/+}$ or $MJ23^+$ *Ccr2*$^{-/-}$ CD4SP thymocytes found in the Semimature (SM, MHC-I^{neg}), Mature 1 (M1, MHC-I^+ $CD69^+$), and Mature 2 (M2, MHC-I^+ $CD69^{neg}$), enriched from the thymus of chimeric mice. Each bar segment represents the mean of each $MJ23^+$ compartment within mice. (* = $P < 0.05$, *** = $P < 0.001$; 2-way ANOVA). (E) Representative flow cytometric analysis of MJ23 $donor^+$ or polyclonal $host^+$ $CD4^+$ T cells isolated from the indicated organ of LF chimeric mice. Plots depict Foxp3 vs. CCR2 expression (left) and CD62L vs. CD44 expression (right) by $CD4^+$ T cells. The frequency of cells within the indicated gates is denoted. (F) Summary plots of pooled data showing the frequency of Foxp3+ cells amongst $MJ23^+$ *Ccr2*$^{+/+}$ or $MJ23^+$ *Ccr2*$^{-/-}$ $CD4^+$ T cells enriched from the thymus of chimeric mice. Each symbol pair represents one mouse. (** = $P < 0.01$; two-tailed paired t test).

Driver Tconv cells activated by Lm-derived antigen license prostate infiltration by endogenous Passenger T cells that display hallmarks of self-reactivity but are tolerant in the steady-state repertoire

C4/I-A^b-specific Tconv cells rapidly initiate T cell infiltration of the prostate following *Lm[C4]* infection when Treg cells of matched specificity are absent from the system, indicating that activated C4/I-A^b-specific Tconv cells are necessary for the development of autoimmune prostatitis in this setting. However, most T cells recovered from the prostatic lesion are not specific for C4/I-A^b and do not normally infiltrate the prostate when C4/I-A^b-specific Tconv cells are constrained during *Lm[C4]* infection (Figure 16, D) or fail to activate during *Lm[parent]* infection (Figure 15, F). Thus, C4/I-A^b-specific Tconv cells can be defined as autoimmune "Driver" T cell clones when *Lm[C4]* infection breaks tolerance, while prostate-infiltrating non-specific T cells operate as "Passenger" T cells that uniquely depend on the Driver specificity to enter the lesion. To gain deeper insight into the relationship between Passenger T cells and Driver T cells, we performed a series of experiments to characterize these populations, perturb their abundance, and modulate their interactions during infection.

We first sought to test whether the degree of Passenger T cell infiltration is related to the number of C4/I-A^b-specific Driver Tconv cells activated by *Lm[C4]* infection. We titrated increasing numbers of MJ23 Tconv cells from TCR transgenic mice into $C4^{WT}$ mice and measured prostate infiltration a week after infection (Figure 30, A). When mice received 100 MJ23 Tconv cells, these cells could be readily observed in the spleen but were rarely detected in the prostate (Figure 30, B-E), indicating that these cells are sufficiently constrained by endogenous C4/I-A^b-specific Treg cells and consistent with the notion that these Treg cells impede trafficking of C4/I-A^b-specific Tconv cells from the SLOs (Figure 28). Expectedly, mice that received 100 MJ23 Tconv cells had very few polyclonal $CD4^+$ T cells in the prostate (Figure 30, E) that did not exceed the number of cells in the prostate of uninfected $C4^{WT}$ mice (Figure 14, F) or mice that remained tolerant after *Lm[C4]* infection (Figure 16, F). In contrast, mice that received 1000 MJ23 Tconv cells presented with prostatic infiltration by both Driver MJ23 Tconv and Passenger polyclonal $CD4^+$ and $CD8^+$ T cells (Figure 30, E), indicating that antigen-specific Treg suppression can be overcome by increasing the number of MJ23 Tconv cells, and suggesting that this mechanisms of Treg suppression ultimately operates by conferring such cells with a numeric advantage over their Tconv counterparts. The degree of Passenger T cell infiltration further increased with 10^4 donor MJ23 Tconv cells but remained steady with 10^5 donor cells, indicating that Passenger T cell licensing is dependent on the number of Driver T cells, and suggesting that a limited number of T cells with the potential to become Passenger cells exist in the steady-state repertoire.

The finding that tolerance to the C4 peptide can be numerically overcome with antigen-specific Tconv cells suggests that any self-reactive T cell specificity has the potential to be a Driver clone, provided it has access to self-antigen. We therefore hypothesized that the F1/I-A^b-specific SP33 clone would function as a Driver clone following *Lm[F1]* infection. To test this, we

transferred SP33 Tconv cells into *C4*^{WT} mice and analyzed prostatic T cell infiltration following *Lm[F1]* challenge (Figure 30, F). We also used C4/I-A^b and LLO/I-A^b tetramers to determine whether these antigen-specific populations contributed to the Passenger T cell pool. Following infection with *Lm[F1]*, SP33 T cells robustly expanded, entered the prostate, and drove infiltration of Passenger polyclonal T cells (Figure 30, G-H). Importantly, *Lm[C4]* infection did not enable SP33 Tconv cells to become Drivers, indicating that antigen recognition in the context of infection was critical for this differentiation step. Of the Passenger T cells, a significant proportion were specific for LLO/I-A^b (Figure 30, G-H), suggesting that at least some Passenger cells infiltrate in an antigen-nonspecific manner, perhaps due to the upregulation of integrins or chemokine receptors following activation by the pathogen. However, a small but significant number of Passenger T cells were specific for C4/I-A^b and were mostly Treg cells (Figure 20, H-I), indicating that Passenger cells also consist of T cells that infiltrate in an antigen-dependent manner. This remarkable heterogeneity in the Passenger T cell compartment was globally captured by the phenotype of polyclonal CD4$^+$ T cells that did not bind tetramer, which consisted of PD-1$^+$ Tconv cells, PD-1^{neg} cells, and Treg cells (Figure 30, G and J), suggesting that cells within the lesion consist of both non-autoreactive clones and self-reactive clones that are licensed to evade tolerance mechanisms in the presence of a Driver specificity.

We next aimed to understand how the context of antigen presentation to Driver and Passenger T cells impacts the response and licensing of these populations. During the *Lm[F1]* infection, SP33 T cells were presumably activated alongside LLO/I-A^b specific T cells at a site distal to the prostate, while C4/I-A^b-specific T cells could only sense self-derived antigen in the prostate-draining LN. While both LLO/I-A^b-specific and C4/I-A^b-specific cells became Passenger T cells in this context, the degree of T cell infiltration of the prostate differed, suggesting that the

context of antigen recognition may be important for Passenger licensing. To force concurrent antigen presentation to SP33 Driver and C4/I-A^b Passenger T cells on the same APC, we created a *Lm* strain that expressed covalently linked C4 and F1 peptides that could not be decoupled (termed "*Lm[C4+F1]*"). This enabled us to compare the C4/I-A^b Passenger T cell response when activation occurred on the same APC (*Lm[C4+F1]*) or at different anatomical sites (*Lm[F1]*). When SP33 recipient mice were infected with *Lm[C4+F1]*, the number of C4/I-A^b-specific Passenger T cells that infiltrated the prostate markedly increased compared with those following *Lm[F1]* (Figure 30, G-H). Furthermore, the number of SP33 Driver T cells that infiltrated the prostate also increased, implying the existence of a bidirectional positive-feedback loop between these specificities that either promotes greater T cell expansion or enables a higher degree of licensing. Notably, although their absolute number increased, C4/I-A^b Passenger T cells were still mostly Treg cells (Figure 30, I), suggesting that SP33 Driver T cells do not enable C4/I-A^b-specific Tconv cells to escape Treg-mediated control, but instead increase the number of antigen-specific cells in both T cell compartments. Curiously, the number of LLO/I-A^b-specific cells or polyclonal $CD4^+$ T cells in the prostate was not different between *Lm[F1]* and *Lm[C4+F1]* infection (Figure 30, H), although the proportion of polyclonal Tconv cells and PD-1^{neg} Tconv cells increased in the latter condition (Figure 30, I-J), which could imply that Passenger T cell licensing is permissive to a greater number of non-specific T cell clones when C4/I-A^b and F1/I-A^b-specific cells are activated in tandem. Finally, $C4^{WT}$ mice that did not receive donor cells were completely protected from prostate infiltration following *Lm[C4+F1]* infection (Figure 30, H), underscoring the fact that tolerance to one antigen must be independently breached to create a Driver T cell specificity and elicit a response from Passenger T cells.

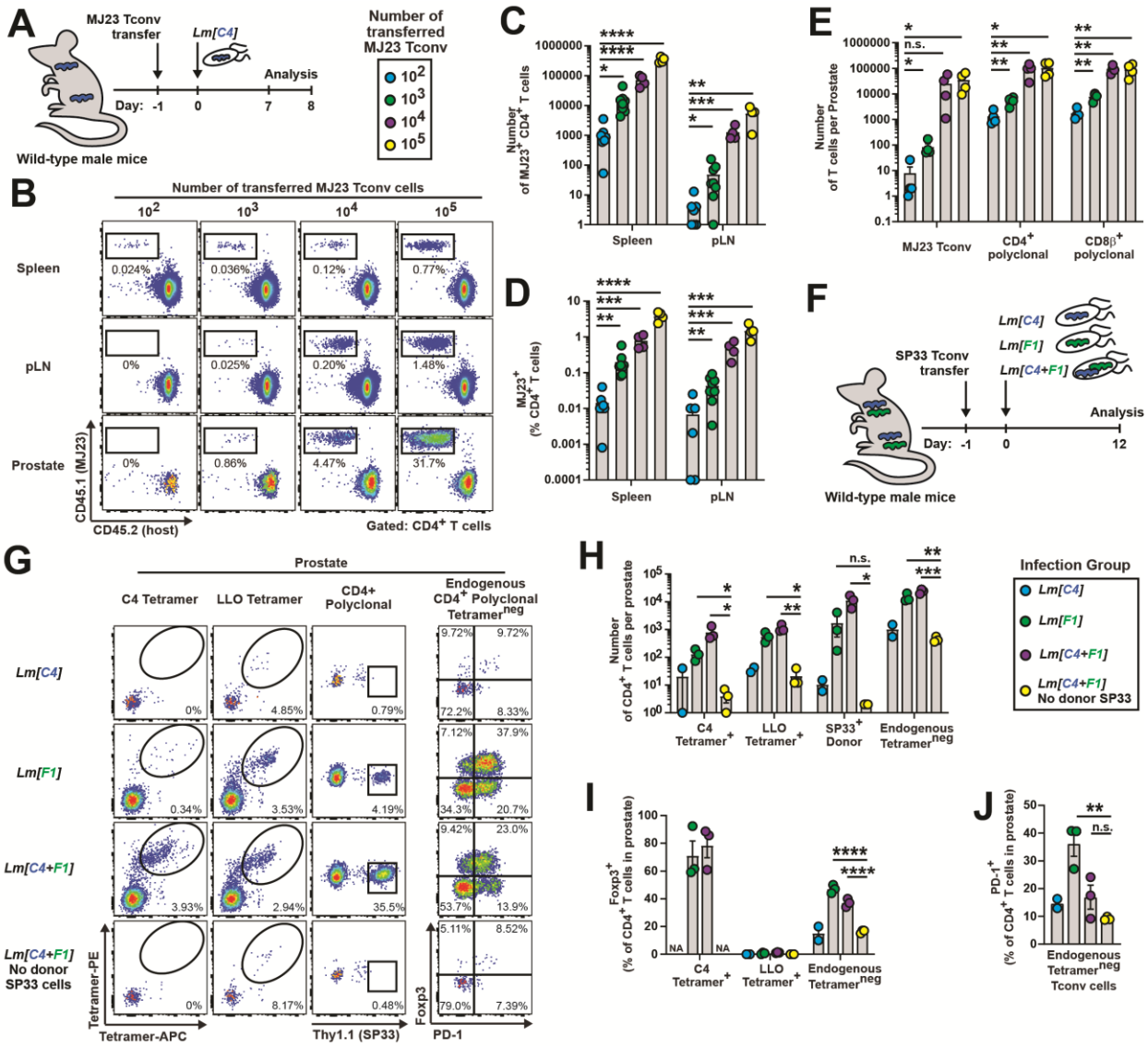

FIGURE 30. Driver Tconv cells activated by *Lm*-derived antigen license prostate infiltration by endogenous Passenger T cells that display hallmarks of self-reactivity but are tolerant in the steady-state repertoire.

(A) Experimental schematic for panels (B-E). Wild-type male hosts received the indicated number of donor naive MJ23 Tconv cells, and were challenged 1 day later with 10^7 CFU *Lm[C4]*. 7-8 days post-infection, the fate of MJ23 T cells and endogenous T cells were assessed in the indicated organ by flow cytometry. n = 4-7, 10^2; n = 4-7, 10^3; n = 4, 10^4; n = 4, 10^5. Data represent 2-3 independent experiments. (B) Representative flow cytometric analysis of polyclonal $CD4^+$ T cells isolated from the indicated organ of host mice. Plots depict CD45.1 (MJ23) vs. CD45.2 (host) polyclonal $CD4^+$ T cells. The frequency of cells within the indicated gates is denoted. (C) Summary plot of pooled data showing the number of $MJ23^+$ T cells isolated from the indicated organ of host mice. Each symbol represents one mouse. Mean ± SEM is indicated. (* = P < 0.05, ** = P < 0.01, *** = P < 0.001, **** = P < 0.0001; Welch's t test). (D) Summary plot of pooled data showing the frequency of MJ23+ CD4+ Tconv cells amongst $CD4^+$ T cells isolated from the indicated organ of host mice. Each symbol represents one mouse. Mean

FIGURE 30, continued
± SEM is indicated. (** = P < 0.01, *** = P < 0.001, **** = P < 0.0001; Welch's t test). (E) Summary plot of pooled data showing the number of MJ23$^+$ or polyclonal T cells isolated from the prostate of host mice. Each symbol represents one mouse. Mean ± SEM is indicated. (* = P < 0.05, ** = P < 0.01; Welch's t test). (F) Experimental schematic for panels (G-J). Wild-type male mice received 10^5 SP33 Tconv donor cells or no cells, and were infected 1 day later with the indicated strain of *Lm*. 12 days post-infection, the fate of donor SP33 T cells, endogenous C4/I-A^b or LLO/I-A^b Tetramer$^+$ T cells, and endogenous CD4$^+$ T cells were assessed in the prostate by flow cytometry. n = 2, *Lm[C4]*; n = 3, *Lm[F1]*; n = 3, *Lm[C4+F1]*; n = 3, *Lm[C4+F1]* with no donor SP33. Data represent one experiment. (G) Representative flow cytometric analysis of polyclonal CD4$^+$ T cells isolated from the indicated organ of host mice. Plots depict C4 or LLO Tetramer expression by polyclonal CD4$^+$ T cells (left), Thy1.1 expression to denote donor SP33 T cells (middle), and PD-1 vs. Foxp3 expression by endogenous Tetramer^{neg} polyclonal CD4$^+$ T cells. The frequency of cells within the indicated gates is denoted. (H) Summary plot of pooled data showing the number of C4/I-A^b Tetramer$^+$, LLO/I-A^b Tetramer$^+$, SP33$^+$, or endogenous Tetramer^{neg} polyclonal CD4$^+$ T cells isolated from the prostate of host mice infected with the indicated *Lm* strain. Each symbol represents one mouse. Mean ± SEM is indicated. (* = P < 0.05, ** = P < 0.01, *** = P < 0.001; Welch's t test). (I) Summary plot of pooled data showing the frequency of Foxp3$^+$ cells amongst C4/I-A^b Tetramer$^+$, LLO/I-A^b Tetramer$^+$, SP33$^+$, or endogenous Tetramer^{neg} polyclonal CD4$^+$ T cells isolated from the prostate of host mice infected with the indicated *Lm* strain. Each symbol represents one mouse. Mean ± SEM is indicated. (**** = P < 0.0001; Welch's t test). (J) Summary plot of pooled data showing the frequency of PD-1$^+$ cells amongst endogenous Tetramer^{neg} polyclonal CD4$^+$ Tconv cells isolated from the prostate of host mice infected with the indicated *Lm* strain. Each symbol represents one mouse. Mean ± SEM is indicated. (** = P < 0.01; Welch's t test).

Absence of C4/I-A^b-specific Treg cells in C4$^{\Delta TEC}$ mice enables a Tconv-dominated response to F1/I-A^b following Lm[C4+F1] infection

Increasing the number of self-specific C4/I-A^b or F1/I-A^b Tconv cells enabled their escape from endogenous antigen-specific Treg control following *Lm* infection and endowed such cells with the ability to orchestrate prostatic infiltration of other polyclonal T cells (Figure 30). Furthermore, Driver F1/I-A^b-specific Tconv cells enhanced prostatic infiltration by C4/I-A^b-specific cells when antigen presentation was linked, yet the C4/I-A^b-specific response remained Treg-dominated, suggesting that the addition of Driver F1/I-A^b-specific T cells alone does not break tolerance to C4/I-A^b. Since removal of C4/I-A^b-specific Treg cells also allows those Tconv

cells to assume a Driver specificity role (Figure 16), it remained possible that removing Treg cells of one specificity could break tolerance to the other specificity when the antigens are concurrently presented.

To address this, we infected *C4*^{WT} and *C4*$^{\Delta TEC}$ mice with *Lm[C4+F1]*, and analyzed the responses of T cells reactive to C4/I-A^b and F1/I-A^b over time (Figure 31, A). In this way, the response to F1/I-A^b could be compared in the presence and absence of C4/I-A^b-specific Treg cells. We also measured the response to LLO/I-A^b as a control, since C4/I-A^b-specific Treg cells do not impact the response to this nonself pMHC (Figure 16). Following infection of *C4*^{WT} mice with *Lm[C4+F1]*, C4/I-A^b- and F1/I-A^b-specific Treg and Tconv cells briefly expanded in the spleen (Figure 31, B-D), but the Tconv responses were ultimately controlled and the mice did not exhibit T cell infiltration of the prostate (Figure 31, E-I). In *C4*$^{\Delta TEC}$ mice, C4/I-A^b-specific Tconv cells accumulated in the spleen (Figure 31, D) and infiltrated the prostate (Figure 31, G), as expected. Surprisingly, F1/I-A^b-specific Tconv cells also expanded and contributed to the prostate infiltrate in *C4*$^{\Delta TEC}$ mice (Figure 31, C-D and H), despite the lack of a response from these cells in *C4*$^{\Delta TEC}$ mice following *Lm[F1]* infection without the linked C4 peptide (Figure 19). Furthermore, *Lm[C4+F1]* infection did not alter the response from LLO/I-A^b-specific T cells between *C4*^{WT} and *C4*$^{\Delta TEC}$ mice (Figure 31, B-C). These results suggest that the absence of C4/I-A^b-specific Treg cells enables escape by F1/I-A^b specific Tconv cells when the specificities are concurrently activated, implying that antigen-specific Treg control may extend to self-reactive T cells of related specificities in certain contexts. Escape of F1/I-A^b-specific Tconv cells is unlikely to result from the emergence of C4/I-A^b-specific Driver Tconv cells, given that the addition of F1/I-A^b Driver cells alone did not alter the Treg/Tconv ratio of C4/I-A^b specific cells previously (Figure 30, I).

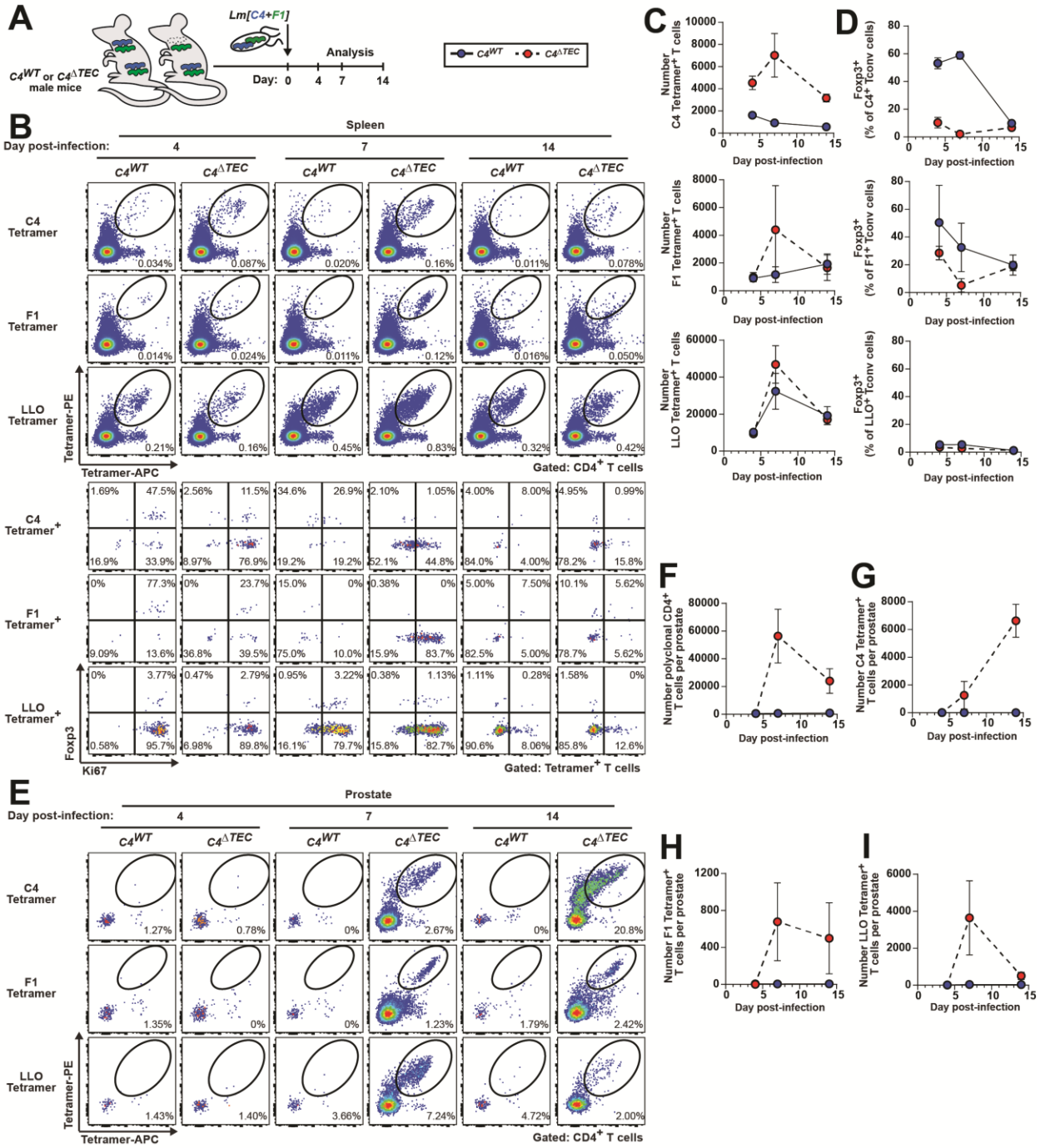

FIGURE 31. Absence of C4/I-A^b-specific Treg cells in *C4$^{\Delta TEC}$* mice enables a Tconv-dominated response to F1/I-A^b following *Lm[C4+F1]* infection

(A) Experimental schematic. *C4^{WT}* and *C4$^{\Delta TEC}$* mice were challenged intravenously with 10^7 CFU *Lm[C4+F1]*. Recall that F1/I-A^b-specific T cells remain tolerant in *C4$^{\Delta TEC}$* (Figure 19). On the indicated day post-infection, T cells were isolated from the indicated organ, labelled with C4/I-A^b, F1/I-A^b, or LLO/I-A^b tetramers, and analyzed by flow cytometry. Data are representative of 1 experiment. n = 2 mice in each genotype at each timepoint. Stats were not included due to insufficient group sizes. In all summary plots, each symbol represents the mean

FIGURE 31, continued
± SEM of pooled mice. **(**B) Representative flow cytometric analysis of $CD4^+$ T cells isolated from the spleen of mice of the indicated genotype on the indicated day post-infection. Plots depict C4/I-A^b, F1/I-A^b, or LLO/I-A^b tetramer-APC vs -PE expression by polyclonal $CD4^+$ T cells, and Ki67 vs Foxp3 expression by C4/I-A^b, F1/I-A^b, or LLO/I-A^b $tetramer^+$ T cells. The frequency of cells within the indicated gates are denoted. (C) Summary plots of pooled data showing the number of dual C4/I-A^b $tetramer^+$ (top), F1/I-A^b $tetramer^+$ (middle), and LLO/I-A^b $tetramer^+$ (bottom) $CD4^+$ T cells recovered from the spleens of mice of the indicated genotype and day post-infection. (D) Summary plots of pooled data showing the frequency of C4/I-A^b $tetramer^+$ (top), F1/I-A^b $tetramer^+$ (middle), and LLO/I-A^b $tetramer^+$ (bottom) $CD4^+$ T cells expressing Ki67 in the spleen of the indicated genotype and day post-infection. (E) Representative flow cytometric analysis of $CD4^+$ T cells isolated from the prostate of mice of the indicated genotype on the indicated day post-infection. Plots depict C4/I-A^b, F1/I-A^b, or LLO/I-A^b tetramer-APC vs -PE expression by polyclonal $CD4^+$ T cells, and Ki67 vs Foxp3 expression by C4/I-A^b, F1/I-A^b, or LLO/I-A^b $tetramer^+$ T cells. The frequency of cells within the indicated gates are denoted. (F-I) Summary plots of pooled data showing the number of polyclonal $CD4^+$ T cells (F), dual C4/I-A^b $tetramer^+$ (G), F1/I-A^b $tetramer^+$ (H), and 2W/I-A^b $tetramer^+$ (I) $CD4^+$ T cells recovered from the prostates of mice of the indicated genotype and day post-infection.

Thymic selection on C4/I-A^b does not impact the T cell responses against the Lm-derived 2W or OVA peptide antigens when covalently linked to the C4 peptide

The finding that C4/I-A^b-specific Treg cells may impact the F1/I-A^b-specific T cell response but do not alter the LLO/I-A^b-specific response prompted an effort to explore what is happening at the T cell:APC interface within individual micro clusters of responding cells. Conceptually, it could be that C4/I-A^b- F1/I-A^b- and LLO/I-A^b-specific cells are all activated within the same microdomain, and the C4/I-A^b-specific Treg cells can outcompete C4/I-A^b- and F1/I-A^b-reactive Tconv cells but not LLO/I-A^b-specific Tconv cells owing to a higher activation barrier in the Tconv cells that developed in the presence of self-agonist peptide prior to infection. A second possibility is that directly linking the C4 and F1 peptides in *Lm* promoted the co-localization of these T cell specificities in a way that does not occur when the C4 and LLO peptides are derived from different proteins. It could also be that an unexplored interaction occurs between

C4/I-A^b- and F1/I-A^b-specific following their arrival at the pLN, given that the peptides remain coupled at this site as they derive from the same self-protein. We therefore developed a set of tools to address these and other possibilities.

We first attempted to identify canonical LLO/I-A^b-specific T cell clones that could be expressed using our retrogenic system to track the response of such cells in imaging studies. We infected mice expressing a fixed TCRβ chain utilized by MJ23 and SP33 T cells with *Lm[parent]* to sort LLO/I-A^b tetramer$^+$ cells at the peak of the response (Figure 32, A). Unexpectedly, LLO/I-A^b-specific cells were completely absent from the spleen of mice expressing this TCRβ chain (Figure 32, B), suggesting that the TCRβ chain is critical for LLO/I-A^b recognition. Therefore, while fixed TCRβ mice are populated by a diverse repertoire, holes in the repertoire likely exist for some antigen specifies. To circumvent this, we created two novel strains of *Lm* with foreign peptides linked to C4, termed "*Lm[C4+2W]*" and "*Lm[C4+OVAp]*". These strains enabled us to track pathogen-reactive Tconv cells in the presence and absence of C4/I-A^b-specific Treg cells using both polyclonal 2W/I-A^b tetramer$^+$ Tconv cells and monoclonal OT-II$^+$ Tconv cells specific for the pathogen-derived peptide when it is covalently linked to the C4 peptide (Figure 32, C and H).

First, we infected $C4^{WT}$ and $C4^{\Delta TEC}$ mice with *Lm[C4+2W]* and measured T cell responses against C4/I-A^b and 2W/I-A^b at days 7 and 14 post-infection. We observed no difference in the magnitude or Ki67 status of 2W/I-A^b-specific Tconv cells in the spleen at either day (Figure 32, D-F), demonstrating that C4/I-A^b-specific Treg cells do not constrain pathogen-specific Tconv cell responses even when antigen presentation is spatially coupled, and further supporting a model in which C4/I-A^b-specific Treg cells constrain Tconv cells of matched specificity primarily by competition for C4/I-A^b antigen (Figure 27). $C4^{\Delta TEC}$ mice infected with *Lm[C4+2W]* developed

prostatic infiltration by C4/I-A^b-specific, 2W/I-A^b-specific, and polyclonal Passenger T cells as expected (Figure 32, G). Interestingly, the degree of C4/I-A^b-specific Tconv expansion and prostatic infiltration following *Lm[C4+2W]* infection (Figure 32, E and G) was markedly less than that observed in $C4^{\Delta TEC}$ mice infected with *Lm[C4]* (Figure 16, C-D and J). While this stark difference might be explained if the expression and presentation of the C4 antigen is significantly lower in the *Lm[C4+2W]* strain than the *Lm[C4]* strain, it's also possible that linking the peptides forces competition between C4/I-A^b-specific and 2W/I-A^b-specific T cells within each microdomain, which could be tested by measuring the magnitude of the C4/I-A^b or 2W/I-A^b-specific response when Tconv cells of the opposite specificity are titrated into the system (similar to Figure 30, A). A decrease in the 2W/I-A^b response with increasing MJ23 Tconv cells would strongly imply a fundamental role for heterologous immune responses and antigen dominance hierarchies in coordinating antigen-specific Treg suppression, and would provide a critical clue for understanding how the decision to respond or constrain is conferred within each antigen-relevant microdomain (see *Conclusions and Discussion*).

The magnitude of the endogenous T cell responses against two pathogen-derived peptides – LLO (Figure 16) and 2W (Figure 32, D-G) – were not impacted by the presence of C4/I-A^b-specific Treg cells, but it remained possible that such Treg cells were altering the clonal composition of the pathogen-reactive T cell pools such that hyper-expansion of some clones was able to compensate for the constraint of others. To remove clonal variability and complement our findings for endogenous pathogen-specific T cells, we employed an experiment using monoclonal self-specific and pathogen-specific $CD4^+$ T cells (Figure 32, H). We created low-frequency MJ23 chimeras in $C4^{WT}$ and $C4^{\Delta TEC}$ mice, seeded these hosts with congenically-distinct donor OT-II transgenic Tconv cells, and infected the mice with *Lm[C4+OVAp]*. In this way, the pathogen-

specific OT-II Tconv response and self-specific MJ23 Tconv response could be measured in the presence and absence of MJ23 Treg cells when the peptides were covalently linked. At day 6 post-infection, far fewer C4/I-A^b-specific MJ23 Tconv cells were elicited in $C4^{WT}$ when compared to $C4^{\Delta TEC}$ mice as expected and previously observed (Figure 24, D), but the number of OT-II Tconv cells elicited in the two settings was comparable (Figure 32, I-J). Taken together, these studies of endogenous polyclonal and monoclonal Treg and Tconv cells reactive to linked peptide antigens strongly suggest that Treg cells primarily constrain Tconv cells of matched specificity at the level of the pMHC-II complex and not via modulation of the APCs or local microenvironment. Notably, the monoclonal system established for this series of experiments (Figure 32, H) enables spatial analysis of self-specific and pathogen-specific T cells using confocal immunofluorescence imaging to understand how C4/I-A^b-specific Treg cells coordinate these divergent outcomes (data in progress).

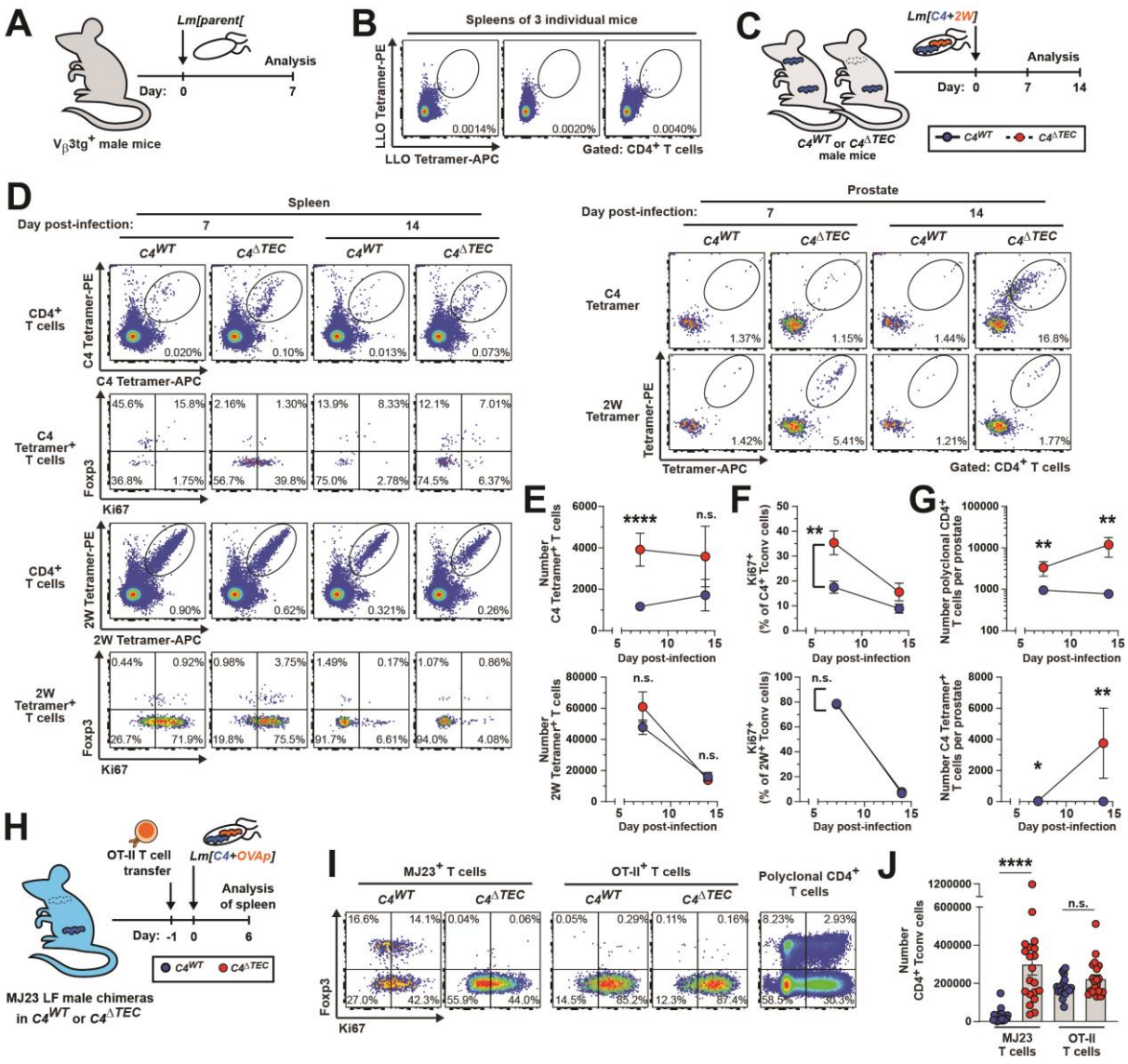

FIGURE 32. Thymic selection on C4/I-A^b does not impact the T cell responses against the *Lm*-derived 2W or OVA peptide antigens when covalently linked to the C4 peptide

(A) Experimental schematic for panel (B). To identify endogenous *Lm*-reactive T cell clones specific for LLO/I-A^b, Vβ3tg$^+$ mice expressing the MJ23-derived Vβ chain on all T cells were challenged with 10^7 CFU *Lm[parent]*. 7 days post-infection, CD4$^+$ T cells were enriched from the spleens, labelled with LLO/I-A^b tetramers, and analyzed by flow cytometry. Data represent 3 mice in one experiment. (B) Flow cytometric analysis of CD4$^+$ T cells isolated from the prostates of mice of the indicated genotype on the indicated day post-infection. Plots depict LLO/I-A^b tetramer-APC vs -PE expression by polyclonal CD4$^+$ T cells. The frequency of cells within the indicated gates are denoted. (C) Experimental schematic for (D-G). *C4^{WT}* and *C4$^{\Delta TEC}$* mice were challenged intravenously with 10^7 CFU *Lm[C4+2W]*. On the indicated day post-infection, T cells were isolated from the indicated organ, labelled with C4/I-A^b or 2W/I-A^b tetramers, and analyzed by flow cytometry. Data are representative of 3 experiments. n = 9, *C4^{WT}* d7; n = 9, *C4$^{\Delta TEC}$* d7; n = 6, *C4^{WT}* d14; n = 9, *C4$^{\Delta TEC}$* d14. (D) Representative flow

FIGURE 32, continued
cytometric analysis of $CD4^+$ T cells isolated from the spleens (left) or prostates (right) of mice of the indicated genotype on the indicated day post-infection. Plots depict C4/I-A^b or 2W/I-A^b tetramer-APC vs -PE expression by polyclonal $CD4^+$ T cells, and Ki67 vs Foxp3 expression by C4/I-A^b or 2W/I-A^b $tetramer^+$ T cells. The frequency of cells within the indicated gates are denoted. (E) Summary plots of data pooled from (D) showing the number of dual C4/I-A^b $tetramer^+$ (top) and 2W/I-A^b $tetramer^+$ (bottom) $CD4^+$ T cells recovered from the spleens of mice of the indicated genotype and day post-infection. Each symbol represents the mean ± SEM of pooled mice. (**** = $P < 0.0001$; n.s. = $P > 0.05$; two-tailed non-parametric Mann-Whitney test). (E) Summary plots of data pooled from (D) showing the number of dual C4/I-A^b $tetramer^+$ (top) and 2W/I-A^b $tetramer^+$ (bottom) $CD4^+$ T cells recovered from the spleens of mice of the indicated genotype and day post-infection. Each symbol represents the mean ± SEM of pooled mice. (**** = $P < 0.0001$; n.s. = $P > 0.05$; two-tailed non-parametric Mann-Whitney test). (F) Summary plots of data pooled from (D) showing the frequency of dual C4/I-A^b $tetramer^+$ (top) or 2W/I-A^b $tetramer^+$ (bottom) $CD4^+$ Tconv cells expressing Ki67 in the spleens of mice of the indicated genotype and day post-infection. Each symbol represents the mean ± SEM of all mice.(** = $P < 0.01$; ordinary 2-way ANOVA). (G) Summary plots of data pooled from (D) showing the number of polyclonal $CD4^+$ T cells (top) and dual C4/I-A^b $tetramer^+$ $CD4^+$ T cells (bottom) recovered from the prostates of mice of the indicated genotype and day post-infection. Each symbol represents the mean ± SEM of pooled mice. (* = $P < 0.05$; * = $P < 0.01$; n.s. = $P > 0.05$; two-tailed non-parametric Mann-Whitney test). (H) Experimental schematic for (I-J). Low-frequency MJ23 chimeras were established in $C4^{WT}$ and $C4^{\Delta TEC}$ male mice. >6 weeks post-reconstitution, mice received 10^4 OT-II $CD4^+$ T cells from transgenic donor mice, and were challenged intravenously 1 day post-transfer with 10^7 CFU *Lm[C4+OVAp]*. 6 days post-infection, T cells were isolated from the indicated spleen, labelled and analyzed by flow cytometry. Data are representative of 3 experiments. n = 21, $C4^{WT}$; n = 20, $C4^{\Delta TEC}$. (I) Representative flow cytometric analysis of $CD4^+$ T cells isolated from the spleens of mice of the indicated genotype. Plots depict Ki67 vs Foxp3 expression by MJ23tg^+, OT-IItg^+, or polyclonal $CD4^+$ T cells. The frequency of cells within the indicated gates are denoted. (J) Summary plot of data pooled from (I) showing the number of MJ23tg^+ and OT-IItg^+ T cells recovered from the spleens of mice of the indicated genotype. Each symbol represents one mouse. The mean ± SEM is indicated (**** = $P = 0.0001$; n.s. = $P > 0.05$; Welch's t test).

Production of anti-C4/I-A^b antibody clones and V5-epitope tagged Lm strains to identify APCs that present the C4 peptide

Our studies have extensively described the impact of self-specific Treg cells on Tconv cells of shared specificity and Tconv cells reactive to other non-self peptides by measuring T cell responses in various settings, including their phenotype, positioning, trafficking, and anatomical location. While these metrics have been pivotal for elucidating the contexts and mechanisms of

antigen-specific Treg suppression, a black box persists around the priming events and relevant antigen-presenting cells that coordinate this process. Crucially, it remains outstanding whether antigen-responsive Treg cells alter the maturation and costimulatory potential of APCs presenting self-derived and pathogen-derived peptide, as has been suggested in other systems as a mechanism of Treg suppression [256,464-466], or whether these populations are the same or distinct.

To identify the APCs that present *Lm*-derived peptides during infection, we created a set of *Lm* strains engineered to express the C4 peptide covalently linked to an identifiable V5 epitope tag (Figure 12, B), with the goal of identifying cells presenting the C4/I-Ab complex using an anti-V5 tag antibody (Figure 33, A). To globally identify APCs that present the C4/I-A^b complex, we raised a set of antibodies against the pMHC complex. We immunized Balb/c mice, which lack the I-A^b haplotype, with C4/I-A^b monomer using an increasing antigen dose regimen and created hybridoma clones using splenic B cells enriched for C4/I-A^b tetramer binding (Figure 33, B and *Methods*). By ELISA assay, we identified 48 of 480 total hybridoma clones whose supernatants specifically bound C4/I-A^b but not control CLIP/I-A^b monomer (Figure 33, C). We also raised hybridomas specific for the I-A^b molecule and non-specific clones. We proceeded to expand and purify αC4/I-A^b antibodies from 3 of the hybridoma lines, all of which selectively inhibited the activation of MJ23 Tconv but not control OT-II Tconv cells in *in vitro* proliferation experiments (Figure 33, D-F). Finally, fluorophore-conjugated αC4/I-A^b clones faithfully detected C4/I-A^b complex on the surface of peptide-pulsed splenic DCs by flow cytometry (Figure 33, G). Additionally, aV5-epitope antibodies robustly identified C4-V5 pulsed DCs but not those pulsed with V5 or C4 peptide alone (Figure 33, G), indicating that the "peptide overhang" strategy may be viable for detecting such cells following infection (Figure 33, A).

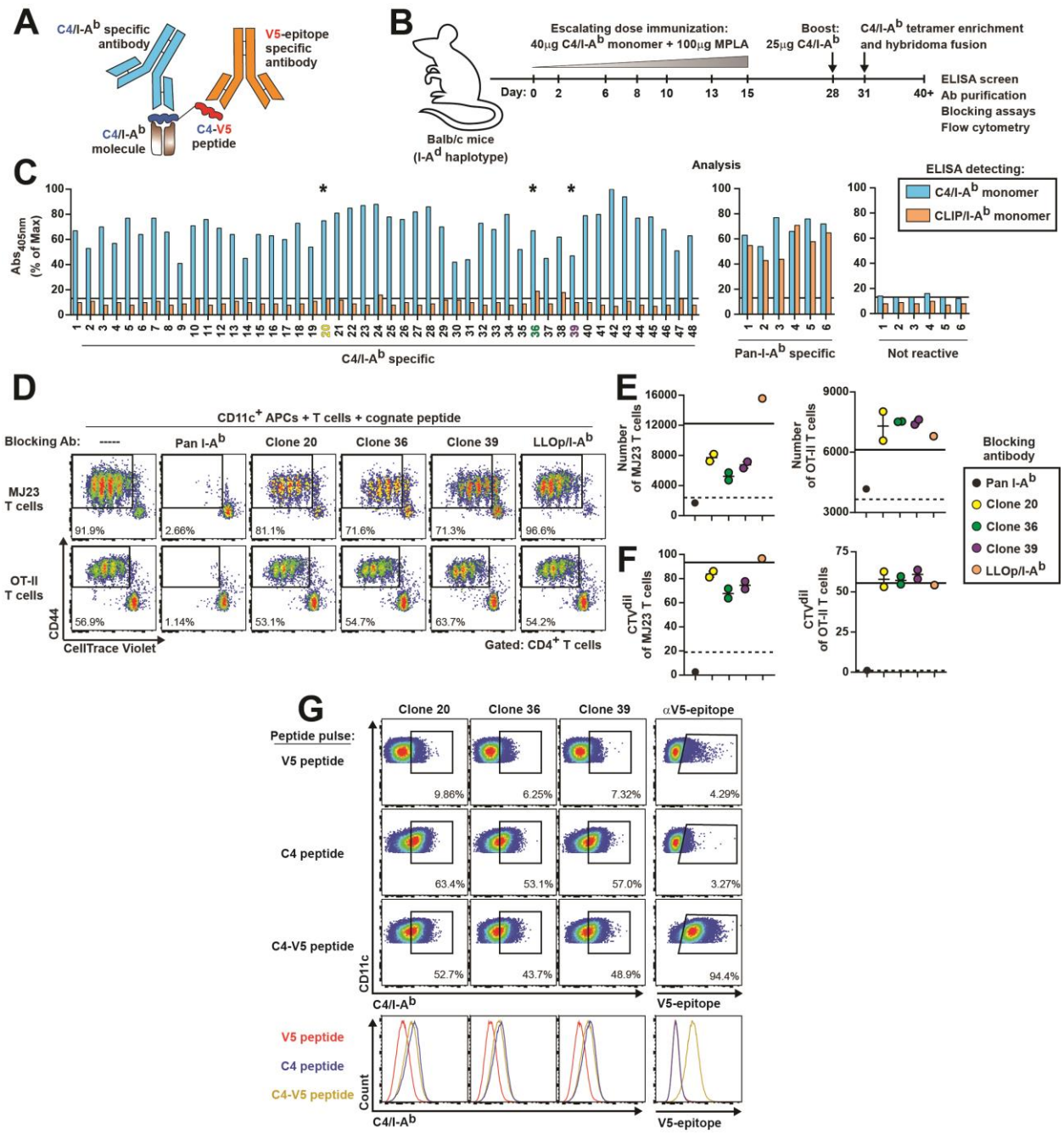

FIGURE 33. Production of anti-C4/I-A^b antibody clones and V5-epitope tagged *Lm* strains to identify APCs that present C4 peptide

(A) Experimental objective. Endogenous APCs presenting the C4/I-A^b antigen might be directly identified using an antibody raised to specifically bind to the C4 peptide complexed with the I-A^b molecule. Alternatively, expression of the C4 peptide may be engineered in tandem with a covalently-linked V5 epitope tag, and C4/I-A^b-presenting APCs might be indirectly identified using commercially-available anti-V5 antibody clones. (B) Experimental schematic used to raise anti-C4/I-A^b antibody clones. Balb/c mice, which lack the I-A^b molecule, were immunized subcutaneously with an escalating dose regiment of C4/I-A^b monomer with the adjuvant MPLA.

FIGURE 33, continued
Following primary immunization schedule, mice were boosted intravenously with C4/I-A^b monomer. 3 days post-boost, C4/I-A^b tetramer-binding B cells were magnetically enriched from the spleens of immunized mice and fused with SP2/0-Ag14 myeloma cells to create hybridomas (see methods), which were subsequently screened for antigen specificity. In total, 480 hybridoma clones were generated and screened. (C) ELISA results of select hybridoma clones. Plates were coated with C4/I-A^b monomer or CLIP/I-A^b monomer and incubated with supernatants from the hybridoma clones. HRP-conjugated anti-mouse IgG was used as the detection antibody. Solid lines indicate the average absorbance values for wells that contained media alone. 48 total C4/I-A^b-specific candidate clones were detected by ELISA. Select I-A^b-specific and non-I-A^b-specific clones are also depicted. * indicates clones selected for colony expansion and antibody purification, based on preliminary in vitro blocking results (data not shown). (D-F) In vitro proliferation and blocking assays. CTV-labeled C4/I-A^b-specific MJ23 T cells (top) or OVAp/I-A^b-specific OT-II T cells (bottom) were incubated with splenic APCs, 1-2nM of respective peptide, and 10μg/ml of purified antibody as indicated. 3 days later, CTV dilution and CD44 upregulation were analyzed by flow cytometry. (D) Representative flow cytometric analysis of MJ23 and OT-II $CD4^+$ T cells. Plots depict CTV vs CD44 expression by the indicated monoclonal T cells. The Pan I-Ab antibody is a commercially-available anti-I-A^b clone derived from the Balb/c strain, while the LLOp/I-A^b clone was raised in a similar manner to (B) and gifted from the Jenkins/Fife laboratories [341]. (E-F) Summary plots of data from (D) depicting the absolute number (E) or frequency of CTV-diluted cells (F) recovered from MJ23 (left) or OT-II (right) T cell cultures. Each symbol depicts one replicate well. The solid lines depict cells recovered from samples that were not incubated with antibody, while the dotted lines depict cells recovered from clutures that did not recieve peptide.
(G) Detection of C4 peptide-pulsed APCs by flow cytometry. Splenic APCs isolaed from B6 mice were pulsed with recombinant C4 peptide, V5 peptide, or covanently-linked C4-V5 peptide and stained with the indicated AF647-conjugated anti-C4/I-A^b or PE-conjugated anti-V5-epitope antibodies and analyzed by flow cytometry. Plots and histograms depict antibody staining of $CD11c^+$ cells following in vitro peptide pulse. Recombinant strains of *Lm* were engineered to express linked C4-V5 peptides for future studies (see Figure 12 and *Lm* strain table).

Tolerance to the C4/I-A^b antigen is instructed independent of B cells or B cell antigen specificity

Both DCs and B cells act as canonical APCs that express MHC-II and can present antigen to $CD4^+$ T cells. DCs are professional APCs known to present a broad array of extracellular and intracellular antigen at steady-state and prime T cell responses upon immune challenge, while B cells are primarily thought to present specific antigens that react with the BCR to evoke $CD4^+$ T cell help during a germinal center reaction [467]. However, it has been suggested that B cells can

present self-antigens to $CD4^+$ T cells at steady state [358] and may be required for the development of $CD4^+$ T cell mediated autoimmune disease [468]. In particular, the existence of Tcaf3-specific autoantibodies in *Aire*$^{-/-}$ mice suggests that C4/I-A^b-specific T cells interface with endogenous B cells during autoimmune reactions [101]. To determine whether B cells were required for C4/I-A^b-specific T cell infiltration of the prostate in autoimmune disease, we crossed *Ighm*$^{-/-}$ mice, which lack functional B cells [469], with *Aire*$^{-/-}$ mice, which develop spontaneous autoimmune disease to multiple organs including C4/I-A^b-specific T cell infiltration of the prostate [138]. *Aire*$^{-/-}$ *Ighm*$^{-/-}$ and *Aire*$^{-/-}$ *Ighm*$^{+/-}$ mice had similar numbers of C4/I-A^b-specific and polyclonal T cells in the prostate, which was elevated compared to *Aire*$^{+/+}$ mice (Figure 34, A-B), indicating that B cells are not required for priming C4/I-A^b-specific autoimmune responses.

It remained possible that B cells were playing a role in mediating tolerance upon immune challenge that is distinct from other APC subsets. To investigate this, we immunized *Ighm*$^{-/-}$ mice on Aire-sufficient and -deficient backgrounds with C4 peptide in CFA and analyzed the antigen specific T cell response in the SLOs 14 days later. Surprisingly, B cell deficiency caused a ~10fold reduction in the number of C4/I-A^b-specific cells elicited when compared to sufficient controls (Figure 34, C-D), but did not alter the Treg/Tconv ratio in *Aire*$^{+/+}$ or *Aire*$^{-/-}$ mice (Figure 34, E). These results suggest that B cells may present antigen and promote expansion of C4/I-A^b-specific Treg and Tconv cells during immune challenge. However, since B cells are known to promote the development of lymphoid tissue [470,471], it remained possible that C4/I-A^b-specific T cells failed to expand for reasons unrelated to antigen presentation by B cells. We therefore performed experiments in $MD4^+$ B cell transgenic hosts, which harbor monoclonal B cells specific for the foreign protein HEL and would not present C4 antigen to T cells. C4/I-A^b-specific Treg and Tconv cells readily expanded in $MD4^+$ mice following C4 peptide immunization (Figure 34, F-H),

indicating that the lack of expansion of such cells in *Ighm*$^{-/-}$ mice was likely an artefact of the absence of B cells. Additionally, MD4^{+} mice remained protected from prostatitis following Lm[C4] infection (Figure 34, I-J), indicating that antigen-specific B cells do not impose tolerance on T cells of related specificity in this setting. Collectively, our results suggest that B cells do not play a role as APCs in the maintenance or breakdown of tolerance to the C4/I-A^{b} self antigen.

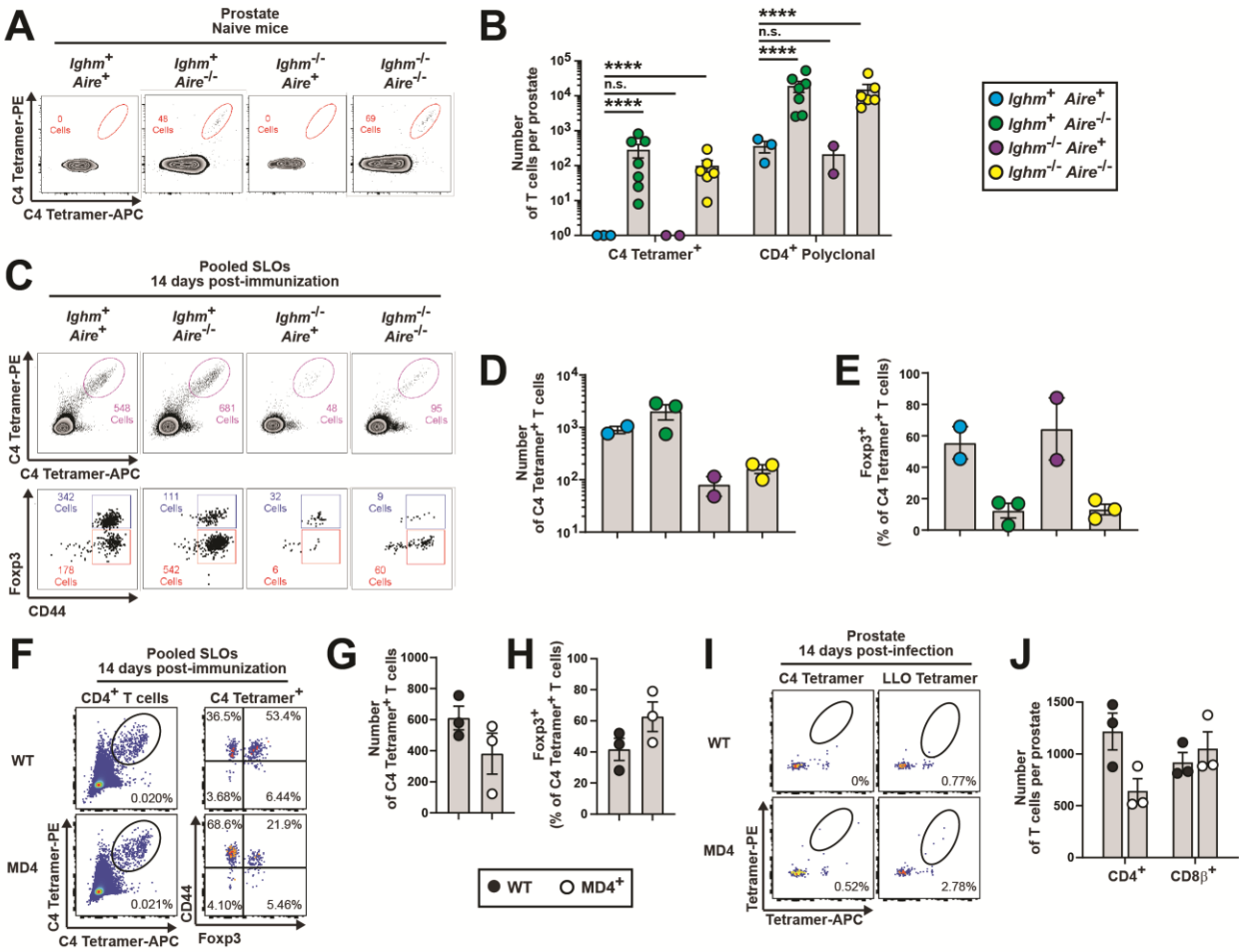

FIGURE 34. Tolerance to the C4/I-A^b antigen is instructed independent of B cells or B cell antigen specificity.

(A-B) Naive male mice of the indicated genotype were aged to >12 weeks and analyzed for prostatic T cell infiltration by flow cytometry. *Ighm*$^{-/-}$ mice lack B cells, while *Aire*$^{-/-}$ mice typically develop spontaneous CD4 T cell-dependent prostatitis. Data represent 2-3 independent experiments. n = 3, *Ighm*$^{+}$ *Aire*$^{+}$; n = 7, *Ighm*$^{+}$ *Aire*$^{-/-}$; n = 2, *Ighm*$^{-/-}$ *Aire*$^{+}$; n = 6, *Ighm*$^{-/-}$ *Aire*$^{-/-}$. (A) Representative flow cytometric analysis of CD4$^+$ T cells isolated from the prostates of mice of the indicated genotype. Plots depict dual C4/I-A^b tetramer staining of polyclonal CD4$^+$ cells. The absolute number of cells within the indicated gates is denoted. (B) Summary plot of pooled data from (A) showing the absolute number of C4/I-A^b tetramer$^+$ and CD4$^+$ cells isolated from the prostates of mice of the indicated genotype. Each symbol represents one mouse. Mean ± SEM is indicated. (two-tailed nonparametric Mann-Whitney test).

(C-E) Mice of the indicated genotype were immunized subcutaneously with 100µg C4 peptide emulsified in CFA. 14 days after immunization, CD4$^+$ T cells were isolated, and C4/I-A^b tetramer-binding cells were enriched from the pooled SLOs and analyzed by flow cytometry. Data are representative of 1 independent experiment. n = 2, *Ighm*$^{+}$ *Aire*$^{+}$; n = 3, *Ighm*$^{+}$ *Aire*$^{-/-}$; n = 2, *Ighm*$^{-/-}$ *Aire*$^{+}$; n = 3, *Ighm*$^{-/-}$ *Aire*$^{-/-}$. (C) Representative flow cytometric analysis of CD4$^+$ T cells enriched from the pooled SLOs of mice of the indicated genotype. The top plots depict C4/I-A^b tetramer-APC vs -PE expression by polyclonal CD4$^+$ T cells, whereas the bottom plots depict Foxp3 vs CD44 expression by dual C4/I-A^b tetramer$^+$ CD4$^+$ T cells. The absolute number

FIGURE 34, continued
of cells within the indicated gates are denoted. (D-E) Summary plots of data pooled from (C) showing the absolute number of dual C4/I-A^b tetramer$^+$ CD4$^+$ T cells (D) and frequency of such cells expressing Foxp3 (E) enriched from the pooled SLOs from mice of the indicated genotype. Each symbol represents one mouse. Mean ± SEM is indicated.
(F-H) Mice of the indicated genotype were treated and analyzed as in (C-E). MD4$^+$ mice harbor a monoclonal population of naive B cells that recognize the non-self protein Hen Egg Lysozyme. Data represent 1 independent experiment. n = 3, WT; n = 3, MD4$^+$. (F) Representative flow cytometric analysis of CD4$^+$ T cells enriched from the pooled SLOs of mice of the indicated genotype. The left plots depict C4/I-A^b tetramer-APC vs -PE expression by polyclonal CD4$^+$ T cells, whereas the right plots depict Foxp3 vs CD44 expression by dual C4/I-A^b tetramer$^+$ CD4$^+$ T cells. The frequency of cells within the indicated gates are denoted. (G-H) Summary plots of data pooled from (F) showing the absolute number of dual C4/I-A^b tetramer$^+$ CD4$^+$ T cells (G) and frequency of such cells expressing Foxp3 (H) enriched from the pooled SLOs from mice of the indicated genotype. Each symbol represents one mouse. Mean ± SEM is indicated.
(I-J) Male mice of the indicated genotype were infected intravenously with 10^7 CFU *Lm[C4].* 14 days post-infection, mice were analyzed for prostatic T cell infiltration by flow cytometry. *Ighm*$^{-/-}$ mice lack B cells, while *Aire*$^{-/-}$ mice typically develop spontaneous CD4 T cell-dependent prostatitis. Data represent 1 independent experiment. n = 3, WT; n = 3, MD4$^+$. (I) Representative flow cytometric analysis of CD4$^+$ T cells isolated from the prostates of mice of the indicated genotype. Plots depict C4/I-A^b tetramer-APC vs -PE (left) and LLO/I-A^b tetramer-APC vs -PE (right) expression by polyclonal CD4$^+$ T cells. The frequency of cells within the indicated gates are denoted. (J) Summary plot of pooled data from (I) showing the absolute number of polyclonal CD4$^+$ and CD8β$^+$ cells isolated from the prostates of mice of the indicated genotype. Each symbol represents one mouse. Mean ± SEM is indicated.

Presentation of the C4/I-A^b antigen in the periphery at steady state may alter the pool of antigen-specific T cells and the response to Lm[C4] infection

Our studies demonstrate an essential role for C4 peptide expression in the thymus in protecting the host from autoimmune susceptibility (Figures 5 and 16) by enabling the development of C4/I-A^b-specific Treg cells that selectively constrain Tconv cells of matched antigen specificity in settings of inflammation. C4/I-A^b-specific T cells also sense antigen in the prostate-draining LN at steady-state of male mice prior to infection (Figure 11, D-F), so peripheral antigen recognition could play an additional role in maintaining tolerance. In this regard, previous studies have shown that peripheral antigen recognition can increase the frequency of antigen-

specific Treg cells at the skin and during pregnancy [428,429]. Given that autoimmune protection to C4/I-A^b is conferred, at least in part, by a numeric Treg advantage over Tconv cells in the periphery (Figure 30), we sought to determine if peripheral antigen was acting to shape the repertoire of such cells.

We hypothesized that C4/I-A^b recognition at the pLN at steady-state was enabling a Treg-dominated antigen-specific response upon immune challenge. To establish a scenario in which C4/I-A^b-specific T cells developed in the same environment and peripheral antigen is either removed or maintained, we transferred polyclonal $CD4^+$ T cells from $C4^{WT}$ mice into T cell-deficient $Tcra^{-/-}$ hosts that expressed or lacked the C4 peptide (Figure 35, A). Following an equilibration period of ~2 months, host mice were challenged with C4 peptide + CFA, and C4/I-A^b-specific Treg and Tconv cells were enumerated in the SLOs 2 weeks later. On average, a greater number of total C4/I-A^b-specific T cells were elicited in $C4^{WT}$ hosts than $C4^{-/-}$ hosts, and a higher fraction of these cells expressed Foxp3, although these results did not reach statistical significance owing to variability between hosts (Figure 35, B-D). The numeric increase mapped to the Treg compartment (Figure 35, E-F), suggesting that peripheral recognition of C4/I-A^b may serve to increase the precursor pool of antigen-specific Treg cells or confer these cells with a greater capacity for expansion. To test the functional implications of this advantage, we challenged the same host mice with *Lm[C4]* and enumerated the cells 1 week later (Figure 35, G), reasoning that the decease in C4/I-A^b-specific Treg cells may enable a larger burst at the peak of infection. While the fraction of cells elicited in $C4^{WT}$ or $C4^{-/-}$ host mice did not differ at this timepoint, the absolute number of cells elicited was greater in mice lacking C4 peptide (Figure 35, H-J). Taken together, these results suggest that recognition of the C4 peptide at steady-state may confer C4/I-A^b-specific Treg cells with a superior ability to control antigen-specific responses upon immune challenge. It

remains outstanding whether this advantage is strictly quantitative in nature, or if antigen recognition also confers qualitative changes in antigen-specific Treg and Tconv cells which enforce unique effector or anergic phenotypes, as observed in other studies [186,225,226].

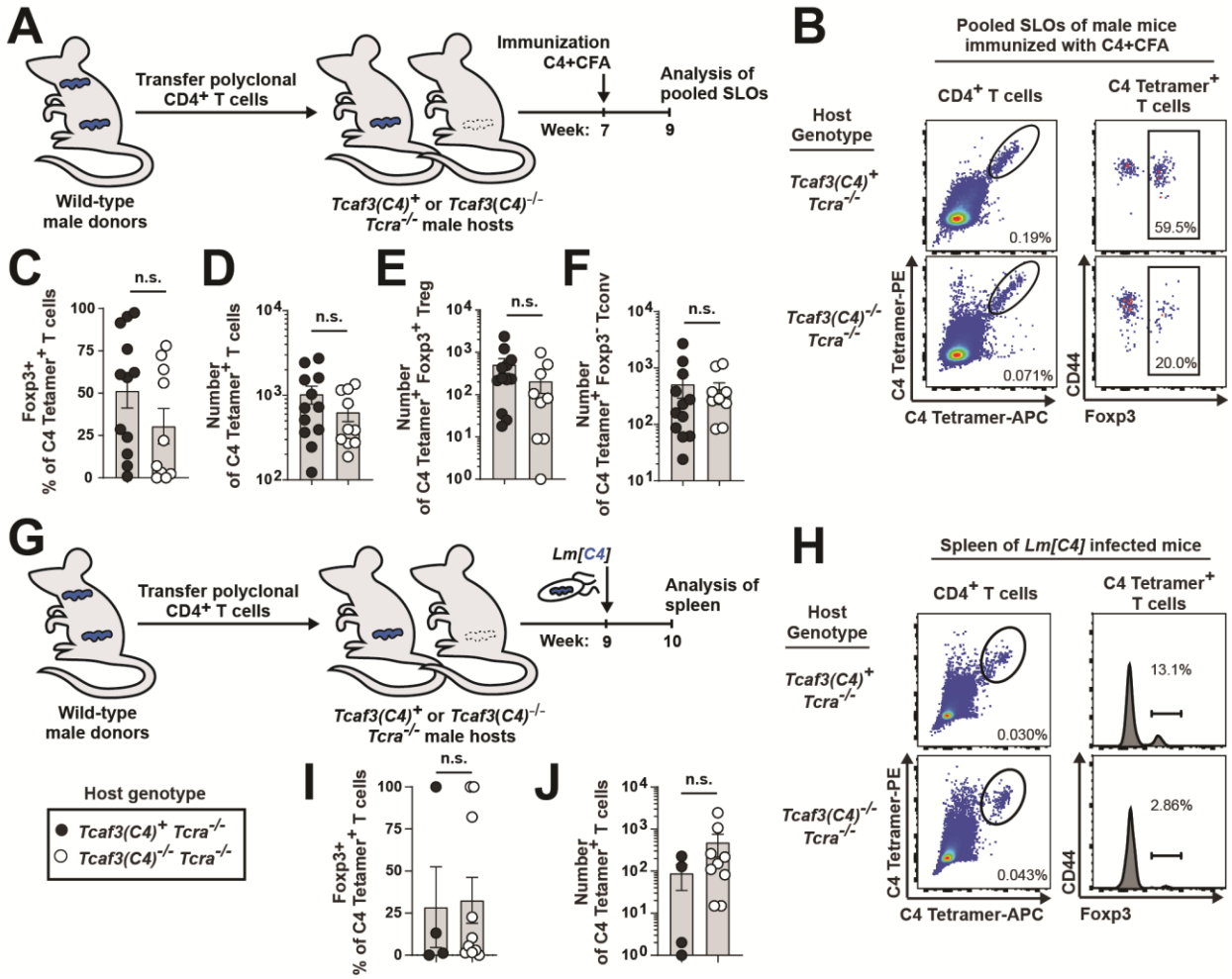

FIGURE 35. In a reconstitution setting of lymphodeplete hosts, peripheral C4 antigen may alter the pool of C4/I-A^b-specific T cells and the response to *Lm[C4]* infection

(A) Experimental schematic for panels (B-F). 10^7 polyclonal CD4$^+$ T cells were isolated from the pooled secondary lymphoid organs (SLOs) of wild-type male donors and transferred intravenously into *Tcaf3(C4)$^+$ Tcra$^{-/-}$* or *Tcaf3(C4)$^{-/-}$ Tcra$^{-/-}$* male recipients. 7 weeks after transfer, host mice were immunized subcutaneously with 100µg C4 peptide emulsified in CFA. 2 weeks post-immunization, C4/I-A^b tetramer$^+$ cells were enriched from the pooled SLOs and analyzed by flow cytometry. Data are pooled from 3 independent experiments. n = 12, *Tcaf3(C4)$^+$ Tcra$^{-/-}$*; n = 9, *Tcaf3(C4)$^{-/-}$ Tcra$^{-/-}$*. (B) Representative flow cytometric analysis of CD4$^+$ T cells isolated from host males of the indicated genotype. The left plots depict C4/I-A^b tetramer-APC vs -PE expression by polyclonal CD4$^+$ cells, whereas the right plots depict CD44 vs. Foxp3 expression by dual C4/I-A^b tetramer$^+$ T cells. The frequency of cells within the indicated gates is denoted. (C) Summary plots of data pooled from (B) showing the frequency of dual C4/I-A^b tetramer$^+$ CD4$^+$ T cells expressing Foxp3 in the pooled SLOs of host mice of the indicated genotype. Each symbol represents one mouse. Mean ± SEM is indicated. (n.s., not significant $p > 0.05$; Welch's t-test). (D-F) Summary plots of data pooled from (B) showing the number of dual C4/I-A^b tetramer$^+$ CD4$^+$ T cells (D), dual C4/I-A^b tetramer$^+$ Foxp3$^+$ Treg cells (E), and dual C4/I-A^b tetramer$^+$ Foxp3^{neg} Tconv cells (F) in the pooled SLOs of host mice of the indicated genotype. Each symbol represents one mouse. Mean ± SEM is indicated. (n.s., not

FIGURE 35, continued
significant $p > 0.05$; Welch's t-test). (G) Experimental schematic for panels (H-J). 10^7 polyclonal $CD4^+$ T cells were isolated from the pooled secondary lymphoid organs (SLOs) of wild-type male donors and transferred intravenously into *Tcaf3(C4)*$^+$ *Tcra*$^{-/-}$ or *Tcaf3(C4)*$^{-/-}$ *Tcra*$^{-/-}$ male recipients. 9 weeks after transfer, host mice were infected intravenously with 10^7 CFU *Lm[C4]*. 1 week post-infection, C4/I-A^b tetramer$^+$ cells were isolated from the spleen and analyzed by flow cytometry. Data are pooled from 1 independent experiments. n = 4, *Tcaf3(C4)*$^+$ *Tcra*$^{-/-}$; n = 9, *Tcaf3(C4)*$^{-/-}$ *Tcra*$^{-/-}$. (H) Representative flow cytometric analysis of $CD4^+$ T cells isolated from host males of the indicated genotype. The left plots depict C4/I-A^b tetramer-APC vs -PE expression by polyclonal $CD4^+$ cells, whereas the right plots depict Foxp3 expression by dual C4/I-A^b tetramer$^+$ T cells. The frequency of cells within the indicated gates is denoted. (I) Summary plots of data pooled from (H) showing the frequency of dual C4/I-A^b tetramer$^+$ $CD4^+$ T cells expressing Foxp3 in the spleen of host mice of the indicated genotype. Each symbol represents one mouse. Mean ± SEM is indicated. (n.s., not significant $p > 0.05$; Welch's t-test). (J) Summary plots of data pooled from (H) showing the number of dual C4/I-A^b tetramer$^+$ $CD4^+$ T cells in the spleen of host mice of the indicated genotype. Each symbol represents one mouse. Mean ± SEM is indicated. (n.s., not significant $p > 0.05$; Welch's t-test).

Repeated infection of C4^{WT} mice with Lm[C4] enables prostatic infiltration of C4/I-A^b-specific T cells

Genetic factors that influence expression of the C4 peptide in the thymus and periphery can genetically predispose the host to autoimmune attack by altering the natural "setpoint" of self-reactive Treg and Tconv cells specific for C4/I-A^b. The finding that organ-specific tolerance hinges on constraint by such antigen-specific Treg cells in inflammatory contexts implies that genetic susceptibility is not a prerequisite for autoimmune disease if external factors alone can alter the Treg setpoint. Environmental tuning of antigen-specific T cell populations is readily evidenced in T cells reactive to commensal microbes, where Treg cell induction depends on antigen expression by the microbial targets [153,170,427], and the emergence of pathogenic commensals is associated with a loss of antigen-specific Treg cells [152,171]. Intriguingly, infection of mice with *M. Tuberculosis* causes Treg cells specific for a pathogen-derived peptide to disappear from the periphery of such mice [220], suggesting that cross-reactivity with pathogen antigens may rewire the Treg/Tconv ratio

of self-specific T cells and render a host with no obvious genetic predisposition now susceptible to autoimmune attack.

C4^{WT} mice present with a strongly Treg-dominated antigen-specific response early after *Lm[C4]* infection that is gradually lost after infection (Figure 16, H). To determine if infection with a mimetope-bearing pathogen promotes autoimmune susceptibility in tolerant hosts, we performed a repeat challenge experiment. *C4^{WT}* mice, which are protected from prostatitis following *Lm[C4]* infection, were subjected to a secondary challenge with *Lm[C4]* between 2 and 4 weeks following the primary infection (Figure 36, A). If the primary infection promotes alterations in the pool of C4/I-A^b-specific Treg cells, loss of tolerance to C4/I-A^b may follow. C4/I-A^b-specific T cells were observed in the prostate of some mice following secondary challenge with *Lm[C4]* but not with control *Lm[parent]* (Figure 36, B-C). However, neither polyclonal CD4$^+$ or CD8β$^+$ T cells were elevated in the prostates of mice that had received dual *Lm[C4]* infection (Figure 36, D-E), indicating that tolerance had not been completely broken in this setting. These results suggest that primary exposure to pathogen-derived C4 peptide can act as an environmental cue that reinstructs the recall response. While a complete breakdown of tolerance was not observed in this setting, it remains possible that a kinetic window of optimal susceptibility exists in which C4/I-A^b-specific Treg cells have not recovered from the primary response.

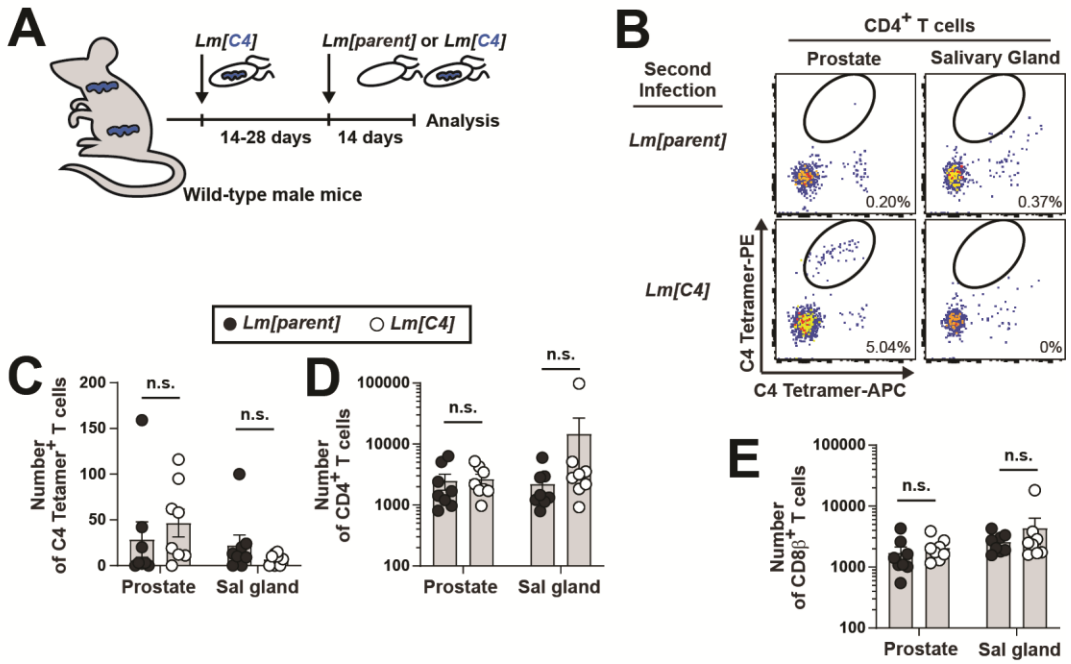

FIGURE 36. Repeated infection of wild-type mice with *Lm[C4]* may enable prostatic infiltration of C4/I-A^b-specific T cells

(A) Wild-type male mice were challenged intravenously with 10^7 CFU *Lm[C4]*, allowed to recover for 14-28 days, and re-challenged with 10^7 CFU of either *Lm[C4]* or *Lm[parent]*. 14 days post-secondary infection, T cells were isolated from the indicated organ, labelled with C4/I-A^b tetramers, and analyzed by flow cytometry. Data are representative of 2 experiments. n = 8, *Lm[parent]* secondary; n = 8, *Lm[C4]* secondary. (B) Representative flow cytometric analysis of CD4$^+$ T cells isolated from the prostates (left) or salivary glands (right) of mice that received the indicated *Lm* stain for the second infection. Plots depict C4/I-A^b tetramer-APC vs -PE expression by polyclonal CD4$^+$ T cells. The frequency of cells within the indicated gates are denoted. (C) Summary plots of pooled data showing the number of dual C4/I-A^b tetramer$^+$ CD4$^+$ T cells recovered from the indicated organ of mice that received the indicated *Lm* stain for the second infection. Each symbol represents one mouse. Mean ± SEM is indicated. (n.s. = P > 0.05; Welch's t-test). (C) Summary plots of pooled data showing the number of dual C4/I-A^b tetramer$^+$ CD4$^+$ T cells recovered from the indicated organ of mice that received the indicated *Lm* stain for the second infection. Each symbol represents one mouse. Mean ± SEM is indicated. (n.s. = P > 0.05; Welch's t-test). (D-E) Summary plots of pooled data showing the number of polyclonal CD4+ (D) and polyclonal CD8β$^+$ (E) T cells recovered from the indicated organ of mice that received the indicated *Lm* stain for the second infection. Each symbol represents one mouse. Mean ± SEM is indicated. (n.s. = P > 0.05; Welch's t-test).

CONCLUSIONS AND DISCUSSION

In this chapter, we interrogate the mechanisms that enable self-pMHCII-specific Treg cells to control Tconv cells of matched antigen specificity during infection. Using a monoclonal population of self-pMHCII-specific transgenic T cells, mice lacking this single self antigen, and high-parameter three-dimensional confocal microcopy, we demonstrate that antigen-specific Treg cells locally compete with Tconv cells of matched specificity for TCR-dependent and -independent signals to prevent such Tconv cells from adopting cell states permissive to prolonged proliferation. In the absence of Treg cells of matched antigen specificity, some self-reactive Tconv cells are controlled by local polyclonal Treg cells via bystander mechanisms of suppression, while others receive high TCR-mediated signals to escape Treg control and adopt a hyperproliferative cell state. Treg cells are poised to accumulate more rapidly than Tconv cells expressing the same TCR, endowing such cells with a numeric competitive advantage intrinsic to the Treg program that may act to prevent such Tconv cells from trafficking to distal sites. Increasing the number of self-specific Tconv cells prior to infection enabled prostatitis development in wild-type mice following infection, further implicating the antigen-specific Treg/Tconv ratio as a critical determinant of Tconv control or escape. Antigen-specific suppression was found to act independent of B cell specificity but may be bolstered by antigen recognition in the periphery prior to infection. We discovered a critical role for the receptor CCR2 for driving the development of Treg cells but not Tconv cells specific for Aire-dependent self antigen. Using a series of pathogens expressing covalently-linked peptide antigens, we found that self-specific Treg cells do not quantitatively or qualitatively alter the Tconv response to a second pathogen-derived epitope. However, the loss of tolerance to one self-antigen numerically or phenotypically altered the response to a related self-antigen following infection, suggesting the existence of crosstalk between some T cell specificities

but not others. Finally, repeated infection with a pathogen expressing self-antigen enabled the accumulation of antigen-reactive T cells in the prostate, implying a degree of plasticity in antigen-specific tolerance. Thus, both genetic and environmental factors cooperate to enable tolerance to antigenic self-peptides by ensuring a Treg-dominated response that outcompetes Tconv cells of matched antigen specificity and prevents autoimmune attack.

Heterologous immunity and antigen dominance

During T cell development, the T cell repertoire is selected on host MHC molecules that present host-derived peptides. These clones are expected to populate the periphery and mount robust responses to unknown foreign peptide antigens that have not been previously encountered. The TCR must therefore possess a degree of cross-reactivity to peptide antigens by nature to ensure robust responses during infection. Consequently, individual T cell responses against truly novel peptide antigens may not all necessarily begin from a naïve state, given that the host is exposed to diverse pathogens throughout life that can activate cross-reactive T cell clones. This concept, classically termed "heterologous immunity", creates a scenario in which T cell clones possessing differing histories of antigen encounter compete for limited activating resources during immune challenge [472-474], and has been described for both $CD8^+$ [475,476] and $CD4^+$ [477] T cell subsets. Clonal heterogeneity may exist within a single antigenic determinant due to differences in TCR cross-reactivity or functional affinity to heterologous antigens, and can differ between host mice with identical genetic background and infection history due to varied clonal compositions within antigen-specific T cell populations [478,479]. An additional layer of complexity resides in the existence of multiple immunodominant peptide epitopes during immune challenge, which forces inter-specificity competition for TCR/pMHCII-independent activating factors. Together, these

factors ultimately establish antigen dominance hierarchies in the T cell response to a pathogen [366,376], which can be reinforced or broken upon subsequent homogenous or heterologous antigen exposure [480,481].

Spatial *in situ* analysis of MJ23 Treg and Tconv cells during the critical window of infection-induced activation, together with temporal studies of the resulting population responses, enabled an unprecedented level of insight into heterologous immunity at the clonal level that elucidated the role of both antigen-specific and polyclonal Treg cells in establishing dominance hierarchies. Many autoreactive MJ23 Tconv cells could be controlled by proximal polyclonal Treg cells, indicating that bystander mechanisms of Treg suppression remain operative during infection and likely contribute to patterns of heterologous immunity for both self- and pathogen-derived antigens. The phenotypes of these polyclonal Treg cells suggest two mechanisms by which Treg cells of mismatched antigen specificity can mediate "bystander" Treg suppression: 1) Treg cells respond to early Tconv activation using TCR-mediated signals from unrelated antigens and the high-affinity IL-2 receptor to actively outcompete local Tconv cells for proliferation signals (Figure 27, Clusters A2 and S2), 2) Treg cells existing at high density create local deserts that passively restrict Tconv cell activation (Figure 27, Cluster S3). Treg cells following the latter "density" mechanism were largely devoid of pSTAT5, indicating that these cells were probably not acting as IL-2 sinks, but retained PD-1 expression, suggesting that they may be providing other suppressive factors downstream of TCR such as IL-10 [282]. In wild-type mice, the MJ23 Tconv cells that were not controlled via bystander Treg suppression were uniquely controlled by antigen-specific Treg cells, which exhibited the highest level of activation among all Treg cells (Figure 27, Cluster S1). In these regions, polyclonal Treg cells were strikingly devoid of Ki67 and pSTAT5 despite signs of TCR-mediated signaling, strongly suggesting that local MJ23 Treg cells hoard

proliferation and differentiation factors from all other proximal T cells following their activation. Notably, MJ23 Tregs located proximal to MJ23 Tconv cells had universally high PD-1 expression while those Tregs located distal expressed low levels of PD-1, implicating MJ23 Treg "hypercompetition" for antigen as a major mechanism of antigen-specific control of Tconv cells, and suggesting that MJ23 Treg cells take on "bystander" suppression roles characteristic of polyclonal Treg cells in regions with low antigen availability. In $C4^{\Delta TEC}$ mice that lack MJ23 Treg cells, some MJ23 Tconv cells escaped bystander Treg suppression and acted as hyper-competitors, as evidenced by local polyclonal Treg cells that were completely inactivated (Figure 27, Cluster A1) and analogous to what was observed for MJ23 Treg cells performing antigen-specific suppression.

The heterogeneity observed for MJ23 Tconv cell responses in $C4^{\Delta TEC}$ might be expected to reflect activation patterns of pathogen-specific Tconv cell populations, given the paucity of Treg cells with matched specificity. What insights are revealed by extrapolating our imaging analysis to a typical productive immune response to foreign antigens? First, a remarkable degree of variability exists in the phenotypes of individual monoclonal MJ23 Tconv cells, indicating that heterologous immunity can exist within individual clonal populations independent of affinity for antigen. This heterogeneity is likely to be instructed by a combination of stochastic factors such as local antigen availability and the ability of local polyclonal Treg cells to outcompete for response resources. It is also possible that heterologous responses are partially instructed by cues that occur prior to immune challenge. For example, one Tconv cell of a clonal population may have been exposed to different cross-reactive self-antigens than another cell, which could endow such cells with distinct activation potential from unique histories of TCR stimulation. Second, our results revealed that only a few MJ23 Tconv cells became highly activated during the response,

suggesting that only a few activated T cells give rise to the antigen-specific burst that is observed in any given productive T cell response. This prediction aligns with a previous pair of studies demonstrating that most LLOp/I-A^b-speciifc T cells responding to infection at day 7 arise from a single transferred Tconv cell clone [482,483]. Here, the size of the clonal burst corelated with both the degree of effector cell formation and memory cell consolidation, which provides a conceptually satisfying basis for how a few escaping MJ23 Tconv cells can go on to promote and sustain a fulminant autoimmune response following infection. Finally, we observed that both escaping MJ23 Tconv cells were always observed in regions with low polyclonal Treg activation, suggesting that the few clones in the heterologous response that give rise to most of the expanded cells are likely capable of outcompeting all other local cells for activating resources. Importantly, activated MJ23 Treg cells were never found near escaping MJ23 Tconv cells, indicating that Treg cells of matched specificity always "win" in a competitive scenario. The rapid accumulation of MJ23 Treg cells relative to Tconv cells is likely to endow such cells with the ability to outcompete MJ23 Tconv cells in all scenarios (Figure 26), and implies that Treg cells may be programed to undergo small but rapid clonal bursts following antigenic stimulation, as opposed to the relatively slow but large burst expected for escaping MJ23 Tconv cells [454,455]. Notably, all suppressed MJ23 Tconv cells in *C4*$^{\Delta TEC}$ mice were surrounded by polyclonal Treg cells with high PD-1 expression that were expected to have recently seen antigen. While speculative, this could suggest that Treg cells are uniquely capable of rapid proliferation because they only require TCR input signal. Thus, for foreign antigen-specific Tconv cells, a productive response is mounted by a few clones that integrate activation signals in regions that probably have a low density of Treg-specific self-ligands.

Having established a conceptual framework for heterologous immunity of single antigen specificities responding to pathogen infection, how might this model explain observations of antigen dominance and interclonal competition in our system? Specifically, we demonstrated that C4/I-A^b-specific Treg cells could selectively styme the activation of Tconv cells of matched antigen specificity without impacting the response to the LLO/I-A^b pathogen-derived antigen (Figure 16). In this experiment, the antigenic peptides are expressed by different proteins of the same pathogen, so each APC is likely to present both antigens simultaneously, but the density of either pMHC complex on the surface of a given APC may vary between cells. This establishes a scenario, on a single APC, in which C4/I-A^b-specific or LLO/I-A^b-specific T cell populations start with a competitive advantage based on ligand density. If all three populations of cells – C4/I-A^b-specific Treg cells, C4/I-A^b-specific Tconv cells, and LLO/I-A^b-specific Tconv cells – simultaneously arrive at the APC, two possible outcomes may occur: 1) LLO/I-A^b-specific Tconv cells outcompete both C4/I-A^b-specific populations, 2) C4/I-A^b-specific Treg cells outcompete both antigen-matched Tconv cells and LLO/I-A^b-specific Tconv cells. C4/I-A^b-specific Tconv cells will never outcompete when C4/I-A^b-specific Treg cells are in the system, as demonstrated in our studies. Therefore, local competition with C4/I-A^b-specific Treg cells will prevent the expansion of some LLO/I-A^b-specific Tconv cells but not others, ultimately establishing an antigen-dominance hierarchy manifested in the accumulation of LLO/I-A^b-specific Tconv cells in $C4^{WT}$ mice. In the absence of C4/I-A^b-specific Treg cells, only C4/I-A^b-specific and LLO/I-A^b-specific Tconv cells compete in the same local environment, where some C4/I-A^b-specific Tconv cells can now outcompete LLO/I-A^b-specific Tconv cells in the absence of C4/I-A^b-specific Treg cells. The dominance hierarchy for LLO/I-A^b-specific Tconv cells in $C4^{\Delta TEC}$ mice does not change because the competing antigen does not change – the only difference is the type of cell that is

competing against the LLO/I-A^b-specific Tconv cell. If this model is correct, the magnitude of the LLO-specific Tconv response is expected to be larger during *Lm[parent]* infection than during *Lm[C4]* infection, given the absence of interclonal competition with C4/I-A^b-specific T cells, though this has yet to be explicitly tested. Alternatively, it is possible that decreasing interclonal competition would increase the degree of intraclonal competition between LLO/I-A^b-specific Tconv cells, which could be confirmed if *Lm[parent]* infected mice had a less oligoclonal response to LLO/I-A^b than mice infected with *Lm[C4]*. In this regard, when an additional specificity of 2W/I-A^b-specific Tconv cells was recruited into the pathogen-reactive immune response by covalently linking the C4 peptide to the 2W peptide, the magnitude of the C4/I-A^b-specific response was markedly decreased (Figure 32) compared to *Lm[C4]* infection. Notably, there is expected to be less heterogeneity amongst individual APCs in the relative amount of C4/I-A^b and 2W/I-A^b complexes since these peptides are expressed in tandem, so the dominance hierarchy might be more dependent on the precursor frequency of antigen-specific T cells in the naïve repertoire, which is 100x greater for 2W/I-A^b-specific T cells (Figure 3 and [350]). Thus, the addition of MJ23 Tconv cells prior to *Lm[C4+2W]* infection may impact the magnitude or clonality of the response to 2W/I-A^b, though this experiment has yet to be performed.

Driver and Passenger T cells, epitope spreading, and the Riot Hypothesis

Our collective study revealed that the activation of a single self-reactive Tconv cell specificity unleashes targeted organ infiltration by polyclonal $CD4^+$ and $CD8^+$ T cells. This simple yet definitive observation, recurrently demonstrated in multiple models and experiments throughout, unearths a trove of questions with the potential to challenge long-held paradigms that span multiple immunology-related fields. What is the ontogeny and specificity of polyclonal

infiltrating cells? How does the initiating antigen, target organ, and T cell specificity alter this pool of cells? How are normally-tolerant T cells "licensed" to infiltrate a single target organ? How are they contributing to tissue destruction, and what factors are supporting their sustained response? The following paragraphs attempt to construct the "Riot Hypothesis" – that single activated T cells direct an array of unrelated T cell specificities to "start a riot" – by addressing these questions through the lens of our experimental system, and attempting to integrate observations from other models of autoimmunity, tumor immunology, and pathogen response. The term "Driver" will describe a single activated T cell specificity that initiates a targeted T cell response, and the term "Passenger" will refer to all T cell specificities whose response, location, or phenotype changes in the presence of a Driver.

By definition, Passenger T cells must originate from a pre-existing pool of tolerant cells that are likely to be heterogeneous in origin, location, and phenotype. What is the nature of these cells at steady state? A few $CD4^+$ and $CD8^+$ T cells exist in the prostate in the absence of a Driver specificity (Figures 16 and 30-31), so at least some Passenger T cells are expected to comprise these tissue-resident cells. It is possible that Passenger T cells are exclusively derived from pre-existing cells in the tissue that expand in response to cues from the Driver specificity, but this is unlikely given that Passenger T cell numbers rapidly increase >10-fold before the driver specificity accumulates in the prostate (Figure 16). Therefore, many Passenger T cells are expected to originate from circulating cells. Circulating Passenger cells could infiltrate either in an antigen-directed manner enabled by reactivity to antigens in the target organ, or in an antigen-independent manner via recognition of inflammatory or chemotactic cues. In our model, both prostate-reactive C4/I-A^b-specific T cells and pathogen-reactive LLO/I-A^b-specific T cells contribute to the Passenger cell infiltrate when an F1/I-A^b-specific Driver specificity is operative (Figure 30),

indicating that both modes of infiltration can occur simultaneously for different subsets of Passenger cells. LLO/I-A^b-specific T cell contribution to the Passenger infiltrate suggests that memory T cells with a history of activation may be uniquely endowed with the ability to act as Passenger cells at sites of ongoing inflammation, perhaps via a surface receptor that is expressed as part of the memory program. One candidate for memory-derived Passenger infiltration is the IL-15Rβ chain CD122, as IL-15 is expressed and presented in damaged tissues to promote memory cell recruitment and retention [484]. Since SPF mice have no history of pathogen exposure, the pool of memory cells from which this subset of Passenger cells could arise is narrower than what would be anticipated from a typical organism in a non-sterile environment. However, a population of "Memory Phenotype" $CD8^+$ T cells exist at homeostasis in SPF mice which share a phenotype with true memory cells including expression of CD122 [485-487]. Notably, clones derived from this population were recently shown to exhibit hallmarks of self-reactivity despite their tolerance at steady-state [488], implicating these cells as prime candidates for contributing to the Passenger T cell population. Relatedly, $CD4^+$ Passenger T cells consisted of a substantial population of PD-1^+ Tconv cells, suggesting that some Passenger clones are self-reactive and continue to receive TCR stimulation in the tissue (Figure 30). Thus, a combination of self-reactive cells, memory T cells, and tissue-resident specificities contribute to the Passenger T cell infiltrate. Notably, this suggests two separate target organs will have overlapping Passenger specificities – namely those specific for widely expressed self-antigens and those with a history of pathogen exposure – as well as some distinct specificities reactive to tissue-restricted self antigens. A picture capturing the heterogeneity of the global Passenger T cell infiltrate, such as a carefully-defined scRNAseq dataset, will be required to directly address the contribution and ontogeny of these subpopulations.

The presence of a Driver specificity was the sole determinant of whether Passenger T cells could infiltrate the prostate or remained tolerant. How might the Driver specificity authorize such a response from Passenger T cells? Driver T cells were initially activated in SLOs distal to the prostate in our infection models, so it's difficult to imagine how Passenger licensing would take place at these sites. For this to occur, Driver cells would need to be imprinted with the knowledge of Prostate self-reactivity prior to infection, and be able to transfer this intelligence to potential Passenger T cells at distal sites. We showed that monoclonal C4/I-A^b- or F1/I-A^b-specific cells from female mice could become Driver T cells following pathogen-mediated activation in male hosts (Figure 30), strongly suggesting that *a priori* knowledge of prostate reactivity is not a prerequisite for the Driver program. A second possibility is that activated Driver T cells home directly to the prostate and act as an inflammatory beacon to entice potential Passenger cells to enter from surrounding tissues or draining SLOs. This scenario would require antigen-directed entry of the Driver specificity, given that the prostate is not uniquely inflammatory without these cells. Epithelial cells of the prostate do not express MHC-II in the mouse [405], so a Driver cell stochastically passing through the tissue would need to find a rare antigen-presenting APC and mount a robust secondary proliferative response. This is an arbitrary series of events that would probably yield a high degree of variability in prostatic infiltration between mice, which is not what is experimentally observed (Figure 16). The most likely scenario is that Passenger licensing occurs in the prostate-draining LN following activation and recirculation of Driver cells from distal SLOs. It follows that Passenger T cells are primarily derived from a pool of T cells that are in the prostate dLN alongside the Driver specificity or circulate to this site after the Driver specificity has entered. Notably, this "second hit" model of autoimmune induction implies the existence of an additional layer of Treg-mediated protection in the prostate dLN that helps to prevent prostatitis in the wild-

type host (discussed with Figure 17). In this model, an activated Driver cell recognizing its cognate pMHC on an APC could license Passenger T cells either directly via secreted factors or cell-cell contact, or indirectly by instructing qualitative changes to the APC. Considering that SLOs typically drain multiple tissues, a Driver T cell with no prior knowledge of prostate reactivity must somehow direct Passenger cells – and itself – to specifically infiltrate the prostate. The only cell in this scenario that could link the antigen to the tissue-of-origin is an APC that migrates from the tissue. This logic strongly implies the existence of a "reciprocal licensing" phenomenon between the Driver specificity and the APC – whereby a migratory APC imprinted with a tissue-specific signature passes this knowledge to T cells in the LN, and the Driver T cell permits the APC to give the same signals to other potential Passenger cells. There is precedent for tissue-specific imprinting of DCs and integrin-mediated T cell homing [489], particularly at mucosal sites [490], and a recent study demonstrated that Treg cells almost exclusively interact with migratory DC subsets in the LN [457], which would also be expected to present antigens to Driver T cells. While the exact molecular events that enable this reciprocal licensing are unclear, one can speculate that the Driver cell might raise the activation potential of an APC by forcing upregulation of costimulatory molecules that effectively lower the threshold to activation for surrounding Passenger T cell, such as those with low reactivity to self-antigens or unelated memory cells that are primed to respond via bystander activation mechanisms [491]. One major clue to this mechanism comes from a study that mapped T cell-APC interactions *in vivo* [492], where T cells initially only made contact with DCs in a TCR/pMHCII-dependent manner, but were subsequently able to form stable interactions and change the expression profile of non-cognate DCs via CD40/CD40L. If this extends to Driver T cells, it follows that such cells can impart other APCs not only with increased stimulatory capacity, but also with ability to pass along a molecular "zipcode" for the prostate.

How might the quality of the Driver specificity or antigenic determinant impact the Passenger cell response? Possible contributing factors include Driver TCR affinity for antigen, antigen load during activation and at the licensing site, the inflammatory stimulus driving initial activation, the absolute number of Driver T cells, and whether multiple Driver specificities are elicited. Our studies provide minimal insight in this regard, but hypotheses can be extrapolated from other disease systems where Driver and Passenger T cells might operate. We will look to studies of tumor immunology – a setting where Driver and Passenger responses observed in our autoimmune model are most likely to extend – given that neoantigen expression (Driver antigen) in multiple tumor models promotes lymphocyte infiltration (Passenger cells) [493,494], and that mutational burden correlates with measures of T cell infiltration and function [495,496]. In our study, we did observe increased Passenger T cell infiltration that ultimately plateaued with increasing numbers of a single specificity of Driver T cells (Figure 30), indicating that more Driver cells enable a greater degree of Passenger cell licensing, up to a point. It remains unknown and is difficult to speculate whether a greater number of Driver cells broadens the repertoire and antigen specificities of Passenger cells, increases the clonal expansion of such cells, or both. Regarding antigen affinity, one elegant study altered the TCR contact residues of a subcutaneous melanoma tumor neoantigen epitope to create a panel of tumors expressing peptides with varying affinity for cognate T cells [497]. When single TCR clones were introduced following tumor inoculation, all cells robustly proliferated and entered the tumor, suggesting that affinity does not play a major role in creating a Driver T cell. A separate study using an autochthonous lung tumor model demonstrated the same principle [498]. However, this study also found that a T cell specificity with a higher affinity for a co-expressed neoantigen inhibited the T cell response to a lower affinity antigen in a competitive scenario, suggesting the quality of the Driver antigen becomes important when

multiple Driver specificities are elicited simultaneously. Notably, peptide vaccination not only overcame the dominance hierarchy established by affinity, but also greatly increased the number of tumor-infiltrating neoantigen-specific cells, suggesting that the density of activating antigen and/or the activating adjuvant play a role in shaping the Driver T cell response. Engineered CAR T cells are also likely candidates to serve as Driver specificities, and it's notable that many tumors that regress following CAR therapy have very few CAR T cells but a large polyclonal T cell infiltrate [499]. Furthermore, *in vivo* activation of transferred CAR T cells promoted enhanced T cell infiltration that was required for tumor rejection [500], providing additional evidence that the activating stimulus plays a role in coordinating the Driver and Passenger T cell responses.

What is the contribution of Driver and Passenger T cells to disease? The lack of well-defined Driver and Passenger T cell populations in most previous studies leaves this question largely open. However, the nearly 30-year-old observation that mice which had rejected an OVA-expressing tumor cell line largely survived subsequent challenge with the parental tumor line suggests a consequential role for Passenger T cells in disease [501]. Furthermore, a recent landmark study of the T cell tumor infiltrate pre- and post- checkpoint blockade demonstrated that the primary mechanism of action was to drive new clones into the tumor to promote regression rather than to reactivate preexisting exhausted clones [502], highlighting the importance of defining and defining and studying these Driver and Passenger populations. Relatedly, a single autoreactive B cell clone was previously shown to drive other autoreactive B cell specificities to undergo sustained and productive germinal center reactions culminating with the production of autoantibodies against multiple self-proteins [503], implicating of Driver and Passenger T cells as potential "gatekeepers" to autoimmune attack from multiple cellular fronts. Two recent studies also described a phenomenon whereby long-lived germinal centers are continually replaced by

new clones of undefined specificity [504,505], which could propose a role for Driver or Passenger T cell specificities in regulating such germinal center reactions at steady-state or during disease. Unfortunately, testable hypotheses require depletion or addition experiments that are largely precluded without an understanding of Passenger cell heterogeneity and the forces that enable them to respond. An understanding of the mechanisms of Passenger cell licensing would enable studies of their contribution to both autoimmunity and anti-tumor immunity by blocking their infiltration. Defining subsets within the Passenger T cell infiltrate by gene expression would further enable specific depletion experiments *in vivo* using genetic models. Similarly, a carefully controlled Driver specificity could be removed following Passenger infiltration to define the T cell populations required to sustain an autoimmune response. Once these populations and their contributions have been defined, points of therapeutic intervention will likely become apparent. A brief experimental plan for one potential study of Driver and Passenger T cells will be discussed in *Discussion of Thesis & Future Directions*. A biological system of this nature – where Driver specificities orchestrate immune responses from Passenger T cells in the SLOs – does not have any intrinsic features that necessarily require settings of autoimmunity or disease to operate. The Driver specificity can easily be substituted by a T cell specificity reactive to a bona fide pathogen-derived peptide, which would implicate Passenger T cells as regular contributors to protective responses upon infection. In addition to the apparent relevance to the tumor context, this finding may challenge the long-held paradigm of pathogen-specific T cell specificities as the prototypical contributors to an adaptive immune response, and open new horizons reshape the field's understanding of what it means to mount a protective adaptive immune response.

Treg antigenic training

Antigen-specific Treg control of Tconv cells appears to operate at a quantitative level – the relative number of Treg cells to Tconv cells of a given specificity is related to the magnitude of the Tconv response, or lack thereof. This assertion is supported by the following observations in our studies: 1) recipient mice were protected from prostatitis when donor cells were transferred from mice with a Treg-biased C4/I-A^b-specific population (Figure 5), 2) an early proliferative burst by C4/I-A^b-specific or MJ23 Treg cells dampened the accumulation of matched Tconv cells (Figures 16 & 26), 3) the addition of MJ23 Tconv cells to wild-type mice enabled escape from endogenous C4/I-A^b-specific Treg control (Figure 30), 4) MJ23 Treg cells culled the response of MJ23 Tconv cells via local numeric enrichment (Figure 27), 5) A small number of C4/I-A^b-specific Treg cells in *C4*$^{\Delta TEC}$ mice existed but were unable to prevent prostatitis following infection (Figure 16), 6) a small number of LLO/I-A^b-specific Treg cells expanded upon infection but were unable to prevent the Tconv response (Figure 16). While our proposed mechanism of suppression ultimately depends on a numeric threshold of antigen-specific Treg cells per Tconv cell, qualitative differences set prior to infection may also enable robust numeric enrichment of Treg cells.

Recognition of antigen in the periphery following thymic egress is an evident extrinsic cue that could reshape the antigen-specific repertoire of T cells. Antigenic stimulation of Tconv cells without inflammatory cues has been well documented to promote tolerance by forcing the deletion or functional inactivation of such cells in some systems [506]. However, a host of autoreactive cells continue to persist in the periphery and can be reactivated upon Treg removal [19,186], indicating that Tconv antigen recognition primarily serves to raise the activation threshold for an autoreactive Tconv cell rather than to ablate its functional capacity. From the Treg perspective, TCR stimulation at regional SLOs [221,225,226] enables these cells to differentiate from a "central" (cTreg) phenotype

and adopt an "effector" (eTreg) program at steady state [224], the latter of which is required to control Tconv cells. Notably, it is known that cognate self-antigen in the prostate dLN similarly alters the activation status of C4/I-A^b-specific MJ23 Treg and Tconv cells at steady-state (Figure 11 and [70]). This result implies that peripheral antigen recognition may serve to qualitatively boost Treg activation and function in contrast to its potential inhibitory role for Tconv cells. A recent preliminary report demonstrated that peripheral expression of a model self-antigen in the lung enabled preferential expansion of antigen-specific Treg over Tconv cells following local injury [507], despite that the antigen is not expressed in the thymus for Treg selection during development [97], implying some level of preferential Treg selection, retention, or expansion following antigen recognition in the periphery.

Antigen recognition may also serve to quantitatively refine the pre-existing number of Treg and Tconv cells of a given specificity. It's been well-documented that pTreg induction readily occurs at barrier sites in response to tissue-expressed, commensal-derived, or food antigen [152,153,172,174,179-181,427,429], which likely acts to simultaneously divert Tconv cells away from pathogenic cell fates and quantitatively boost the number of antigen-specific Tregs in the system. Interestingly, in a setting of pregnancy where the fetus expressed an antigen that the mother had never been exposed to, the precursor population of antigen-specific T cells became more Treg-dominated over time in the draining LN throughout gestation, but reverted back to the baseline population dominated by Tconv cells following birth [428]. Notably, these findings align with our observation that removing peripheral C4/I-A^b antigen may alter the Treg/Tconv ratio and response of antigen-specific T cells (Figure 35). Taken together, these findings suggest that active antigen sensing in the steady-state periphery can simultaneously increase the number of antigen-specific Treg cells, decrease the number of antigen-specific Tconv cells, and alter the cell state of both

populations. Thus, antigen-specific tolerance is likely conferred via two sequential modalities: 1) the degree of self-antigen reactivity in the thymus during development predicts the likelihood of autoreactivity in the periphery and creates a numeric Treg/Tconv setpoint, 2) recognition of agonist ligand, or lack thereof, in the steady-state periphery refines the initial setpoint to effectively allow for a dynamic and adaptable definition of self or nonself.

The operation of such a tiered system of antigen-specific tolerance must be reconciled with arguments regarding ontogeny and context. Aire expression is required only for the first 3 weeks of life in a mouse to maintain tolerance [135], and Treg cells that arise as early as the first two weeks of life are sufficient to prevent autoimmune disease [136,137], suggesting that an early-life setpoint is critical for sustained immune tolerance. While it is currently unknown when C4/I-A^b-specific Treg and Tconv cells temporally egress from the thymus, it is likely that a wave of Treg development occurs early in life given their dependency on Aire [102]. If this is the case, how might the C4/I-A^b-specific Treg setpoint recover if it is reshaped by peripheral antigen, as suggested in our study (Figure 35)? In female mice, which have thymic development of C4/I-A^b-specific Treg cells but lack antigen in the periphery [102], it may be that the C4/I-A^b-specific T cell population is more prone to mount a response to *Lm[C4]* than that in male mice which have peripheral antigen. If this extends to other "cryptic" antigens that are not expressed in the thymus but are expressed later in life, such as puberty-dependent or fetal antigens, it implies that there exists a temporal window of autoimmune susceptibility before the antigen-specific T cell population has been "trained" on the novel antigen. Finally, both our and other studies have observed that antigen expression in the inflammatory context of a pathogen creates a Tconv-dominated of antigen-specific T cells in the periphery (Figure 16 and [220]), suggesting that a similar temporal window for autoimmune development may exist after such an inflammatory event. In this regard, we found that C4/I-A^b-

specific T cells could infiltrate the prostate of wild-type mice following a repeated challenge with *Lm[C4]* (Figure 36). Further exploration of this dynamic window of tolerance may reveal novel insights into how autoimmunity can be initiated within a repertoire that is not pre-disposed to autoimmune development, which is predicted to enable unique therapeutic development in cancer biology.

DISCUSSION OF THESIS

&

FUTURE DIRECTIONS

In this thesis, we set out to define the role of a single self-derived peptide and T cell antigen specificity in conferring tolerance to the host, determine the relevant cellular players coordinating tolerance to individual antigens, and elucidate the mechanisms by which self-reactive T cell responses are selectively controlled while foreign-directed responses are simultaneously mounted. We tackled these questions by studying monoclonal and endogenous polyclonal T cell specificities reactive to distinct self-derived and pathogen-derived antigens. C4/I-A^b-specific T cells, an endogenous population of lymphocytes specific for the C4 peptide antigen derived from the prostatic protein Tcaf3, populate both the Treg and Tconv compartments in wild-type mice and require Aire-mediated expession of Tcaf3 protein in the thymus to develop into the Treg lineage [102]. F1/I-A^b-specific T cells exist as Treg and Tconv cells in mice in a similar manner, and recognize a second Tcaf3-derived peptide termed F1. Importantly, both C4/I-A^b- and F1/I-A^b-specific T cells infiltrate the prostates of *Aire*$^{-/-}$ mice, implicating these specificities as potential mediators of autoimmune disease (Figure 1). Here, we summarize our findings using unique mouse models with a set of cutting-edge experimental techniques, and attempt to synthesize the data into working models with an emphasis on outstanding questions.

Regulatory T cells enforce self-nonself discrimination by constraining conventional T cells of matched self-specificity during infection

To define the role of selection on a single self-antigen in tolerance and autoimmunity, we generated and characterized *C4*$^{-/-}$ mice (also termed *Tcaf3(C4)*$^{-/-}$), which harbor a deletion in the germline region of *Tcaf3* that encodes the C4 peptide but retain expression and presentation of the F1 peptide (Figure 2). Tetramer analysis of endogenous C4/I-A^b-specific $CD4^+$ T cells revealed that both *C4*^{WT} (wild-type) and *C4*$^{-/-}$ mice have the same number of cells in the pre-immune and

post-immune repertoires – approximately 24 and 1000 cells respectively – suggesting that selection on C4 does not prune the number of antigen-specific T cells in the periphery (Figures 3 and 4). Following immunization, C4/I-A^b-specific T cells were a mix of both Treg and Tconv cells in $C4^{WT}$ mice but heavily populated the Tconv compartment in $C4^{-/-}$ mice, indicating that selection on C4 is required to select a fraction of cells into the Treg lineage and to mount a Treg-biased immune response. $CD4^+$ T cell transfer from $C4^{-/-}$ mice into lymphodeplete hosts resulted in prostate-directed T cell infiltration of C4/I-A^b-specific and polyclonal T cells and tissue destruction in recipient mice (Figures 5 and 6), demonstrating that T cell selection on this single peptide is the sole determinant of tolerance or autoimmunity, and cannot be controlled by all the other Treg cell specificities in this setting. Lineage-tracking transfers showed negligible pTreg conversion amongst C4/I-A^b-specific T cells (Figure 7), and experiments with Bim-deficient mixed bone-marrow chimeras confirmed that selection on C4/I-A^b has a minimal impact on C4/I-A^b-specific T cell deletion (Figure 8). Nude recipients grafted with $C4^{-/-}$ thymi did not develop spontaneous prostatitis (Figure 9), implying that C4/I-A^b-specific T cells may only become dangerous in distinct settings or following certain triggers. Finally, we identified and characterized two clones found in the ocular lesions of $C4^{-/-}$ mice (Figure 10), extending our findings to a second autoimmune organ.

To determine how tolerance to the C4/I-A^b antigen is conferred, we utilized a model of infection using the pathogen *L.monocytogenes*, engineered a stain to express the C4 peptide (Figure 12), and generated $C4^{\Delta TEC}$ mice with a conditional deletion of C4 peptide only in the thymus. Sustained polyclonal Treg ablation of thymectomized mice resulted in rapid fatal autoimmunity, indicating that Treg-mediated control is an ongoing process, and infection of with *Lm* did not prevent C4/I-A^b antigen recognition in the prostate by MJ23 T cells (Figure 11). $C4^{\Delta TEC}$

mice did not develop spontaneous prostatitis at steady-state or following various systemic immune challenges (Figures 14 and 15), indicating that polyclonal Treg cells and bystander mechanisms of Treg-mediated tolerance are sufficient in settings without elevated levels of antigen. Infection of $C4^{\Delta TEC}$ mice with *Lm[C4]* resulted in rapid fulminant autoimmunity while infected $C4^{WT}$ mice were completely protected (Figures 13, 16, and 17), and protection was dependent on Treg cell control rather than Tconv inactivation (Figure 18). Divergent responses to the C4/I-A^b antigen were autonomous, with no impact on responses to other pathogen-derived antigens (Figure 32). Infection with *Lm[F1]* did not elicit prostatitis in $C4^{\Delta TEC}$ mice (Figure 19), indicating independent regulation of tolerance to antigens within the same protein. Attempts to alter the ratio of C4/I-A^b-specific Treg and Tconv cells did not enable or prevent autoimmunity (Figures 20-22), likely due to technical limitations that prevented such manipulations from reaching the numeric tipping point. Single-cell RNA sequencing of C4/I-A^b-specific T cells in $C4^{WT}$ and $C4^{\Delta TEC}$ mice infected with *Lm[C4]* revealed that Tconv cells preferentially adopted non-proliferative or division-permissive cell states, respectively (Figure 23). C4/I-A^b-specific Treg and controlled Tconv cells in $C4^{WT}$ mice highly expressed CCR2 following infection, which was found to be required for the development of MJ23 Treg but not Tconv cells in the thymus in mixed chimeras (Figure 29). Finally, infection of LF MJ23 chimeras revealed that the non-proliferative Tconv cell state was dependent on the presence of MJ23 Treg cells (Figures 24 and 25), directly implicating C4/I-A^b-specific Treg cells in controlling potential autoimmune responses elicited by Tconv cells of matched specificity following infection.

To elucidate how C4/I-A^b-specific Treg cells were selectively conferring tolerance of Tconv cells of matched antigen specificity, we used temporal analyses, *in situ* immunofluorescent imaging, and other genetically manipulated strain of mice and *Lm*. Careful tracking of MJ23 T cell

responses in $C4^{WT}$ and $C4^{\Delta TEC}$ chimeras revealed that MJ23 Treg cells accumulated faster than MJ23 Tconv cells in mice of either genotype, implying that Treg cells are inherently more competitive than Tconv cells early in the response (Figure 26). Visualization of MJ23 Tconv cells in the LN at this timepoint demonstrated a pattern of heterologous immunity whereby some MJ23 Tconv cells were controlled by polyclonal Treg cell domains, while others required local enrichment of activated MJ23 Treg cells (Figure 27), absent which these MJ23 Tconv cells escaped control due to enhanced TCR signaling and access to antigen. Following escape, MJ23 Tconv cells readily entered the circulation and ultimately landed in the prostate (Figure 28). Tolerance was broken in $C4^{WT}$ mice with the addition of 1000 but not 100 naïve Tconv cells prior to *Lm[C4]* infection, indicating that antigen-specific Treg suppression can be overcome following the breach of a numeric threshold (Figure 30), which could also be achieved for F1/I-A^b-specific SP33 Tconv cells. Immunization or infection responses from C4/I-A^b-specific Treg and Tconv cells were slightly altered by antigen exposure prior to immune challenge (Figures 35 and 36), implying that the history of antigen encounter may alter the numeric setpoint of Treg and Tconv cells within that specificity. When either C4/I-A^b-specific or F1/I-A^b-specific Tconv cells acted as an autoimmune Driver specificity, infection with *Lm[C4+F1]* elicited a Passenger response from the other specificity, indicating active cross-talk between these cells during the initial response or at the prostate dLN (Figures 30 and 31). Finally, antigen-presentation by B cells was dispensable for autoimmune development or protection (Figure 34), suggesting that DCs may be the APC coordinating self-directed responses following infection, and C4/I-A^b-specific antibody clones were raised to identify the relevant APC subsets in future studies (Figure 33).

Taken together, this thesis supports a model in which Treg cells of matched antigen specificity are uniquely required in settings of inflammation and elevated antigen to selectively

prevent their Tconv counterparts from mounting an effective response (Figure D1). In $C4^{WT}$ mice, both Treg and Tconv cells specific for antigenic self-peptides co-exist in the repertoire, while foreign-reactive T cell specificities exist largely as Tconv cells owing to the lack of steady-state selection on agonist ligands. At homeostasis, bystander mechanisms of Treg-mediated suppression are sufficient to prevent overt activation of self-reactive Tconv cells. These bystander mechanisms continue to function in settings where fulminant Tconv cell activation thresholds might be breached – such as upon infection with a mimetope-bearing pathogen, in settings of acute lymphopenia, or in settings of inflammation and overt tissue damage – and function locally to constrain some self-reactive and pathogen-reactive Tconv cells in the system. An additional antigen-specific mechanism of Treg-mediated suppression also becomes operative in this setting, where Treg cells unilaterally outcompete Tconv cells of matched antigen specificity following initial priming by rapidly proliferating to interrupt TCR signals. In effect, this mechanism enables the selective control of self-reactive Tconv specificities while allowing those pathogen-reactive cells which escape bystander mechanisms of Treg-mediated suppression to mount productive responses against their cognate antigens. In $C4^{\Delta TEC}$ mice which have a paucity of Treg cells specific for a single self-antigen, some Tconv cells reactive to the same antigen are now able to escape bystander mechanisms of suppression in settings of inflammation and mount pathogenic responses to coordinate organ-targeted T cell infiltration and autoimmune disease.

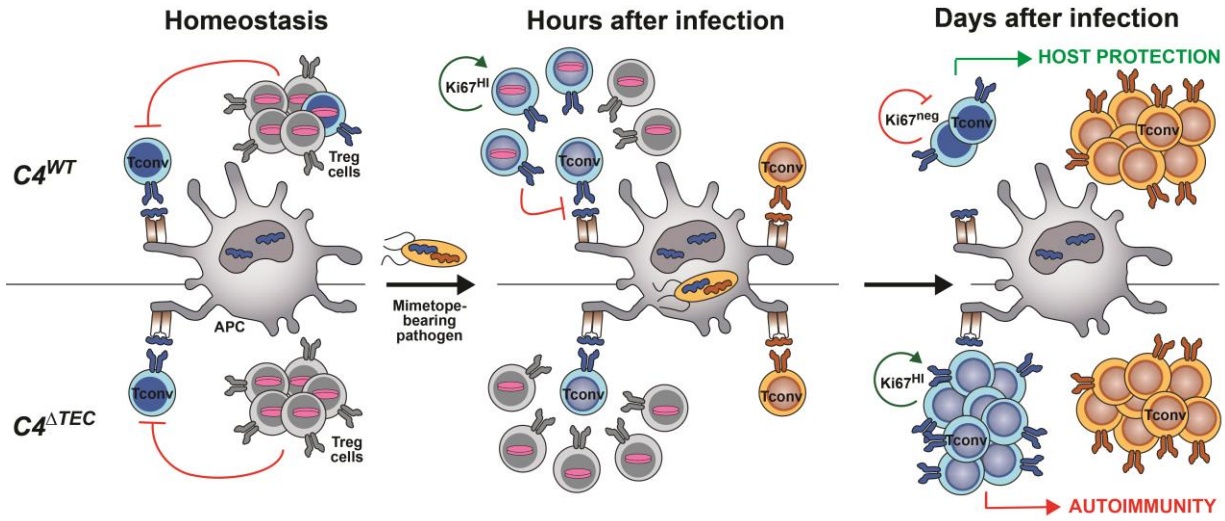

FIGURE D1. Summary of major conclusions
A normal T cell repertoire is furnished with Treg cells reactive to antigenic self-peptides (blue). Upon infection, a setting associated with increased self- and pathogen-derived peptide presentation contextualized by inflammation, self-reactive Tconv cells are initially primed but ultimately controlled by rapidly expanding Treg cells of matched specificity, while some pathogen-reactive Tconv cells escape bystander mechanisms of Treg suppression to mount a productive response (top). In a host in which Treg selection of a single T cell specificity was incomplete or otherwise lost, some self-reactive Tconv cells of matched antigen specificity properly integrate signals and give rise to a self-renewing population of Tconv cells that go on to elicit autoimmunity after the infection has been cleared (bottom).

Directed entry of the prostate following activation at distal sites

C4/I-A^b-specific Tconv cells escape Treg control to become "Driver" cells in *C4*$^{\Delta TEC}$ mice following activation by *Lm[C4]* primarily in the spleen and liver dLN. A series of events must subsequently occur to elicit prostatic T cell infiltration of a distal sterile organ (Figure D2). Following activation, Driver Tconv cells must first egress from the distal SLOs, migrate through the circulation, and end up in the prostate dLN. It is very unlikely that such cells migrate directly to the prostate given the lack of inflammation and the absence of I-A^b expession on prostatic epithelial cells that would enable antigen-directed entry. At the prostate dLN, Driver T cells must participate in an event that directs their subsequent migration specifically to the prostate and not to other target organs that share the same LNs. Such an event is most probably involves a "second

hit" of TCR stimulation dependent on self-derived C4/I-A^b antigen, given that *C4*$^{-/-}$ mice do not develop C4/I-A^b-driven prostatitis and that the only conceivable link between a C4/I-A^b-specific T cell and a prostate-derived APC vs. another APC is the C4/I-A^b antigen. At this point, for the observed outcomes of C4/I-A^b-specific and polyclonal T cell infiltration of the prostate to occur, the following conditions must be true: 1) the C4/I-A^b-bearing APC must have an intrinsic "memory" of a recent visit to the prostate, 2) the APC must have the ability to transfer such memory to the Driver T cell specificity, 3) either the APC or the Driver T cells must subsequently be able to both transfer such memory to other Passenger T cells and give them permission to enter the tissue.

The molecular basis for these reciprocal licensing events remain largely undefined save that they require the Driver specificity and depend on Driver recognition of tissue-derived cognate antigen. It is well documented that DCs and other cells within tissues adopt transcriptional programs unique from the same cells in other tissues [508,509], so it is probable that some prostate-specific transcripts such as unique integrins become upregulated on DCs following C4 peptide capture and prior to tissue egress. But a prostate-unique receptor is unlikely to transfer prostate memory to the Driver T cell since such a cell is initially agnostic of the tissue and would not express a unique ligand for the receptor, unless activated T cells express a unique ligand for every possible tissue. Thus, the molecular basis for sterile tissue memory transfer from the DC to the Driver T cell remains elusive, though we hypothesize that it may involve the direct transmission of surface proteins or transcription factor transcripts to the Driver cells. Following Driver licensing, Passenger T cells must also be directed for tissue entry. This could be orchestrated by the Driver in the prostate, by the Driver in the LN, or by the DC that licensed the Driver in the LN. A subset of Passenger T cells are probably directed into the prostate by infiltrating Driver cells via

general inflammatory chemokines that act as "beacons". This class of Passenger cell is likely to consist primarily of memory cells that had been previously activated and harbor general receptors associated with inflammatory chemotaxis, as demonstrated by LLO/I-A^b-specific infiltration of the inflamed prostate (Figure 30). If clonal populations of Passenger T cells with hallmarks of self-reactivity also exist in the prostate, it is unlikely that Driver cells in the LN are directly imparting such cells with the ability to infiltrate, since this implies a dependency on antigen recognition and Driver cells would not present antigen directly, at least to $CD4^+$ T cells. Instead, it would strongly argue for licensing from the DC. Given that the DC cannot promote tissue infiltration without the Driver, it is implied that a reciprocal licensing event occurs from the Driver T cell to the DC. We hypothesize that this involves the upregulation of costimulatory molecules and activating cytokines which function to lower the activation threshold for interacting T cell specificities. In this way, T cells with a sub-threshold level of self-reactivity at steady-state can now become activated and infiltrate the tissue. Notably, these events may happen more rapidly than the Driver cell licensing, given that a huge Passenger T cell infiltrate exists before almost any Driver cells are observed in the tissue (Figure 16). Finally, as highlighted in the Chapter 3 Discussion, the contribution of each of these populations to tissue destruction remain unknown.

Future questions to be solved center on defining the relationships between Driver T cells, Passenger T cells, and target tissue. While these topics are wide-ranging enough to build an entire research program, here we highlight some initial directions and preliminary experiments. A series of first steps would be to comprehensively define subsets within the Passenger T cell compartment and determine how their composition is shaped by the Driver specificity and tissue target. A series of tissue-specific Cre strains crossed to the *Rosa26*$^{\text{LSL-YFP}}$ strain would be used as a platform for these studies. Specifically, *Chd16*-Cre^+ *Rosa26*-LSL-YFP^+ (*Chd16*^{CreYFP}), *Ins2*-Cre^+ *Rosa26*-LSL-

YFP$^+$ (*Ins2*^{CreYFP}), and *CC10*-Cre$^+$ *Rosa26*-LSL-YFP$^+$ (*CC10*^{CreYFP}) strains would be used to express both Cre and YFP in the kidney, pancreas, or lung, respectively. Each of these proteins contains an immunodominant epitope that is presented on I-A^b for recognition by CD4$^+$ T cells [97,98], which would be used as the Driver specificity. In the first experiment, each strain would receive naive pCre/I-A^b- or pYFP/I-A^b-specific transgenic T cells and be infected with the corresponding *Lm* strain engineered to express the cognate peptide, initiating autoimmunity of the Cre-expressing organ by the transgenic Driver clone. Organ-infiltrating T cells would be subsequently isolated, stained with a barcoded tetramer to identify the Driver specificity, and subjected to scRNA and scTCR sequencing. In this way, the impact of both the Driver T cell and the targeted organ on the Passenger T cell infiltrate can be established. The resultant dataset would reveal signatures of Passenger T cell subsets that can be used to investigate their ontogeny and contribution to the anti-tissue response. Some of these subsets are predicted to overlap between organs while others are expected to remain distinct based on the nature of the antigens that they recognize. From here, downstream studies include recombinant expression and antigen screening of expanded Passenger T cell clones within subsets, *in vivo* studies of Passenger clone development and behavior, co-transfers of transgenic or retrogenic Driver and Passenger T cell clones to tack licensing and infiltration phenomena, the identification of endogenous subsets of Passenger T cells using RNA expression profiles and flow cytometry, and depletion experiments of Driver or Passenger T cell subsets following disease onset to determine their contribution to sustaining the autoimmune reaction.

A second line of inquiry would be to discern the molecular events surrounding T cell and DC licensing for organ infiltration or Passenger cell activation. This would require methods to ascertain prostate-derived DCs from other DCs within the LN. One possible avenue would be to

create a mouse that expresses a fluorescent protein or tractable surface antigen under a prostate-specific promoter such that migrating DCs would be tagged. It may also be necessary to identify which of these DCs are actively presenting C4/I-A^b antigen, which could be done using αC4/I-A^b-specific antibodies or by artificially expressing a C4-V5tag fusion peptide under the *Tcaf3* promoter (Figure 33). To capture whether Driver T cells reciprocally license DCs and identify potential molecular pathways involved, a comparative phenotypic and transcriptomic analysis could be performed using DCs from *Lm[C4]*-infected wild-type mice that had or had not received MJ23 Driver T cells prior to infection. The recently-developed uLIPSTIC system [457] could also be used to tag DCs that interact with MJ23 Driver T cells. To determine the molecular factors that enable Driver T cells to infiltrate the prostate, a similar comparative analysis could be performed for MJ23 Driver T cells isolated from the prostate dLN of $C4^{WT}$ and $C4^{-/-}$ mice; where antigen-dependent prostate licensing of MJ23 T cells is expected to occur in the former but not the latter condition. The same type of experiment could be performed for Passenger T cell clones identified in the previous paragraph by introducing such cells into mice with or without Driver T cells. Candidate molecular factors for each licensing event would be subsequently tested using genetic manipulation of the relevant cell populations to ultimately create a detailed mechanism of reciprocal licensing.

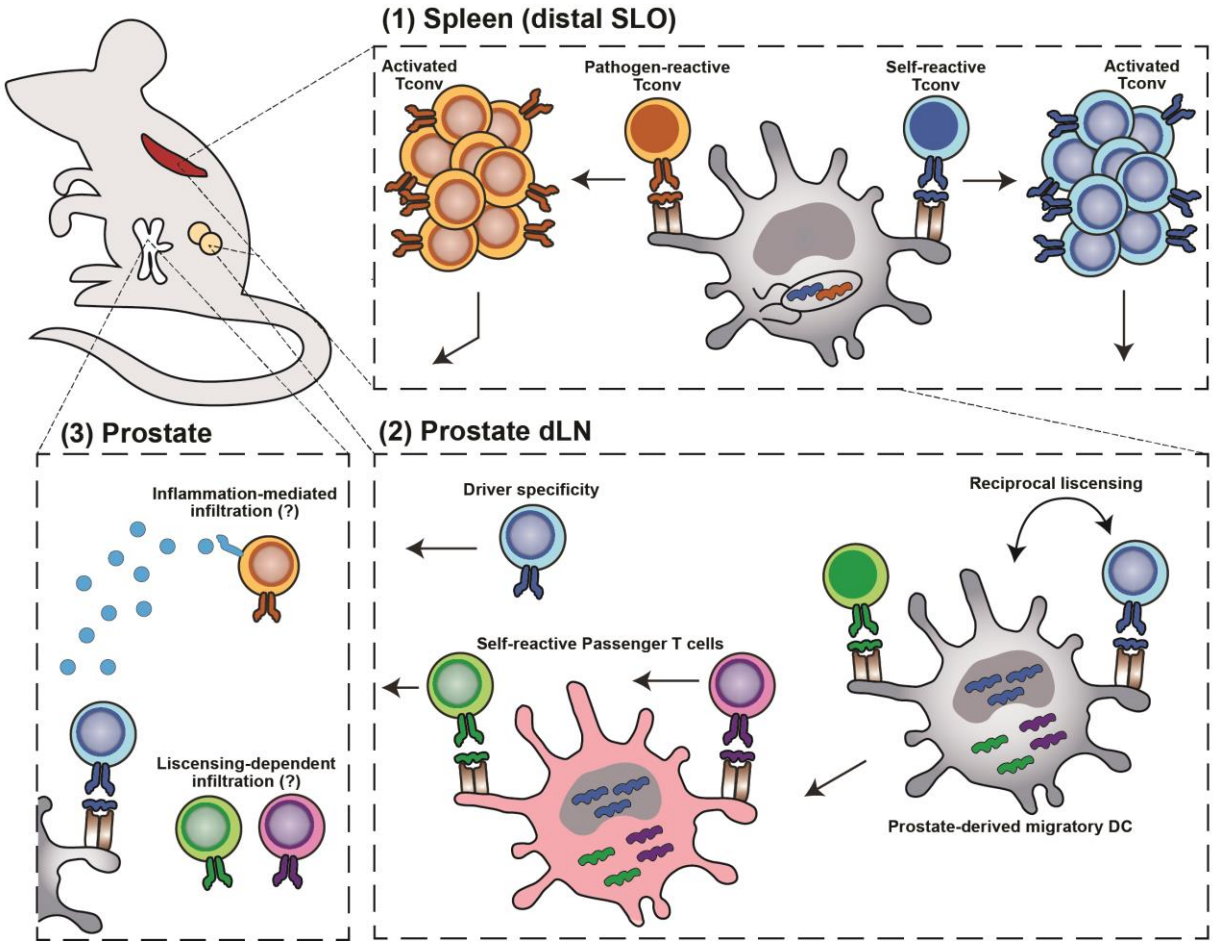

FIGURE D2. Model of autoimmune initiation by pathogen-associated epitope mimicry
In the absence of Treg cells of matched antigen specificity, self-reactive Tconv cells become activated at a distal site via cross-reactivity to a pathogen-derived epitope and enter the circulation. In the prostate-draining LN, activated clones recognize their cognate self-antigen presented on DCs migrating from the prostate. A reciprocal licensing event occurs, whereby the DC provides the self-reactive "Driver" T cell with the molecular zipcode for the prostate, and the Driver T cell enhances the activation potential of the DC. The activated DC goes on to activate other self-reactive specificities that are normally tolerant at steady-state. The Driver and Passenger T cells subsequently enter the prostate. It remains unknown if the Driver T cell actively creates an inflammatory environment and promotes tissue damage to bring in Passenger cells via chemokines, or if Passenger T cells must first receive signals from a licensed DC.

Local competition as a determinant of heterologous responses to self- and pathogen-derived antigens

In situ imaging analysis of the LN during a critical window of activation following infection revealed heterologous patterns of Tconv control or escape from Treg-mediated

suppression (Figure 27). These decisions appeared to occur in local isolation and operate through competition for activation signals with a winner-take-all result. Conceptually, these local domains are analogous in many respects to a germinal center reaction undergone by B cells in that spatially constrained lymphocytes undergo classic Darwinian selection to ensure the most useful clones rapidly accumulate and contribute to the immune response. Temporal analysis of $C4^{WT}$ and $C4^{\Delta TEC}$ mice following *Lm[C4]* infection also revealed that C4/I-A^b-specific Treg cells could constrain a response to the C4/I-A^b antigen without impacting the response to pathogen-derived LLO/I-A^b antigen (Figure 16), though the basis for this selectivity remained a mystery at the time. Given that MJ23 Tconv cells in $C4^{\Delta TEC}$ mice are essentially a surrogate for pathogen-reactive specificities, in that there is a paucity of Treg cells with matched antigen specificity in the system, the observed patterns of MJ23 Tconv cells *in situ* may be extrapolated to create a conceptually-satisfying model of self-nonself discrimination that argues for heterologous T cell responses as the mechanism of selective control (Figure D3).

Consider a three-cell scenario as the initial condition of each local microdomain: an APC simultaneously presenting self- and pathogen-derived peptides, and two Tconv cells being primed by their respective peptide. In one microdomain, local polyclonal Treg cells rapidly accumulate in the microdomain, either via proliferation following activation by other self-antigens on the APC or by stochastic enrichment. In this case, both Tconv cells receive relevant TCR signals but are deprived of subsequent signals by the Treg cells and fail to mount a fulminant response (akin to Clusters A2, S2, and S3 in Figure 27). In another microdomain, polyclonal Treg cells fail to respond but are replaced by a Treg cell specific for the same self-antigen as the Tconv cell. This Treg always finds a microdomain when polyclonal Tregs are not present as observed in the data; the mechanism remains uncertain but may involve antigen-driven enrichment or reflect

chemotactic homing in response to initial priming of the Tconv cell. Since this Treg cell has an intrinsic competitive advantage over the self-specific Tconv cell, this cell has lost the competition in this microdomain and will not mount a response. Simultaneously, Tconv cells specific for the pathogen continue to integrate and compete for activation signals and one of two outcomes will emerge from this microdomain: either the self-specific Treg cells will win and suppress both Tconv specificities, or the pathogen-reactive Tconv cells will win and prevent further activation of the self-specific Treg or Tconv cells. Competitive factors that may contribute to the outcome include the time of TCR engagement, the relative density of antigen, pre-existing surface phenotype and growth factors on either cell, and the affinity for cognate antigen, but the relative contribution of these remain undefined. When too few Treg cells specific for the self-antigen exist in the system, the competition within a given Treg-low microdomain would instead occur between the pathogen-specific and self-specific Tconv cells, with each winning in some microdomains but not others and resulting in the fulminant activation of some self-specific Tconv cells. Importantly, because the antigens do not change in either scenario, the ultimate response of the pathogen-reactive specificity does not change – the anti-pathogen response is bounded by competition with self-specific T cells without regard to the identity of such cells.

Future studies might investigate the cellular and molecular factors that scale heterologous T cell responses, antigen dominance hierarchies, and the consequence for response outcome. It is known that the number of T cells of a given specificity capable of being elicited during an immune response is related to the precursor frequency in the naïve repertoire, which was demonstrated using isolated subcutaneous immunization of single peptides in CFA [350]. Assuming no other specificities are meaningfully recruited into the response in this setting, this might be considered the maximum response threshold for a given specificity. To test whether precursor size contributes

to competitive advantage in a heterologous response, additional peptides might be added to the immunization for which new specificities of defined precursor frequencies are known, and the magnitude of the T cell responses could be compared to those of single peptide immunization. The peptides could also be linked with spacers containing cathepsin-cleavable sites to ensue presentation by the same APC and competition amongst specificities. In an orthogonal approach, the baseline endogenous T cell responses to two linked peptides could first be established, and then compared to responses where transgenic T cell clones reactive to one peptide or the other were added into the system prior to immunization. If precursor frequency plays a role, the larger specificity would mount the highest numeric response at the expense of specificities with smaller precursor pools. Antigen affinity for pMHC or cognate T cells could also play a role in establishing dominance hierarchies, and could be tested in similar experimental systems where the peptide residues are mutated within the agonist core. These responses could be measured globally by flow cytometric analysis, or locally measured using *in situ* imaging and a spatial transcriptomic approach, and the immunizing antigens could be coupled to a fluorescent reported to identify the presenting APCs and relevant microdomains. In addition to typical immune responses and autoimmune disease, elucidating the underpinnings of heterologous responses may also reveal novel and exploitable aspects of anti-tumor immunity. Intratumoral T cells reactive to tumor-expressed antigens often adopt an irreversible state of exhaustion driven by negative feedback from chronic antigen signals [510]. Approaches that enable multiple specificities to target a given tumor may reduce the activation state of all specificities through competition, allowing such cells to adopt long-lived effector cell states that are slower to reach exhaustion [511]. Relatedly, tumor cells have been shown to evolve such that they lose expression of single MHC alleles [512], a phenomenon termed “loss of heterozygosity” which is thought to result from selective pressure

imposed by T cells. While this is typically thought to be detrimental from the host perspective, given that tumor-reactive specificities that recognize antigens presented on the downregulated allele would be rendered functionally irrelevant, this scenario may enable a situation where antigen dominance constraints are removed, opening unique windows of opportunity for therapeutic intervention such as the use of checkpoint inhibitors.

A second avenue that warrants future study is the observation that MJ23 Treg cells are always found near antigen-responsive MJ23 Tconv cells when polyclonal Treg cells are not present or capable of mediating suppression. Such enrichment implies the existence of a directed migration by MJ23 Treg cells in response to initial MJ23 Tconv cell activation – analogous to firefighters responding to a call about an active fire. An unbiased approach to uncover MJ23 Treg-intrinsic factors driving enrichment, such as an *in vivo* CRISPR screen, would be laborious to execute and difficult to interpret given that both spatial and transcript information would need to be retained in the assay and not all MJ23 Treg cells in an operative system are enriched around MJ23 Tconv. Single-cell RNA sequencing of responding C4/I-A^b-specific cells in the spleen following *Lm[C4]* infection revealed high expression of the chemokine receptor CCR2 on both Treg cells and Tconv cells that populated the "suppressed" Cluster 5 enriched in $C4^{WT}$ mice (Figure 23), suggesting that it may play a key role during infection to coordinate Tconv control. Our studies attempted to discern the role of CCR2 during infection using a CCR2-deficient MJ23 transgenic mouse line, but we unexpectedly found that CCR2 was required for MJ23 Treg development in the thymus (Figure 29), and could thus not be selectively removed from MJ23 Treg cells during infection. A future study could definitively test the role of CCR2 using *Foxp3*-CreERT2 and *Ccr2*-floxed alleles. In one approach, *Foxp3*-CreERT2$^+$ x $Ccr2^{f/f}$ would be treated with tamoxifen prior to infection with *Lm[C4]* to remove CCR2 on all endogenous Treg cells. Depletion would continue

to occur for the first few days of infection, since this is the temporal window for Treg-mediated suppression. If CCR2 is important for mediating this process, mice should develop prostatic T cell infiltration by 14 days post infection as observed for *C4*$^{\Delta TEC}$ mice. It is also possible that these mice would present with autoimmunity in multiple target organs, given that other self-reactive specificities which may be activated by infection will also lack CCR2 in the Treg compartment. In a complementary approach, low-frequency chimeras could be established using MJ23^{+} x *Foxp3*-CreERT2^{+} x *Ccr2*$^{f/f}$ marrow. In this system, MJ23 Treg cells would seed the periphery of the host and CCR2 could be removed just prior to infection. In this system, MJ23 Treg and Tconv positioning and phenotypes could be compared between tamoxifen-treated and control mice following *Lm[C4]* infection using both imaging and flow cytometry-based approaches.

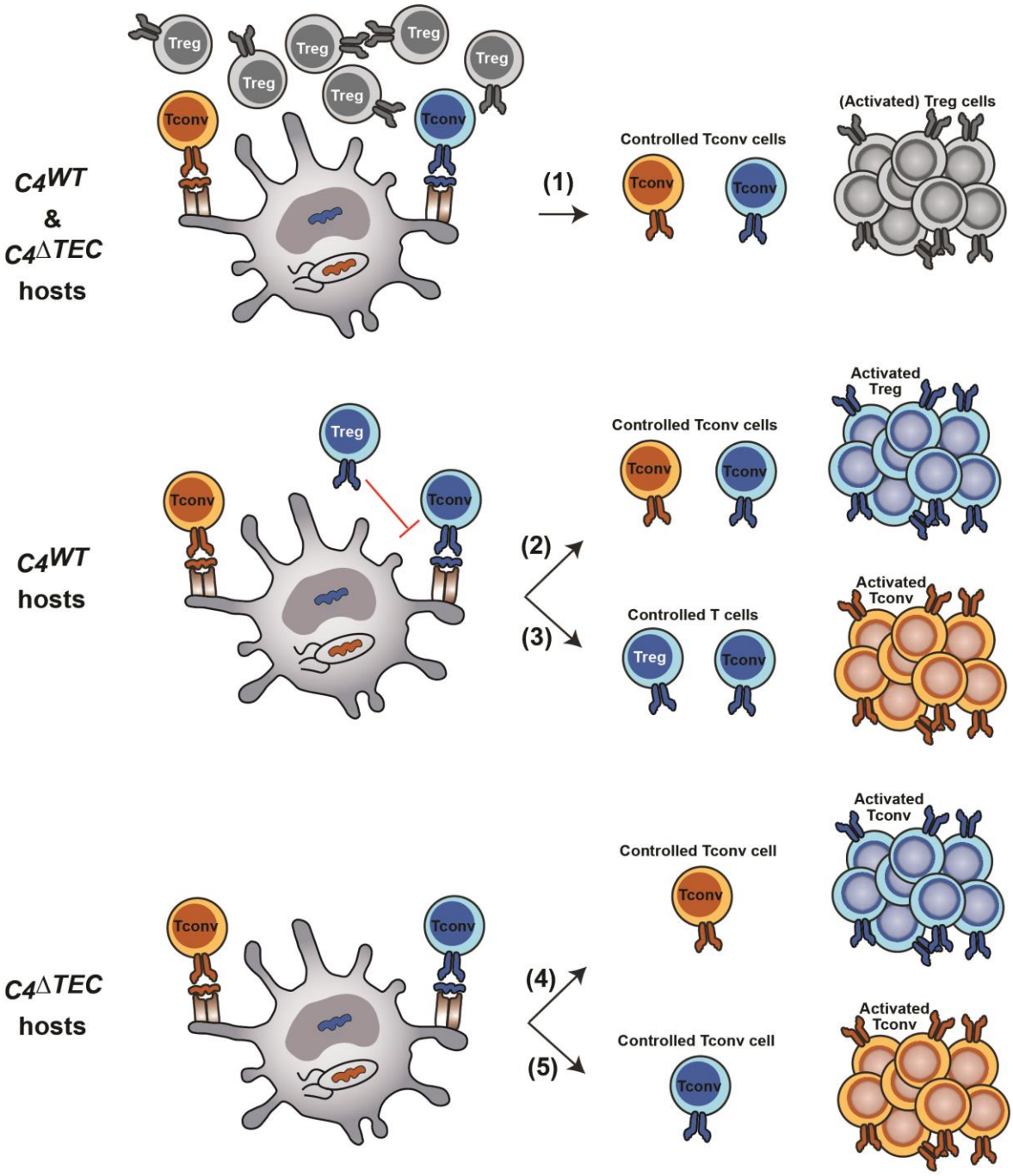

FIGURE D3. Expected patterns of heterologous immunity and antigen dominance
Upon infection, the "choice" for an individual Tconv cell to mount a response is decided in microdomains and is dependent on neighboring T cell specificities. In microdomains containing either a high density or activated polyclonal Treg cells, such Treg cells outcompete other Tconv cells for activating resources and effectively control all Tconv cells via bystander mechanisms of suppression (1). In a wild-type host where self-reactive Treg and Tconv cells co-exist alongside pathogen-reactive Tconv cells, either the self-reactive Treg wins the local competition

FIGURE D3, continued
to control the Tconv of matched specificity and the pathogen-reactive Tconv cell (2), or the pathogen-reactive Tconv cell outcompetes the self-reactive Treg and Tconv cells (3). Notably, the self-reactive Tconv cell can never outcompete the Treg cell of matched specificity, so it will always be controlled via bystander Treg suppression, antigen-specific Treg suppression, or competition with the pathogen-reactive specificity. In the absence of a self-reactive Treg specificity, either the self-reactive Tconv (4) or the pathogen-reactive Tconv (5) ultimately respond, effectively depriving the other of activating resources. In this way, the presence or absence of the self-reactive Treg cell does not impact the response of the pathogen-reactive Tconv cell because the self-reactive cells occupy the same dominance hierarchy.

Signal integration events of Tconv cell activation and temporal windows for Treg-mediated suppression

Treg-mediated suppression of Tconv cells does not operate by preventing the initial priming and activation of Tconv cells, revealing the existence of a temporal window in which all mechanisms of constraint operate. To model this window in both space and time, the kinetics of the Tconv and Treg responses will first be considered. Following *in vivo* exposure to activating ligand, reactive Tconv cells do not undergo cell division for the first few days, but accumulate very rapidly and proliferate many times over in the subsequent hours [454,455]. During this lag period, Tconv cells make long-duration contacts with APCs presenting cognate antigen [513]. Furthermore, persistent antigen is necessary for a fulminant Tconv response to occur, without which cell division rapidly ceases [450]. In contrast, antigen-specific Treg cells accumulate earlier than Tconv cells of matched specificity (Figure 26) but the magnitude of this response is smaller than what might occur for a Tconv cell after the lag period. Accordingly, Treg cells are much more motile within the SLOs and make short-duration contacts with APCs [453]. Taken together, these observations propose a model in which Tconv cells spend a prolonged period of time integrating activation signals to instruct a single and substantial bursting event, while Treg cells accumulate in a linear fashion via rapid signal integration and small clonal bursts. Supporting this notion, one study

demonstrated that active TCR signalling is antagonistic to proliferation, and that T cells disengage from APCs prior to proliferation [514]. Therefore, both bystander and antigen-specific mechanisms of Treg control would operate during this lag period by depriving Tconv cells of activation signals through competition (Figure 4D).

Consider an APC-defined microdomain with co-presentation of self- and pathogen-derived antigens very early after infection. Tconv cells reactive to either antigen arrive in the microdomain with a basal state of activation – this may be higher or lower depending on previous antigen exposure or memory status, but would be relatively comparable between two naïve Tconv cells. Each cell makes contact with antigen and begins integrating TCR-dependent activations signals. From this point until the end of signal integration and the Tconv bursting event, antigen-specific mechanisms of Treg suppression can begin to operate. A self-specific Treg cell may enter the microdomain and rapidly proliferate, causing interruption of TCR signaling in the Tconv cell of shared antigen specificity, which becomes more frequent as the Treg cells continue to accumulate. These Treg cells have effectively deprived self-specific Tconv cells of a critical signal integration component without impacting those Tconv cells reactive to the pathogen, and those Tregs that stay in the microdomain will continue to operate in this fashion. Over time, antigen-independent secondary activation signals will begin to appear in the microdomain, including costimulatory molecule upregulation on the APC, local IL-2 production by the ligated pathogen-reactive Tconv cell, and other lineage-instructing soluble factors. Bystander mechanisms of Treg control will become operative during this "second phase" of signal integration that may dampen activation signals via costimulatory masking or stripping, IL-2 hoarding, and secretion of tolerogenic molecules. This tug-of-war between activating and suppressive factors will dictate whether the

pathogen-reactive cell will undergo a large clonal burst upon disengaging the APC or fail to mount a response.

Two major unknowns in this model are 1) the translation of each activation signal to the bursting response and 2) the impact of signal interruption on the Tconv cell state. Activation signals could be strictly additive, where all signals linearly sum to instruct both the magnitude of the burst and the differentiation state adopted in the progeny. The propensity for a given $CD4^+$ T cell to differentiate into an effector or follicular-helper is thought to depend on both TCR signal strength and IL-2 availability [515], which could fit with an additive model of signal integration. Alternatively, each class of activation signal could instruct a different aspect of the response, implicating the existence of a hierarchy of signals that non-redundantly contribute to host protection. Given that intracellular signaling circuits differ between well-established activation signals [270,516], and that the differentiation lineage of a single specificity can be instructed by the environment and pathogen [517,518], it is unlikely that the signals are strictly additive. In this regard, one study [47] carefully manipulated the strength and duration of TCR signaling, and the concentration of IL-2, in OT-II Tconv cells expressing a Nur77 TCR signaling reporter to uncouple these events. Their findings were two-fold: 1) TCR signal strength instructs the number of divisions a cell will undergo within 24hrs of TCR engagement, 2) IL-2 does not impact the number of divisions a given cell can undergo but rather increases the number of cells that can divide. These observations, though limited, argue that IL-2 may function to lower the threshold for proliferation while TCR signal strength instructs sustained division.

C4/I-A^b-specific Treg cells prevented both the accumulation and memory formation of C4/I-A^b-specific Tconv cells, but such Tconv cells retained the ability to upregulate a Th1-like short-lived effector program (Figure 23), suggesting that TCR signaling in Tconv cells may be

crucially important for the T cell burst and memory consolidation phases but expendable for their differentiation program. Testing such a hypothesis would require a system in which proliferation could be measured independent from differentiation. One potential avenue may employ a recently-developed mouse model where endogenous T cells express a fate-mapped allele following multiple rounds of cell division [519]. Here, proliferation-experienced and non-accumulated Tconv cells within a given specificity could be compared to uncouple the activation signals driving proliferation from other differentiation signals. To determine the potency of antigen-specific Treg suppression compared to other bystander mechanisms, it will be important to determine how TCR signal interruption impacts the Tconv cell response. One possibility is that the activation state of a Tconv cell slowly decreases following TCR interruption, indicating that Treg cells of matched specificity must continually compete for antigenic signals to enable constraint. Alternatively, the transient TCR signaling loss may rapidly return the Tconv cell to a basal state, in which case a few interruption events may have a large effect on constraining the response. One study used intravital imaging to compare antigen-specific Tconv cells that had formed stable or transient contacts with APCs in the LN [520]. In this model, nuclear localization of NFAT remained stable for a period of time following APC disengagement, suggesting that T cells harbor "memory" of antigen recognition. Despite this, NFAT failed to promote expression of the effector molecule IFNγ upon ligand disengagement, suggesting that prolonged TCR signals may impart a different differentiation program than short serial engagements. Another study [521] employed a CAR T cell model that had been engineered to acutely cease TCR signal transduction upon exposure to light, and observed that TCR signal interruption as short as 15 minutes was enough to completely abrogate the phosphorylation or gene expression of activation molecules including Erk, Fos, and NFAT, suggesting that transient Treg-mediated interruption of antigenic signals may be enough to

force Tconv cells of matched specificity into sub-optimal activation states. Fully testing the effect of signal interruption *in vivo* will likely require a novel mouse model engineered with a Dox-inducible negative regulator of TCR signal transduction, such as a kinase-dead Zap-70 molecule. In this system, TCR signal transduction could be transiently and temporally interrupted during infection with the addition of Doxycycline, which would trigger short-lived production of a molecule that would compete against endogenous Zap-70 to attenuate TCR signal transduction for a short time. An alternative approach may be a FRET-inspired system, where the addition of a small molecule would prevent the association of two molecules involved in TCR signal transduction, such as the association of TCR with the CD3 signaling complex.

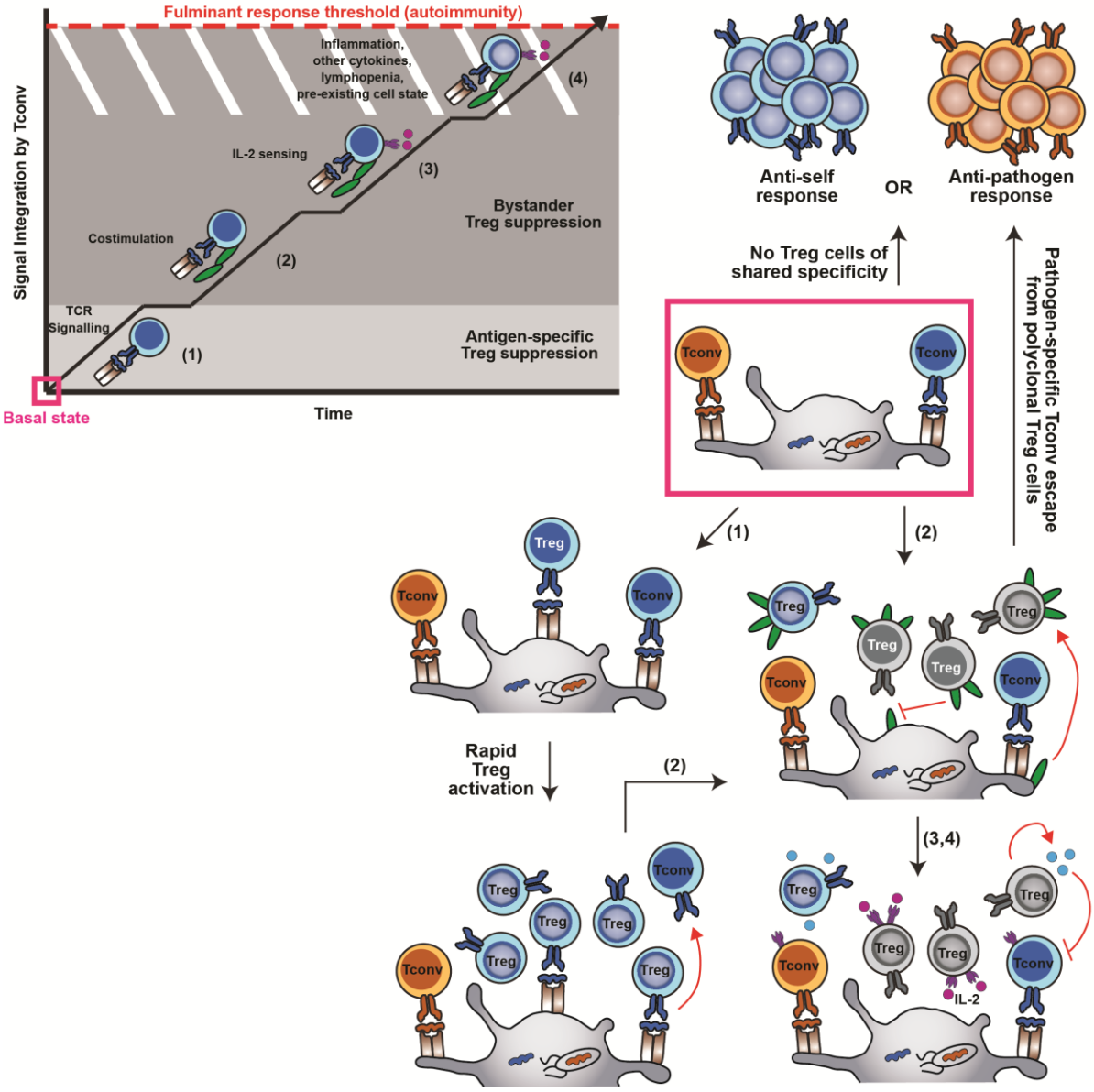

FIGURE D4. Model of Tconv signal integration events required for activation and autoimmunity

(Left) Upon ligand recognition on an APC, a Tconv cell begins propogating TCR signal events that are amplified by concurrent ligation of costimulatory molecules. The Tconv cell begins prodcing IL-2 and upregulating the high-affinity receptor CD25 to continue boosting activation signals and the prolifeation potential. Other known and unknown factors ultimately determine the extent to which the Tconv cell will differentiate and which effector and memory lineages it will give rise to, including previous antigen encounter, availabiliy and identity of available cytokines, and other positive or negative accesory signals in the environment. (Right) Various mechasisms of Treg-mediated suppression can operate at each stage of Tconv activation to disrupt or attenuate signal integration and repress the response. Bystander mechanisms of Treg suppression can operate in the vacinity of the Tconv cell and the APC to effectively raise the

FIGURE D4, continued
response threshold for the Tconv cell, denoted by (2), (3), and (4), while an antigen-specific mechanism of Treg suppression operates at the level of the TCR/pMHC (1) to attenuate TCR signalling in Tconv cells of matched specificity. At this point, Antigen-specific Tregs will act as polyclonal Tregs and compete with other neighboing Tconv specificities, which will control such Tconv cells in some cases but not all. Notably, other factors such as Tconv cell memory or anergy can function to raise or lower the basal state, respectively.

Antigenic memory and antigen-specific Treg and Tconv setpoints

C4/I-A^b antigen expression in the thymus during T cell development was the sole determinant of whether mice developed prostatic T cell infiltration following *Lm[C4]* infection. In effect, thymic selection on C4/I-A^b served to both increase the number of antigen-specific Tregs and decrease the number of Tconv cells in the periphery during an inflammatory response to establish an antigen-specific "setpoint", which enabled Treg cells to locally compete with and constrain Tconv cells of matched specificity (Figure D5). In male mice, C4/I-A^b-specific Treg and Tconv cells that exit the thymus continue to have access to the same self-derived ligand in the prostate dLN following puberty and continuing throughout the life of the mouse. The consequence of this peripheral antigen recognition on the C4/I-A^b-specific Treg/Tconv setpoint remains understudied. Notably, TCR expression on polyclonal Treg cells in the periphery endows such cells with a proliferative effector (eTreg) phenotype [225,226,519], suggesting that peripheral antigen ligation may serve to bolster the number or responsive capacity of C4/I-A^b-specific Treg cells and enhance autoimmune protection. Recognition of peripherally-expressed antigen by Tconv cells at steady-state has been shown to both numerically prune and render such cells hyporesponsive to immune challenge [522], further altering the antigen-specific setpoint. Furthermore, a population of Treg cells reactive to an epitope derived from the pathogen *M. tuberculosis* is completely lost from the peripheral repertoire following primary infection [220], implying that the context of antigen

recognition is likely a key determinant for the setpoint. A biological system with fluid tolerogenic setpoints may have deliberately evolved to navigate constant changes to the host environment. Initial education of the T cell repertoire first occurs in the thymus, where it must attempt to optimize for reactivity to foreign peptides while remaining completely agnostic of such antigens. While this process is remarkably efficient given receptor complexity and the nature of the directive, some specificities that would be protective against pathogens are likely to be sorted into the "tolerance bin" as collateral. Furthermore, mature T cell specificities reactive to foreign peptides derived from commensal microbes, food, and innocuous environmental antigens – many of which are constantly in flux throughout the life of the organism – need to be tolerized upon exiting the thymus. While specialized APC subsets mediate parts of this process via pTreg induction in the digestive tract [298], the principle of setpoint fluidity remains the same: an antigen-specific setpoint favoring the Tconv response upon thymic egress can be re-tuned for tolerance based on homeostatic antigen cues in the periphery. Likewise, a tolerant antigen-specific setpoint exiting the thymus could be further reinforced by recognition of innocuous antigen at homeostasis or re-established as a responsive setpoint following repeated recognition during inflammation.

Future studies will be required to determine the relative contribution of the thymus, homeostatic periphery, and inflamed periphery to the establishment of antigen-specific setpoints. Although C4/I-A^b antigen acts to set a critical tolerogenic setpoint in the thymus, it remains unclear whether this mechanistic arm operates throughout life to continually add to the peripheral Treg pool or is primarily required during a distinct temporal window. In this regard, it is know that expression of Aire is only required for the first three weeks of the life of a mouse to maintain tolerance [135], and that Treg cells which arise in the first two weeks of life are uniquely capable of preventing Aire-dependent or Foxp3null-induced disease [136,137]. Since C4/I-A^b is an Aire-

dependent peptide, may be that most antigen-specific Treg cells arise early in life and are sufficient to prevent *Lm[C4]*-induced autoimmunity. To test this, the existing *Aire*-CreERT2 strain [523] could be interbred with the $C4^{\Delta TEC}$ line to establish *Aire*-CreERT2^{+} x $Tcaf3(C4)^{f/f}$ mice. In these mice, the C4 peptide could be temporally removed from the thymus upon tamoxifen administration, which would be administered to different groups of mice at various timepoints post-birth. Comparing prostatic infiltration amongst groups following *Lm[C4]* infection will determine how long the peptide must be expressed in the thymus to confer tolerance and thus when the thymic antigen-specific setpoint is established.

To understand the role of peripheral C4/I-A^b antigen is coordinating the Treg/Tconv setpoint, a series of studies could be done comparing cells from male mice to female mice, which have and lack expression of antigen in the periphery, respectively. As an orthogonal approach, castration could be used to remove the C4 antigen from the periphery of male mice, as has been demonstrated previously [70]. First, the endogenous C4/I-A^b-specific Treg and Tconv responses to *Lm[C4]* infection could be compared in aged mice between the groups. If the response is greater in mice lacking peripheral antigen, it would imply that the setpoint can be influenced by memory of antigen at steady-state. To determine how peripheral antigen impacts the responses in both the Treg and Tconv compartment against the pathogen, MJ23 Treg and Tconv cells from *Lm[C4]*-infected male and female mice could be sorted following challenge and subjected to RNA sequencing, where a comparison of differentially regulated genes between groups could be used to generate hypothesis about how antigenic memory programs either compartment. To understand whether peripheral changes in the setpoint are consequential for tolerance, a series of transfer experiments could be performed using male and female donor cells into hosts that express the antigen in the periphery as a target for autoimmunity. The use of castrated mice would be

especially useful in this third set of experiments, as non-tolerized specificities reactive to prostatic antigens other than C4 may exist in the repertoire of female mice and account for observed autoimmunity.

A primary infection with the *Lm[C4]* pathogen does not cause a break in tolerance of wild-type mice. However, the proportion of C4/I-Ab-specific Treg cells appears to decease in the periphery of such mice over time (Figure 16) in a manner that is reminiscent of *M.tuberculosis*-reactive Treg cells [220]. It may be advantageous to the host to "recalibrate" the antigen-specific setpoint following infection as a means of giving pathogen-reactive T cell specificities that failed to mount a response a "second chance" upon subsequent inflammatory challenge. To determine whether primary infection impacts the C4/I-A^b setpoint and define the consequence on tolerance, a series of iterative infection experiments can be performed in wild-type mice that are normally tolerant. Here, mice would be infected two and three times and the C4/I-A^b-specific T cell response would be compared against mice challenged with a single infection. Since a "recalibration" window may be temporally-dependent, such that the setpoint recovers after a period of time, the interval between infections would also be varied in a separate series of experiments. Finally, given that pre-existing immunity to the pathogen may impact the availability of C4 peptide in secondary and tertiary infections, mice could be infected with a different set of pathogens that all express recombinant C4 peptide. A tolerogenic break in any group would indicate that the setpoint and thus tolerance to defined self-antigens can be modulated by antigen contextualized with inflammation; a first-of-its-kind finding that may be selectively leveraged to overcome barriers to anti-tumor immunity.

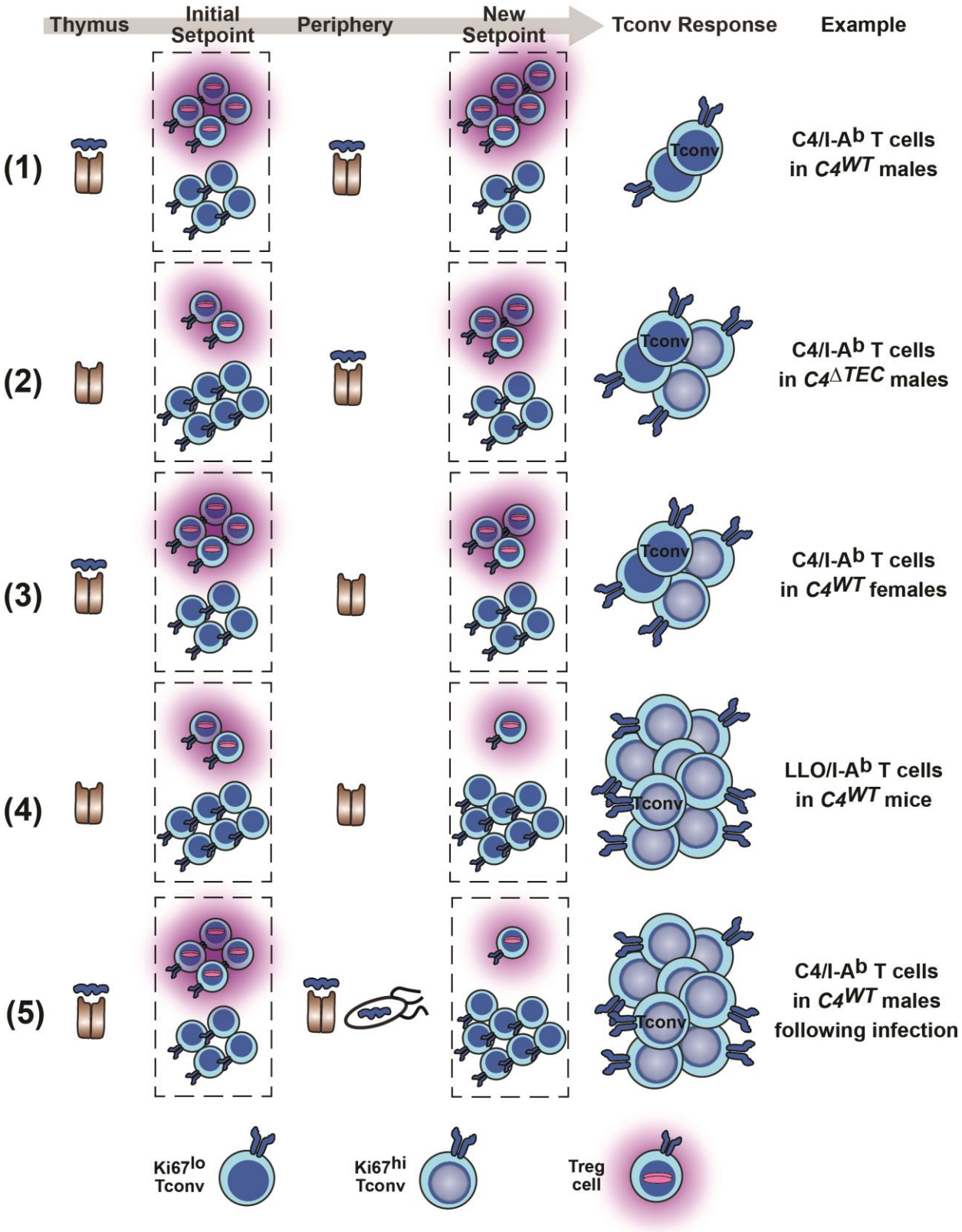

FIGURE D5. Potential modes of establishing antigen-specific Treg and Tconv setpoints

FIGURE D5, continued
For a given anigen specificity, the decision to mount or suppress a response depends on the number of Treg cells in relation to the number of Tconv cells during inital signal integration events. This "setpoint" is at least partially established by the preexisting number of Treg and Tconv cells in the pre-immune repertoire. In this model, the thymus is the primary mode by which the initial setpoint is established. Following thymic egress, antigen-specific populations are modulated by peripheral antigen recgonition and the context of antigen to establish new setpoints, which likely retain a degree of plasticity thoughout life. The new setpint could be established via quantitative actions such as pTreg induction, tTreg expansion, or Tconv deletion, but may also be established qualitatively by frocing Treg cells into effector states that enhance suppression. Ultimately, the degree of Tconv responsiveness is inimately linked to the setpoint at the time of immune challenge

REFERENCES

1 Mackay, I. R. Travels and travails of autoimmunity: a historical journey from discovery to rediscovery. *Autoimmun Rev* **9**, A251-258, doi:10.1016/j.autrev.2009.10.007 (2010).

2 Ehrlich P, M. J. Ueber Hämolysine. *Berl Klin Wochenschr* **38**, 251–257 (1901).

3 Donath J, L. K. Ueber paroxysmale Hämaglobinurie. *Munch Med Wochenschr* **51**, 1590–1593 (1904).

4 Freund, J., Stern, E. R. & Pisani, T. M. Isoallergic encephalomyelitis and radiculitis in guinea pigs after one injection of brain and Mycobacteria in water-in-oil emulsion. *J Immunol* **57**, 179-194 (1947).

5 FM, B. The Clonal Selection of Acquired Immunity. *London: Cambridge University Press* (1959).

6 Burnet, F. M. The impact of ideas on immunology. *Cold Spring Harbor Symp Quant Biol* **32** (1967).

7 Jerne, N. K. Summary: Waiting for the end. *Cold Spring Harbor Symp Quant Biol* **32**, 591 (1967).

8 Lederberg, J. Genes and antibodies. *Science* **129**, 1649-1653, doi:10.1126/science.129.3364.1649 (1959).

9 Bretscher, P. & Cohn, M. A theory of self-nonself discrimination. *Science* **169**, 1042-1049, doi:10.1126/science.169.3950.1042 (1970).

10 Jerne, N. K. The common sense of immunology. *Cold Spring Harbor Symp Quant Biol* **41**, 1 (1976).

11 Jenkins, M. K., Pardoll, D. M., Mizuguchi, J., Chused, T. M. & Schwartz, R. H. Molecular events in the induction of a nonresponsive state in interleukin 2-producing helper T-lymphocyte clones. *Proc Natl Acad Sci U S A* **84**, 5409-5413, doi:10.1073/pnas.84.15.5409 (1987).

12 Jenkins, M. K. & Schwartz, R. H. Antigen presentation by chemically modified splenocytes induces antigen-specific T cell unresponsiveness in vitro and in vivo. *J Exp Med* **165**, 302-319, doi:10.1084/jem.165.2.302 (1987).

13 Jenkins, M. K., Pardoll, D. M., Mizuguchi, J., Quill, H. & Schwartz, R. H. T-cell unresponsiveness in vivo and in vitro: fine specificity of induction and molecular characterization of the unresponsive state. *Immunol Rev* **95**, 113-135, doi:10.1111/j.1600-065x.1987.tb00502.x (1987).

14 Janeway, C. A., Jr. Approaching the asymptote? Evolution and revolution in immunology. *Cold Spring Harb Symp Quant Biol* **54 Pt 1**, 1-13, doi:10.1101/sqb.1989.054.01.003 (1989).

15 Matzinger, P. Tolerance, danger, and the extended family. *Annu Rev Immunol* **12**, 991-1045, doi:10.1146/annurev.iy.12.040194.005015 (1994).

16 Medzhitov, R., Preston-Hurlburt, P. & Janeway, C. A., Jr. A human homologue of the Drosophila Toll protein signals activation of adaptive immunity. *Nature* **388**, 394-397, doi:10.1038/41131 (1997).

17 Kawai, T. & Akira, S. Toll-like receptor and RIG-I-like receptor signaling. *Ann N Y Acad Sci* **1143**, 1-20, doi:10.1196/annals.1443.020 (2008).

18 Rojas, M. *et al.* Molecular mimicry and autoimmunity. *J Autoimmun* **95**, 100-123, doi:10.1016/j.jaut.2018.10.012 (2018).

19 Kim, J. M., Rasmussen, J. P. & Rudensky, A. Y. Regulatory T cells prevent catastrophic autoimmunity throughout the lifespan of mice. *Nat Immunol* **8**, 191-197, doi:10.1038/ni1428 (2007).
20 Romo-Tena, J., Gomez-Martin, D. & Alcocer-Varela, J. CTLA-4 and autoimmunity: new insights into the dual regulator of tolerance. *Autoimmun Rev* **12**, 1171-1176, doi:10.1016/j.autrev.2013.07.002 (2013).
21 Goudy, K. *et al.* Human IL2RA null mutation mediates immunodeficiency with lymphoproliferation and autoimmunity. *Clin Immunol* **146**, 248-261, doi:10.1016/j.clim.2013.01.004 (2013).
22 Cavanillas, M. L. *et al.* Polymorphisms in the IL2, IL2RA and IL2RB genes in multiple sclerosis risk. *Eur J Hum Genet* **18**, 794-799, doi:10.1038/ejhg.2010.15 (2010).
23 Alcina, A. *et al.* IL2RA/CD25 gene polymorphisms: uneven association with multiple sclerosis (MS) and type 1 diabetes (T1D). *PLoS One* **4**, e4137, doi:10.1371/journal.pone.0004137 (2009).
24 Matesanz, F. *et al.* IL2RA/CD25 polymorphisms contribute to multiple sclerosis susceptibility. *J Neurol* **254**, 682-684, doi:10.1007/s00415-006-0416-4 (2007).
25 Matesanz, F. *et al.* Allelic expression and interleukin-2 polymorphisms in multiple sclerosis. *J Neuroimmunol* **119**, 101-105 (2001).
26 Vella, A. *et al.* Localization of a type 1 diabetes locus in the IL2RA/CD25 region by use of tag single-nucleotide polymorphisms. *Am J Hum Genet* **76**, 773-779, doi:10.1086/429843 (2005).
27 Sollid, L. M., Pos, W. & Wucherpfennig, K. W. Molecular mechanisms for contribution of MHC molecules to autoimmune diseases. *Curr Opin Immunol* **31**, 24-30, doi:10.1016/j.coi.2014.08.005 (2014).
28 Nishizuka, Y. & Sakakura, T. Thymus and reproduction: sex-linked dysgenesia of the gonad after neonatal thymectomy in mice. *Science* **166**, 753-755, doi:10.1126/science.166.3906.753 (1969).
29 Tung, K. S., Smith, S., Teuscher, C., Cook, C. & Anderson, R. E. Murine autoimmune oophoritis, epididymoorchitis, and gastritis induced by day 3 thymectomy. Immunopathology. *Am J Pathol* **126**, 293-302 (1987).
30 Sakaguchi, S., Sakaguchi, N., Asano, M., Itoh, M. & Toda, M. Immunologic self-tolerance maintained by activated T cells expressing IL-2 receptor alpha-chains (CD25). Breakdown of a single mechanism of self-tolerance causes various autoimmune diseases. *J Immunol* **155**, 1151-1164 (1995).
31 Asano, M., Toda, M., Sakaguchi, N. & Sakaguchi, S. Autoimmune disease as a consequence of developmental abnormality of a T cell subpopulation. *J Exp Med* **184**, 387-396, doi:10.1084/jem.184.2.387 (1996).
32 Fontenot, J. D., Gavin, M. A. & Rudensky, A. Y. Foxp3 programs the development and function of CD4+CD25+ regulatory T cells. *Nat Immunol* **4**, 330-336, doi:10.1038/ni904 (2003).
33 Hori, S., Nomura, T. & Sakaguchi, S. Control of regulatory T cell development by the transcription factor Foxp3. *Science* **299**, 1057-1061, doi:10.1126/science.1079490 (2003).
34 Khattri, R., Cox, T., Yasayko, S. A. & Ramsdell, F. An essential role for Scurfin in CD4+CD25+ T regulatory cells. *Nat Immunol* **4**, 337-342, doi:10.1038/ni909 (2003).

35 Bennett, C. L. *et al.* The immune dysregulation, polyendocrinopathy, enteropathy, X-linked syndrome (IPEX) is caused by mutations of FOXP3. *Nat Genet* **27**, 20-21, doi:10.1038/83713 (2001).
36 Chatila, T. A. *et al.* JM2, encoding a fork head-related protein, is mutated in X-linked autoimmunity-allergic disregulation syndrome. *J Clin Invest* **106**, R75-81, doi:10.1172/JCI11679 (2000).
37 Wildin, R. S. *et al.* X-linked neonatal diabetes mellitus, enteropathy and endocrinopathy syndrome is the human equivalent of mouse scurfy. *Nat Genet* **27**, 18-20, doi:10.1038/83707 (2001).
38 Russell, W. L., Russell, L. B. & Gower, J. S. Exceptional Inheritance of a Sex-Linked Gene in the Mouse Explained on the Basis That the X/O Sex-Chromosome Constitution Is Female. *Proc Natl Acad Sci U S A* **45**, 554-560, doi:10.1073/pnas.45.4.554 (1959).
39 Godfrey, V. L., Wilkinson, J. E. & Russell, L. B. X-linked lymphoreticular disease in the scurfy (sf) mutant mouse. *Am J Pathol* **138**, 1379-1387 (1991).
40 Brunkow, M. E. *et al.* Disruption of a new forkhead/winged-helix protein, scurfin, results in the fatal lymphoproliferative disorder of the scurfy mouse. *Nat Genet* **27**, 68-73, doi:10.1038/83784 (2001).
41 Hsieh, C. S. *et al.* Recognition of the peripheral self by naturally arising CD25+ CD4+ T cell receptors. *Immunity* **21**, 267-277, doi:10.1016/j.immuni.2004.07.009 (2004).
42 Pacholczyk, R. *et al.* Nonself-antigens are the cognate specificities of Foxp3+ regulatory T cells. *Immunity* **27**, 493-504, doi:10.1016/j.immuni.2007.07.019 (2007).
43 Wong, J. *et al.* Adaptation of TCR repertoires to self-peptides in regulatory and nonregulatory CD4+ T cells. *J Immunol* **178**, 7032-7041, doi:10.4049/jimmunol.178.11.7032 (2007).
44 Bautista, J. L. *et al.* Intraclonal competition limits the fate determination of regulatory T cells in the thymus. *Nat Immunol* **10**, 610-617, doi:10.1038/ni.1739 (2009).
45 Leung, M. W., Shen, S. & Lafaille, J. J. TCR-dependent differentiation of thymic Foxp3+ cells is limited to small clonal sizes. *J Exp Med* **206**, 2121-2130, doi:10.1084/jem.20091033 (2009).
46 Moran, A. E. *et al.* T cell receptor signal strength in Treg and iNKT cell development demonstrated by a novel fluorescent reporter mouse. *J Exp Med* **208**, 1279-1289, doi:10.1084/jem.20110308 (2011).
47 Au-Yeung, B. B. *et al.* A sharp T-cell antigen receptor signaling threshold for T-cell proliferation. *Proc Natl Acad Sci U S A* **111**, E3679-3688, doi:10.1073/pnas.1413726111 (2014).
48 Stadinski, B. D. *et al.* A temporal thymic selection switch and ligand binding kinetics constrain neonatal Foxp3(+) Treg cell development. *Nat Immunol* **20**, 1046-1058, doi:10.1038/s41590-019-0414-1 (2019).
49 Salomon, B. *et al.* B7/CD28 costimulation is essential for the homeostasis of the CD4+CD25+ immunoregulatory T cells that control autoimmune diabetes. *Immunity* **12**, 431-440, doi:10.1016/s1074-7613(00)80195-8 (2000).
50 Tai, X., Cowan, M., Feigenbaum, L. & Singer, A. CD28 costimulation of developing thymocytes induces Foxp3 expression and regulatory T cell differentiation independently of interleukin 2. *Nat Immunol* **6**, 152-162, doi:10.1038/ni1160 (2005).

51 Lio, C. W., Dodson, L. F., Deppong, C. M., Hsieh, C. S. & Green, J. M. CD28 facilitates the generation of Foxp3(-) cytokine responsive regulatory T cell precursors. *J Immunol* **184**, 6007-6013, doi:10.4049/jimmunol.1000019 (2010).
52 Almeida, A. R., Legrand, N., Papiernik, M. & Freitas, A. A. Homeostasis of peripheral CD4+ T cells: IL-2R alpha and IL-2 shape a population of regulatory cells that controls CD4+ T cell numbers. *J Immunol* **169**, 4850-4860, doi:10.4049/jimmunol.169.9.4850 (2002).
53 Malek, T. R., Yu, A., Vincek, V., Scibelli, P. & Kong, L. CD4 regulatory T cells prevent lethal autoimmunity in IL-2Rbeta-deficient mice. Implications for the nonredundant function of IL-2. *Immunity* **17**, 167-178 (2002).
54 Papiernik, M., de Moraes, M. L., Pontoux, C., Vasseur, F. & Penit, C. Regulatory CD4 T cells: expression of IL-2R alpha chain, resistance to clonal deletion and IL-2 dependency. *Int Immunol* **10**, 371-378, doi:10.1093/intimm/10.4.371 (1998).
55 Bayer, A. L., Yu, A., Adeegbe, D. & Malek, T. R. Essential role for interleukin-2 for CD4(+)CD25(+) T regulatory cell development during the neonatal period. *J Exp Med* **201**, 769-777, doi:10.1084/jem.20041179 (2005).
56 Setoguchi, R., Hori, S., Takahashi, T. & Sakaguchi, S. Homeostatic maintenance of natural Foxp3(+) CD25(+) CD4(+) regulatory T cells by interleukin (IL)-2 and induction of autoimmune disease by IL-2 neutralization. *J Exp Med* **201**, 723-735, doi:10.1084/jem.20041982 (2005).
57 Burchill, M. A., Yang, J., Vogtenhuber, C., Blazar, B. R. & Farrar, M. A. IL-2 receptor beta-dependent STAT5 activation is required for the development of Foxp3+ regulatory T cells. *J Immunol* **178**, 280-290, doi:10.4049/jimmunol.178.1.280 (2007).
58 Fan, M. Y. *et al.* Differential Roles of IL-2 Signaling in Developing versus Mature Tregs. *Cell Rep* **25**, 1204-1213 e1204, doi:10.1016/j.celrep.2018.10.002 (2018).
59 Fontenot, J. D., Dooley, J. L., Farr, A. G. & Rudensky, A. Y. Developmental regulation of Foxp3 expression during ontogeny. *J Exp Med* **202**, 901-906, doi:10.1084/jem.20050784 (2005).
60 D'Cruz, L. M. & Klein, L. Development and function of agonist-induced CD25+Foxp3+ regulatory T cells in the absence of interleukin 2 signaling. *Nat Immunol* **6**, 1152-1159, doi:10.1038/ni1264 (2005).
61 Bayer, A. L., Lee, J. Y., de la Barrera, A., Surh, C. D. & Malek, T. R. A function for IL-7R for CD4+CD25+Foxp3+ T regulatory cells. *J Immunol* **181**, 225-234, doi:10.4049/jimmunol.181.1.225 (2008).
62 Vang, K. B. *et al.* IL-2, -7, and -15, but not thymic stromal lymphopoeitin, redundantly govern CD4+Foxp3+ regulatory T cell development. *J Immunol* **181**, 3285-3290, doi:10.4049/jimmunol.181.5.3285 (2008).
63 Burchill, M. A. *et al.* Linked T cell receptor and cytokine signaling govern the development of the regulatory T cell repertoire. *Immunity* **28**, 112-121, doi:10.1016/j.immuni.2007.11.022 (2008).
64 Yao, Z. *et al.* Nonredundant roles for Stat5a/b in directly regulating Foxp3. *Blood* **109**, 4368-4375, doi:10.1182/blood-2006-11-055756 (2007).
65 Vang, K. B. *et al.* Cutting edge: CD28 and c-Rel-dependent pathways initiate regulatory T cell development. *J Immunol* **184**, 4074-4077, doi:10.4049/jimmunol.0903933 (2010).

66 Hinterberger, M., Wirnsberger, G. & Klein, L. B7/CD28 in central tolerance: costimulation promotes maturation of regulatory T cell precursors and prevents their clonal deletion. *Front Immunol* **2**, 30, doi:10.3389/fimmu.2011.00030 (2011).
67 Ouyang, W., Beckett, O., Ma, Q. & Li, M. O. Transforming growth factor-beta signaling curbs thymic negative selection promoting regulatory T cell development. *Immunity* **32**, 642-653, doi:10.1016/j.immuni.2010.04.012 (2010).
68 Coquet, J. M. *et al.* Epithelial and dendritic cells in the thymic medulla promote CD4+Foxp3+ regulatory T cell development via the CD27-CD70 pathway. *J Exp Med* **210**, 715-728, doi:10.1084/jem.20112061 (2013).
69 Mahmud, S. A. *et al.* Costimulation via the tumor-necrosis factor receptor superfamily couples TCR signal strength to the thymic differentiation of regulatory T cells. *Nat Immunol* **15**, 473-481, doi:10.1038/ni.2849 (2014).
70 Leventhal, D. S. *et al.* Dendritic Cells Coordinate the Development and Homeostasis of Organ-Specific Regulatory T Cells. *Immunity* **44**, 847-859, doi:10.1016/j.immuni.2016.01.025 (2016).
71 Yang-Snyder, J. A. & Rothenberg, E. V. Spontaneous expression of interleukin-2 in vivo in specific tissues of young mice. *Dev Immunol* **5**, 223-245 (1998).
72 Owen, D. L. *et al.* Identification of Cellular Sources of IL-2 Needed for Regulatory T Cell Development and Homeostasis. *J Immunol* **200**, 3926-3933, doi:10.4049/jimmunol.1800097 (2018).
73 Hemmers, S. *et al.* IL-2 production by self-reactive CD4 thymocytes scales regulatory T cell generation in the thymus. *J Exp Med* **216**, 2466-2478, doi:10.1084/jem.20190993 (2019).
74 Weist, B. M., Kurd, N., Boussier, J., Chan, S. W. & Robey, E. A. Thymic regulatory T cell niche size is dictated by limiting IL-2 from antigen-bearing dendritic cells and feedback competition. *Nat Immunol* **16**, 635-641, doi:10.1038/ni.3171 (2015).
75 Lio, C. W. & Hsieh, C. S. A two-step process for thymic regulatory T cell development. *Immunity* **28**, 100-111, doi:10.1016/j.immuni.2007.11.021 (2008).
76 Owen, D. L. *et al.* Thymic regulatory T cells arise via two distinct developmental programs. *Nat Immunol* **20**, 195-205, doi:10.1038/s41590-018-0289-6 (2019).
77 Tai, X. *et al.* Foxp3 transcription factor is proapoptotic and lethal to developing regulatory T cells unless counterbalanced by cytokine survival signals. *Immunity* **38**, 1116-1128, doi:10.1016/j.immuni.2013.02.022 (2013).
78 Owen, D. L., La Rue, R. S., Munro, S. A. & Farrar, M. A. Tracking Regulatory T Cell Development in the Thymus Using Single-Cell RNA Sequencing/TCR Sequencing. *J Immunol* **209**, 1300-1313, doi:10.4049/jimmunol.2200089 (2022).
79 Bensinger, S. J., Bandeira, A., Jordan, M. S., Caton, A. J. & Laufer, T. M. Major histocompatibility complex class II-positive cortical epithelium mediates the selection of CD4(+)25(+) immunoregulatory T cells. *J Exp Med* **194**, 427-438, doi:10.1084/jem.194.4.427 (2001).
80 Liston, A. *et al.* Differentiation of regulatory Foxp3+ T cells in the thymic cortex. *Proc Natl Acad Sci U S A* **105**, 11903-11908, doi:10.1073/pnas.0801506105 (2008).
81 Ribot, J. *et al.* Shaping of the autoreactive regulatory T cell repertoire by thymic cortical positive selection. *J Immunol* **179**, 6741-6748, doi:10.4049/jimmunol.179.10.6741 (2007).

82 Fontenot, J. D. *et al.* Regulatory T cell lineage specification by the forkhead transcription factor foxp3. *Immunity* **22**, 329-341, doi:10.1016/j.immuni.2005.01.016 (2005).
83 Lee, H. M. & Hsieh, C. S. Rare development of Foxp3+ thymocytes in the CD4+CD8+ subset. *J Immunol* **183**, 2261-2266, doi:10.4049/jimmunol.0901304 (2009).
84 Thiault, N. *et al.* Peripheral regulatory T lymphocytes recirculating to the thymus suppress the development of their precursors. *Nat Immunol* **16**, 628-634, doi:10.1038/ni.3150 (2015).
85 Hinterberger, M. *et al.* Autonomous role of medullary thymic epithelial cells in central CD4(+) T cell tolerance. *Nat Immunol* **11**, 512-519, doi:10.1038/ni.1874 (2010).
86 Khan, I. S. *et al.* Enhancement of an anti-tumor immune response by transient blockade of central T cell tolerance. *J Exp Med* **211**, 761-768, doi:10.1084/jem.20131889 (2014).
87 Malchow, S. *et al.* Aire Enforces Immune Tolerance by Directing Autoreactive T Cells into the Regulatory T Cell Lineage. *Immunity* **44**, 1102-1113, doi:10.1016/j.immuni.2016.02.009 (2016).
88 Metzger, T. C. *et al.* Lineage tracing and cell ablation identify a post-Aire-expressing thymic epithelial cell population. *Cell Rep* **5**, 166-179, doi:10.1016/j.celrep.2013.08.038 (2013).
89 Perry, J. S. A. *et al.* Distinct contributions of Aire and antigen-presenting-cell subsets to the generation of self-tolerance in the thymus. *Immunity* **41**, 414-426, doi:10.1016/j.immuni.2014.08.007 (2014).
90 Inglesfield, S., Cosway, E. J., Jenkinson, W. E. & Anderson, G. Rethinking Thymic Tolerance: Lessons from Mice. *Trends Immunol* **40**, 279-291, doi:10.1016/j.it.2019.01.011 (2019).
91 Hsieh, C. S., Lee, H. M. & Lio, C. W. Selection of regulatory T cells in the thymus. *Nat Rev Immunol* **12**, 157-167, doi:10.1038/nri3155 (2012).
92 Apostolou, I., Sarukhan, A., Klein, L. & von Boehmer, H. Origin of regulatory T cells with known specificity for antigen. *Nat Immunol* **3**, 756-763, doi:10.1038/ni816 (2002).
93 Cabarrocas, J. *et al.* Foxp3+ CD25+ regulatory T cells specific for a neo-self-antigen develop at the double-positive thymic stage. *Proc Natl Acad Sci U S A* **103**, 8453-8458, doi:10.1073/pnas.0603086103 (2006).
94 Jordan, M. S. *et al.* Thymic selection of CD4+CD25+ regulatory T cells induced by an agonist self-peptide. *Nat Immunol* **2**, 301-306, doi:10.1038/86302 (2001).
95 Lee, H. M., Bautista, J. L., Scott-Browne, J., Mohan, J. F. & Hsieh, C. S. A broad range of self-reactivity drives thymic regulatory T cell selection to limit responses to self. *Immunity* **37**, 475-486, doi:10.1016/j.immuni.2012.07.009 (2012).
96 Lee, T., Sprouse, M. L., Banerjee, P., Bettini, M. & Bettini, M. L. Ectopic Expression of Self-Antigen Drives Regulatory T Cell Development and Not Deletion of Autoimmune T Cells. *J Immunol* **199**, 2270-2278, doi:10.4049/jimmunol.1700207 (2017).
97 Legoux, F. P. *et al.* CD4+ T Cell Tolerance to Tissue-Restricted Self Antigens Is Mediated by Antigen-Specific Regulatory T Cells Rather Than Deletion. *Immunity* **43**, 896-908, doi:10.1016/j.immuni.2015.10.011 (2015).
98 Malhotra, D. *et al.* Tolerance is established in polyclonal CD4(+) T cells by distinct mechanisms, according to self-peptide expression patterns. *Nat Immunol* **17**, 187-195, doi:10.1038/ni.3327 (2016).

99 Picca, C. C. *et al.* Thymocyte deletion can bias Treg formation toward low-abundance self-peptide. *Eur J Immunol* **39**, 3301-3306, doi:10.1002/eji.200939709 (2009).
100 van Santen, H. M., Benoist, C. & Mathis, D. Number of T reg cells that differentiate does not increase upon encounter of agonist ligand on thymic epithelial cells. *J Exp Med* **200**, 1221-1230, doi:10.1084/jem.20041022 (2004).
101 Klawon, D. E. J. *et al.* Altered selection on a single self-ligand promotes susceptibility to organ-specific T cell infiltration. *J Exp Med* **218**, doi:10.1084/jem.20200701 (2021).
102 Malchow, S. *et al.* Aire-dependent thymic development of tumor-associated regulatory T cells. *Science* **339**, 1219-1224, doi:10.1126/science.1233913 (2013).
103 Hassler, T. *et al.* Inventories of naive and tolerant mouse CD4 T cell repertoires reveal a hierarchy of deleted and diverted T cell receptors. *Proc Natl Acad Sci U S A* **116**, 18537-18543, doi:10.1073/pnas.1907615116 (2019).
104 Villasenor, J., Besse, W., Benoist, C. & Mathis, D. Ectopic expression of peripheral-tissue antigens in the thymic epithelium: probabilistic, monoallelic, misinitiated. *Proc Natl Acad Sci U S A* **105**, 15854-15859, doi:10.1073/pnas.0808069105 (2008).
105 Derbinski, J., Pinto, S., Rosch, S., Hexel, K. & Kyewski, B. Promiscuous gene expression patterns in single medullary thymic epithelial cells argue for a stochastic mechanism. *Proc Natl Acad Sci U S A* **105**, 657-662, doi:10.1073/pnas.0707486105 (2008).
106 Moon, J. J. *et al.* Quantitative impact of thymic selection on Foxp3+ and Foxp3- subsets of self-peptide/MHC class II-specific CD4+ T cells. *Proc Natl Acad Sci U S A* **108**, 14602-14607, doi:10.1073/pnas.1109806108 (2011).
107 Klein, L., Robey, E. A. & Hsieh, C. S. Central CD4(+) T cell tolerance: deletion versus regulatory T cell differentiation. *Nat Rev Immunol* **19**, 7-18, doi:10.1038/s41577-018-0083-6 (2019).
108 Li, M. O. & Rudensky, A. Y. T cell receptor signalling in the control of regulatory T cell differentiation and function. *Nat Rev Immunol* **16**, 220-233, doi:10.1038/nri.2016.26 (2016).
109 Adamopoulou, E. *et al.* Exploring the MHC-peptide matrix of central tolerance in the human thymus. *Nat Commun* **4**, 2039, doi:10.1038/ncomms3039 (2013).
110 Collado, J. A. *et al.* Composition of the HLA-DR-associated human thymus peptidome. *Eur J Immunol* **43**, 2273-2282, doi:10.1002/eji.201243280 (2013).
111 Marrack, P., Ignatowicz, L., Kappler, J. W., Boymel, J. & Freed, J. H. Comparison of peptides bound to spleen and thymus class II. *J Exp Med* **178**, 2173-2183, doi:10.1084/jem.178.6.2173 (1993).
112 Dengjel, J. *et al.* Autophagy promotes MHC class II presentation of peptides from intracellular source proteins. *Proc Natl Acad Sci U S A* **102**, 7922-7927, doi:10.1073/pnas.0501190102 (2005).
113 Schmid, D., Pypaert, M. & Munz, C. Antigen-loading compartments for major histocompatibility complex class II molecules continuously receive input from autophagosomes. *Immunity* **26**, 79-92, doi:10.1016/j.immuni.2006.10.018 (2007).
114 Nedjic, J., Aichinger, M., Emmerich, J., Mizushima, N. & Klein, L. Autophagy in thymic epithelium shapes the T-cell repertoire and is essential for tolerance. *Nature* **455**, 396-400, doi:10.1038/nature07208 (2008).

115 Atibalentja, D. F., Byersdorfer, C. A. & Unanue, E. R. Thymus-blood protein interactions are highly effective in negative selection and regulatory T cell induction. *J Immunol* **183**, 7909-7918, doi:10.4049/jimmunol.0902632 (2009).
116 Atibalentja, D. F., Murphy, K. M. & Unanue, E. R. Functional redundancy between thymic CD8alpha+ and Sirpalpha+ conventional dendritic cells in presentation of blood-derived lysozyme by MHC class II proteins. *J Immunol* **186**, 1421-1431, doi:10.4049/jimmunol.1002587 (2011).
117 Hanahan, D. Peripheral-antigen-expressing cells in thymic medulla: factors in self-tolerance and autoimmunity. *Curr Opin Immunol* **10**, 656-662 (1998).
118 Guerri, L. *et al.* Analysis of APC types involved in CD4 tolerance and regulatory T cell generation using reaggregated thymic organ cultures. *J Immunol* **190**, 2102-2110, doi:10.4049/jimmunol.1202883 (2013).
119 Wirnsberger, G., Mair, F. & Klein, L. Regulatory T cell differentiation of thymocytes does not require a dedicated antigen-presenting cell but is under T cell-intrinsic developmental control. *Proc Natl Acad Sci U S A* **106**, 10278-10283, doi:10.1073/pnas.0901877106 (2009).
120 Proietto, A. I. *et al.* Dendritic cells in the thymus contribute to T-regulatory cell induction. *Proc Natl Acad Sci U S A* **105**, 19869-19874, doi:10.1073/pnas.0810268105 (2008).
121 Hadeiba, H. *et al.* Plasmacytoid dendritic cells transport peripheral antigens to the thymus to promote central tolerance. *Immunity* **36**, 438-450, doi:10.1016/j.immuni.2012.01.017 (2012).
122 Yamano, T. *et al.* Thymic B Cells Are Licensed to Present Self Antigens for Central T Cell Tolerance Induction. *Immunity* **42**, 1048-1061, doi:10.1016/j.immuni.2015.05.013 (2015).
123 Anderson, M. S. *et al.* The cellular mechanism of Aire control of T cell tolerance. *Immunity* **23**, 227-239, doi:10.1016/j.immuni.2005.07.005 (2005).
124 Anderson, M. S. *et al.* Projection of an immunological self shadow within the thymus by the aire protein. *Science* **298**, 1395-1401, doi:10.1126/science.1075958 (2002).
125 Nitta, T. *et al.* Fibroblasts as a source of self-antigens for central immune tolerance. *Nat Immunol* **21**, 1172-1180, doi:10.1038/s41590-020-0756-8 (2020).
126 Koble, C. & Kyewski, B. The thymic medulla: a unique microenvironment for intercellular self-antigen transfer. *J Exp Med* **206**, 1505-1513, doi:10.1084/jem.20082449 (2009).
127 Millet, V., Naquet, P. & Guinamard, R. R. Intercellular MHC transfer between thymic epithelial and dendritic cells. *Eur J Immunol* **38**, 1257-1263, doi:10.1002/eji.200737982 (2008).
128 Perry, J. S. A. *et al.* Transfer of Cell-Surface Antigens by Scavenger Receptor CD36 Promotes Thymic Regulatory T Cell Receptor Repertoire Development and Allo-tolerance. *Immunity* **48**, 923-936 e924, doi:10.1016/j.immuni.2018.04.007 (2018).
129 Derbinski, J., Schulte, A., Kyewski, B. & Klein, L. Promiscuous gene expression in medullary thymic epithelial cells mirrors the peripheral self. *Nat Immunol* **2**, 1032-1039, doi:10.1038/ni723 (2001).
130 Finnish-German, A. C. An autoimmune disease, APECED, caused by mutations in a novel gene featuring two PHD-type zinc-finger domains. *Nat Genet* **17**, 399-403, doi:10.1038/ng1297-399 (1997).
131 Nagamine, K. *et al.* Positional cloning of the APECED gene. *Nat Genet* **17**, 393-398, doi:10.1038/ng1297-393 (1997).

132 Giraud, M. *et al.* Aire unleashes stalled RNA polymerase to induce ectopic gene expression in thymic epithelial cells. *Proc Natl Acad Sci U S A* **109**, 535-540, doi:10.1073/pnas.1119351109 (2012).
133 Sansom, S. N. *et al.* Population and single-cell genomics reveal the Aire dependency, relief from Polycomb silencing, and distribution of self-antigen expression in thymic epithelia. *Genome Res* **24**, 1918-1931, doi:10.1101/gr.171645.113 (2014).
134 Lin, J. *et al.* Increased generation of Foxp3(+) regulatory T cells by manipulating antigen presentation in the thymus. *Nat Commun* **7**, 10562, doi:10.1038/ncomms10562 (2016).
135 Guerau-de-Arellano, M., Martinic, M., Benoist, C. & Mathis, D. Neonatal tolerance revisited: a perinatal window for Aire control of autoimmunity. *J Exp Med* **206**, 1245-1252, doi:10.1084/jem.20090300 (2009).
136 Yang, S., Fujikado, N., Kolodin, D., Benoist, C. & Mathis, D. Immune tolerance. Regulatory T cells generated early in life play a distinct role in maintaining self-tolerance. *Science* **348**, 589-594, doi:10.1126/science.aaa7017 (2015).
137 Hu, W. *et al.* Regulatory T cells function in established systemic inflammation and reverse fatal autoimmunity. *Nat Immunol* **22**, 1163-1174, doi:10.1038/s41590-021-01001-4 (2021).
138 Leonard, J. D. *et al.* Identification of Natural Regulatory T Cell Epitopes Reveals Convergence on a Dominant Autoantigen. *Immunity* **47**, 107-117 e108, doi:10.1016/j.immuni.2017.06.015 (2017).
139 Setiady, Y. Y. *et al.* Physiologic self antigens rapidly capacitate autoimmune disease-specific polyclonal CD4+ CD25+ regulatory T cells. *Blood* **107**, 1056-1062, doi:10.1182/blood-2005-08-3088 (2006).
140 Kieback, E. *et al.* Thymus-Derived Regulatory T Cells Are Positively Selected on Natural Self-Antigen through Cognate Interactions of High Functional Avidity. *Immunity* **44**, 1114-1126, doi:10.1016/j.immuni.2016.04.018 (2016).
141 Spence, A. *et al.* Revealing the specificity of regulatory T cells in murine autoimmune diabetes. *Proc Natl Acad Sci U S A* **115**, 5265-5270, doi:10.1073/pnas.1715590115 (2018).
142 Gabler, J., Arnold, J. & Kyewski, B. Promiscuous gene expression and the developmental dynamics of medullary thymic epithelial cells. *Eur J Immunol* **37**, 3363-3372, doi:10.1002/eji.200737131 (2007).
143 Lei, Y. *et al.* Aire-dependent production of XCL1 mediates medullary accumulation of thymic dendritic cells and contributes to regulatory T cell development. *J Exp Med* **208**, 383-394, doi:10.1084/jem.20102327 (2011).
144 Hu, Z. *et al.* CCR7 Modulates the Generation of Thymic Regulatory T Cells by Altering the Composition of the Thymic Dendritic Cell Compartment. *Cell Rep* **21**, 168-180, doi:10.1016/j.celrep.2017.09.016 (2017).
145 Aichinger, M., Wu, C., Nedjic, J. & Klein, L. Macroautophagy substrates are loaded onto MHC class II of medullary thymic epithelial cells for central tolerance. *J Exp Med* **210**, 287-300, doi:10.1084/jem.20122149 (2013).
146 Hildner, K. *et al.* Batf3 deficiency reveals a critical role for CD8alpha+ dendritic cells in cytotoxic T cell immunity. *Science* **322**, 1097-1100, doi:10.1126/science.1164206 (2008).
147 Li, J., Park, J., Foss, D. & Goldschneider, I. Thymus-homing peripheral dendritic cells constitute two of the three major subsets of dendritic cells in the steady-state thymus. *J Exp Med* **206**, 607-622, doi:10.1084/jem.20082232 (2009).

148 Breed, E. R. *et al.* Type 2 cytokines in the thymus activate Sirpalpha(+) dendritic cells to promote clonal deletion. *Nat Immunol* **23**, 1042-1051, doi:10.1038/s41590-022-01218-x (2022).
149 Liu, T. T. *et al.* Ablation of cDC2 development by triple mutations within the Zeb2 enhancer. *Nature* **607**, 142-148, doi:10.1038/s41586-022-04866-z (2022).
150 Dudziak, D. *et al.* Differential antigen processing by dendritic cell subsets in vivo. *Science* **315**, 107-111, doi:10.1126/science.1136080 (2007).
151 Curotto de Lafaille, M. A., Lino, A. C., Kutchukhidze, N. & Lafaille, J. J. CD25- T cells generate CD25+Foxp3+ regulatory T cells by peripheral expansion. *J Immunol* **173**, 7259-7268, doi:10.4049/jimmunol.173.12.7259 (2004).
152 Xu, M. *et al.* c-MAF-dependent regulatory T cells mediate immunological tolerance to a gut pathobiont. *Nature* **554**, 373-377, doi:10.1038/nature25500 (2018).
153 Wegorzewska, M. M. *et al.* Diet modulates colonic T cell responses by regulating the expression of a Bacteroides thetaiotaomicron antigen. *Sci Immunol* **4**, doi:10.1126/sciimmunol.aau9079 (2019).
154 Apostolou, I. & von Boehmer, H. In vivo instruction of suppressor commitment in naive T cells. *J Exp Med* **199**, 1401-1408, doi:10.1084/jem.20040249 (2004).
155 Gottschalk, R. A., Corse, E. & Allison, J. P. TCR ligand density and affinity determine peripheral induction of Foxp3 in vivo. *J Exp Med* **207**, 1701-1711, doi:10.1084/jem.20091999 (2010).
156 Kretschmer, K. *et al.* Inducing and expanding regulatory T cell populations by foreign antigen. *Nat Immunol* **6**, 1219-1227, doi:10.1038/ni1265 (2005).
157 Sun, C. M. *et al.* Small intestine lamina propria dendritic cells promote de novo generation of Foxp3 T reg cells via retinoic acid. *J Exp Med* **204**, 1775-1785, doi:10.1084/jem.20070602 (2007).
158 Thornton, A. M. *et al.* Expression of Helios, an Ikaros transcription factor family member, differentiates thymic-derived from peripherally induced Foxp3+ T regulatory cells. *J Immunol* **184**, 3433-3441, doi:10.4049/jimmunol.0904028 (2010).
159 Weiss, J. M. *et al.* Neuropilin 1 is expressed on thymus-derived natural regulatory T cells, but not mucosa-generated induced Foxp3+ T reg cells. *J Exp Med* **209**, 1723-1742, S1721, doi:10.1084/jem.20120914 (2012).
160 Yadav, M. *et al.* Neuropilin-1 distinguishes natural and inducible regulatory T cells among regulatory T cell subsets in vivo. *J Exp Med* **209**, 1713-1722, S1711-1719, doi:10.1084/jem.20120822 (2012).
161 Akimova, T., Beier, U. H., Wang, L., Levine, M. H. & Hancock, W. W. Helios expression is a marker of T cell activation and proliferation. *PLoS One* **6**, e24226, doi:10.1371/journal.pone.0024226 (2011).
162 Gottschalk, R. A., Corse, E. & Allison, J. P. Expression of Helios in peripherally induced Foxp3+ regulatory T cells. *J Immunol* **188**, 976-980, doi:10.4049/jimmunol.1102964 (2012).
163 Petzold, C. *et al.* Fluorochrome-based definition of naturally occurring Foxp3(+) regulatory T cells of intra- and extrathymic origin. *Eur J Immunol* **44**, 3632-3645, doi:10.1002/eji.201444750 (2014).

164 Schliesser, U. *et al.* Generation of highly effective and stable murine alloreactive Treg cells by combined anti-CD4 mAb, TGF-beta, and RA treatment. *Eur J Immunol* **43**, 3291-3305, doi:10.1002/eji.201243292 (2013).
165 Szurek, E. *et al.* Differences in Expression Level of Helios and Neuropilin-1 Do Not Distinguish Thymus-Derived from Extrathymically-Induced CD4+Foxp3+ Regulatory T Cells. *PLoS One* **10**, e0141161, doi:10.1371/journal.pone.0141161 (2015).
166 Josefowicz, S. Z. *et al.* Extrathymically generated regulatory T cells control mucosal TH2 inflammation. *Nature* **482**, 395-399, doi:10.1038/nature10772 (2012).
167 Schlenner, S. M., Weigmann, B., Ruan, Q., Chen, Y. & von Boehmer, H. Smad3 binding to the foxp3 enhancer is dispensable for the development of regulatory T cells with the exception of the gut. *J Exp Med* **209**, 1529-1535, doi:10.1084/jem.20112646 (2012).
168 Zheng, Y. *et al.* Role of conserved non-coding DNA elements in the Foxp3 gene in regulatory T-cell fate. *Nature* **463**, 808-812, doi:10.1038/nature08750 (2010).
169 Samstein, R. M., Josefowicz, S. Z., Arvey, A., Treuting, P. M. & Rudensky, A. Y. Extrathymic generation of regulatory T cells in placental mammals mitigates maternal-fetal conflict. *Cell* **150**, 29-38, doi:10.1016/j.cell.2012.05.031 (2012).
170 Lathrop, S. K. *et al.* Peripheral education of the immune system by colonic commensal microbiota. *Nature* **478**, 250-254, doi:10.1038/nature10434 (2011).
171 Chai, J. N. *et al.* Helicobacter species are potent drivers of colonic T cell responses in homeostasis and inflammation. *Sci Immunol* **2**, doi:10.1126/sciimmunol.aal5068 (2017).
172 Nutsch, K. *et al.* Rapid and Efficient Generation of Regulatory T Cells to Commensal Antigens in the Periphery. *Cell Rep* **17**, 206-220, doi:10.1016/j.celrep.2016.08.092 (2016).
173 Solomon, B. D. & Hsieh, C. S. Antigen-Specific Development of Mucosal Foxp3+RORgammat+ T Cells from Regulatory T Cell Precursors. *J Immunol* **197**, 3512-3519, doi:10.4049/jimmunol.1601217 (2016).
174 Hong, S. W. *et al.* Immune tolerance of food is mediated by layers of CD4(+) T cell dysfunction. *Nature* **607**, 762-768, doi:10.1038/s41586-022-04916-6 (2022).
175 Cebula, A. *et al.* Thymus-derived regulatory T cells contribute to tolerance to commensal microbiota. *Nature* **497**, 258-262, doi:10.1038/nature12079 (2013).
176 Ohnmacht, C. *et al.* MUCOSAL IMMUNOLOGY. The microbiota regulates type 2 immunity through RORgammat(+) T cells. *Science* **349**, 989-993, doi:10.1126/science.aac4263 (2015).
177 Sefik, E. *et al.* MUCOSAL IMMUNOLOGY. Individual intestinal symbionts induce a distinct population of RORgamma(+) regulatory T cells. *Science* **349**, 993-997, doi:10.1126/science.aaa9420 (2015).
178 Russler-Germain, E. V. *et al.* Gut Helicobacter presentation by multiple dendritic cell subsets enables context-specific regulatory T cell generation. *Elife* **10**, doi:10.7554/eLife.54792 (2021).
179 Akagbosu, B. *et al.* Novel antigen-presenting cell imparts T(reg)-dependent tolerance to gut microbiota. *Nature* **610**, 752-760, doi:10.1038/s41586-022-05309-5 (2022).
180 Kedmi, R. *et al.* A RORgammat(+) cell instructs gut microbiota-specific T(reg) cell differentiation. *Nature* **610**, 737-743, doi:10.1038/s41586-022-05089-y (2022).
181 Lyu, M. *et al.* ILC3s select microbiota-specific regulatory T cells to establish tolerance in the gut. *Nature* **610**, 744-751, doi:10.1038/s41586-022-05141-x (2022).

182 van der Veeken, J. *et al.* Genetic tracing reveals transcription factor Foxp3-dependent and Foxp3-independent functionality of peripherally induced Treg cells. *Immunity* **55**, 1173-1184 e1177, doi:10.1016/j.immuni.2022.05.010 (2022).
183 Jacobsen, J. T. *et al.* Expression of Foxp3 by T follicular helper cells in end-stage germinal centers. *Science* **373**, doi:10.1126/science.abe5146 (2021).
184 Schallenberg, S., Tsai, P. Y., Riewaldt, J. & Kretschmer, K. Identification of an immediate Foxp3(-) precursor to Foxp3(+) regulatory T cells in peripheral lymphoid organs of nonmanipulated mice. *J Exp Med* **207**, 1393-1407, doi:10.1084/jem.20100045 (2010).
185 Paiva, R. S. *et al.* Recent thymic emigrants are the preferential precursors of regulatory T cells differentiated in the periphery. *Proc Natl Acad Sci U S A* **110**, 6494-6499, doi:10.1073/pnas.1221955110 (2013).
186 Kalekar, L. A. *et al.* CD4(+) T cell anergy prevents autoimmunity and generates regulatory T cell precursors. *Nat Immunol* **17**, 304-314, doi:10.1038/ni.3331 (2016).
187 Bernard, N. F., Ertug, F. & Margolese, H. High incidence of thyroiditis and anti-thyroid autoantibodies in NOD mice. *Diabetes* **41**, 40-46, doi:10.2337/diab.41.1.40 (1992).
188 Miller, F. W., Moore, G. F., Weintraub, B. D. & Steinberg, A. D. Prevalence of thyroid disease and abnormal thyroid function test results in patients with systemic lupus erythematosus. *Arthritis Rheum* **30**, 1124-1131, doi:10.1002/art.1780301006 (1987).
189 Riley, W. J., Winer, A. & Goldstein, D. Coincident presence of thyro-gastric autoimmunity at onset of type 1 (insulin-dependent) diabetes. *Diabetologia* **24**, 418-421, doi:10.1007/BF00257339 (1983).
190 Thomas, D. J., Young, A., Gorsuch, A. N., Bottazzo, G. F. & Cudworth, A. G. Evidence for an association between rheumatoid arthritis and autoimmune endocrine disease. *Ann Rheum Dis* **42**, 297-300, doi:10.1136/ard.42.3.297 (1983).
191 Sternthal, E., Like, A. A., Sarantis, K. & Braverman, L. E. Lymphocytic thyroiditis and diabetes in the BB/W rat. A new model of autoimmune endocrinopathy. *Diabetes* **30**, 1058-1061, doi:10.2337/diab.30.12.1058 (1981).
192 Irvine, W. J., Clarke, B. F., Scarth, L., Cullen, D. R. & Duncan, L. J. Thyroid and gastric autoimmunity in patients with diabetes mellitus. *Lancet* **2**, 163-168, doi:10.1016/s0140-6736(70)92531-6 (1970).
193 Like, A. A., Rossini, A. A., Guberski, D. L., Appel, M. C. & Williams, R. M. Spontaneous diabetes mellitus: reversal and prevention in the BB/W rat with antiserum to rat lymphocytes. *Science* **206**, 1421-1423, doi:10.1126/science.388619 (1979).
194 Shizuru, J. A., Taylor-Edwards, C., Banks, B. A., Gregory, A. K. & Fathman, C. G. Immunotherapy of the nonobese diabetic mouse: treatment with an antibody to T-helper lymphocytes. *Science* **240**, 659-662, doi:10.1126/science.2966437 (1988).
195 Wofsy, D. & Seaman, W. E. Successful treatment of autoimmunity in NZB/NZW F1 mice with monoclonal antibody to L3T4. *J Exp Med* **161**, 378-391, doi:10.1084/jem.161.2.378 (1985).
196 Londei, M., Bottazzo, G. F. & Feldmann, M. Human T-cell clones from autoimmune thyroid glands: specific recognition of autologous thyroid cells. *Science* **228**, 85-89, doi:10.1126/science.3871967 (1985).
197 Kojima, A. & Prehn, R. T. Genetic susceptibility to post-thymectomy autoimmune diseases in mice. *Immunogenetics* **14**, 15-27, doi:10.1007/BF00344296 (1981).

198 Penhale, W. J., Farmer, A., McKenna, R. P. & Irvine, W. J. Spontaneous thyroiditis in thymectomized and irradiated Wistar rats. *Clin Exp Immunol* **15**, 225-236 (1973).
199 Sakaguchi, S., Fukuma, K., Kuribayashi, K. & Masuda, T. Organ-specific autoimmune diseases induced in mice by elimination of T cell subset. I. Evidence for the active participation of T cells in natural self-tolerance; deficit of a T cell subset as a possible cause of autoimmune disease. *J Exp Med* **161**, 72-87, doi:10.1084/jem.161.1.72 (1985).
200 Powrie, F., Leach, M. W., Mauze, S., Caddle, L. B. & Coffman, R. L. Phenotypically distinct subsets of CD4+ T cells induce or protect from chronic intestinal inflammation in C. B-17 scid mice. *Int Immunol* **5**, 1461-1471, doi:10.1093/intimm/5.11.1461 (1993).
201 Morrissey, P. J., Charrier, K., Braddy, S., Liggitt, D. & Watson, J. D. CD4+ T cells that express high levels of CD45RB induce wasting disease when transferred into congenic severe combined immunodeficient mice. Disease development is prevented by cotransfer of purified CD4+ T cells. *J Exp Med* **178**, 237-244, doi:10.1084/jem.178.1.237 (1993).
202 Sugihara, S., Fujiwara, H. & Shearer, G. M. Autoimmune thyroiditis induced in mice depleted of particular T cell subsets. Characterization of thyroiditis-inducing T cell lines and clones derived from thyroid lesions. *J Immunol* **150**, 683-694 (1993).
203 Smith, H., Lou, Y. H., Lacy, P. & Tung, K. S. Tolerance mechanism in experimental ovarian and gastric autoimmune diseases. *J Immunol* **149**, 2212-2218 (1992).
204 Powrie, F. & Mason, D. OX-22high CD4+ T cells induce wasting disease with multiple organ pathology: prevention by the OX-22low subset. *J Exp Med* **172**, 1701-1708, doi:10.1084/jem.172.6.1701 (1990).
205 McKeever, U. *et al.* Adoptive transfer of autoimmune diabetes and thyroiditis to athymic rats. *Proc Natl Acad Sci U S A* **87**, 7618-7622, doi:10.1073/pnas.87.19.7618 (1990).
206 Blair, P. J. *et al.* CD4+CD8- T cells are the effector cells in disease pathogenesis in the scurfy (sf) mouse. *J Immunol* **153**, 3764-3774 (1994).
207 Schubert, L. A., Jeffery, E., Zhang, Y., Ramsdell, F. & Ziegler, S. F. Scurfin (FOXP3) acts as a repressor of transcription and regulates T cell activation. *J Biol Chem* **276**, 37672-37679, doi:10.1074/jbc.M104521200 (2001).
208 Tommasini, A. *et al.* X-chromosome inactivation analysis in a female carrier of FOXP3 mutation. *Clin Exp Immunol* **130**, 127-130, doi:10.1046/j.1365-2249.2002.01940.x (2002).
209 Lahl, K. *et al.* Selective depletion of Foxp3+ regulatory T cells induces a scurfy-like disease. *J Exp Med* **204**, 57-63, doi:10.1084/jem.20061852 (2007).
210 Arpaia, N. *et al.* A Distinct Function of Regulatory T Cells in Tissue Protection. *Cell* **162**, 1078-1089, doi:10.1016/j.cell.2015.08.021 (2015).
211 Burzyn, D. *et al.* A special population of regulatory T cells potentiates muscle repair. *Cell* **155**, 1282-1295, doi:10.1016/j.cell.2013.10.054 (2013).
212 Feuerer, M. *et al.* Lean, but not obese, fat is enriched for a unique population of regulatory T cells that affect metabolic parameters. *Nat Med* **15**, 930-939, doi:10.1038/nm.2002 (2009).
213 Ali, N. *et al.* Regulatory T Cells in Skin Facilitate Epithelial Stem Cell Differentiation. *Cell* **169**, 1119-1129 e1111, doi:10.1016/j.cell.2017.05.002 (2017).
214 Hsieh, C. S., Zheng, Y., Liang, Y., Fontenot, J. D. & Rudensky, A. Y. An intersection between the self-reactive regulatory and nonregulatory T cell receptor repertoires. *Nat Immunol* **7**, 401-410, doi:10.1038/ni1318 (2006).

215 Wojciech, L. *et al.* The same self-peptide selects conventional and regulatory CD4(+) T cells with identical antigen receptors. *Nat Commun* **5**, 5061, doi:10.1038/ncomms6061 (2014).
216 Wolf, K. J., Emerson, R. O., Pingel, J., Buller, R. M. & DiPaolo, R. J. Conventional and Regulatory CD4+ T Cells That Share Identical TCRs Are Derived from Common Clones. *PLoS One* **11**, e0153705, doi:10.1371/journal.pone.0153705 (2016).
217 Ooi, J. D. *et al.* Dominant protection from HLA-linked autoimmunity by antigen-specific regulatory T cells. *Nature* **545**, 243-247, doi:10.1038/nature22329 (2017).
218 Su, L. F., Del Alcazar, D., Stelekati, E., Wherry, E. J. & Davis, M. M. Antigen exposure shapes the ratio between antigen-specific Tregs and conventional T cells in human peripheral blood. *Proc Natl Acad Sci U S A* **113**, E6192-E6198, doi:10.1073/pnas.1611723113 (2016).
219 Bacher, P. *et al.* Regulatory T Cell Specificity Directs Tolerance versus Allergy against Aeroantigens in Humans. *Cell* **167**, 1067-1078 e1016, doi:10.1016/j.cell.2016.09.050 (2016).
220 Shafiani, S. *et al.* Pathogen-specific Treg cells expand early during mycobacterium tuberculosis infection but are later eliminated in response to Interleukin-12. *Immunity* **38**, 1261-1270, doi:10.1016/j.immuni.2013.06.003 (2013).
221 Lathrop, S. K., Santacruz, N. A., Pham, D., Luo, J. & Hsieh, C. S. Antigen-specific peripheral shaping of the natural regulatory T cell population. *J Exp Med* **205**, 3105-3117, doi:10.1084/jem.20081359 (2008).
222 Huehn, J. *et al.* Developmental stage, phenotype, and migration distinguish naive- and effector/memory-like CD4+ regulatory T cells. *J Exp Med* **199**, 303-313, doi:10.1084/jem.20031562 (2004).
223 Huehn, J., Siegmund, K. & Hamann, A. Migration rules: functional properties of naive and effector/memory-like regulatory T cell subsets. *Curr Top Microbiol Immunol* **293**, 89-114, doi:10.1007/3-540-27702-1_5 (2005).
224 Smigiel, K. S. *et al.* CCR7 provides localized access to IL-2 and defines homeostatically distinct regulatory T cell subsets. *J Exp Med* **211**, 121-136, doi:10.1084/jem.20131142 (2014).
225 Levine, A. G., Arvey, A., Jin, W. & Rudensky, A. Y. Continuous requirement for the TCR in regulatory T cell function. *Nat Immunol* **15**, 1070-1078, doi:10.1038/ni.3004 (2014).
226 Vahl, J. C. *et al.* Continuous T cell receptor signals maintain a functional regulatory T cell pool. *Immunity* **41**, 722-736, doi:10.1016/j.immuni.2014.10.012 (2014).
227 DiToro, D. *et al.* Differential IL-2 expression defines developmental fates of follicular versus nonfollicular helper T cells. *Science* **361**, doi:10.1126/science.aao2933 (2018).
228 Burzyn, D., Benoist, C. & Mathis, D. Regulatory T cells in nonlymphoid tissues. *Nat Immunol* **14**, 1007-1013, doi:10.1038/ni.2683 (2013).
229 Sullivan, J. M., Hollbacher, B. & Campbell, D. J. Cutting Edge: Dynamic Expression of Id3 Defines the Stepwise Differentiation of Tissue-Resident Regulatory T Cells. *J Immunol* **202**, 31-36, doi:10.4049/jimmunol.1800917 (2019).
230 Li, C. *et al.* TCR Transgenic Mice Reveal Stepwise, Multi-site Acquisition of the Distinctive Fat-Treg Phenotype. *Cell* **174**, 285-299 e212, doi:10.1016/j.cell.2018.05.004 (2018).

231 Tontonoz, P. & Spiegelman, B. M. Fat and beyond: the diverse biology of PPARgamma. *Annu Rev Biochem* **77**, 289-312, doi:10.1146/annurev.biochem.77.061307.091829 (2008).
232 Kolodin, D. *et al.* Antigen- and cytokine-driven accumulation of regulatory T cells in visceral adipose tissue of lean mice. *Cell Metab* **21**, 543-557, doi:10.1016/j.cmet.2015.03.005 (2015).
233 Vasanthakumar, A. *et al.* The transcriptional regulators IRF4, BATF and IL-33 orchestrate development and maintenance of adipose tissue-resident regulatory T cells. *Nat Immunol* **16**, 276-285, doi:10.1038/ni.3085 (2015).
234 Sather, B. D. *et al.* Altering the distribution of Foxp3(+) regulatory T cells results in tissue-specific inflammatory disease. *J Exp Med* **204**, 1335-1347, doi:10.1084/jem.20070081 (2007).
235 Koch, M. A. *et al.* T-bet(+) Treg cells undergo abortive Th1 cell differentiation due to impaired expression of IL-12 receptor beta2. *Immunity* **37**, 501-510, doi:10.1016/j.immuni.2012.05.031 (2012).
236 Tan, T. G., Mathis, D. & Benoist, C. Singular role for T-BET+CXCR3+ regulatory T cells in protection from autoimmune diabetes. *Proc Natl Acad Sci U S A* **113**, 14103-14108, doi:10.1073/pnas.1616710113 (2016).
237 Dikiy, S. & Rudensky, A. Y. Principles of regulatory T cell function. *Immunity* **56**, 240-255, doi:10.1016/j.immuni.2023.01.004 (2023).
238 Panduro, M., Benoist, C. & Mathis, D. Tissue Tregs. *Annu Rev Immunol* **34**, 609-633, doi:10.1146/annurev-immunol-032712-095948 (2016).
239 Campbell, C. & Rudensky, A. Roles of Regulatory T Cells in Tissue Pathophysiology and Metabolism. *Cell Metab* **31**, 18-25, doi:10.1016/j.cmet.2019.09.010 (2020).
240 Gratz, I. K. & Campbell, D. J. Organ-specific and memory treg cells: specificity, development, function, and maintenance. *Front Immunol* **5**, 333, doi:10.3389/fimmu.2014.00333 (2014).
241 Thornton, A. M. & Shevach, E. M. CD4+CD25+ immunoregulatory T cells suppress polyclonal T cell activation in vitro by inhibiting interleukin 2 production. *J Exp Med* **188**, 287-296, doi:10.1084/jem.188.2.287 (1998).
242 Thornton, A. M. & Shevach, E. M. Suppressor effector function of CD4+CD25+ immunoregulatory T cells is antigen nonspecific. *J Immunol* **164**, 183-190, doi:10.4049/jimmunol.164.1.183 (2000).
243 Tang, Q. *et al.* Visualizing regulatory T cell control of autoimmune responses in nonobese diabetic mice. *Nat Immunol* **7**, 83-92, doi:10.1038/ni1289 (2006).
244 Takahashi, T. *et al.* Immunologic self-tolerance maintained by CD25(+)CD4(+) regulatory T cells constitutively expressing cytotoxic T lymphocyte-associated antigen 4. *J Exp Med* **192**, 303-310, doi:10.1084/jem.192.2.303 (2000).
245 Read, S., Malmstrom, V. & Powrie, F. Cytotoxic T lymphocyte-associated antigen 4 plays an essential role in the function of CD25(+)CD4(+) regulatory cells that control intestinal inflammation. *J Exp Med* **192**, 295-302, doi:10.1084/jem.192.2.295 (2000).
246 Zheng, Y. & Rudensky, A. Y. Foxp3 in control of the regulatory T cell lineage. *Nat Immunol* **8**, 457-462, doi:10.1038/ni1455 (2007).
247 Marson, A. *et al.* Foxp3 occupancy and regulation of key target genes during T-cell stimulation. *Nature* **445**, 931-935, doi:10.1038/nature05478 (2007).

248 Wu, Y. *et al.* FOXP3 controls regulatory T cell function through cooperation with NFAT. *Cell* **126**, 375-387, doi:10.1016/j.cell.2006.05.042 (2006).
249 Waterhouse, P. *et al.* Lymphoproliferative disorders with early lethality in mice deficient in Ctla-4. *Science* **270**, 985-988, doi:10.1126/science.270.5238.985 (1995).
250 Tivol, E. A. *et al.* Loss of CTLA-4 leads to massive lymphoproliferation and fatal multiorgan tissue destruction, revealing a critical negative regulatory role of CTLA-4. *Immunity* **3**, 541-547, doi:10.1016/1074-7613(95)90125-6 (1995).
251 Kuehn, H. S. *et al.* Immune dysregulation in human subjects with heterozygous germline mutations in CTLA4. *Science* **345**, 1623-1627, doi:10.1126/science.1255904 (2014).
252 Carreno, B. M. & Collins, M. The B7 family of ligands and its receptors: new pathways for costimulation and inhibition of immune responses. *Annu Rev Immunol* **20**, 29-53, doi:10.1146/annurev.immunol.20.091101.091806 (2002).
253 Acuto, O. & Michel, F. CD28-mediated co-stimulation: a quantitative support for TCR signalling. *Nat Rev Immunol* **3**, 939-951, doi:10.1038/nri1248 (2003).
254 Egen, J. G. & Allison, J. P. Cytotoxic T lymphocyte antigen-4 accumulation in the immunological synapse is regulated by TCR signal strength. *Immunity* **16**, 23-35, doi:10.1016/s1074-7613(01)00259-x (2002).
255 Corse, E. & Allison, J. P. Cutting edge: CTLA-4 on effector T cells inhibits in trans. *J Immunol* **189**, 1123-1127, doi:10.4049/jimmunol.1200695 (2012).
256 Wing, K. *et al.* CTLA-4 control over Foxp3+ regulatory T cell function. *Science* **322**, 271-275, doi:10.1126/science.1160062 (2008).
257 Ovcinnikovs, V. *et al.* CTLA-4-mediated transendocytosis of costimulatory molecules primarily targets migratory dendritic cells. *Sci Immunol* **4**, doi:10.1126/sciimmunol.aaw0902 (2019).
258 Qureshi, O. S. *et al.* Trans-endocytosis of CD80 and CD86: a molecular basis for the cell-extrinsic function of CTLA-4. *Science* **332**, 600-603, doi:10.1126/science.1202947 (2011).
259 Oderup, C., Cederbom, L., Makowska, A., Cilio, C. M. & Ivars, F. Cytotoxic T lymphocyte antigen-4-dependent down-modulation of costimulatory molecules on dendritic cells in CD4+ CD25+ regulatory T-cell-mediated suppression. *Immunology* **118**, 240-249, doi:10.1111/j.1365-2567.2006.02362.x (2006).
260 Paterson, A. M. *et al.* Deletion of CTLA-4 on regulatory T cells during adulthood leads to resistance to autoimmunity. *J Exp Med* **212**, 1603-1621, doi:10.1084/jem.20141030 (2015).
261 Klocke, K., Sakaguchi, S., Holmdahl, R. & Wing, K. Induction of autoimmune disease by deletion of CTLA-4 in mice in adulthood. *Proc Natl Acad Sci U S A* **113**, E2383-2392, doi:10.1073/pnas.1603892113 (2016).
262 Sharpe, A. H. & Pauken, K. E. The diverse functions of the PD1 inhibitory pathway. *Nat Rev Immunol* **18**, 153-167, doi:10.1038/nri.2017.108 (2018).
263 Tan, C. L. *et al.* PD-1 restraint of regulatory T cell suppressive activity is critical for immune tolerance. *J Exp Med* **218**, doi:10.1084/jem.20182232 (2021).
264 Fallarino, F. *et al.* Modulation of tryptophan catabolism by regulatory T cells. *Nat Immunol* **4**, 1206-1212, doi:10.1038/ni1003 (2003).
265 Liang, B. *et al.* Regulatory T cells inhibit dendritic cells by lymphocyte activation gene-3 engagement of MHC class II. *J Immunol* **180**, 5916-5926, doi:10.4049/jimmunol.180.9.5916 (2008).

266 Sarris, M., Andersen, K. G., Randow, F., Mayr, L. & Betz, A. G. Neuropilin-1 expression on regulatory T cells enhances their interactions with dendritic cells during antigen recognition. *Immunity* **28**, 402-413, doi:10.1016/j.immuni.2008.01.012 (2008).
267 Sage, P. T., Paterson, A. M., Lovitch, S. B. & Sharpe, A. H. The coinhibitory receptor CTLA-4 controls B cell responses by modulating T follicular helper, T follicular regulatory, and T regulatory cells. *Immunity* **41**, 1026-1039, doi:10.1016/j.immuni.2014.12.005 (2014).
268 Shevach, E. M. Mechanisms of foxp3+ T regulatory cell-mediated suppression. *Immunity* **30**, 636-645, doi:10.1016/j.immuni.2009.04.010 (2009).
269 Vignali, D. A., Collison, L. W. & Workman, C. J. How regulatory T cells work. *Nat Rev Immunol* **8**, 523-532, doi:10.1038/nri2343 (2008).
270 Ross, S. H. & Cantrell, D. A. Signaling and Function of Interleukin-2 in T Lymphocytes. *Annu Rev Immunol* **36**, 411-433, doi:10.1146/annurev-immunol-042617-053352 (2018).
271 Savage, P. A., Klawon, D. E. J. & Miller, C. H. Regulatory T Cell Development. *Annu Rev Immunol* **38**, 421-453, doi:10.1146/annurev-immunol-100219-020937 (2020).
272 Fontenot, J. D., Rasmussen, J. P., Gavin, M. A. & Rudensky, A. Y. A function for interleukin 2 in Foxp3-expressing regulatory T cells. *Nat Immunol* **6**, 1142-1151, doi:10.1038/ni1263 (2005).
273 Cheng, G., Yu, A. & Malek, T. R. T-cell tolerance and the multi-functional role of IL-2R signaling in T-regulatory cells. *Immunol Rev* **241**, 63-76, doi:10.1111/j.1600-065X.2011.01004.x (2011).
274 O'Gorman, W. E. *et al.* The initial phase of an immune response functions to activate regulatory T cells. *J Immunol* **183**, 332-339, doi:10.4049/jimmunol.0900691 (2009).
275 Liu, Z. *et al.* Immune homeostasis enforced by co-localized effector and regulatory T cells. *Nature* **528**, 225-230, doi:10.1038/nature16169 (2015).
276 Wong, H. S. *et al.* A local regulatory T cell feedback circuit maintains immune homeostasis by pruning self-activated T cells. *Cell* **184**, 3981-3997 e3922, doi:10.1016/j.cell.2021.05.028 (2021).
277 Oyler-Yaniv, A. *et al.* A Tunable Diffusion-Consumption Mechanism of Cytokine Propagation Enables Plasticity in Cell-to-Cell Communication in the Immune System. *Immunity* **46**, 609-620, doi:10.1016/j.immuni.2017.03.011 (2017).
278 Fiorentino, D. F., Bond, M. W. & Mosmann, T. R. Two types of mouse T helper cell. IV. Th2 clones secrete a factor that inhibits cytokine production by Th1 clones. *J Exp Med* **170**, 2081-2095, doi:10.1084/jem.170.6.2081 (1989).
279 Kuhn, R., Lohler, J., Rennick, D., Rajewsky, K. & Muller, W. Interleukin-10-deficient mice develop chronic enterocolitis. *Cell* **75**, 263-274, doi:10.1016/0092-8674(93)80068-p (1993).
280 Moore, K. W., de Waal Malefyt, R., Coffman, R. L. & O'Garra, A. Interleukin-10 and the interleukin-10 receptor. *Annu Rev Immunol* **19**, 683-765, doi:10.1146/annurev.immunol.19.1.683 (2001).
281 Groux, H. *et al.* A CD4+ T-cell subset inhibits antigen-specific T-cell responses and prevents colitis. *Nature* **389**, 737-742, doi:10.1038/39614 (1997).
282 Maynard, C. L. *et al.* Regulatory T cells expressing interleukin 10 develop from Foxp3+ and Foxp3- precursor cells in the absence of interleukin 10. *Nat Immunol* **8**, 931-941, doi:10.1038/ni1504 (2007).

283 Rubtsov, Y. P. *et al.* Regulatory T cell-derived interleukin-10 limits inflammation at environmental interfaces. *Immunity* **28**, 546-558, doi:10.1016/j.immuni.2008.02.017 (2008).
284 Burkhart, C., Liu, G. Y., Anderton, S. M., Metzler, B. & Wraith, D. C. Peptide-induced T cell regulation of experimental autoimmune encephalomyelitis: a role for IL-10. *Int Immunol* **11**, 1625-1634, doi:10.1093/intimm/11.10.1625 (1999).
285 Chen, Y., Kuchroo, V. K., Inobe, J., Hafler, D. A. & Weiner, H. L. Regulatory T cell clones induced by oral tolerance: suppression of autoimmune encephalomyelitis. *Science* **265**, 1237-1240, doi:10.1126/science.7520605 (1994).
286 Kullberg, M. C. *et al.* Bacteria-triggered CD4(+) T regulatory cells suppress Helicobacter hepaticus-induced colitis. *J Exp Med* **196**, 505-515, doi:10.1084/jem.20020556 (2002).
287 Shull, M. M. *et al.* Targeted disruption of the mouse transforming growth factor-beta 1 gene results in multifocal inflammatory disease. *Nature* **359**, 693-699, doi:10.1038/359693a0 (1992).
288 Chen, W. *et al.* Conversion of peripheral CD4+CD25- naive T cells to CD4+CD25+ regulatory T cells by TGF-beta induction of transcription factor Foxp3. *J Exp Med* **198**, 1875-1886, doi:10.1084/jem.20030152 (2003).
289 Harrington, L. E. *et al.* Interleukin 17-producing CD4+ effector T cells develop via a lineage distinct from the T helper type 1 and 2 lineages. *Nat Immunol* **6**, 1123-1132, doi:10.1038/ni1254 (2005).
290 Park, H. *et al.* A distinct lineage of CD4 T cells regulates tissue inflammation by producing interleukin 17. *Nat Immunol* **6**, 1133-1141, doi:10.1038/ni1261 (2005).
291 Langrish, C. L. *et al.* IL-23 drives a pathogenic T cell population that induces autoimmune inflammation. *J Exp Med* **201**, 233-240, doi:10.1084/jem.20041257 (2005).
292 Murphy, C. A. *et al.* Divergent pro- and antiinflammatory roles for IL-23 and IL-12 in joint autoimmune inflammation. *J Exp Med* **198**, 1951-1957, doi:10.1084/jem.20030896 (2003).
293 Cua, D. J. *et al.* Interleukin-23 rather than interleukin-12 is the critical cytokine for autoimmune inflammation of the brain. *Nature* **421**, 744-748, doi:10.1038/nature01355 (2003).
294 Bettelli, E. *et al.* Reciprocal developmental pathways for the generation of pathogenic effector TH17 and regulatory T cells. *Nature* **441**, 235-238, doi:10.1038/nature04753 (2006).
295 Chaudhry, A. *et al.* Interleukin-10 signaling in regulatory T cells is required for suppression of Th17 cell-mediated inflammation. *Immunity* **34**, 566-578, doi:10.1016/j.immuni.2011.03.018 (2011).
296 Huber, S. *et al.* Th17 cells express interleukin-10 receptor and are controlled by Foxp3(-) and Foxp3+ regulatory CD4+ T cells in an interleukin-10-dependent manner. *Immunity* **34**, 554-565, doi:10.1016/j.immuni.2011.01.020 (2011).
297 Xiao, S. *et al.* Retinoic acid increases Foxp3+ regulatory T cells and inhibits development of Th17 cells by enhancing TGF-beta-driven Smad3 signaling and inhibiting IL-6 and IL-23 receptor expression. *J Immunol* **181**, 2277-2284, doi:10.4049/jimmunol.181.4.2277 (2008).
298 Brown, C. C. & Rudensky, A. Y. Spatiotemporal regulation of peripheral T cell tolerance. *Science* **380**, 472-478, doi:10.1126/science.adg6425 (2023).

299 Korn, T. *et al.* IL-21 initiates an alternative pathway to induce proinflammatory T(H)17 cells. *Nature* **448**, 484-487, doi:10.1038/nature05970 (2007).
300 Levine, A. G. *et al.* Suppression of lethal autoimmunity by regulatory T cells with a single TCR specificity. *J Exp Med* **214**, 609-622, doi:10.1084/jem.20161318 (2017).
301 Akkaya, B. *et al.* Regulatory T cells mediate specific suppression by depleting peptide-MHC class II from dendritic cells. *Nat Immunol* **20**, 218-231, doi:10.1038/s41590-018-0280-2 (2019).
302 Yang, S. J. *et al.* Pancreatic islet-specific engineered T(regs) exhibit robust antigen-specific and bystander immune suppression in type 1 diabetes models. *Sci Transl Med* **14**, eabn1716, doi:10.1126/scitranslmed.abn1716 (2022).
303 Yi, J. *et al.* Antigen-specific depletion of CD4(+) T cells by CAR T cells reveals distinct roles of higher- and lower-affinity TCRs during autoimmunity. *Sci Immunol* **7**, eabo0777, doi:10.1126/sciimmunol.abo0777 (2022).
304 Dominguez-Villar, M. & Hafler, D. A. Regulatory T cells in autoimmune disease. *Nat Immunol* **19**, 665-673, doi:10.1038/s41590-018-0120-4 (2018).
305 Tay, C., Tanaka, A. & Sakaguchi, S. Tumor-infiltrating regulatory T cells as targets of cancer immunotherapy. *Cancer Cell* **41**, 450-465, doi:10.1016/j.ccell.2023.02.014 (2023).
306 Noval Rivas, M. & Chatila, T. A. Regulatory T cells in allergic diseases. *J Allergy Clin Immunol* **138**, 639-652, doi:10.1016/j.jaci.2016.06.003 (2016).
307 Chong, A. S., Sage, P. T. & Alegre, M. L. Regulation of Alloantibody Responses. *Front Cell Dev Biol* **9**, 706171, doi:10.3389/fcell.2021.706171 (2021).
308 Romano, M., Fanelli, G., Albany, C. J., Giganti, G. & Lombardi, G. Past, Present, and Future of Regulatory T Cell Therapy in Transplantation and Autoimmunity. *Front Immunol* **10**, 43, doi:10.3389/fimmu.2019.00043 (2019).
309 Arvey, A. *et al.* Inflammation-induced repression of chromatin bound by the transcription factor Foxp3 in regulatory T cells. *Nat Immunol* **15**, 580-587, doi:10.1038/ni.2868 (2014).
310 van der Veeken, J. *et al.* Memory of Inflammation in Regulatory T Cells. *Cell* **166**, 977-990, doi:10.1016/j.cell.2016.07.006 (2016).
311 Saravia, J., Chapman, N. M. & Chi, H. Helper T cell differentiation. *Cell Mol Immunol* **16**, 634-643, doi:10.1038/s41423-019-0220-6 (2019).
312 Campbell, D. J. & Koch, M. A. Phenotypical and functional specialization of FOXP3+ regulatory T cells. *Nat Rev Immunol* **11**, 119-130, doi:10.1038/nri2916 (2011).
313 Koch, M. A. *et al.* The transcription factor T-bet controls regulatory T cell homeostasis and function during type 1 inflammation. *Nat Immunol* **10**, 595-602, doi:10.1038/ni.1731 (2009).
314 Chaudhry, A. *et al.* CD4+ regulatory T cells control TH17 responses in a Stat3-dependent manner. *Science* **326**, 986-991, doi:10.1126/science.1172702 (2009).
315 Levine, A. G. *et al.* Stability and function of regulatory T cells expressing the transcription factor T-bet. *Nature* **546**, 421-425, doi:10.1038/nature22360 (2017).
316 Martinez, R. J. *et al.* Type III interferon drives thymic B cell activation and regulatory T cell generation. *Proc Natl Acad Sci U S A* **120**, e2220120120, doi:10.1073/pnas.2220120120 (2023).
317 Belkaid, Y., Piccirillo, C. A., Mendez, S., Shevach, E. M. & Sacks, D. L. CD4+CD25+ regulatory T cells control Leishmania major persistence and immunity. *Nature* **420**, 502-507, doi:10.1038/nature01152 (2002).

318 Mendez, S., Reckling, S. K., Piccirillo, C. A., Sacks, D. & Belkaid, Y. Role for CD4(+) CD25(+) regulatory T cells in reactivation of persistent leishmaniasis and control of concomitant immunity. *J Exp Med* **200**, 201-210, doi:10.1084/jem.20040298 (2004).
319 Lund, J. M., Hsing, L., Pham, T. T. & Rudensky, A. Y. Coordination of early protective immunity to viral infection by regulatory T cells. *Science* **320**, 1220-1224, doi:10.1126/science.1155209 (2008).
320 Oldenhove, G. *et al.* Decrease of Foxp3+ Treg cell number and acquisition of effector cell phenotype during lethal infection. *Immunity* **31**, 772-786, doi:10.1016/j.immuni.2009.10.001 (2009).
321 Rowe, J. H., Ertelt, J. M., Aguilera, M. N., Farrar, M. A. & Way, S. S. Foxp3(+) regulatory T cell expansion required for sustaining pregnancy compromises host defense against prenatal bacterial pathogens. *Cell Host Microbe* **10**, 54-64, doi:10.1016/j.chom.2011.06.005 (2011).
322 Srivastava, S., Koch, M. A., Pepper, M. & Campbell, D. J. Type I interferons directly inhibit regulatory T cells to allow optimal antiviral T cell responses during acute LCMV infection. *J Exp Med* **211**, 961-974, doi:10.1084/jem.20131556 (2014).
323 Pace, L. *et al.* Regulatory T cells increase the avidity of primary CD8+ T cell responses and promote memory. *Science* **338**, 532-536, doi:10.1126/science.1227049 (2012).
324 Laidlaw, B. J. *et al.* Production of IL-10 by CD4(+) regulatory T cells during the resolution of infection promotes the maturation of memory CD8(+) T cells. *Nat Immunol* **16**, 871-879, doi:10.1038/ni.3224 (2015).
325 Dolina, J. S. *et al.* Developmentally distinct CD4(+) T(reg) lineages shape the CD8(+) T cell response to acute Listeria infection. *Proc Natl Acad Sci U S A* **119**, e2113329119, doi:10.1073/pnas.2113329119 (2022).
326 Ertelt, J. M. *et al.* Selective priming and expansion of antigen-specific Foxp3- CD4+ T cells during Listeria monocytogenes infection. *J Immunol* **182**, 3032-3038, doi:10.4049/jimmunol.0803402 (2009).
327 Brincks, E. L. *et al.* Antigen-specific memory regulatory CD4+Foxp3+ T cells control memory responses to influenza virus infection. *J Immunol* **190**, 3438-3446, doi:10.4049/jimmunol.1203140 (2013).
328 Sanchez, A. M., Zhu, J., Huang, X. & Yang, Y. The development and function of memory regulatory T cells after acute viral infections. *J Immunol* **189**, 2805-2814, doi:10.4049/jimmunol.1200645 (2012).
329 Quadros, R. M. *et al.* Easi-CRISPR: a robust method for one-step generation of mice carrying conditional and insertion alleles using long ssDNA donors and CRISPR ribonucleoproteins. *Genome Biol* **18**, 92, doi:10.1186/s13059-017-1220-4 (2017).
330 Shi, J., Getun, I., Torres, B. & Petrie, H. T. Foxn1[Cre] Expression in the Male Germline. *PLoS One* **11**, e0166967, doi:10.1371/journal.pone.0166967 (2016).
331 McDonald, B. D., Bunker, J. J., Erickson, S. A., Oh-Hora, M. & Bendelac, A. Crossreactive alphabeta T Cell Receptors Are the Predominant Targets of Thymocyte Negative Selection. *Immunity* **43**, 859-869, doi:10.1016/j.immuni.2015.09.009 (2015).
332 Turner, V. M., Gardam, S. & Brink, R. Lineage-specific transgene expression in hematopoietic cells using a Cre-regulated retroviral vector. *J Immunol Methods* **360**, 162-166, doi:10.1016/j.jim.2010.06.007 (2010).

333 Morita, S., Kojima, T. & Kitamura, T. Plat-E: an efficient and stable system for transient packaging of retroviruses. *Gene therapy* **7**, 1063-1066, doi:10.1038/sj.gt.3301206 (2000).
334 Moon, J. J. *et al.* Naive CD4(+) T cell frequency varies for different epitopes and predicts repertoire diversity and response magnitude. *Immunity* **27**, 203-213, doi:10.1016/j.immuni.2007.07.007 (2007).
335 Tungatt, K. *et al.* Antibody stabilization of peptide-MHC multimers reveals functional T cells bearing extremely low-affinity TCRs. *J Immunol* **194**, 463-474, doi:10.4049/jimmunol.1401785 (2015).
336 Legoux, F. P. & Moon, J. J. Peptide:MHC tetramer-based enrichment of epitope-specific T cells. *J Vis Exp*, doi:10.3791/4420 (2012).
337 Yan, L. *et al.* Selected prfA* mutations in recombinant attenuated Listeria monocytogenes strains augment expression of foreign immunogens and enhance vaccine-elicited humoral and cellular immune responses. *Infect Immun* **76**, 3439-3450, doi:10.1128/IAI.00245-08 (2008).
338 Stuart, T. *et al.* Comprehensive Integration of Single-Cell Data. *Cell* **177**, 1888-1902 e1821, doi:10.1016/j.cell.2019.05.031 (2019).
339 McCarthy, D. J., Chen, Y. & Smyth, G. K. Differential expression analysis of multifactor RNA-Seq experiments with respect to biological variation. *Nucleic Acids Res* **40**, 4288-4297, doi:10.1093/nar/gks042 (2012).
340 Robinson, M. D., McCarthy, D. J. & Smyth, G. K. edgeR: a Bioconductor package for differential expression analysis of digital gene expression data. *Bioinformatics* **26**, 139-140, doi:10.1093/bioinformatics/btp616 (2010).
341 Spanier, J. A. *et al.* Efficient generation of monoclonal antibodies against peptide in the context of MHCII using magnetic enrichment. *Nat Commun* **7**, 11804, doi:10.1038/ncomms11804 (2016).
342 Tam, H. H. *et al.* Sustained antigen availability during germinal center initiation enhances antibody responses to vaccination. *Proc Natl Acad Sci U S A* **113**, E6639-E6648, doi:10.1073/pnas.1606050113 (2016).
343 Klein, L., Kyewski, B., Allen, P. M. & Hogquist, K. A. Positive and negative selection of the T cell repertoire: what thymocytes see (and don't see). *Nat Rev Immunol* **14**, 377-391, doi:10.1038/nri3667 (2014).
344 Josefowicz, S. Z., Lu, L. F. & Rudensky, A. Y. Regulatory T cells: mechanisms of differentiation and function. *Annu Rev Immunol* **30**, 531-564, doi:10.1146/annurev.immunol.25.022106.141623 (2012).
345 Fan, Y. *et al.* Thymus-specific deletion of insulin induces autoimmune diabetes. *EMBO J* **28**, 2812-2824, doi:10.1038/emboj.2009.212 (2009).
346 DeVoss, J. *et al.* Spontaneous autoimmunity prevented by thymic expression of a single self-antigen. *J Exp Med* **203**, 2727-2735, doi:10.1084/jem.20061864 (2006).
347 Taniguchi, R. T. *et al.* Detection of an autoreactive T-cell population within the polyclonal repertoire that undergoes distinct autoimmune regulator (Aire)-mediated selection. *Proc Natl Acad Sci U S A* **109**, 7847-7852, doi:10.1073/pnas.1120607109 (2012).
348 Thebault-Baumont, K. *et al.* Acceleration of type 1 diabetes mellitus in proinsulin 2-deficient NOD mice. *J Clin Invest* **111**, 851-857, doi:10.1172/JCI16584 (2003).
349 Meng, J. *et al.* Testosterone regulates tight junction proteins and influences prostatic autoimmune responses. *Horm Cancer* **2**, 145-156, doi:10.1007/s12672-010-0063-1 (2011).

350 Nelson, R. W. *et al.* T cell receptor cross-reactivity between similar foreign and self peptides influences naive cell population size and autoimmunity. *Immunity* **42**, 95-107, doi:10.1016/j.immuni.2014.12.022 (2015).
351 Zehn, D. & Bevan, M. J. T cells with low avidity for a tissue-restricted antigen routinely evade central and peripheral tolerance and cause autoimmunity. *Immunity* **25**, 261-270, doi:10.1016/j.immuni.2006.06.009 (2006).
352 Moon, J. J. *et al.* Tracking epitope-specific T cells. *Nat Protoc* **4**, 565-581, doi:10.1038/nprot.2009.9 (2009).
353 Samy, E. T., Parker, L. A., Sharp, C. P. & Tung, K. S. Continuous control of autoimmune disease by antigen-dependent polyclonal CD4+CD25+ regulatory T cells in the regional lymph node. *J Exp Med* **202**, 771-781, doi:10.1084/jem.20041033 (2005).
354 Bouillet, P. *et al.* BH3-only Bcl-2 family member Bim is required for apoptosis of autoreactive thymocytes. *Nature* **415**, 922-926, doi:10.1038/415922a (2002).
355 Savage, P. A., Boniface, J. J. & Davis, M. M. A kinetic basis for T cell receptor repertoire selection during an immune response. *Immunity* **10**, 485-492 (1999).
356 Crawford, F., Kozono, H., White, J., Marrack, P. & Kappler, J. Detection of antigen-specific T cells with multivalent soluble class II MHC covalent peptide complexes. *Immunity* **8**, 675-682 (1998).
357 Xing, Y. & Hogquist, K. A. T-cell tolerance: central and peripheral. *Cold Spring Harb Perspect Biol* **4**, doi:10.1101/cshperspect.a006957 (2012).
358 Lee, V. *et al.* The endogenous repertoire harbors self-reactive CD4(+) T cell clones that adopt a follicular helper T cell-like phenotype at steady state. *Nat Immunol*, doi:10.1038/s41590-023-01425-0 (2023).
359 Brugnera, E. *et al.* Coreceptor reversal in the thymus: signaled CD4+8+ thymocytes initially terminate CD8 transcription even when differentiating into CD8+ T cells. *Immunity* **13**, 59-71, doi:10.1016/s1074-7613(00)00008-x (2000).
360 Zhu, Y., Rudensky, A. Y., Corper, A. L., Teyton, L. & Wilson, I. A. Crystal structure of MHC class II I-Ab in complex with a human CLIP peptide: prediction of an I-Ab peptide-binding motif. *J Mol Biol* **326**, 1157-1174, doi:10.1016/s0022-2836(02)01437-7 (2003).
361 Sewell, A. K. Why must T cells be cross-reactive? *Nat Rev Immunol* **12**, 669-677, doi:10.1038/nri3279 (2012).
362 Stone, J. D., Chervin, A. S. & Kranz, D. M. T-cell receptor binding affinities and kinetics: impact on T-cell activity and specificity. *Immunology* **126**, 165-176, doi:10.1111/j.1365-2567.2008.03015.x (2009).
363 Bankovich, A. J., Girvin, A. T., Moesta, A. K. & Garcia, K. C. Peptide register shifting within the MHC groove: theory becomes reality. *Mol Immunol* **40**, 1033-1039, doi:10.1016/j.molimm.2003.11.016 (2004).
364 Dileepan, T. *et al.* MHC class II tetramers engineered for enhanced binding to CD4 improve detection of antigen-specific T cells. *Nat Biotechnol* **39**, 943-948, doi:10.1038/s41587-021-00893-9 (2021).
365 Sibener, L. V. *et al.* Isolation of a Structural Mechanism for Uncoupling T Cell Receptor Signaling from Peptide-MHC Binding. *Cell* **174**, 672-687 e627, doi:10.1016/j.cell.2018.06.017 (2018).
366 Yewdell, J. W. Confronting complexity: real-world immunodominance in antiviral CD8+ T cell responses. *Immunity* **25**, 533-543, doi:10.1016/j.immuni.2006.09.005 (2006).

367 Lehmann, P. V., Forsthuber, T., Miller, A. & Sercarz, E. E. Spreading of T-cell autoimmunity to cryptic determinants of an autoantigen. *Nature* **358**, 155-157, doi:10.1038/358155a0 (1992).
368 Stadinski, B. D. *et al.* A temporal thymic selection switch and ligand binding kinetics constrain neonatal Foxp3(+) T(reg) cell development. *Nat Immunol* **20**, 1046-1058, doi:10.1038/s41590-019-0414-1 (2019).
369 Rosen, A. & Casciola-Rosen, L. Autoantigens as Partners in Initiation and Propagation of Autoimmune Rheumatic Diseases. *Annu Rev Immunol* **34**, 395-420, doi:10.1146/annurev-immunol-032414-112205 (2016).
370 Wang, L. *et al.* Epitope-Specific Tolerance Modes Differentially Specify Susceptibility to Proteolipid Protein-Induced Experimental Autoimmune Encephalomyelitis. *Front Immunol* **8**, 1511, doi:10.3389/fimmu.2017.01511 (2017).
371 Nakayama, M. *et al.* Prime role for an insulin epitope in the development of type 1 diabetes in NOD mice. *Nature* **435**, 220-223, doi:10.1038/nature03523 (2005).
372 Spanier, J. A. *et al.* Increased Effector Memory Insulin-Specific CD4(+) T Cells Correlate With Insulin Autoantibodies in Patients With Recent-Onset Type 1 Diabetes. *Diabetes* **66**, 3051-3060, doi:10.2337/db17-0666 (2017).
373 Cortes, L. M. *et al.* Repertoire analysis and new pathogenic epitopes of IRBP in C57BL/6 (H-2b) and B10.RIII (H-2r) mice. *Invest Ophthalmol Vis Sci* **49**, 1946-1956, doi:10.1167/iovs.07-0868 (2008).
374 Landegren, N. *et al.* Transglutaminase 4 as a prostate autoantigen in male subfertility. *Sci Transl Med* **7**, 292ra101, doi:10.1126/scitranslmed.aaa9186 (2015).
375 Meyer, S. *et al.* AIRE-Deficient Patients Harbor Unique High-Affinity Disease-Ameliorating Autoantibodies. *Cell* **166**, 582-595, doi:10.1016/j.cell.2016.06.024 (2016).
376 Sercarz, E. E. *et al.* Dominance and crypticity of T cell antigenic determinants. *Annu Rev Immunol* **11**, 729-766, doi:10.1146/annurev.iy.11.040193.003501 (1993).
377 Murata, S. *et al.* Regulation of CD8+ T cell development by thymus-specific proteasomes. *Science* **316**, 1349-1353, doi:10.1126/science.1141915 (2007).
378 Nemazee, D. Receptor selection in B and T lymphocytes. *Annu Rev Immunol* **18**, 19-51, doi:10.1146/annurev.immunol.18.1.19 (2000).
379 Mathis, D. & Benoist, C. Back to central tolerance. *Immunity* **20**, 509-516, doi:10.1016/s1074-7613(04)00111-6 (2004).
380 Yu, W. *et al.* Clonal Deletion Prunes but Does Not Eliminate Self-Specific alphabeta CD8(+) T Lymphocytes. *Immunity* **42**, 929-941, doi:10.1016/j.immuni.2015.05.001 (2015).
381 Yan, J. & Mamula, M. J. Autoreactive T cells revealed in the normal repertoire: escape from negative selection and peripheral tolerance. *J Immunol* **168**, 3188-3194, doi:10.4049/jimmunol.168.7.3188 (2002).
382 Bouneaud, C., Kourilsky, P. & Bousso, P. Impact of negative selection on the T cell repertoire reactive to a self-peptide: a large fraction of T cell clones escapes clonal deletion. *Immunity* **13**, 829-840, doi:10.1016/s1074-7613(00)00080-7 (2000).
383 Pandiyan, P., Zheng, L., Ishihara, S., Reed, J. & Lenardo, M. J. CD4+CD25+Foxp3+ regulatory T cells induce cytokine deprivation-mediated apoptosis of effector CD4+ T cells. *Nat Immunol* **8**, 1353-1362, doi:10.1038/ni1536 (2007).

384 von Boehmer, H. Mechanisms of suppression by suppressor T cells. *Nat Immunol* **6**, 338-344, doi:10.1038/ni1180 (2005).
385 Wong, H. S. & Germain, R. N. Robust control of the adaptive immune system. *Semin Immunol* **36**, 17-27, doi:10.1016/j.smim.2017.12.009 (2018).
386 Mogensen, T. H. Pathogen recognition and inflammatory signaling in innate immune defenses. *Clin Microbiol Rev* **22**, 240-273, Table of Contents, doi:10.1128/CMR.00046-08 (2009).
387 Kratky, W., Reis e Sousa, C., Oxenius, A. & Sporri, R. Direct activation of antigen-presenting cells is required for CD8+ T-cell priming and tumor vaccination. *Proc Natl Acad Sci U S A* **108**, 17414-17419, doi:10.1073/pnas.1108945108 (2011).
388 Nace, G., Evankovich, J., Eid, R. & Tsung, A. Dendritic cells and damage-associated molecular patterns: endogenous danger signals linking innate and adaptive immunity. *J Innate Immun* **4**, 6-15, doi:10.1159/000334245 (2012).
389 Gallucci, S., Lolkema, M. & Matzinger, P. Natural adjuvants: endogenous activators of dendritic cells. *Nat Med* **5**, 1249-1255, doi:10.1038/15200 (1999).
390 Kono, H. & Rock, K. L. How dying cells alert the immune system to danger. *Nat Rev Immunol* **8**, 279-289, doi:10.1038/nri2215 (2008).
391 Cusick, M. F., Libbey, J. E. & Fujinami, R. S. Molecular mimicry as a mechanism of autoimmune disease. *Clin Rev Allergy Immunol* **42**, 102-111, doi:10.1007/s12016-011-8294-7 (2012).
392 Yang, X. *et al.* Autoimmunity-associated T cell receptors recognize HLA-B*27-bound peptides. *Nature* **612**, 771-777, doi:10.1038/s41586-022-05501-7 (2022).
393 Harris, J. E. *et al.* Early growth response gene-2, a zinc-finger transcription factor, is required for full induction of clonal anergy in CD4+ T cells. *J Immunol* **173**, 7331-7338, doi:10.4049/jimmunol.173.12.7331 (2004).
394 Portnoy, D. A., Auerbuch, V. & Glomski, I. J. The cell biology of Listeria monocytogenes infection: the intersection of bacterial pathogenesis and cell-mediated immunity. *J Cell Biol* **158**, 409-414, doi:10.1083/jcb.200205009 (2002).
395 Hamon, M., Bierne, H. & Cossart, P. Listeria monocytogenes: a multifaceted model. *Nat Rev Microbiol* **4**, 423-434, doi:10.1038/nrmicro1413 (2006).
396 Lauer, P., Chow, M. Y., Loessner, M. J., Portnoy, D. A. & Calendar, R. Construction, characterization, and use of two Listeria monocytogenes site-specific phage integration vectors. *J Bacteriol* **184**, 4177-4186, doi:10.1128/JB.184.15.4177-4186.2002 (2002).
397 Shetron-Rama, L. M. *et al.* Isolation of Listeria monocytogenes mutants with high-level in vitro expression of host cytosol-induced gene products. *Mol Microbiol* **48**, 1537-1551, doi:10.1046/j.1365-2958.2003.03534.x (2003).
398 Mueller, K. J. & Freitag, N. E. Pleiotropic enhancement of bacterial pathogenesis resulting from the constitutive activation of the Listeria monocytogenes regulatory factor PrfA. *Infect Immun* **73**, 1917-1926, doi:10.1128/IAI.73.4.1917-1926.2005 (2005).
399 Schroder, B. The multifaceted roles of the invariant chain CD74--More than just a chaperone. *Biochim Biophys Acta* **1863**, 1269-1281, doi:10.1016/j.bbamcr.2016.03.026 (2016).
400 Pepper, M., Pagan, A. J., Igyarto, B. Z., Taylor, J. J. & Jenkins, M. K. Opposing signals from the Bcl6 transcription factor and the interleukin-2 receptor generate T helper 1 central

and effector memory cells. *Immunity* **35**, 583-595, doi:10.1016/j.immuni.2011.09.009 (2011).

401 Gordon, J. *et al.* Specific expression of lacZ and cre recombinase in fetal thymic epithelial cells by multiplex gene targeting at the Foxn1 locus. *BMC Dev Biol* **7**, 69, doi:10.1186/1471-213X-7-69 (2007).

402 Cossart, P. & Mengaud, J. Listeria monocytogenes. A model system for the molecular study of intracellular parasitism. *Mol Biol Med* **6**, 463-474 (1989).

403 Brundage, R. A., Smith, G. A., Camilli, A., Theriot, J. A. & Portnoy, D. A. Expression and phosphorylation of the Listeria monocytogenes ActA protein in mammalian cells. *Proc Natl Acad Sci U S A* **90**, 11890-11894, doi:10.1073/pnas.90.24.11890 (1993).

404 Endres, R. *et al.* Listeriosis in p47(phox-/-) and TRp55-/- mice: protection despite absence of ROI and susceptibility despite presence of RNI. *Immunity* **7**, 419-432, doi:10.1016/s1074-7613(00)80363-5 (1997).

405 Nanda, N. K., Birch, L., Greenberg, N. M. & Prins, G. S. MHC class I and class II molecules are expressed in both human and mouse prostate tumor microenvironment. *Prostate* **66**, 1275-1284, doi:10.1002/pros.20432 (2006).

406 Gearty, S. V. *et al.* An autoimmune stem-like CD8 T cell population drives type 1 diabetes. *Nature* **602**, 156-161, doi:10.1038/s41586-021-04248-x (2022).

407 Philip, M. *et al.* Chromatin states define tumour-specific T cell dysfunction and reprogramming. *Nature* **545**, 452-456, doi:10.1038/nature22367 (2017).

408 Cyster, J. G. Chemokines, sphingosine-1-phosphate, and cell migration in secondary lymphoid organs. *Annu Rev Immunol* **23**, 127-159, doi:10.1146/annurev.immunol.23.021704.115628 (2005).

409 Krueger, P. D., Osum, K. C. & Jenkins, M. K. CD4(+) Memory T-Cell Formation during Type 1 Immune Responses. *Cold Spring Harb Perspect Biol* **13**, doi:10.1101/cshperspect.a038141 (2021).

410 Escobar, G., Mangani, D. & Anderson, A. C. T cell factor 1: A master regulator of the T cell response in disease. *Sci Immunol* **5**, doi:10.1126/sciimmunol.abb9726 (2020).

411 Siddiqui, I. *et al.* Intratumoral Tcf1(+)PD-1(+)CD8(+) T Cells with Stem-like Properties Promote Tumor Control in Response to Vaccination and Checkpoint Blockade Immunotherapy. *Immunity* **50**, 195-211 e110, doi:10.1016/j.immuni.2018.12.021 (2019).

412 Nish, S. A. *et al.* CD4+ T cell effector commitment coupled to self-renewal by asymmetric cell divisions. *J Exp Med* **214**, 39-47, doi:10.1084/jem.20161046 (2017).

413 Miller, B. C. *et al.* Subsets of exhausted CD8(+) T cells differentially mediate tumor control and respond to checkpoint blockade. *Nat Immunol* **20**, 326-336, doi:10.1038/s41590-019-0312-6 (2019).

414 Greenbaum, D., Colangelo, C., Williams, K. & Gerstein, M. Comparing protein abundance and mRNA expression levels on a genomic scale. *Genome Biol* **4**, 117, doi:10.1186/gb-2003-4-9-117 (2003).

415 Grossman, Z. & Paul, W. E. Dynamic tuning of lymphocytes: physiological basis, mechanisms, and function. *Annu Rev Immunol* **33**, 677-713, doi:10.1146/annurev-immunol-032712-100027 (2015).

416 Heinzel, S. *et al.* A Myc-dependent division timer complements a cell-death timer to regulate T cell and B cell responses. *Nat Immunol* **18**, 96-103, doi:10.1038/ni.3598 (2017).

417 Zabriskie, J. B. & Freimer, E. H. An immunological relationship between the group. A streptococcus and mammalian muscle. *J Exp Med* **124**, 661-678, doi:10.1084/jem.124.4.661 (1966).
418 Fujinami, R. S. & Oldstone, M. B. Amino acid homology between the encephalitogenic site of myelin basic protein and virus: mechanism for autoimmunity. *Science* **230**, 1043-1045, doi:10.1126/science.2414848 (1985).
419 Gough, S. C. & Simmonds, M. J. The HLA Region and Autoimmune Disease: Associations and Mechanisms of Action. *Curr Genomics* **8**, 453-465, doi:10.2174/138920207783591690 (2007).
420 Chowdhury, R. R. *et al.* Human Coronary Plaque T Cells Are Clonal and Cross-React to Virus and Self. *Circ Res* **130**, 1510-1530, doi:10.1161/CIRCRESAHA.121.320090 (2022).
421 Miller, F. W. The increasing prevalence of autoimmunity and autoimmune diseases: an urgent call to action for improved understanding, diagnosis, treatment, and prevention. *Curr Opin Immunol* **80**, 102266, doi:10.1016/j.coi.2022.102266 (2023).
422 Lerner, A. & Matthias, T. Changes in intestinal tight junction permeability associated with industrial food additives explain the rising incidence of autoimmune disease. *Autoimmun Rev* **14**, 479-489, doi:10.1016/j.autrev.2015.01.009 (2015).
423 Trost, B. *et al.* No human protein is exempt from bacterial motifs, not even one. *Self Nonself* **1**, 328-334, doi:10.4161/self.1.4.13315 (2010).
424 Wang, P. *et al.* A systematic assessment of MHC class II peptide binding predictions and evaluation of a consensus approach. *PLoS Comput Biol* **4**, e1000048, doi:10.1371/journal.pcbi.1000048 (2008).
425 Jones, E. Y., Fugger, L., Strominger, J. L. & Siebold, C. MHC class II proteins and disease: a structural perspective. *Nat Rev Immunol* **6**, 271-282, doi:10.1038/nri1805 (2006).
426 Bousbaine, D. *et al.* A conserved Bacteroidetes antigen induces anti-inflammatory intestinal T lymphocytes. *Science* **377**, 660-666, doi:10.1126/science.abg5645 (2022).
427 Scharschmidt, T. C. *et al.* A Wave of Regulatory T Cells into Neonatal Skin Mediates Tolerance to Commensal Microbes. *Immunity* **43**, 1011-1021, doi:10.1016/j.immuni.2015.10.016 (2015).
428 Rowe, J. H., Ertelt, J. M., Xin, L. & Way, S. S. Pregnancy imprints regulatory memory that sustains anergy to fetal antigen. *Nature* **490**, 102-106, doi:10.1038/nature11462 (2012).
429 Rosenblum, M. D. *et al.* Response to self antigen imprints regulatory memory in tissues. *Nature* **480**, 538-542, doi:10.1038/nature10664 (2011).
430 Jabri, B. & Sollid, L. M. T Cells in Celiac Disease. *J Immunol* **198**, 3005-3014, doi:10.4049/jimmunol.1601693 (2017).
431 Abadie, V., Sollid, L. M., Barreiro, L. B. & Jabri, B. Integration of genetic and immunological insights into a model of celiac disease pathogenesis. *Annu Rev Immunol* **29**, 493-525, doi:10.1146/annurev-immunol-040210-092915 (2011).
432 Jabri, B. & Sollid, L. M. Tissue-mediated control of immunopathology in coeliac disease. *Nat Rev Immunol* **9**, 858-870, doi:10.1038/nri2670 (2009).
433 Coleman, T. J., Gamble, D. R. & Taylor, K. W. Diabetes in mice after Coxsackie B 4 virus infection. *Br Med J* **3**, 25-27, doi:10.1136/bmj.3.5870.25 (1973).
434 Tai, N. *et al.* Microbial antigen mimics activate diabetogenic CD8 T cells in NOD mice. *J Exp Med* **213**, 2129-2146, doi:10.1084/jem.20160526 (2016).

435 Filippi, C. M., Estes, E. A., Oldham, J. E. & von Herrath, M. G. Immunoregulatory mechanisms triggered by viral infections protect from type 1 diabetes in mice. *J Clin Invest* **119**, 1515-1523, doi:10.1172/JCI38503 (2009).
436 Filippi, C. M. & von Herrath, M. G. Viral trigger for type 1 diabetes: pros and cons. *Diabetes* **57**, 2863-2871, doi:10.2337/db07-1023 (2008).
437 Bach, J. F. The effect of infections on susceptibility to autoimmune and allergic diseases. *N Engl J Med* **347**, 911-920, doi:10.1056/NEJMra020100 (2002).
438 Oliveira, G. *et al.* Landscape of helper and regulatory antitumour CD4(+) T cells in melanoma. *Nature* **605**, 532-538, doi:10.1038/s41586-022-04682-5 (2022).
439 Ahmadzadeh, M. *et al.* Tumor-infiltrating human CD4(+) regulatory T cells display a distinct TCR repertoire and exhibit tumor and neoantigen reactivity. *Sci Immunol* **4**, doi:10.1126/sciimmunol.aao4310 (2019).
440 Wu, W. H., Zegarra-Ruiz, D. F. & Diehl, G. E. Intestinal Microbes in Autoimmune and Inflammatory Disease. *Front Immunol* **11**, 597966, doi:10.3389/fimmu.2020.597966 (2020).
441 Ruff, W. E. *et al.* Pathogenic Autoreactive T and B Cells Cross-React with Mimotopes Expressed by a Common Human Gut Commensal to Trigger Autoimmunity. *Cell Host Microbe* **26**, 100-113 e108, doi:10.1016/j.chom.2019.05.003 (2019).
442 Horai, R. *et al.* Microbiota-Dependent Activation of an Autoreactive T Cell Receptor Provokes Autoimmunity in an Immunologically Privileged Site. *Immunity* **43**, 343-353, doi:10.1016/j.immuni.2015.07.014 (2015).
443 Galván-Peña, S., Zhu, Y., Hanna, B. S., Mathis, D. & Benoist, C. A dynamic atlas of immunocyte migration from the gut. *bioRxiv*, 2022.2011.2016.516757, doi:10.1101/2022.11.16.516757 (2022).
444 Hanna, B. S. *et al.* The gut microbiota promotes distal tissue regeneration via RORgamma(+) regulatory T cell emissaries. *Immunity*, doi:10.1016/j.immuni.2023.01.033 (2023).
445 Merana, G. R. *et al.* Intestinal inflammation alters the antigen-specific immune response to a skin commensal. *Cell Rep* **39**, 110891, doi:10.1016/j.celrep.2022.110891 (2022).
446 Binnewies, M. *et al.* Unleashing Type-2 Dendritic Cells to Drive Protective Antitumor CD4(+) T Cell Immunity. *Cell* **177**, 556-571 e516, doi:10.1016/j.cell.2019.02.005 (2019).
447 Chudnovskiy, A. *et al.* Proximity-dependent labeling identifies dendritic cells that prime the antitumor CD4⁺ T cell response. *bioRxiv*, 2022.2010.2025.513771, doi:10.1101/2022.10.25.513771 (2022).
448 Canesso, M. C. C. *et al.* Identification of dendritic cell-T cell interactions driving immune responses to food. *bioRxiv*, 2022.2010.2026.513772, doi:10.1101/2022.10.26.513772 (2022).
449 Marchingo, J. M. *et al.* T cell signaling. Antigen affinity, costimulation, and cytokine inputs sum linearly to amplify T cell expansion. *Science* **346**, 1123-1127, doi:10.1126/science.1260044 (2014).
450 Obst, R., van Santen, H. M., Mathis, D. & Benoist, C. Antigen persistence is required throughout the expansion phase of a CD4(+) T cell response. *J Exp Med* **201**, 1555-1565, doi:10.1084/jem.20042521 (2005).

451 Kim, C., Wilson, T., Fischer, K. F. & Williams, M. A. Sustained interactions between T cell receptors and antigens promote the differentiation of CD4(+) memory T cells. *Immunity* **39**, 508-520, doi:10.1016/j.immuni.2013.08.033 (2013).
452 Jing, Y. *et al.* Increased TCR signaling in regulatory T cells is disengaged from TCR affinity. *bioRxiv*, 2023.2001.2017.523999, doi:10.1101/2023.01.17.523999 (2023).
453 Marangoni, F. *et al.* Expansion of tumor-associated Treg cells upon disruption of a CTLA-4-dependent feedback loop. *Cell* **184**, 3998-4015 e3919, doi:10.1016/j.cell.2021.05.027 (2021).
454 Whitmire, J. K., Benning, N. & Whitton, J. L. Precursor frequency, nonlinear proliferation, and functional maturation of virus-specific CD4+ T cells. *J Immunol* **176**, 3028-3036, doi:10.4049/jimmunol.176.5.3028 (2006).
455 Quiel, J. *et al.* Antigen-stimulated CD4 T-cell expansion is inversely and log-linearly related to precursor number. *Proc Natl Acad Sci U S A* **108**, 3312-3317, doi:10.1073/pnas.1018525108 (2011).
456 Mueller, D. L. Mechanisms maintaining peripheral tolerance. *Nat Immunol* **11**, 21-27, doi:10.1038/ni.1817 (2010).
457 Nakandakari-Higa, S. *et al.* Universal recording of cell-cell contacts in vivo for interaction-based transcriptomics. *bioRxiv*, doi:10.1101/2023.03.16.533003 (2023).
458 Eisenbarth, S. C. Dendritic cell subsets in T cell programming: location dictates function. *Nat Rev Immunol* **19**, 89-103, doi:10.1038/s41577-018-0088-1 (2019).
459 Allison, K. A. *et al.* Affinity and dose of TCR engagement yield proportional enhancer and gene activity in CD4+ T cells. *Elife* **5**, doi:10.7554/eLife.10134 (2016).
460 Liao, W., Lin, J. X. & Leonard, W. J. IL-2 family cytokines: new insights into the complex roles of IL-2 as a broad regulator of T helper cell differentiation. *Curr Opin Immunol* **23**, 598-604, doi:10.1016/j.coi.2011.08.003 (2011).
461 Breed, E. R., Watanabe, M. & Hogquist, K. A. Measuring Thymic Clonal Deletion at the Population Level. *J Immunol* **202**, 3226-3233, doi:10.4049/jimmunol.1900191 (2019).
462 Zuklys, S. *et al.* Normal thymic architecture and negative selection are associated with Aire expression, the gene defective in the autoimmune-polyendocrinopathy-candidiasis-ectodermal dystrophy (APECED). *J Immunol* **165**, 1976-1983, doi:10.4049/jimmunol.165.4.1976 (2000).
463 Zhan, Y. *et al.* CCR2 enhances CD25 expression by FoxP3(+) regulatory T cells and regulates their abundance independently of chemotaxis and CCR2(+) myeloid cells. *Cell Mol Immunol* **17**, 123-132, doi:10.1038/s41423-018-0187-8 (2020).
464 Wohn, C. *et al.* Absence of MHC class II on cDC1 dendritic cells triggers fatal autoimmunity to a cross-presented self-antigen. *Sci Immunol* **5**, doi:10.1126/sciimmunol.aba1896 (2020).
465 Muth, S., Schutze, K., Schild, H. & Probst, H. C. Release of dendritic cells from cognate CD4+ T-cell recognition results in impaired peripheral tolerance and fatal cytotoxic T-cell mediated autoimmunity. *Proc Natl Acad Sci U S A* **109**, 9059-9064, doi:10.1073/pnas.1110620109 (2012).
466 Onishi, Y., Fehervari, Z., Yamaguchi, T. & Sakaguchi, S. Foxp3+ natural regulatory T cells preferentially form aggregates on dendritic cells in vitro and actively inhibit their maturation. *Proc Natl Acad Sci U S A* **105**, 10113-10118, doi:10.1073/pnas.0711106105 (2008).

467 Victora, G. D. & Nussenzweig, M. C. Germinal Centers. *Annu Rev Immunol* **40**, 413-442, doi:10.1146/annurev-immunol-120419-022408 (2022).
468 Gavanescu, I., Benoist, C. & Mathis, D. B cells are required for Aire-deficient mice to develop multi-organ autoinflammation: A therapeutic approach for APECED patients. *Proc Natl Acad Sci U S A* **105**, 13009-13014, doi:10.1073/pnas.0806874105 (2008).
469 Kitamura, D., Roes, J., Kuhn, R. & Rajewsky, K. A B cell-deficient mouse by targeted disruption of the membrane exon of the immunoglobulin mu chain gene. *Nature* **350**, 423-426, doi:10.1038/350423a0 (1991).
470 Ansel, K. M. *et al.* A chemokine-driven positive feedback loop organizes lymphoid follicles. *Nature* **406**, 309-314, doi:10.1038/35018581 (2000).
471 Luther, S. A., Lopez, T., Bai, W., Hanahan, D. & Cyster, J. G. BLC expression in pancreatic islets causes B cell recruitment and lymphotoxin-dependent lymphoid neogenesis. *Immunity* **12**, 471-481, doi:10.1016/s1074-7613(00)80199-5 (2000).
472 Selin, L. K. *et al.* Memory of mice and men: CD8+ T-cell cross-reactivity and heterologous immunity. *Immunol Rev* **211**, 164-181, doi:10.1111/j.0105-2896.2006.00394.x (2006).
473 Selin, L. K. *et al.* CD8 memory T cells: cross-reactivity and heterologous immunity. *Semin Immunol* **16**, 335-347, doi:10.1016/j.smim.2004.08.014 (2004).
474 Welsh, R. M. & Selin, L. K. No one is naive: the significance of heterologous T-cell immunity. *Nat Rev Immunol* **2**, 417-426, doi:10.1038/nri820 (2002).
475 Clute, S. C. *et al.* Broad cross-reactive TCR repertoires recognizing dissimilar Epstein-Barr and influenza A virus epitopes. *J Immunol* **185**, 6753-6764, doi:10.4049/jimmunol.1000812 (2010).
476 Selin, L. K., Nahill, S. R. & Welsh, R. M. Cross-reactivities in memory cytotoxic T lymphocyte recognition of heterologous viruses. *J Exp Med* **179**, 1933-1943, doi:10.1084/jem.179.6.1933 (1994).
477 Mathurin, K. S., Martens, G. W., Kornfeld, H. & Welsh, R. M. CD4 T-cell-mediated heterologous immunity between mycobacteria and poxviruses. *J Virol* **83**, 3528-3539, doi:10.1128/JVI.02393-08 (2009).
478 Welsh, R. M. Private specificities of heterologous immunity. *Curr Opin Immunol* **18**, 331-337, doi:10.1016/j.coi.2006.03.002 (2006).
479 Kim, S. K. *et al.* Private specificities of CD8 T cell responses control patterns of heterologous immunity. *J Exp Med* **201**, 523-533, doi:10.1084/jem.20041337 (2005).
480 Kim, S. K., Brehm, M. A., Welsh, R. M. & Selin, L. K. Dynamics of memory T cell proliferation under conditions of heterologous immunity and bystander stimulation. *J Immunol* **169**, 90-98, doi:10.4049/jimmunol.169.1.90 (2002).
481 Brehm, M. A. *et al.* T cell immunodominance and maintenance of memory regulated by unexpectedly cross-reactive pathogens. *Nat Immunol* **3**, 627-634, doi:10.1038/ni806 (2002).
482 Tubo, N. J. *et al.* Most microbe-specific naive CD4(+) T cells produce memory cells during infection. *Science* **351**, 511-514, doi:10.1126/science.aad0483 (2016).
483 Tubo, N. J. *et al.* Single naive CD4+ T cells from a diverse repertoire produce different effector cell types during infection. *Cell* **153**, 785-796, doi:10.1016/j.cell.2013.04.007 (2013).
484 Jabri, B. & Abadie, V. IL-15 functions as a danger signal to regulate tissue-resident T cells and tissue destruction. *Nat Rev Immunol* **15**, 771-783, doi:10.1038/nri3919 (2015).

485 White, J. T., Cross, E. W. & Kedl, R. M. Antigen-inexperienced memory CD8(+) T cells: where they come from and why we need them. *Nat Rev Immunol* **17**, 391-400, doi:10.1038/nri.2017.34 (2017).
486 Jameson, S. C., Lee, Y. J. & Hogquist, K. A. Innate memory T cells. *Adv Immunol* **126**, 173-213, doi:10.1016/bs.ai.2014.12.001 (2015).
487 Haluszczak, C. *et al.* The antigen-specific CD8+ T cell repertoire in unimmunized mice includes memory phenotype cells bearing markers of homeostatic expansion. *J Exp Med* **206**, 435-448, doi:10.1084/jem.20081829 (2009).
488 Miller, C. H. *et al.* Eomes identifies thymic precursors of self-specific memory-phenotype CD8(+) T cells. *Nat Immunol* **21**, 567-577, doi:10.1038/s41590-020-0653-1 (2020).
489 Denucci, C. C., Mitchell, J. S. & Shimizu, Y. Integrin function in T-cell homing to lymphoid and nonlymphoid sites: getting there and staying there. *Crit Rev Immunol* **29**, 87-109, doi:10.1615/critrevimmunol.v29.i2.10 (2009).
490 Berlin, C. *et al.* Alpha 4 beta 7 integrin mediates lymphocyte binding to the mucosal vascular addressin MAdCAM-1. *Cell* **74**, 185-195, doi:10.1016/0092-8674(93)90305-a (1993).
491 Kim, T. S. & Shin, E. C. The activation of bystander CD8(+) T cells and their roles in viral infection. *Exp Mol Med* **51**, 1-9, doi:10.1038/s12276-019-0316-1 (2019).
492 Pasqual, G. *et al.* Monitoring T cell-dendritic cell interactions in vivo by intercellular enzymatic labelling. *Nature* **553**, 496-500, doi:10.1038/nature25442 (2018).
493 Matsushita, H. *et al.* Cancer exome analysis reveals a T-cell-dependent mechanism of cancer immunoediting. *Nature* **482**, 400-404, doi:10.1038/nature10755 (2012).
494 DuPage, M., Mazumdar, C., Schmidt, L. M., Cheung, A. F. & Jacks, T. Expression of tumour-specific antigens underlies cancer immunoediting. *Nature* **482**, 405-409, doi:10.1038/nature10803 (2012).
495 Rooney, M. S., Shukla, S. A., Wu, C. J., Getz, G. & Hacohen, N. Molecular and genetic properties of tumors associated with local immune cytolytic activity. *Cell* **160**, 48-61, doi:10.1016/j.cell.2014.12.033 (2015).
496 Brown, S. D. *et al.* Neo-antigens predicted by tumor genome meta-analysis correlate with increased patient survival. *Genome Res* **24**, 743-750, doi:10.1101/gr.165985.113 (2014).
497 Shakiba, M. *et al.* TCR signal strength defines distinct mechanisms of T cell dysfunction and cancer evasion. *J Exp Med* **219**, doi:10.1084/jem.20201966 (2022).
498 Burger, M. L. *et al.* Antigen dominance hierarchies shape TCF1(+) progenitor CD8 T cell phenotypes in tumors. *Cell* **184**, 4996-5014 e4926, doi:10.1016/j.cell.2021.08.020 (2021).
499 Chen, P. H. *et al.* Activation of CAR and non-CAR T cells within the tumor microenvironment following CAR T cell therapy. *JCI Insight* **5**, doi:10.1172/jci.insight.134612 (2020).
500 Ma, L. *et al.* Eradication of tumors with pre-existing antigenic heterogeneity by vaccine-mediated co-engagement of CAR T and endogenous T-cells. *bioRxiv*, 2022.2010.2005.511036, doi:10.1101/2022.10.05.511036 (2022).
501 Falo, L. D., Jr., Kovacsovics-Bankowski, M., Thompson, K. & Rock, K. L. Targeting antigen into the phagocytic pathway in vivo induces protective tumour immunity. *Nat Med* **1**, 649-653, doi:10.1038/nm0795-649 (1995).
502 Yost, K. E. *et al.* Clonal replacement of tumor-specific T cells following PD-1 blockade. *Nat Med* **25**, 1251-1259, doi:10.1038/s41591-019-0522-3 (2019).

503 Degn, S. E. *et al.* Clonal Evolution of Autoreactive Germinal Centers. *Cell* **170**, 913-926 e919, doi:10.1016/j.cell.2017.07.026 (2017).
504 Hagglof, T. *et al.* Continuous germinal center invasion contributes to the diversity of the immune response. *Cell* **186**, 147-161 e115, doi:10.1016/j.cell.2022.11.032 (2023).
505 de Carvalho, R. V. H. *et al.* Clonal replacement sustains long-lived germinal centers primed by respiratory viruses. *Cell* **186**, 131-146 e113, doi:10.1016/j.cell.2022.11.031 (2023).
506 Schwartz, R. H. T cell anergy. *Annu Rev Immunol* **21**, 305-334, doi:10.1146/annurev.immunol.21.120601.141110 (2003).
507 Shin, D. S. *et al.* Lung injury induces a polarized immune response by self antigen-specific Foxp3 (+) regulatory T cells. *bioRxiv*, doi:10.1101/2023.02.09.527896 (2023).
508 Dominguez Conde, C. *et al.* Cross-tissue immune cell analysis reveals tissue-specific features in humans. *Science* **376**, eabl5197, doi:10.1126/science.abl5197 (2022).
509 Heidkamp, G. F. *et al.* Human lymphoid organ dendritic cell identity is predominantly dictated by ontogeny, not tissue microenvironment. *Sci Immunol* **1**, doi:10.1126/sciimmunol.aai7677 (2016).
510 Jiang, Y., Li, Y. & Zhu, B. T-cell exhaustion in the tumor microenvironment. *Cell Death Dis* **6**, e1792, doi:10.1038/cddis.2015.162 (2015).
511 Zehn, D., Thimme, R., Lugli, E., de Almeida, G. P. & Oxenius, A. 'Stem-like' precursors are the fount to sustain persistent CD8(+) T cell responses. *Nat Immunol* **23**, 836-847, doi:10.1038/s41590-022-01219-w (2022).
512 McGranahan, N. *et al.* Allele-Specific HLA Loss and Immune Escape in Lung Cancer Evolution. *Cell* **171**, 1259-1271 e1211, doi:10.1016/j.cell.2017.10.001 (2017).
513 Tadokoro, C. E. *et al.* Regulatory T cells inhibit stable contacts between CD4+ T cells and dendritic cells in vivo. *J Exp Med* **203**, 505-511, doi:10.1084/jem.20050783 (2006).
514 Bohineust, A., Garcia, Z., Beuneu, H., Lemaitre, F. & Bousso, P. Termination of T cell priming relies on a phase of unresponsiveness promoting disengagement from APCs and T cell division. *J Exp Med* **215**, 1481-1492, doi:10.1084/jem.20171708 (2018).
515 Osum, K. C. & Jenkins, M. K. Toward a general model of CD4(+) T cell subset specification and memory cell formation. *Immunity* **56**, 475-484, doi:10.1016/j.immuni.2023.02.010 (2023).
516 Gaud, G., Lesourne, R. & Love, P. E. Regulatory mechanisms in T cell receptor signalling. *Nat Rev Immunol* **18**, 485-497, doi:10.1038/s41577-018-0020-8 (2018).
517 Yang, Y. *et al.* Focused specificity of intestinal TH17 cells towards commensal bacterial antigens. *Nature* **510**, 152-156, doi:10.1038/nature13279 (2014).
518 Kunzli, M. & Masopust, D. CD4(+) T cell memory. *Nat Immunol*, doi:10.1038/s41590-023-01510-4 (2023).
519 Bresser, K. *et al.* Replicative history marks transcriptional and functional disparity in the CD8(+) T cell memory pool. *Nat Immunol* **23**, 791-801, doi:10.1038/s41590-022-01171-9 (2022).
520 Marangoni, F. *et al.* The transcription factor NFAT exhibits signal memory during serial T cell interactions with antigen-presenting cells. *Immunity* **38**, 237-249, doi:10.1016/j.immuni.2012.09.012 (2013).
521 Harris, M. J., Fuyal, M. & James, J. R. Quantifying persistence in the T-cell signaling network using an optically controllable antigen receptor. *Mol Syst Biol* **17**, e10091, doi:10.15252/msb.202010091 (2021).

522 Valdor, R. & Macian, F. Induction and stability of the anergic phenotype in T cells. *Semin Immunol* **25**, 313-320, doi:10.1016/j.smim.2013.10.010 (2013).

523 Nishikawa, Y. *et al.* Temporal lineage tracing of Aire-expressing cells reveals a requirement for Aire in their maturation program. *J Immunol* **192**, 2585-2592, doi:10.4049/jimmunol.1302786 (2014).